

# Post-translational lysine-acetylation of Ran and its regulation by Sirtuin deacetylases



Inaugural-Dissertation  
zur  
Erlangung des Doktorgrades  
der Mathematisch-Naturwissenschaftlichen Fakultät  
der Universität zu Köln  
vorgelegt von  
**Philipp Knyphausen**  
aus Eckernförde

Hundt Druck GmbH, Köln  
2016

**Post-translational lysine-acetylation of  
Ran and its regulation by Sirtuin  
deacetylases**

Inaugural-Dissertation  
zur  
Erlangung des Doktorgrades  
der Mathematisch-Naturwissenschaftlichen Fakultät  
der Universität zu Köln  
vorgelegt von

**Philipp Knyphausen**  
aus Eckernförde



Berichtersteller:  
(Gutachter)

Dr. Michael Lammers (Betreuer)  
Prof. Dr. Kay Hofmann

Tag der mündlichen Prüfung:

20. Januar 2016



# Zusammenfassung

Durch die Fortschritte in der Hochdurchsatz-Massenspektrometrie hat sich gezeigt, dass posttranslationale N-( $\epsilon$ )-Lysin-Acetylierung bei Tausenden von Proteinen vorkommt. So modifizierte Proteine finden sich beim Menschen und anderen Organismen in allen Zellkompartimenten und sind in vielen Fällen an essentiellen zellulären Prozessen beteiligt. Viele Aspekte posttranslationaler Lysin-Acetylierung sind jedoch nur unvollständig verstanden, einschließlich ihrer Regulierung durch Lysin-Acetyltransferasen und Lysin-Deacetylasen (KDACs). In dieser Arbeit wurde untersucht, welchen Einfluss diese Modifikation auf die Funktion des kleinen GTP-bindenden Proteins Ran hat, dem in der Zelle unter anderem eine zentrale Rolle bei der Regulation des Kerntransports zukommt. Hierzu wurde mit Hilfe eines erweiterten genetischen Codes stellenspezifisch acetyliertes Ran in *E. coli* hergestellt.

Untersucht wurden zunächst fünf zuvor identifizierte Ran-Acetylierungsstellen hinsichtlich ihrer Auswirkungen auf die intrinsische GTP-Hydrolyse Rate von Ran, die Bildung von Exportkomplexen (anhand des Exportrezeptors CRM1 und des Exportsubstrats Spn1) und die Interaktion von Ran mit RanBP1 und dem GTPase-aktivierenden Protein RanGAP. Insgesamt waren sowohl bei der intrinsischen als auch der RanGAP-stimulierten GTP-Hydrolyse nur schwache Effekte zu messen. Dahingegen sorgte die Acetylierung von Ran am Lysin 159 (K159) für eine deutlich gesenkte Affinität von Ran zu RanBP1, wenn Ran im aktiven Zustand vorlag. Darüberhinaus war eine stärkere Bindung von Spn1 an einen Komplex aus CRM1•Ran zu beobachten, wenn Ran an den Stellen K37, K99 oder K159 acetyliert war. Anhand dieser Ergebnisse lässt sich schließen, dass wesentliche Funktionen des Proteins Ran durch Acetylierung beeinflusst werden.

Ein *in vitro* Screen wurde durchgeführt, um potenzielle KDACs für Ran zu identifizieren. NAD<sup>+</sup>-abhängige KDACs der Sirtuin-Klasse zeigten Aktivität gegenüber zwei Acetylierungsstellen von Ran, K37 und K71. Die Spezifität der SIRTs wurde daraufhin anhand einer weiteren acetylierten Variante von Ran (RanAcK38) analysiert. Da bei RanAcK38 im Vergleich zu RanAcK37 eine deutlich langsamere Deacetylierungsrate zu beobachten war, wurde als nächstes di-acetyliertes RanAcK37/38 getestet. Die Deacetylierungsrate von di-acetylierten Ran war erstaunlicherweise vergleichbar mit derjenigen von RanAcK37. Deacetylierungsexperimente unter *single turnover*-Bedingungen ergaben, dass die Deacetylierung im RanAcK37/38-Hintergrund als erstes an der Stelle K38 erfolgen muss. Die Fähigkeit von Sirtuinen zwei benachbarte AcKs zu deacetylieren wurde schließlich anhand

zweier weiterer Proteine untersucht, von denen bekannt war, dass sie unter anderem di-acetyliert vorkommen. Dabei handelte es sich um das Tumorsuppressor-Protein p53 und Phosphoenolpyruvatcarboxykinase 1 (PEPCK1). Es stellte sich heraus, dass p53 an zwei Di-Acetylierungsstellen (K372/372 und K381/382) durch Sirtuin 1 und 2 deacetyliert wird. Entgegen der Erwartungen war bei PEPCK1 keine Deacetylierung durch Sirtuine festzustellen. Diese Ergebnisse lassen einige bedeutende Schlussfolgerungen für die Substratspezifität von Sirtuinen zu.

*“Now my own suspicion is that the Universe is not only queerer than we suppose,  
but queerer than we can suppose.”*

John Burdon Sanderson Haldane, Biologist



# Abstract

Through recent advances in high-throughput mass spectrometry it has become evident that post-translational N-( $\epsilon$ )-lysine-acetylation is a modification found on thousands of proteins of all cellular compartments and all essential physiological processes. Many aspects in the biology of lysine-acetylation are poorly understood, including its regulation by lysine-acetyltransferases and lysine-deacetylases (KDACs). Here, the role of this modification was investigated for the small GTP-binding protein Ran, which, *inter alia*, is essential for the regulation of nucleocytoplasmic transport. To this end, site-specifically acetylated Ran was produced in *E. coli* by genetic code expansion.

For five previously identified sites, Ran acetylation was tested regarding its impact on the intrinsic GTP hydrolysis rate, the assembly of export complexes (modeled *in vitro* with the export receptor CRM1 and the export substrate Spn1) and the interaction of Ran with its GTPase activation protein RanGAP and RanBP1. Overall, mild effects of Ran acetylation were observed for intrinsic and RanGAP-stimulated GTP hydrolysis rates. The interaction of active Ran with RanBP1 was negatively influenced by Ran acetylation at K159. Moreover, CRM1 bound to Ran acetylated at K37, K99 or K159 interacted more strongly with Spn1. Thus, lysine-acetylation interferes with essential aspects of Ran function.

An *in vitro* screen was performed to identify potential Ran KDACs. The NAD<sup>+</sup>-dependent KDACs of the Sirtuin class showed activity towards two acetylation sites of Ran, K37 and K71. The specificity of Sirtuins was further analyzed based on an additional Ran acetylation site, K38. Since deacetylation of RanAcK38 was much slower compared to RanAcK37, di-acetylated RanAcK37/38 was tested next. The deacetylation rate of di-acetylated Ran was comparable to that of RanAcK37. Deacetylation experiments under single turnover conditions revealed that deacetylation occurs first at the K38 site in the di-acetylated RanAcK37/38 background. The ability of Sirtuins to deacetylate two adjacent AcKs was further investigated based on two proteins, which had previously been found to be di-acetylated and targeted by Sirtuins, namely the tumor suppressor protein p53 and phosphoenolpyruvate carboxykinase 1 (PEPCK1). p53 was readily deacetylated at two di-acetylation sites (K372/372 and K381/382), whereas PEPCK1 was not deacetylated *in vitro*. Taken together, these results have important implications for the substrate specificity of Sirtuins.



# Contents

<b>Abstract</b>	<b>i</b>
<b>List of Figures</b>	<b>vii</b>
<b>List of Tables</b>	<b>ix</b>
<b>1 Introduction</b>	<b>1</b>
1.1 The small GTP-binding protein Ran . . . . .	1
1.1.1 Localization of Ras proteins . . . . .	3
1.1.2 Nucleotide exchange and hydrolysis . . . . .	5
1.1.3 Nucleocytoplasmic transport . . . . .	8
1.1.4 Mitotic spindle assembly . . . . .	12
1.1.5 Nuclear envelope formation . . . . .	13
1.2 Lysine-acetylation . . . . .	14
1.2.1 The writers: Lysine-acetyltransferases (KATs) . . . . .	16
1.2.2 The erasers: Lysine-deacetylases (KDACs) . . . . .	17
1.2.3 The readers: Bromodomain containing proteins . . . . .	21
1.2.4 The canonical roles of lysine-acetylation . . . . .	23
1.2.5 The acetylome: Novel roles for lysine-acetylation? . . . . .	25
1.2.6 Lysine-acetylation of Ran . . . . .	27
1.2.7 The genetic code expansion concept (GCEC) . . . . .	28
1.3 Aim of the thesis . . . . .	30
<b>2 Material and Methods</b>	<b>31</b>
2.1 Materials . . . . .	31
2.1.1 Chemicals, kits and enzymes . . . . .	31
2.1.2 Primers . . . . .	31
2.1.3 Vectors and constructs . . . . .	33
2.1.4 Crystallization screens . . . . .	35
2.1.5 Buffers . . . . .	36
2.1.6 Media, Antibiotics and inhibitors . . . . .	38
2.2 Molecular biology techniques . . . . .	38
2.2.1 Purification of DNA . . . . .	38
2.2.2 Polymerase chain reaction (PCR) . . . . .	38
2.2.3 Restriction enzyme-based cloning . . . . .	39

---

2.2.4	Circular polymerase extension cloning (CPEC) . . . . .	39
2.2.5	Site-directed mutagenesis . . . . .	40
2.2.6	Transformation of <i>E. coli</i> . . . . .	40
2.3	Biochemical methods . . . . .	40
2.3.1	Expression of recombinant proteins . . . . .	40
2.3.2	Lysis of cells . . . . .	41
2.3.3	Purification of GST-tagged proteins . . . . .	41
2.3.4	Purification of His <sub>6</sub> -tagged proteins . . . . .	42
2.3.5	Determination of protein concentration . . . . .	42
2.3.6	SDS-polyacrylamide gel electrophoresis (SDS-PAGE) . . . . .	43
2.3.7	Western blotting and immunodetection . . . . .	43
2.3.8	Generation of the RanAcK37-specific antibody . . . . .	44
2.3.9	Exchange of Ran-bound nucleotides . . . . .	45
2.3.10	High pressure liquid chromatography (HPLC) . . . . .	45
2.3.11	Activity assay for deacetylases . . . . .	46
2.3.12	KDAC-screen . . . . .	46
2.3.13	Deacetylase assays . . . . .	47
2.3.14	PEPCK1 activity assay . . . . .	47
2.4	Cell culture . . . . .	48
2.4.1	Cultivation of cell lines . . . . .	48
2.4.2	Transfection . . . . .	48
2.4.3	Ni <sup>2+</sup> -NTA pull-down . . . . .	49
2.5	Biophysical methods . . . . .	50
2.5.1	Isothermal titration calorimetry (ITC) . . . . .	50
2.5.2	Mass spectrometry (MS) . . . . .	50
2.6	Crystallographic methods . . . . .	52
2.6.1	Crystallization . . . . .	52
2.6.2	Preparation of crystals for data collection . . . . .	52
2.6.3	Data collection and processing . . . . .	53
<b>3</b>	<b>Results</b>	<b>55</b>
3.1	Ran acetylation: Effects and regulation . . . . .	55
3.1.1	Purification of acetylated Ran . . . . .	55
3.1.2	Effect of Ran acetylation on intrinsic GTP hydrolysis . . . . .	58
3.1.3	GAP-catalyzed nucleotide hydrolysis and binding to Ran- GAP is not affected by Ran acetylation . . . . .	59
3.1.4	Impact of Ran acetylation on the interaction with RanBP1 . . . . .	64
3.1.5	Ran acetylation interferes with export complex formation . . . . .	65
3.1.6	<i>in vivo</i> acetylation of Ran by KAT overexpression . . . . .	68
3.1.7	An <i>in vitro</i> KDAC screen identifies SIRT1-3 as Ran deacetylases . . . . .	71
3.2	Analysis of di-deacetylation by Sirtuins . . . . .	76
3.2.1	SIRT2 deacetylates Ran at two adjacent lysines . . . . .	76
3.2.2	Mass spectrometric analysis of Ran di-deacetylation . . . . .	77

---

3.2.3	Mutational analysis of the Ran di-deacetylation site . . . . .	80
3.2.4	Structural insights into di-deacetylation . . . . .	81
3.2.5	SIRT1 and SIRT3 are able to di-deacetylate Ran . . . . .	87
3.2.6	PEPCK1 is not deacetylated by SIRT2 <i>in vitro</i> . . . . .	88
3.2.7	Deacetylation of p53-AcK381/382 . . . . .	91
3.2.8	Deacetylation of p53-AcK372/373 . . . . .	93
<b>4</b>	<b>Discussion</b>	<b>99</b>
4.1	Incorporation of acetyl-lysine with the GCEC . . . . .	99
4.2	Ran acetylation in regulation of export complex formation and release	100
4.3	Regulation of Ran acetylation . . . . .	102
4.4	Implications for the substrate specificity of classical KDACs . . . . .	107
4.5	Implications for the substrate specificity of Sirtuins . . . . .	109
4.6	On the role of di-acetylation . . . . .	114
4.7	Conclusions and Outlook . . . . .	114
<b>A</b>	<b>Appendix</b>	<b>117</b>
	<b>Bibliography</b>	<b>125</b>
	<b>Abbreviations</b>	<b>125</b>
	<b>Acknowledgements</b>	<b>167</b>



# List of Figures

1.1	Structural comparison of GDP- and GTP-bound GNBPs . . . . .	3
1.2	The nucleotide exchange cycle . . . . .	5
1.3	Mechanisms of GTPase activation by GAPs . . . . .	8
1.4	The nuclear pore complex (NPC) . . . . .	9
1.5	Ran-dependent nuclear import and export . . . . .	11
1.6	Roles of Ran during mitotic spindle assembly . . . . .	13
1.7	Molecular effects of acetylation of lysine . . . . .	15
1.8	Chemistry and structure of Sirtuin deacetylases . . . . .	19
1.9	Bromodomains are readers of acetylated lysine residues . . . . .	22
1.10	Domain structure and acetylation sites of p53 . . . . .	25
1.11	The genetic code expansion concept (GCEC) . . . . .	29
2.1	Scheme of PEPCK1 activity assay . . . . .	48
3.1	Exemplary purification of acetylated Ran (RanAcK71) . . . . .	56
3.2	Purification of acetylated Ran and Ran interaction partners . . . . .	57
3.3	Effect of Ran acetylation on intrinsic GTP hydrolysis . . . . .	60
3.4	Effect of Ran acetylation on RanGAP-stimulated hydrolysis . . . . .	61
3.5	Interaction of RanGAP with RanGppNHp•RanBP1 . . . . .	63
3.6	Interaction of RanBP1 with acetylated Ran . . . . .	65
3.7	ITC-based <i>in vitro</i> export complex formation assay . . . . .	67
3.8	Impact of Ran acetylation on <i>in vitro</i> export complex formation . . . . .	69
3.9	MS based detection of acetylated Ran in HEK293T cells . . . . .	71
3.10	Activities of recombinant KDACs used for <i>in vitro</i> deacetylase screen . . . . .	72
3.11	<i>In vitro</i> deacetylase screen for recombinant Ran . . . . .	73
3.12	Deacetylation of RanAcK37 and -AcK71 by SIRT1-3 . . . . .	74
3.13	Deacetylation of RanGDP and -GppNHp by SIRT2 . . . . .	75
3.14	SIRT2 can deacetylate Ran at two neighboring lysines . . . . .	78
3.15	Sequential deacetylation of RanAcK37/38 . . . . .	80
3.16	Mutational analysis of RanAcK38 deacetylation . . . . .	82
3.17	Interaction of Ran-derived N-( $\epsilon$ )-trifluoroacetyl-L-lysine peptides with SIRT2 . . . . .	83
3.18	Crystallisation of SIRT2 with a RanTFAcK37 13-mer . . . . .	84
3.19	Structure of SIRT2 with RanTFAcK37 13-mer peptide . . . . .	86
3.20	Molecular interactions between SIRT2 and the RanTFAcK37 13-mer peptide . . . . .	87

---

3.21	Di-deacetylation by SIRT1 and SIRT3 . . . . .	88
3.22	Analysis of PEPCCK1 deacetylation . . . . .	95
3.23	Deacetylation of p53 by SIRT1 . . . . .	96
3.24	Dynamics of p53 deacetylation at the di-acetylation site K381/382 .	97
3.25	Deacetylation of p53 at the di-acetylation site K372/K373 . . . . .	98
4.1	Regulation of Ran functions by lysine-acetylation . . . . .	103
4.2	Sequence context of acetylation sites tested for deacetylation . . . .	111
4.3	Structural context of sites tested for deacetylation . . . . .	113
A.1	Maps of vectors used for GCEC . . . . .	118
A.2	ITC measurements of RanGppNHp•RanBP1 and RanGAP . . . . .	119
A.3	ITC measurements of RanGDP and RanBP1 . . . . .	120
A.4	ITC measurements of RanGppNHp and RanBP1 . . . . .	121
A.5	ITC measurements of RanGppNHp and CRM1•Spn1 . . . . .	122
A.6	ITC measurements of RanGppNHp•CRM1 and Spn1 . . . . .	123
A.7	Ramachandran plots by residue type . . . . .	124

# List of Tables

2.1	Cloning primers . . . . .	32
2.2	Primers for site-directed mutagenesis . . . . .	33
2.3	Constructs for recombinant protein expression . . . . .	35
2.4	Crystallization screens . . . . .	35
2.7	Antibodies . . . . .	44
2.8	Recombinant KDACs used for the screen . . . . .	47
3.1	Data collection, refinement and structure validation of the SIRT2(50-356)•RanTFAcK37-13-mer-peptide structure (molecular replacement).	85
4.1	Lysine-acetylation sites of Ras superfamily members. . . . .	105
4.2	Comparison of Ran acetylation sites with preferred substrate sequences of classical KDACs. . . . .	108



# 1 Introduction

The acquisition of a bacterial endosymbiont by an archeon about two billion years ago marks the beginning of eukaryotic evolution (reviewed in Koonin, 2015; Spang et al., 2015). The energetic gain associated with this symbiosis is thought to have allowed for the seemingly unconstrained genome size and morphological complexity seen in eukaryota (Lane and Martin, 2010). To account for the diverse novel tasks in the evolving eukaryotic cell, many protein families have undergone massive functional diversification, one of which is the Ras superfamily, which is essential for the regulation of cell proliferation, cellular adhesion, the cytoskeleton, vesicular transport and membrane trafficking (Jkely, 2003). Ran (Ras-related nuclear) has taken a central role in establishing the nuclear envelope and the regulation of nuclear transport and mitosis, all three being hallmarks of the eukaryotic domain of life. In this introduction, an overview is presented of the mechanisms of these Ran-directed processes. Furthermore, lysine-acetylation as a conserved and reversible post-translational modification is introduced, which will lead to the question how it might regulate Ran function, a question that will be of central relevance in this thesis.

## 1.1 The small GTP-binding protein Ran

Ran is a member of the Ras superfamily, the founding member of which is Ras (Rat sarcoma). Ras was initially discovered as the factor conferring oncogenicity to two murine viruses, the Kirsten and the Harvey murine sarcoma virus, hence the names K-Ras and H-Ras, respectively (Harvey, 1964; Kirsten et al., 1970). It later turned out that specific point mutations in the Ras sequences lead to this oncogenicity and that their wildtype counterparts are present in rat and human genomes (Capon et al., 1983; Chang et al., 1982; Ellis et al., 1981; Tsuchida et al.,

1982). Ras has since been regarded as a proto-oncogene, having important cellular functions in the non-mutated form but also becoming an oncogenic factor upon mutation of certain amino acid residues.

As stated above, the Ras superfamily has expanded in the early eukaryotic evolution and members of the five major branches (Ras, Rho, Rab, Ran and Arf) can thus be found in all eukaryotes unless they have been lost secondarily (Colicelli, 2004). About 167 members of the Ras superfamily are present in humans. Interestingly and in contrast to the many paralogs of other Ras superfamily members, only one Ran gene is found in mammals and a few often almost identical ones in plants (Rojas et al., 2012). In addition, Ran is one of the most conserved proteins of nucleated cells (Ach and Gruissem, 1994; Bush and Cardelli, 1993; Chen et al., 1994).

All Ras superfamily members have in common that they are relatively small proteins (20-30 kDa), able to bind guanosine di- or triphosphates (GDP and GTP, respectively) with high affinity and to adopt two three-dimensional conformations, depending on which nucleotide is bound. This behavior is referred to as a binary ‘molecular switch’ and makes this protein family particularly well-suited to act in cellular signaling pathways (Vetter and Wittinghofer, 2001). This is reflected by the diverse cellular processes that are regulated by these small guanine nucleotide binding proteins (GNBPs). In addition to the mere binding of GDP or GTP, Ras superfamily members are intrinsically able to hydrolyze bound GTP, although this activity is generally very low and differs substantially between different groups. In particular, the GTPase activity of the Arf members Sar1, SR $\beta$  and Arf are hardly detectable (Bi et al., 2002; Legate and Andrews, 2003; Randazzo and Kahn, 1994).

The shared features of small GNBPs and other GTP binding proteins can be directly attributed to their shared central domain, the G-domain, a fold consisting of a twisted beta sheet with six parallel and anti-parallel beta strands, four alpha helices packed on both sides of the beta sheet and nine connecting loops (de Vos et al., 1988; Pai et al., 1989). This approximately 20-kDa domain possesses characteristic consensus elements, so called G boxes, which on the one hand are required for nucleotide binding (and hydrolysis) and on the other hand mediate the switch-like behavior: G1, GxxxxGK(S/T); G2, x(P/A)T(I//V/L); G3, DxxGQ; G4, (T/N)KxD; and G5, (C/S)A(K/L)(S/T) (Bourne et al., 1991; Dever et al., 1987). While the G4-5 confer specificity for the guanine base over adenine,

the G1 or P-loop makes contacts with the  $\beta$ - and  $\gamma$ -phosphates of GTP and coordinates the  $Mg^{2+}$ -ion, which is needed for high affinity nucleotide binding (Saraste et al., 1990). Interestingly, the G2 and G3, besides also being involved in binding of the  $Mg^{2+}$ -ion, contact the  $\gamma$ -phosphate, which is only present in GTP. Thus, upon GTP hydrolysis these interactions are released, which results in a change in conformation and is the explanation for the switch-like behavior of small GNBPs. Due to this behavior, G2 and G3 are called switch I and switch II, respectively and their GTP-bound conformation has been compared to a loaded spring (Milburn et al., 1990; Vetter and Wittinghofer, 2001). As shown in Fig. 1.1, the switch I and II regions adopt a flexible conformation in the GDP-bound state compared to the rigid conformation seen in the GTP-bound state.

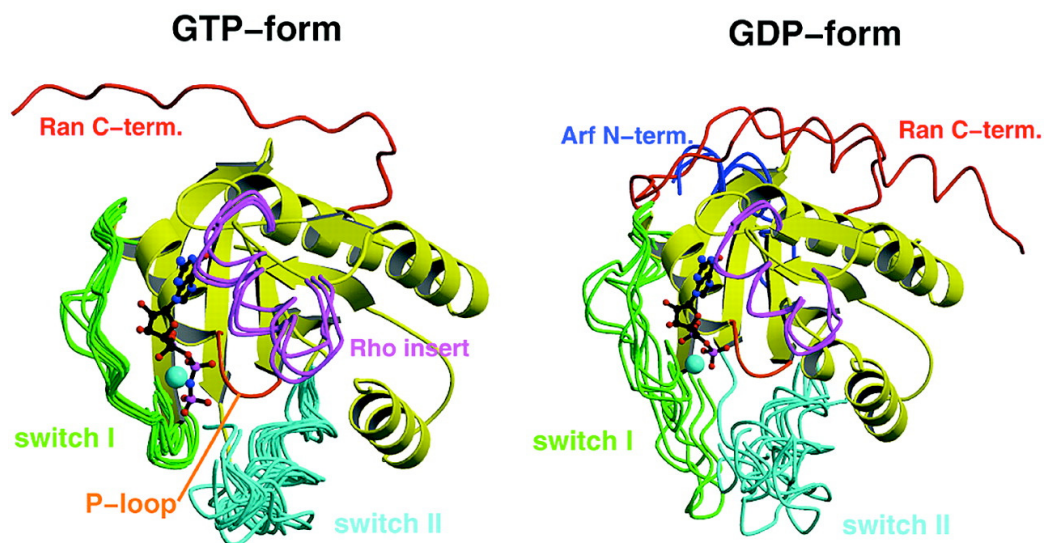


FIGURE 1.1: **Structural comparison of GDP- and GTP-bound GNBPs.** Selected Ras-related proteins in GTP- or GDP-form are shown as superimposed ribbon representations. The switch I and II regions are shown in green and turquoise, respectively. Characteristic elements of Rho, Arf and Ran are indicated (red: C-terminus of Ran, magenta: Rho insert, blue: Arf N-terminal helix) (taken from Vetter and Wittinghofer, 2001).

### 1.1.1 Localization of Ras proteins

Another feature of many Ras superfamily members is their post-translational modification by lipids, which anchor them to cellular membranes. In many cases this reflects their roles in membrane-associated processes. For instance, members of

the Rab and Arf families are important for vesicle formation and transport and the Rho family for the regulation of cell shape changes. However, the type of modification differs between the subfamilies. Ras and Rho family members are modified at a cysteine residue in their C-termini by farnesyltransferase or geranylgeranyltransferase type 1 (GGTase 1), which recognize a C-terminal CAAX motif (C: Cys, A: aliphatic, X: any amino acid) (Andregg et al., 1988; Casey et al., 1989; Clarke et al., 1988; Katayama et al., 1991; Maltese et al., 1990). In addition to the farnesyl- or geranylgeranyl-modifications, a nearby palmitoylation or polybasic patch can further strengthen their membrane attachment and direct their sub-cellular localization through interactions with distinct membrane compartments of different lipid compositions (Apolloni et al., 2000; Choy et al., 1999; Hancock et al., 1990; Rocks et al., 2005; Roy et al., 2005). Similarly, Rab family proteins are geranylgeranylated at their cysteine-containing C-termini by the action of RabGGTase (Jiang et al., 1993; Khosravi-Far et al., 1991). However, in most cases, two prenyl-groups are attached to Rab proteins. This is not specified by a CAAX motif but by an interaction between a conserved surface feature of Rab proteins with the Rab escort protein-1 (REP-1), which in turn interacts with RabGGTase (Andres et al., 1993; Pylypenko et al., 2003). REP-1 can accommodate both hydrophobic prenyl-groups (one in its interior and the other more solvent exposed) and remains bound to Rab proteins after prenylation until delivery to their target membrane (Pylypenko et al., 2006). Besides REP-1, there are also other proteins that can bind prenylated Rho or Rab proteins and regulate their delivery to or retrieval from membranes. These are subsumed under the term GDP-dissociation inhibitor (GDI) and, as the name suggests, preferentially bind to GDP-bound small GNBPs and prevent their activation (Gosser et al., 1997; Longenecker et al., 1999; Sasaki et al., 1990). Another factor that solubilizes a variety of farnesylated proteins, *inter alia* Ras subfamily members, is phosphodiesterase 6  $\delta$  subunit (PDE- $\delta$ ). In this case however, the binding occurs regardless of the GNBPs' nucleotide state (Chandra et al., 2012; Nancy et al., 2002). Members of the Arf family are often anchored to the membrane by a myristoyl-group, which is linked to their N-terminus. In addition to the myristoyl-anchor, an amphipathic N-terminal helix, which is released from an intramolecular sequestration upon GTP-loading, can insert itself into the membrane (Antonny et al., 1997). In fact, some Arf family members, like for instance Sar1, localize to membranes solely based on the action of this helix (Bielli et al., 2005). Ran is one of only a few Ras superfamily members that does not localize to membranes but is instead predominantly found in the nucleus

during interphase (Bischoff and Ponstingl, 1991b). It is furthermore not lipidated (*i.e.* prenylated or modified by fatty acid esterification) and has no poly-basic patch.

### 1.1.2 Nucleotide exchange and hydrolysis

Through their dynamic switch regions, GNBPs have the ability to bind to different interaction partners, depending on which nucleotide is bound. Most interaction partners bind with high affinity to the more rigid conformation of the switch regions of GTP-bound GNBPs and are activated upon binding. These so-called effectors can subsequently exert their down-stream signaling functions or directly mediate effects such as actin nucleation. Nevertheless, there are also many proteins known to interact with the GDP-bound state of GNBPs, which likewise play important roles. The fact that GNBPs usually show slow rates of intrinsic nucleotide exchange and GTP hydrolysis (Bischoff et al., 1990; Klebe et al., 1995), make GNBPs appear not well-suited for dynamic signaling processes. However, both the nucleotide exchange and the GTPase rates can be accelerated over several orders of magnitude by guanine nucleotide exchange factors (GEFs) and GTPase activating proteins (GAPs), which are usually specific for individual GNBPs (reviewed in Bos et al., 2007) (Fig. 1.2).

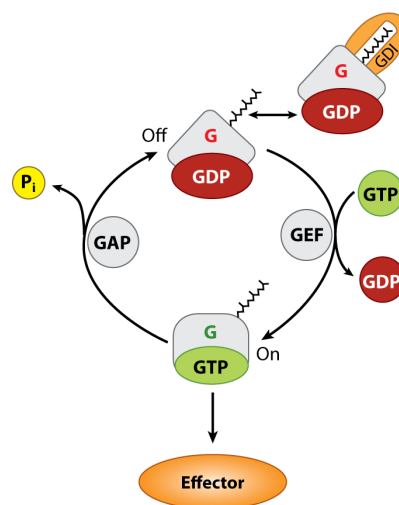


FIGURE 1.2: **The nucleotide exchange cycle.** Overview of the nucleotide exchange cycle of GNBPs (G: small GNBPs, GAP: GTPase activating protein, GEF: guanine nucleotide exchange factor, GDI: GDP dissociation inhibitor) (taken from Bos et al., 2007).

The affinity of GNBPs for nucleotides typically lies in the picomolar range and, as a consequence, the dissociation rate of the nucleotide is very slow (John et al., 1990; Klebe et al., 1995). The binding of a GEF to its cognate GNBPs promotes the dissociation of the bound nucleotide and thus allows for a new nucleotide molecule to bind. For the latter step to take place, the incoming nucleotide has to displace the GEF, which remains bound to the GNBPs after nucleotide release. Since the GEF-GNBPs complex is highly stable (as is the nucleotide-GNBPs complex), the new nucleotide has to modify the affinity of the GEF for the GNBPs, ultimately leading to the release of the GEF. Thus, the exchange reaction relies on the reciprocal negative influence on the affinity of either GEF or nucleotide for the GNBPs and occurs in successive reversible steps (Vetter and Wittinghofer, 2001).

The modulation of the nucleotide affinity by GEFs is achieved by a similar mechanism even though GEFs are structurally unrelated for different Ras superfamily branches (Boriack-Sjodin et al., 1998; Renault et al., 2001; Worthylake et al., 2000). The high affinity for the nucleotide is to a large extent a result of the interactions of the phosphates with the  $Mg^{2+}$ -ion and the P-loop. GEFs use a so-called ‘push-and-pull’ mechanism to interfere with these interactions: The GEF pushes out the  $Mg^{2+}$ -ion by relocating residues of the P-loop and the switch II of the GNBPs or, instead for the latter, by introducing own elements into the nucleotide binding pocket. In addition, the switch I is pulled out of its normal position, which further reduces nucleotide affinity (Vetter and Wittinghofer, 2001). In general, GEFs promote nucleotide exchange of GNBPs irrespective of the nucleotide state of the GNBPs (GTP or GDP) (Haney and Broach, 1994; Lenzen et al., 1998). However, because the concentration of GTP in the cell is about 10-fold higher than that of GDP, the accelerated nucleotide exchange by GEFs effectively lead to GTP-loading of the respective GNBPs. Nevertheless, depending on the physiological state of the cell the GTP:GDP ratio can change substantially and lead to a shift in favor of GDP- or GTP-loading, which, at least in yeast, can have a profound influence on intracellular signaling processes (Rudoni et al., 2001; Sagot et al., 2005). The specific GEF for Ran is RCC1 (regulator of chromatin condensation), which enhances the nucleotide exchange rate of Ran by about  $10^5$ -fold (Bischoff and Ponstingl, 1991a,b; Klebe et al., 1995).

As mentioned above, the GTPase activity of Ras superfamily proteins is generally very low although intrinsically the catalytic machinery is present. The mechanism by which GAPs stimulate the hydrolysis activity involves the stabilization of the

intrinsically mobile catalytic center of GNBPs and, in most cases, the introduction of catalytic residues. However, like GEFs, GAPs are structurally unrelated for distinct GNBPs and thus differences in the molecular details of GTPase activation are found. In principle, GTP-hydrolysis by GNBPs most likely occurs through a substrate assisted catalysis mechanism. This means that GTP itself serves as a base to abstract a proton from a water molecule. The resulting  $\text{OH}^-$  then performs a nucleophilic attack on the  $\gamma$ -phosphate leading to an inversion at the  $\gamma$ -phosphorus atom (Schweins et al., 1995). The reaction probably happens in a single step, a so-called in-line transfer (Feuerstein et al., 1989). For Ras, it was shown that the reaction is catalyzed by stabilization of the transition state by the critical residue glutamine-61, the mutation of which renders Ras unable to hydrolyze GTP (Priv et al., 1992). This glutamine is also critical for the action of RasGAP, which stabilizes it and makes it able to orient the water molecule for nucleophilic attack of the  $\gamma$ -phosphate. Moreover, it inserts an arginine into the phosphate-binding site, which neutralizes negative charges of the  $\beta$  and  $\gamma$ -phosphate and thereby stabilizes the transition state (Scheffzek et al., 1997). A similar mechanism is also observed for Rho and Cdc42 and, with some variations, also for Rab and Sar1 (Bi et al., 2002; Nassar et al., 1998; Pan et al., 2006; Rittinger et al., 1997). The mechanism of Ran GTPase activation through RanGAP is different in that RanGAP does not introduce any catalytic residue into the GTP binding pocket. Instead, RanGAP uses an Asp to correct the, in this case, improperly positioned catalytic glutamine (Gln69). The role of the arginine provided in *trans* by other GAPs is taken over by a tyrosine 39 of Ran that forms hydrogen bonds to the  $\gamma$ -phosphate as well as the Gln69 side chain (Seewald et al., 2002) (see Fig. 1.3).

The location of RCC1 and RanGAP in the cell provides clues for the distribution of RanGDP and RanGTP in the cell. RCC1 associates with chromatin throughout the cell cycle and is thus found in the nucleus during interphase (Ohtsubo et al., 1989). Binding of Ran to RCC1 allosterically promotes the interaction of RCC1 with chromatin, which in turn stimulates nucleotide exchange (Chen et al., 2007; Li et al., 2003a). Thus, RanGTP is generated close to chromatin. By contrast, RanGAP is located in the cytoplasm during interphase, which leads to the conversion of RanGTP into RanGDP in the cytoplasm (Hopper et al., 1990).

This differential distribution of RanGTP and GDP is key for nucleocytoplasmic transport since the stability of import and export complexes is directly regulated by RanGTP. Moreover, it is important for the role of Ran in mitotic spindle

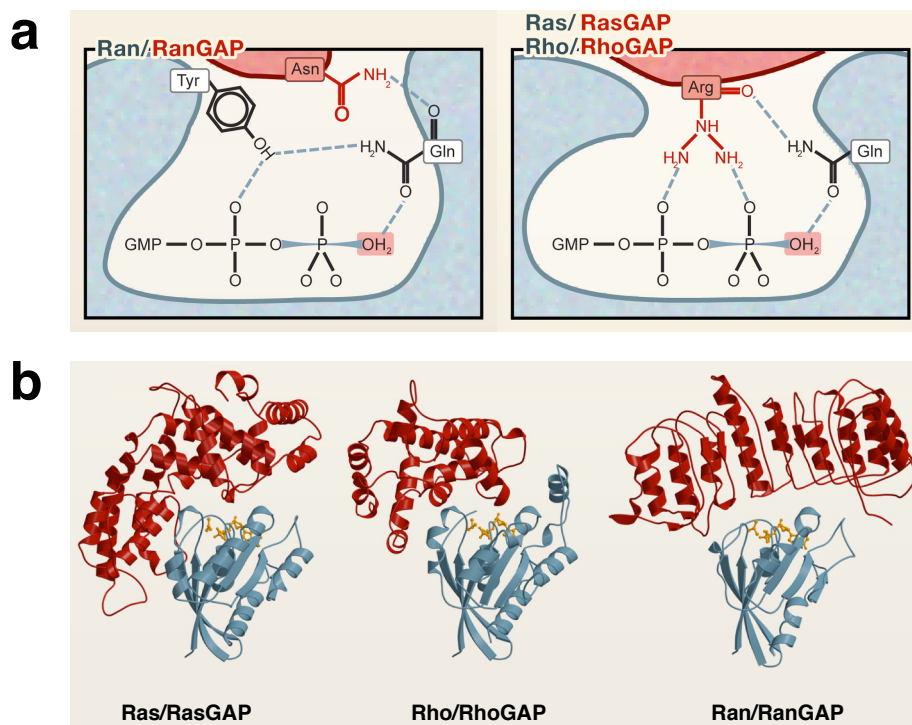


FIGURE 1.3: **Mechanisms of GTPase activation by GAPs.** (a) Depiction of two different mechanisms of GTPase activation for Ran and Ras/Rho. RanGAP induces GTP hydrolysis without introducing an arginine finger. (b) Ribbon representation of different Ras-like proteins (blue) with their cognate GAPs (red). The GNBPs are shown in the same orientation (taken from Bos et al., 2007).

assembly and nuclear envelope formation. These three processes will be briefly introduced in the subsequent sections.

### 1.1.3 Nucleocytoplasmic transport

The nuclear compartment is the most distinctive feature of eukaryotes. It provides a compartmentalization between the cytosol and the nucleoplasm, which is essential for a number of cellular processes and perhaps most importantly to spatially separate transcription and translation, preventing the translation of unspliced mRNAs (Cavalier-Smith, 1991; Martin and Koonin, 2006). The nuclear envelope consists of two parallel membranes and forms a continuous lumen with the endoplasmic reticulum (ER). The two membranes are pierced with nuclear pore complexes (NPCs) that allow the unaided passage of molecules with a diameter of  $\sim 5$  nm, which corresponds to a molecular weight of  $\sim 30$  kDa (Mohr et al., 2009). Larger macromolecules are not able to pass NPCs by passive diffusion or are at

least significantly delayed and their transport thus relies on nuclear transport receptors. Depending on the transport direction they facilitate, these are subdivided in importins and exportins. NPCs are large (125 MDa) protein complexes that, in vertebrates, comprise about 30 different protein species, each multiply represented to form a hollow cylinder with a central pore. The permeability barrier consists of disordered FG-repeat domains (FG: phenylalanine-glycine) that extend into the central pore and form a dense network of filaments. Transport receptors are able to traverse the barrier formed by NPCs by interacting with the FG-repeats while other proteins are rejected (reviewed in Gruenwald et al., 2011) (see Fig. 1.4).

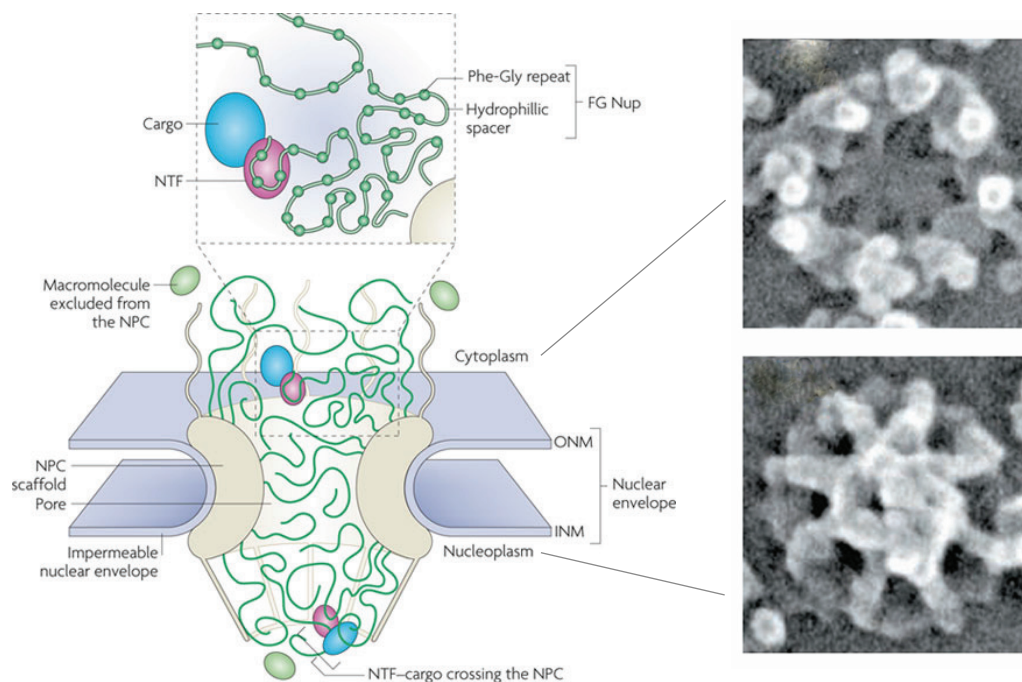


FIGURE 1.4: **The nuclear pore complex (NPC).** (Left) Schematic model of the NPC. NTF: nuclear transport factor, ONM/INM: outer/inner nuclear membrane, Nup: nuclear pore protein (taken from Strambio-De-Castillia et al., 2010). (Right) Electron microscopic pictures of the NPC with top picture showing the cytoplasmic side and bottom picture showing the nucleoplasmic side (taken from Allen et al., 2000).

Importins, such as the prototypical importin- $\beta$ , bind nuclear import signals (NLS) of import cargo (via the adapter protein importin- $\alpha$ ) in the cytoplasm where the level of RanGTP is low (Goerlich et al., 1995, 1994). Once the import receptor-cargo complex enters the nucleoplasm, it encounters the high concentration of RanGTP. Upon binding of RanGTP, the complex disassembles, leading to the release of the cargo (Moroianu et al., 1996). The importin remains bound

to RanGTP until it exits the nucleus where RanGAP can stimulate GTP hydrolysis of Ran. Similarly, exportins, such as CRM1 (chromosomal maintenance 1), that reside predominantly in the nucleus bind to RanGTP. However, in contrast to importins, the interaction of exportins with RanGTP allows the simultaneous binding to cargo molecules that carry nuclear export signals (NES) (Fukuda et al., 1997; Ossareh-Nazari et al., 1997; Stade et al., 1997). Upon binding to its export receptor, the cargo molecule can translocate into the cytoplasm where the export receptor·cargo complex is disassembled and RanGTP converts into RanGDP through the action of RanGAP. Thus, the differential distribution of RanGDP and RanGTP is instrumental for the facilitated transport of macromolecules through the nuclear pore. The fact that each transport event ultimately involves the hydrolysis of a GTP-molecule also satisfies the energetic prerequisites posed by the second law of thermodynamics (Nachury and Weis, 1999). Ran itself is concentrated in the nucleus during interphase. However, for stoichiometric reasons, the import of Ran cannot be mediated by *bona fide* importins (Ribbeck et al., 1998). Instead, Ran is imported specifically by NTF2 (nuclear transport factor 2), which binds Ran only in its GDP-form and drastically accelerates its transport through the NPCs (Ribbeck et al., 1998; Smith et al., 1998). The complex of RanGDP and NTF2 is then disassembled in the nucleus by a yet unknown process (Yamada et al., 2004).

Importins and exportins require an additional factor for the dissociation from Ran, which in mammals is either RanBP1 or RanBP2 (Ran binding protein 1 and 2, respectively). This is due to the fact that Ran is inaccessible to RanGAP when bound to importins/exportins and thus GTP hydrolysis cannot be stimulated. Through the binding of RanBP1 or -2 to exportin/importin-RanGTP complexes RanGAP can efficiently induce GTP hydrolysis and the complex can be disassembled (Lounsbury and Macara, 1997; Maurer et al., 2001; Yaseen and Blobel, 1999). RanBP1 is a ~23 kDa protein with a single Ran binding domain (RanBD) that is essential for its high affinity for RanGTP (Bischoff et al., 1995; Vetter et al., 1999). RanBP2 is a much larger multidomain protein (358 kDa) anchored to NPCs, which not only possesses four RanBDs but also catalyzes the transfer of SUMO1 (small ubiquitin like modifier) and interacts with SUMO-modified proteins. Interestingly, a major target of the SUMOylation activity of RanBP2 is RanGAP, which remains bound to RanBP2 after SUMO-transfer (Mahajan et al., 1997; Matunis et al., 1996; Pichler et al., 2002; Zhu et al., 2006). Thus, the RanBP2·RanGAP

complex combines transport receptor disassembly and GAP activity, both processes occurring immediately at the cytoplasmic side of NPCs (for an overview of nucleocytoplasmic transport see Fig. 1.5).

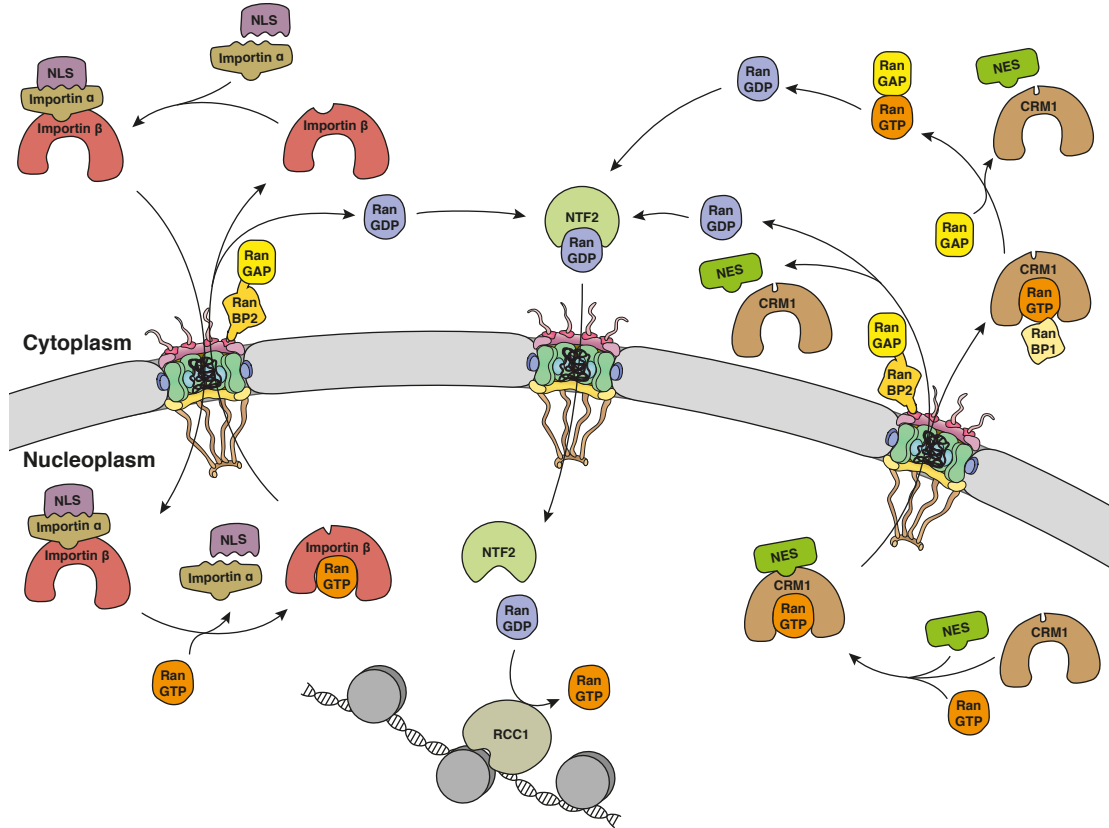


**FIGURE 1.5: Ran-dependent nuclear import and export.** Ran gradient: RanGDP is imported by its cognate transport factor NTF2. RCC1 is chromatin associated and catalyzes the conversion of RanGDP to RanGTP, leading to high RanGTP concentrations in the nucleus. Import: Importin- $\alpha$  and - $\beta$  form a complex in the cytoplasm, which then recognizes a substrate carrying a nuclear localization signal (NLS). The import complex is disassembled after passage through the nuclear pore upon binding of RanGTP. The RanGTP-importin- $\beta$  complex is disassembled by the action of RanBP2/SUMO-RanGAP at the cytoplasmic periphery of the nuclear pore or, alternatively, by soluble RanGAP and RanBP1 (not shown), both leading to the conversion of RanGTP to RanGDP. Export: Export substrates, carrying a nuclear export signal (NES), and RanGTP cooperatively bind to CRM1 to form an export complex. As for importin- $\beta$ , this complex is then disassembled by RanBP2/SUMO-RanGAP or by soluble RanGAP and RanBP1. For clarity reasons, the re-import of CRM1 is not shown (NPC model adapted from Katta et al., 2014).

### 1.1.4 Mitotic spindle assembly

In addition to its role in nucleocytoplasmic transport, Ran plays a central role in the assembly of the bipolar mitotic spindle during cell division. The mitotic spindle is a highly organized microtubule structure responsible for the equal distribution of chromatids to each daughter cell and starts to form after nuclear envelope breakdown. Interestingly, many factors involved in nucleocytoplasmic transport are also important during mitotic spindle assembly. RCC1 remains bound to chromatin during mitosis and, thus, catalyzes the localized nucleotide exchange of GDP to GTP on Ran (Carazo-Salas et al., 1999). The activity of soluble RCC1 is controlled by RanBP1 during mitosis through the formation of an inhibitory complex comprising RanBP1, Ran and RCC1 (Zhang et al., 2014a). The localized source of RanGTP is crucial for the spatially controlled release of inhibitory complexes between importin- $\alpha$ / $\beta$  and NLS-containing spindle assembly factors (SAFs) in the vicinity of the chromatin (Kalab et al., 1999; Nachury et al., 2001; Zhang et al., 1999). One important SAF is TPX2 (Targeting protein for Xklp2), which, after it is released from importin- $\alpha$  / $\beta$  inhibition, interacts with Aurora A kinase and keeps it in an active state (Gruss et al., 2001). Aurora A kinase then phosphorylates microtubule nucleation and stabilization factors around the chromatin (Bayliss et al., 2003; Eyers et al., 2003; Scrofani et al., 2015; Tsai et al., 2003). Thus, the RanGTP gradient is effectively translated into a phosphorylation gradient. The microtubule nucleation-promoting environment in proximity to the chromosomes is further refined by the CPC (chromosomal passenger complex): It is located to the centromeric regions of each chromosome where its kinase subunit Aurora B promotes spindle assembly through phosphorylation of microtubule destabilizing factors (Sampath et al., 2004). Recent studies suggest that the newly formed microtubules then serve as a starting point for microtubule amplification by Augmin, a process that is also stimulated by RanGTP (Petry et al., 2013). Eventually, microtubules are captured by kinetochore proteins and polymerization pushes their (-)-ends towards the spindle poles. The protection of these (-)-ends is mediated by MCRS1 (microspherule protein 1), which, again, is positively regulated by RanGTP (Meunier and Vernos, 2011).

Interestingly, other components of nucleocytoplasmic transport are involved in the formation of the kinetochores. The nucleoporin complex Nup-107-160 (Orjalo et al., 2006) and a complex of RanGAP, RanBP2 and CRM1 are both found at kinetochores and are important for attachment, polymerization and stability of

kinetochore fibers to kinetochores (Arnaoutov et al., 2005; Arnaoutov and Dasso, 2005). Moreover, CRM1 appears to play a role in the proper centromeric localization of the CPC (Knauer et al., 2006) and to antagonize the negative regulation of the kinetochore localization of RanGAP by importin- $\beta$  (Roscioli et al., 2012) (Fig. 1.6).

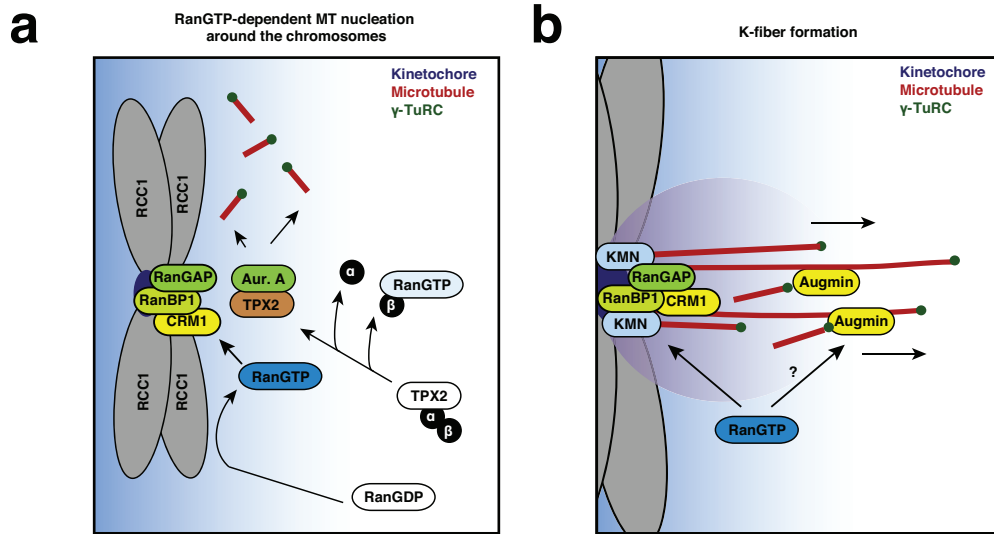


FIGURE 1.6: **Roles of Ran during mitotic spindle assembly.** (a) RanGTP mediates the release of spindle assembly factors like TPX2 from inhibitory complexes with importin- $\alpha/\beta$ . TPX2 can then bind and activate Aurora A kinase, which in turn promotes the microtubule nucleation activity of the  $\gamma$ -Tubulin ring complex ( $\gamma$ -TuRC). RanGTP is also required for the localization of CRM1·RanGAP·RanGTP to kinetochores. (b) Together with other protein complexes, CRM1·RanGAP·RanGTP regulate the stability and formation of kinetochore fibers. These are amplified by the action of Augmin, which is positively regulated by RanGTP (adapted from Scrofani et al., 2015).

### 1.1.5 Nuclear envelope formation

In contrast to fungi and many unicellular ('lower') eukaryotes, in which the nuclear envelope (NE) remains intact during mitosis, in plants and metazoans it is usually completely disassembled during mitosis, a situation referred to as 'open mitosis' (reviewed in Boettcher and Barral, 2013). Reassembly of the NE is temporally controlled by the dephosphorylation of integral inner nuclear membrane proteins (for instance Lamin B receptor), which can then reassociate with chromatin (Foisner and Gerace, 1993; Pfaller et al., 1991; Tseng and Chen, 2011). In addition, the RanGTP gradient is again used by cells to guide the coating of post-mitotic

chromatin by ER sheets (Anderson and Hetzer, 2007; Lu et al., 2011; Zhang and Clarke, 2000). Generation of RanGTP is also required for the reassembly of NPCs after mitosis (Askjaer et al., 2002; Rotem et al., 2009; Zhang et al., 2002). The fact that NE and NPC structures are formed around RanGTP-coated beads convincingly demonstrated the involvement of Ran in both NE and NPC formation (Zhang and Clarke, 2000). These functions of Ran appear to be mediated by the release of NPC components and membrane vesicles on the surface of chromatin, which were previously bound to Importin- $\beta$  (Anderson and Hetzer, 2007; Askjaer et al., 2002; Rotem et al., 2009; Zhang et al., 2002). However, the precise roles of Ran during NE and NPC formation are not fully understood and it is not clear how they are integrated with other pathways involved.

## 1.2 Lysine-acetylation

Acetylation is a very common protein modification in eukaryotes. However, two forms of acetylation exist, one that occurs at the N-( $\alpha$ )- and the other at the N-( $\epsilon$ )-amino group. Approximately 85% of eukaryotic proteins are co-translationally acetylated at their N-( $\alpha$ )-termini (Van Damme et al., 2011), which is catalyzed by N-terminal acetyltransferases (NATs). Despite the fact that many different roles for N-terminal acetylation have been found, it remains largely enigmatic why it is so widespread (Hollebeke et al., 2012). It has been shown to influence the fate of a protein in different and, in some cases, contradictory ways. These include protein stability (Hershko et al., 1984; Hwang et al., 2010), localization (Forte et al., 2011) and protein synthesis (Kamita et al., 2011). The role of acetylation at the  $\epsilon$ -amino group of lysines has been studied only for relatively few cases while for a majority of proteins its role is poorly understood, both functionally and on the level of regulation. Importantly and in contrast to N-( $\alpha$ )-terminal acetylation, N-( $\epsilon$ )-acetylation is highly reversible and is thus potentially involved in many dynamic signaling processes in the cell.

In theory but also from the known examples, it is clear that lysine-acetylation can impact the fate of a protein in several different ways, many of them being a direct consequence of the different chemical properties of acetyl-lysine compared to lysine (for details on immediate molecular effects of lysine-acetylation see Fig. 1.7). For instance, lysine-acetylation of a particular protein can (positively or negatively) influence its affinity to another macromolecule, co-factor or substrate.

More indirect effects of lysine-acetylation include the crosstalk with other post-translational modifications such as ubiquitination or the alteration of subcellular localization of a protein by changing the properties of a specific localization signal (Li et al., 2012). As will be discussed in the following second part of the introduction, post-translational lysine-acetylation has captured the attention of many researchers in recent years. This is mainly due to the identification of many novel acetylation sites throughout the proteome, which was possible through the huge technological advances in high-throughput mass spectrometry (MS). Given that the functional consequences of most of these newly discovered acetylation events is not known, many questions in the acetylation research field remain unanswered and are difficult to address in a high-throughput manner. The next sections will cover the most important proteins subjected to this modification and will give an overview about its regulation.

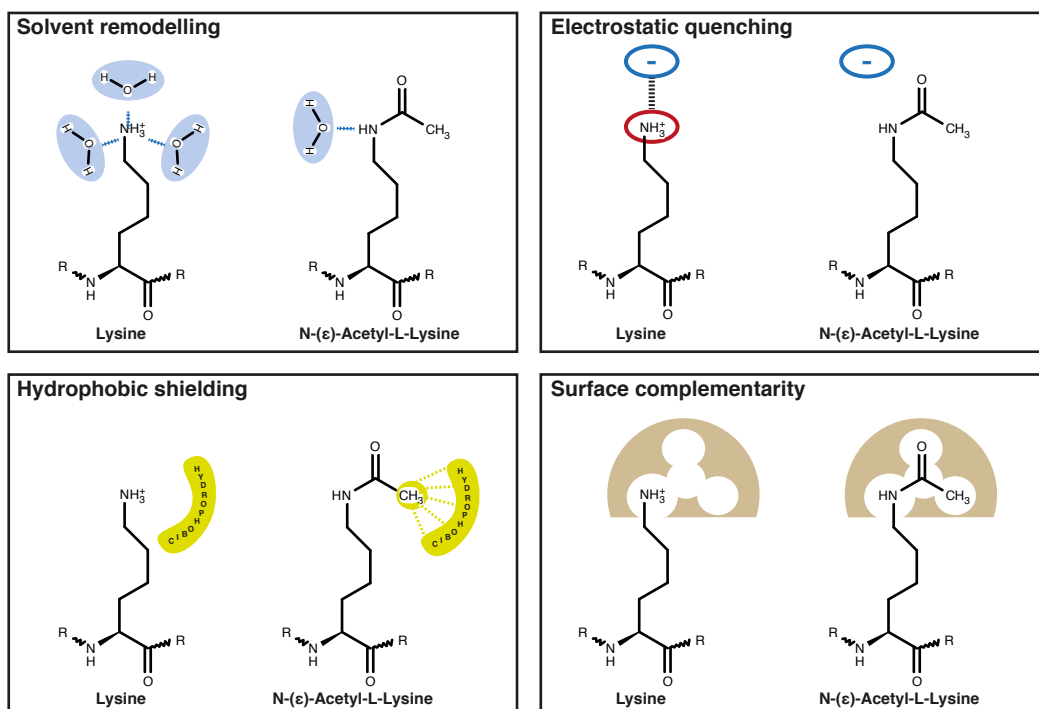


FIGURE 1.7: **Molecular effects of acetylation of lysine.** Illustration of immediate molecular effects of lysine-acetylation (taken from PhD thesis of S. de Boor, 2015).

### 1.2.1 The writers: Lysine-acetyltransferases (KATs)

Lysine-acetyltransferases (KATs) catalyze the transfer of the acetyl-group from acetyl-Coenzyme A (acetyl-CoA) to an N-( $\epsilon$ )-amino group of a lysine side chain. KAT activity was first demonstrated in an enzyme from *Tetrahymena thermophila* that efficiently acetylates lysines in histones and was thus termed histone acetyltransferase type A (HAT A) (Brownell and Allis, 1995; Brownell et al., 1996). HAT A turned out to be a close ortholog of Gcn5 (general control nonrepressed 5), which had previously been identified as a transcriptional regulator and thus the discovery of Gcn5-KAT activity immediately provided a link between histone acetylation and transcriptional regulation. To date, 21 proteins with KAT activity are known to be present in humans (EC 2.3.1.48), the substrates of which are not limited to histones (hence the term KAT instead of HAT) (Glozak et al., 2005; Lee et al., 2007). Based on structure and sequence characteristics, the different KATs have been assigned to one of five subfamilies: HAT1, Gcn5/pCAF, MYST (MOZ, Ybf2, Sas2, and Tip60), p300/CBP, or Rtt109. All KATs discovered until now, share a conserved fold comprising a three-stranded  $\beta$ -sheet and an  $\alpha$ -helix, which is crucial for binding of acetyl-Coenzyme A and substrate coordination. However, despite this similarity, the sequence homology between the KAT subfamilies is remarkably low and different catalytic mechanisms can be observed between KAT subfamilies (Friedmann and Marmorstein, 2013). Importantly, the N- and C-terminal extensions around the core region and also other protein domains (such as bromodomains; see below) are required for their substrate specificity and activity (Polesskaya and Harel-Bellan, 2001). Moreover, KAT activity may be modulated by their intracellular localization, embedding into multi-protein-complexes or post-translational modifications, including auto-acetylation (Creaven et al., 1999; Lee et al., 2007; Poveda et al., 2004; Santos-Rosa et al., 2003). Despite significant advances in the identification of KAT targets it remains largely an open question how KAT specificity is achieved. It seems however that due to the low sequence conservation many more KAT genes remain to be discovered in the human genome (Yuan and Marmorstein, 2013). This view was recently substantiated in a study by Montgomery et al. (2014), in which several proteins with previously unrecognized KAT activity were identified.

### 1.2.2 The erasers: Lysine-deacetylases (KDACs)

Enzymes that catalyze the removal of an acetyl-group from a lysine residue have initially been discovered for histones and hence been termed histone deacetylases (HDACs). To account for their emerging role in deacetylation of non-histone proteins, they are now more generally referred to as lysine-deacetylases (KDACs). To date, two groups of KDACs have been identified, which use remarkably different reaction mechanisms and co-factors. One group comprises the so-called classical KDACs, which catalyze the removal of the acetyl-moiety via a  $\text{Zn}^{+2}$ -dependent hydrolysis reaction. Based on their sequence similarity to yeast homologs and their domain organization, these enzymes have initially been subdivided into different classes (class I: KDAC1, -2, -3 and -8; class IIa: KDAC4, -5, -7 and -9; class IIb: KDAC6 and -10; class IV: KDAC11) (Dokmanovic et al., 2007; Marks et al., 2001). The class I KDACs KDAC1 and KDAC2 are almost identical and can partially compensate for each other (Lagger et al., 2002). Mild phenotypes are observed for most lineage specific knockouts of either KDAC1 or KDAC2 but deletion of both has dramatic effects, leading to blockade of G1-to-S-phase transition (Yamaguchi et al., 2010). Nevertheless, full-body knockout of either one results in perinatal lethality in mice as does the full-body knockout of KDAC3 and -8 (Bhaskara et al., 2008; Haberland et al., 2009a; Montgomery et al., 2007). The effects class I KDAC ablation can in most cases be attributed to their role in regulating transcription. However, they are also involved in splicing, DNA repair, replication, mitosis and meiosis. They are part of large multi-protein complexes such as CoREST and are themselves able to homo- or heterodimerize (Moser et al., 2014, reviewed in). Class IIa KDACs are different from the other classical KDACs in that they possess an N-terminal domain that is an important site for post-translational phosphorylation and is required to establish interactions with transcription factors. Phosphorylation leads to nuclear export and thus prevents repression of their target genes (McKinsey et al., 2000). The expression of class IIa KDACs are often tissue-specific, which is reflected in their tissue-specific functions (Chang et al., 2006; Dequiedt et al., 2003; McKinsey et al., 2000). Relatively little is known about the function of class IIb member KDAC10 and class IV member KDAC11, although the latter has recently gained attraction for its role in suppression of an anti-tumor immune response (Sahakian et al., 2015). In contrast, the second class IIb member, KDAC6, is well described for its role in  $\alpha$ -tubulin deacetylation (see section 1.2.4). In general, KDAC6 appears to have the most

non-histone targets among the classical KDACs (Bertos et al., 2004; Verdel et al., 2000; Zhang et al., 2003). Interestingly, KDAC6 possesses a zinc-finger domain in its C-terminus through which it can bind to ubiquitin and thus establishes a link between ubiquitination and acetylation (Boyault et al., 2006; Hook et al., 2002).

Class III KDACs are unrelated to the classical KDACs and are referred to as Sirtuins based on their homology to the founding member, the yeast Silent information regulator 2 (Sir2). Sir2 is critical for the silencing of mating type loci in yeast, which is mediated by deacetylation of critical lysines of histones H3 and H4 (Imai et al., 2000). For deacetylation, Sirtuins require nicotinamide adenine dinucleotide ( $\text{NAD}^+$ ) as a co-factor, which is broken down to the reaction products nicotinamide (NAM) and 2'- or 3'-O-acetyl-ADP-ribose (OAADPr) (Tanny and Moazed, 2001) (Fig. 1.8a). Interestingly, NAM, is an inhibitor of Sirtuins and, thus, NAM turnover by PNC1 (pyrazinamidase/nicotinamidase 1) modulates Sirtuin activity in the cell (Avalos et al., 2005; Gallo et al., 2004). In addition, the second reaction product, OAADPr is an important signaling molecule and substrate for downstream enzymatic processes (Liou et al., 2005; Tong and Denu, 2010). Given their  $\text{NAD}^+$ -dependence, the activity of Sirtuins is intimately linked to the  $\text{NADH}/\text{NAD}^+$  ratio and thus the metabolic state of the cell. In fact, it is becoming increasingly clear that age-dependent decline of  $\text{NAD}^+$ -levels, which is caused by increased activity of PARPs (poly-ADP-ribose-proteins) in response to DNA damage (PARP1 also uses  $\text{NAD}^+$  as a substrate), leads to a concomitant decline of Sirtuin activity (Bai et al., 2011; Mohamed et al., 2014; Pillai et al., 2005).

Seven Sirtuins are present in human, of which SIRT3, -4 and -5 are predominantly found in mitochondria, SIRT6 and -7 are mostly nuclear and SIRT1 and -2 shuttle between the cytoplasm and the nucleus (Michishita et al., 2005). They all share a conserved domain structure consisting of a small domain that binds a  $\text{Zn}^{2+}$  ion and a second domain in a Rossmann-fold, which is characteristic for  $\text{NAD}^+$ -binding proteins. The two domains are connected by several loops, which form an extended cleft between both domains. Acetyl-lysine and  $\text{NAD}^+$  enter this cleft from opposing sides and meet in a tunnel where they contact the catalytic residues of the enzyme (Sanders et al., 2010) (Fig. 1.8b).

Sirtuins are in fact not restricted to acetyl-lysine as a substrate but can catalyze the removal of other lysine-acylations such as crotonylation (SIRT1, -2, -3; Brooks and Gu, 2011), malonylation and succinylation (SIRT5; Du et al., 2011; Peng et al.,

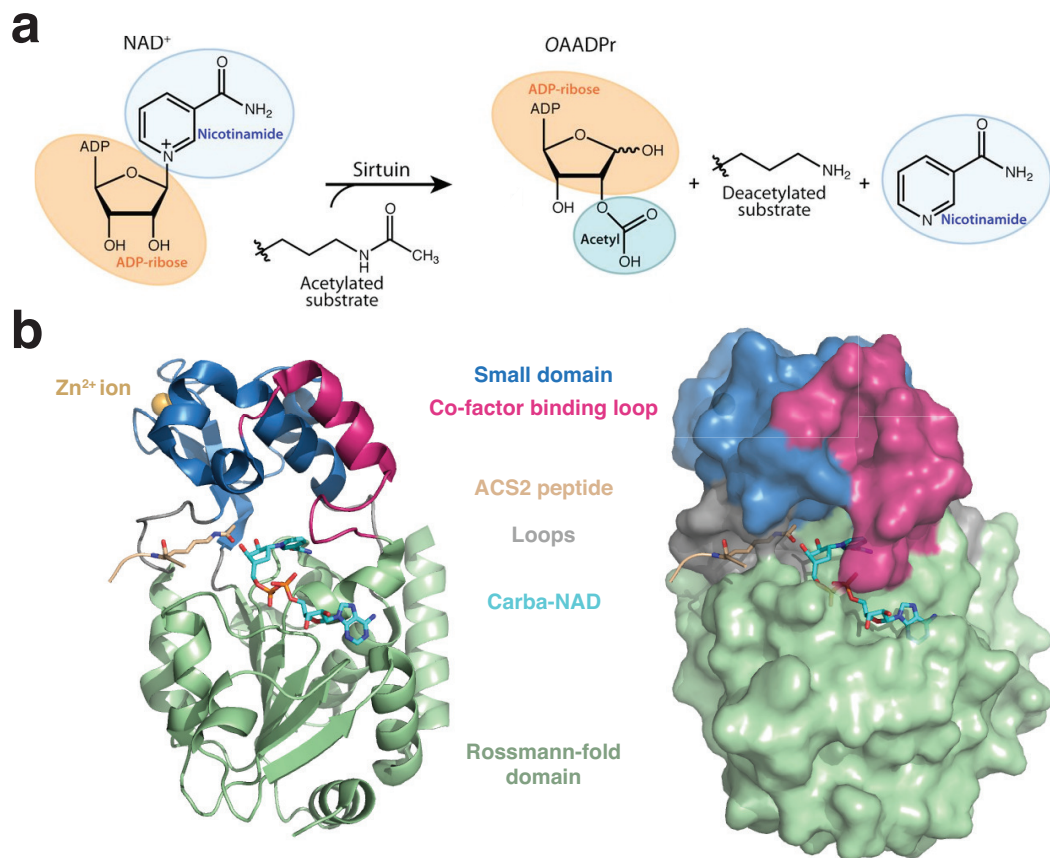


FIGURE 1.8: **Chemistry and structure of Sirtuin deacetylases.** (a) Educts and products of the deacetylation reaction catalyzed by Sirtuins (adapted from Feldman et al., 2012). (b) Structure of SIRT3 in complex with a substrate peptide (ACS2, acetyl-CoA synthetase 2) and a non-reactive NAD<sup>+</sup>-analog (carba-NAD<sup>+</sup>) (PDB: 4FVT). On the left a cartoon representation is shown with the loops connecting the small domain and the Rossmann-fold domain are colored in grey. On the right, the same is shown but as a surface representation of SIRT3.

2011), or long-chain fatty acid acylations (SIRT6, Feldman et al., 2013). Moreover, the deacetylase activity of SIRT6 can be stimulated by free fatty acid, which induce a conformation that promotes acetyl-lysine binding, again emphasizing the role of Sirtuins in metabolic processes (Feldman et al., 2013). Sirtuins are on the one hand involved directly in gene regulation via the deacetylation of histones and nuclear transcription factors and co-factors. On the other hand, most Sirtuins, especially those located in the mitochondria, deacetylate metabolic enzymes.

SIRT1 is the best-studied Sirtuin and well-known for its role in counteracting p53 activation, making SIRT1 a potential pro-oncogene (see section 1.2.4). However, this view is challenged by the fact that other pro-oncogenic and/or pro-inflammatory factors such NF- $\kappa$ B, c-Myc and  $\beta$ -catenin are negatively regulated by SIRT1 (Firestein et al., 2008; Yeung et al., 2004; Yuan et al., 2009). Moreover, SIRT1 is crucial for the lifespan extension effect observed under caloric restriction (Cohen et al., 2004). Such pleiotropic effects are also observed for SIRT2, which can most likely also be attributed to its diverse targets in the nucleus and cytosol (as for example  $\alpha$ -tubulin; see section 1.2.4). For instance, SIRT2 positively regulates myelination by Par-3 (partitioning-defective 3) deacetylation but inhibition of SIRT2 is also neuroprotective by ameliorating the toxic effects of  $\alpha$ -synuclein. Therefore, it is regarded as a potential therapy for Parkinson's disease (Beirowski et al., 2011; Outeiro et al., 2007). The mitochondrial Sirtuins, SIRT3, -4, -5 are particularly important for energy homeostasis. While their precise roles still remain to be identified, it is evident that lack of the mitochondrial Sirtuins lead to metabolic syndrome, obesity and defects in fatty acid oxidation and insulin signaling (Haigis et al., 2006; Hallows et al., 2011; Hirschey et al., 2011; Rardin et al., 2013). SIRT6 has become one of the most interesting Sirtuins for the field of aging research, given its clear progeroid phenotype upon knockout. Overexpression of SIRT6 in turn increases lifespan by 15%. These phenotypes are most likely a result of its function in cellular DNA damage response where on the one hand it mono-ADP-ribosylates the DNA-repair factor PARP1 and on the other hand deacetylates histone H3 to prevent further DNA damage. Moreover, SIRT6 is also able to negatively regulate glycolysis and inflammation. SIRT7 localizes to the nucleolus and controls the production of rRNA by RNA polymerase I (Tsai et al., 2012). Furthermore, it is important for mitochondrial function in that it positively regulates the transcription of nuclear-encoded mitochondrial genes. Loss of SIRT7 thus leads to several age- and metabolism-related phenotypes and a decrease in lifespan (Ryu et al., 2014).

An open question is what exactly determines the specificity of deacylation/deacetylation by Sirtuins. While some studies suggest that SIRT1-3 deacetylate residues that lie in unstructured regions, mostly irrespective of the amino acid sequence (Avalos et al., 2002; Blander et al., 2005; Khan and Lewis, 2005), others reported that substrate recognition is primarily dictated by the residues in direct vicinity of the acetyl-lysine moiety. However, no clear consensus motif was found but instead that substrate recognition is highly contextual. This means that one amino acid

at a certain position might be preferred in combination with another one (also in a certain position) but not so in different combinations (Garske and Denu, 2006; Gurard-Levin et al., 2010; Smith et al., 2011).

### 1.2.3 The readers: Bromodomain containing proteins

In addition to the direct effect on chromatin assembly, the different histone modifications serve as a docking site for a number of DNA/chromatin binding proteins. These proteins are referred to as ‘readers’ since they interpret the histone code and mediate the transcriptional control or play important roles for DNA repair and DNA replication. Monoubiquitinated histones are recognized by the chromatin remodeling complex SWI/SNF (SWItch/Sucrose Non-Fermentable) (Shema-Yaacoby et al., 2013) while several factors such as INO80 and NuA4 can sense phosphorylation of histones (Downs et al., 2004; Morrison et al., 2004). Members of the so-called ‘Royal Family’ or Tudor domain family are readers of protein methylation. This family includes the domains Tudor, plant Agenet, Chromo, PWWP and MBT (Maurer-Stroh et al., 2003), each with a different degree of specificity for the type of methylation: three forms of lysine methylation (mono-, di- and tri-) and three forms of arginine methylation (mono- and symmetric or asymmetric di-) (Aletta et al., 1998; Bannister et al., 2001; Eissenberg, 2012; Kim et al., 2006a; Liu et al., 2010).

To date, the only readers of lysine-acetylation that have been identified are bromodomains (BRDs) (Dhalluin et al., 1999). Interestingly, BRD binding is not limited to histone proteins. The conserved fold of BRDs, comprising a bundle of four  $\alpha$ -helices linked by loop regions that determine the binding specificity for different sequence contexts, provides a deep hydrophobic pocket for the binding of acetyl-lysine (Filippakopoulos et al., 2012; Owen et al., 2000) (Fig. 1.9a). Single or multiple BRDs are present in a number of proteins of different functions such as transcriptional regulation (TRIM/TIF1, TAFs), chromatin remodeling (BAZ1B), methyltransferases (MLL, ASH1L) and helicases (SMARCA) (Muller et al., 2011) (Fig. 1.9b). Interestingly, bromodomains are also found in KATs such as CBP, pCAF and Gen5, immediately implying regulatory feedback between different acetylation events. For instance, CBP not only lysine-acetylates p53 at its C-terminus but the binding of CBP to the acetylated K382 residue of p53 is also required for the recruitment of transcriptional co-activators, which results in

p21-mediated cell cycle arrest (Ito et al., 2001; Mujtaba et al., 2004). Likewise, KATs can in many cases directly bind to histones via their BRDs and stimulate transcription by acetylation of nucleosomal histones and transcription factors in their surrounding or by serving as binding platforms for the basal transcription machinery (Leo and Chen, 2000; Malik and Roeder, 2000; Manning et al., 2001; Schiltz et al., 1999).

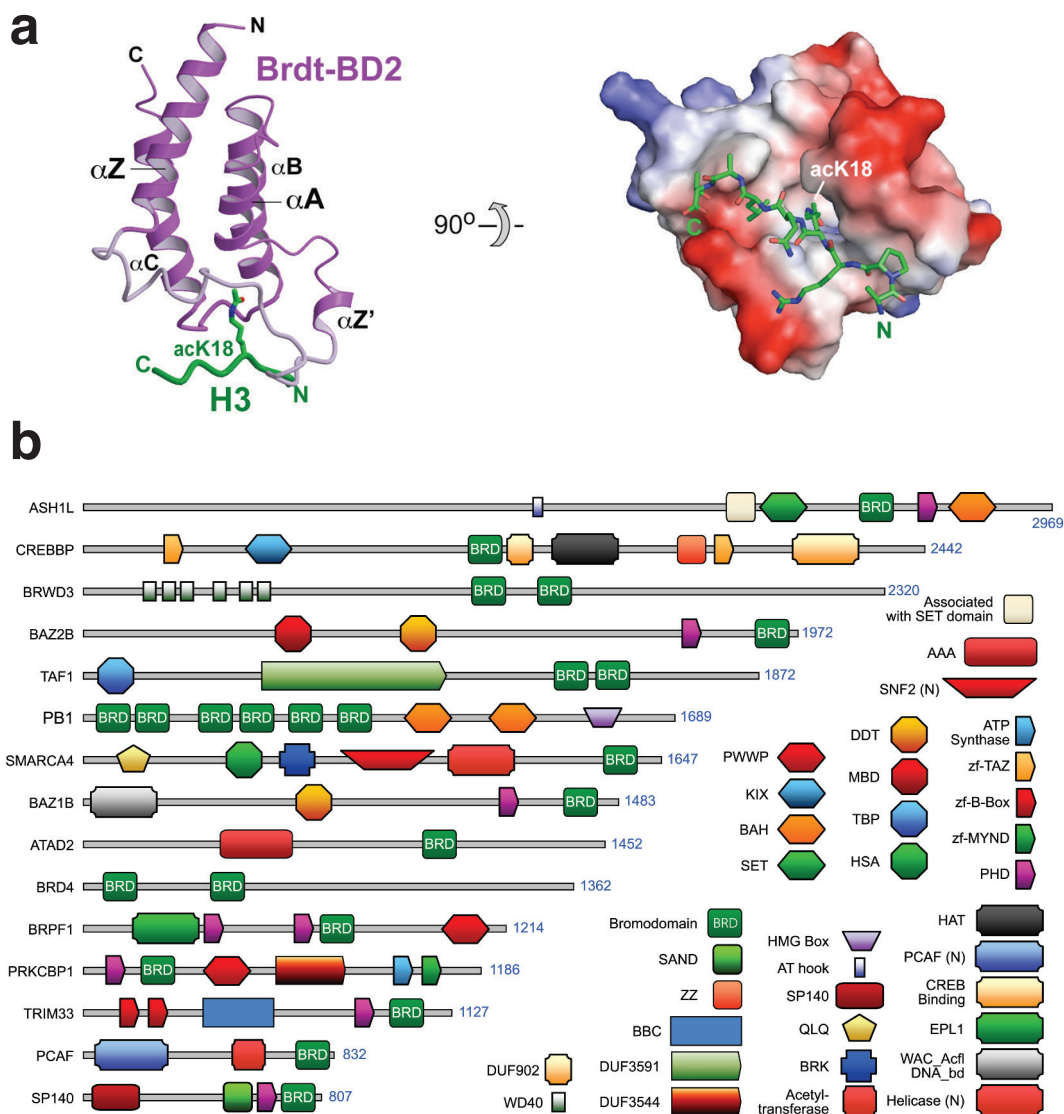


**FIGURE 1.9: Bromodomains are readers of acetylated lysine residues.** (a) Crystal structure (PDB: 2WP1) of the BD2 bromodomain of Brdt, a testis-specific member of the BET protein family, bound to an acetylated H3 peptide (taken from Morinire et al., 2009). (b) A diverse set of proteins contain bromodomains (taken from Filippakopoulos et al., 2012).

### 1.2.4 The canonical roles of lysine-acetylation

Now more than fifty years ago, it became apparent that histones are heavily modified by lysine-acetylation and that it plays an important role in the regulation of gene expression (Allfrey et al., 1964; Phillips, 1963). However, compared to phosphorylation, the regulatory role of acetylation and the responsible enzymes controlling this modification remained largely elusive until the mid-1990s. It is now known that histones are post-translationally modified at their highly conserved N-terminal tails by acetylation, methylation, phosphorylation and ubiquitination. These can, in a combinatorial fashion, both positively and negatively influence gene expression, a fact that has led to the proposition of the histone code (Strahl and Allis, 2000). Post-translational modification of histones affects internucleosomal and histone-DNA interactions and can therefore make DNA more or less accessible for transcription factors and other DNA-binding proteins (Arya and Schlick, 2006; Dorigo et al., 2003; Shogren-Knaak et al., 2006). Acetylation has been described as having mostly an activating effect on gene expression by disrupting higher-order nucleosomal structures and hence enhancing transcription (Shahbazian and Grunstein, 2007). This effect of acetylation in histone tails is only partially a result of charge neutralization. In fact, acetylation-induced charge reduction of only 10% has already a substantial inhibitory effect on chromatin packing (Tse et al., 1998).

Another protein that has been identified relatively early as being highly acetylated is the cytoskeletal protein  $\alpha$ -tubulin (L'Hernault and Rosenbaum, 1983). The site of this acetylation was later mapped to a single lysine residue (K40) (LeDizet and Piperno, 1987), which, interestingly, lies at the luminal surface of microtubules (Nogales et al., 1999). Its major KAT seems to be  $\alpha$ -TAT, formerly MEC-17, which exclusively acetylates  $\alpha$ -tubulin at K40 (Akella et al., 2010).  $\alpha$ -tubulin deacetylation is mediated by the KDAC6 and SIRT2 (Hubbert et al., 2002; North et al., 2003). Both SIRT2 and KDAC6 are able to deacetylate  $\alpha$ -tubulin in the polymerized and the soluble dimer state (North et al., 2003). As for  $\alpha$ -TAT, it is not clear how these enzymes act on the luminal site of microtubules. Initially thought to be important for microtubule stabilization, it turned out that  $\alpha$ -tubulin acetylation can be an indicator of stable microtubules but is probably not causative (Schulze et al., 1987; Webster and Borisy, 1989). In fact, albeit being studied extensively, the role of  $\alpha$ -tubulin acetylation remains poorly understood. It has been suggested that acetylated microtubules can more efficiently recruit the molecular

motors dynein and kinesin-1 and thus promote axonal transport (Dompierre et al., 2007; Reed et al., 2006). Moreover, the recruitment of the chaperone Hsp90 to microtubules is positively affected by acetylation as well as the sliding dynamics of ER cisternae along microtubules (Friedman et al., 2010; Giustiniani et al., 2009). Although mice lacking  $\alpha$ -TAT show loss of  $\alpha$ -tubulin acetylation across multiple tissues, they do not show any overt phenotype, again leaving the question about the precise role of this acetylation unanswered (Kalebic et al., 2013; Kim et al., 2013).

One of the best studied proteins that is subject of extensive post-translational lysine-acetylation is the tumor suppressor p53 protein (Gu and Roeder, 1997). Since the discovery that p53 is acetylated in its regulatory C-terminus, many additional acetylation sites have been described, also in other domains (Fig. 1.10). p53 acetylation prevents its degradation via Mdm2 (mouse double minute 2 homolog) and promotes its association with transcriptional co-activators and target gene promoters, and is essential for the p53-mediated response to DNA damage and the presence of activated oncogenes (Ito et al., 2001; Pearson et al., 2000; Tang et al., 2008). Interestingly, the different acetylation sites of p53 can compensate for each other extensively. In fact, the residues K120, 164, 370, 372, 373, 381, 382 and 386 had to be mutated to arginine (termed 8KR) to render p53 incapable of mediating its anti-tumorigenic effects. This mutant is however still able to activate transcription of its negative regulator, the E3 ubiquitin ligase Mdm2 (Tang et al., 2008). What adds to this complexity is that six different KATs seem to be involved in p53 lysine-acetylation, which can be attributed to the two groups p300/CBP/pCAF and Tip60/MOF/MOZ (Gu and Roeder, 1997; Liu et al., 1999; Rokudai et al., 2013; Sykes et al., 2006; Tang et al., 2006). These are in turn regulated by a diverse set of proteins such as ubiquitin ligases, kinases and viral factors (Jin et al., 2002; Patel et al., 1999; Shiseki et al., 2003).

SIRT1 and KDAC1 are the major deacetylases of p53 and counteract its anti-tumorigenic potential (Luo et al., 2001, 2000; Vaziri et al., 2001). Some evidence also points to deacetylation of p53 mediated by SIRT2 and KDAC6 (Ding et al., 2013; Hoffmann et al., 2014; Jin et al., 2008; Peck et al., 2010). Given that p53 is acetylated at 13 different lysines, it seems unlikely that any one of these deacetylases has the same specificity for all sites. In fact, KDAC1 deacetylates p53 at K320, K373 and K382 (Ito et al., 2002), whereas K382 appears to be the major substrate for SIRT1 (Vaziri et al., 2001). More indirect evidence indicates that

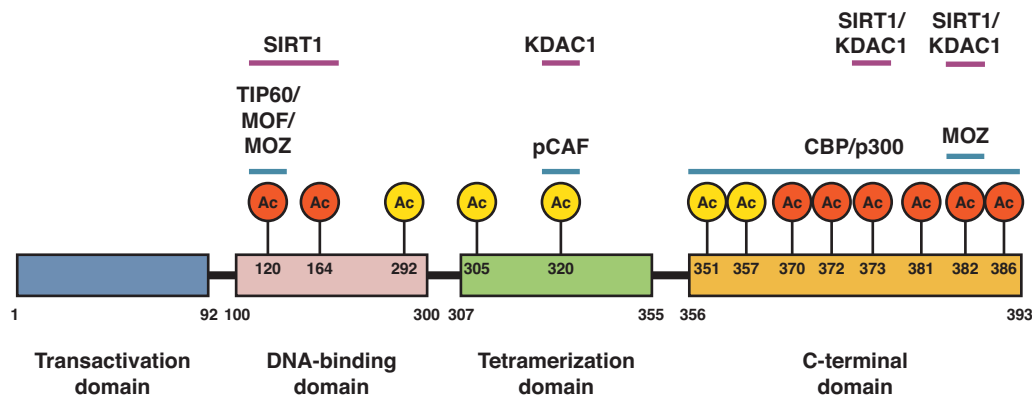


FIGURE 1.10: **Domain structure and acetylation sites of p53.** The known sites of lysine-acetylation of p53 are shown with their respective location in the protein. Acetylation sites that are essential for p53 activation are shown in red. p53 is acetylated by six different KATs (adapted from Brooks and Gu, 2011).

the residues K120 and K164 (Zhang et al., 2014b) as well as K373 might also be deacetylated by SIRT1 (Frazzi et al., 2013; Knights et al., 2006). How KDAC1 and SIRT1 control the function of p53 is however not well understood. This is especially true for SIRT1 since in many cases it negatively regulates p53 activation, suggesting a pro-oncogenic role, but mice lacking SIRT1 display increased tumorigenesis and defects in DNA damage response (Cheng et al., 2003; Wang et al., 2008).

In addition to p53 and  $\alpha$ -tubulin, there is an increasing number of non-histone proteins, often transcription factors, for which lysine-acetylation has been described to have functional consequences, ranging from alterations in protein-protein-interactions to increased or decreased stability and transcriptional activation (Farria et al., 2015; Glozak et al., 2005).

### 1.2.5 The acetylome: Novel roles for lysine-acetylation?

In the last ten years, advances in high-throughput MS have led to the discovery of thousands of acetylation sites in proteins of all cellular compartments and diverse cellular processes (Choudhary et al., 2009; Kim et al., 2006b; Zhao et al., 2010). Interestingly, the notion that acetylation might be of similar importance as phosphorylation was already proposed by Kouzarides (2000) years before these large datasets became available. The number of acetylated proteins and acetylation

sites is in stark contrast to the relatively few proteins for which acetylation had been shown before.

The patterns of acetylation sites are often tissue-specific (Lundby et al., 2012) and change, for instance, in response to metabolic (Yang et al., 2011) or genetic perturbations (Chen et al., 2012). Moreover, lysine-acetylation is found not only in eukaryotes but also in bacteria, where it is strongly influenced by the levels of acetyl-phosphate, a metabolic intermediate between acetate and acetyl-CoA. Interestingly, in bacteria, acetylation appears to happen globally and non-enzymatically at many sites when the cellular acetyl-phosphate concentration rises (Weinert et al., 2013). Similarly, the chemical environment in mitochondria (pH 7.9-8.0, acetyl-CoA concentration of 0.1-1.5 mM) would allow for non-enzymatic acetylation (and other acylations) to occur (Wagner and Payne, 2013). Strikingly, basic patches of proteins were found to be most prone to non-enzymatic acetylation (Baeza et al., 2015), which coincides with the substrate specificity of SIRT3 *in vivo* and *in vitro*, indicating that SIRT3 evolved specifically to deacetylate sites of non-enzymatic acetylation (Hebert et al., 2013; Smith et al., 2011). In fact, acetylation is found in up to 65% of mitochondrial proteins, many of which are key players of mitochondrial metabolism (Hebert et al., 2013; Hirschey et al., 2011), and typically acetylation inhibits the activity of these enzymes (Lin et al., 2012). Taken together, these observations have led to the picture that SIRT3 constitutively suppresses the low-stoichiometry non-enzymatic acetylation in mitochondria to reverse its mostly adverse effects on mitochondrial function (Wagner and Hirschey, 2014; Weinert et al., 2015).

Non-enzymatic acetylation is however less likely to occur in the cytoplasm and nucleus due to the lower pH and acetyl-CoA levels. It has indeed been shown in *S. cerevisiae* that the majority of acetylation sites have a very low stoichiometry in both the nucleocytoplasmic compartment and in mitochondria but that, consistent with their different chemical environments, this basal level is generally higher in the latter. Only the stoichiometry of acetylation sites of histones, transcription factors and proteins embedded in KAT- and KDAC-complexes were exceptionally high (Weinert et al., 2014). However, the fact that many sites are evolutionary conserved and often found in regulatory hot spots of proteins argues for a significant physiological role of acetylation beyond the above protein groups (Beltrao et al., 2012; Weinert et al., 2011). Moreover, there are situations where even a low stoichiometry acetylation can have a strong impact on cellular metabolism

or signaling. For example, acetylation might activate the signaling function of a protein or a new binding partner thereof (such as a kinase or KAT), which would in turn amplify the initially low signaling strength imposed by low stoichiometry acetylation, an effect that could be regarded as a gain-of-function. As another example, the activity of an enzyme might be dependent on its multimerization. Upon acetylation of a small fraction of these enzymes an efficient assembly of multimers could be prevented and thus likewise lead to a strong effect on enzymatic activity, a constellation that would resemble a dominant negative effect.

### 1.2.6 Lysine-acetylation of Ran

Information about the role of post-translational modifications in the regulation of Ran is so far very limited. This does however not apply to other proteins of the Ran interaction network. For instance, as described above, a large fraction of RanGAP is SUMO1-modified throughout the cell cycle (Mahajan et al., 1997). Phosphorylation of RanBP1 is important for the release of RCC1 from the inhibitory Ran•RCC1•RanBP1 complex at the end of mitosis (Zhang et al., 2014a). Acetylation of importin- $\alpha$  has been described as a mechanism to promote nuclear import of mRNA-destabilizing factors in response to metabolic stress (Bannister et al., 2000; Wang et al., 2004). For Ran, recent data shows that it is targeted for SUMOylation by RanBP2-SUMO-E3 complex (Sakin et al., 2015). SUMOylation of Ran had been previously identified for residue K152 (Tammsalu et al., 2014) but *in vitro* it occurred preferentially at K130. Since NTF2 is able to interact with SUMOylated Ran, it has been hypothesized that some cargo proteins might recognize SUMOylated Ran and then piggyback into the nucleus (Sakin et al., 2015). To date, twelve acetylation sites were identified in Ran, all by high-throughput MS (K23, K28, K37, K38, K60, K71, K99, K123, K134, K141/142, K152 and K159). Of these sites, K37, K60, K71, K99 and K159 were initially found by Choudary et al. (2009) in human cell lines treated with deacetylase inhibitors and have since been repeatedly confirmed in other screens, not only in human but also in mouse and rat samples. These five sites were thus selected for investigation in this study. Another site that was also found in human is K38 (albeit with lower confidence in the Choudary screen), which will be of importance in the second experimental part of this work.

### 1.2.7 The genetic code expansion concept (GCEC)

In the last decade, advances in the field of synthetic biology have resulted in the ability to incorporate non-natural amino acids into proteins. These systems have in common that they involve the introduction of an orthogonal translation system into the host. The genetic code is degenerate, with all possible 64 triplet codons assigned to specific amino acids and/or translation termination signals. However, the frequency with which individual codons are being used varies significantly from species to species. One striking example is the amber stop codon (UAG), which, in *E. coli*, is used with a frequency of below 10% (with respect to the other two stop codons) (VanBogelen et al., 1990). In many cases, genetic code expansion relies on the assignment of this low-frequency codon to a non-natural amino acid, which is then incorporated into the nascent polypeptide chain. Other concepts involve the use of quadruplet codons in combination with specifically modified ribosomes (Neumann et al., 2010). A prerequisite for both methods is the availability of a tRNA- and tRNA-synthetase-pair, which does not adversely interfere with the endogenous translational machinery and, *vice versa*, the specificity of which is not compromised by host cell factors (especially tRNA-synthetases and tRNAs). If these conditions are fulfilled a system is referred to as bioorthogonal. One such system is the pyrrolysyl-tRNA synthetase/tRNA<sub>CUA</sub> pair that mediates the incorporation of pyrrolysine in the methanogenic archeon *Methanosarcina barkeri* through amber stop codon suppression (Srinivasan et al., 2002). Neumann et al. (2008) used directed evolution to develop this naturally pyrrolysine-specific tRNA-synthetase into an N-( $\epsilon$ )-acetyl-lysyl-tRNA-synthetase, based on the fact that significant similarities exist between the chemical structure of pyrrolysine and N-( $\epsilon$ )-acetyl-lysine (see Fig. 1.11a). Thus, if the respective evolved gene *PylRS* and the corresponding tRNA-gene *pylT* are introduced into *E. coli* and, in addition, the cells are supplied with exogenous acetyl-lysine, recombinant proteins can be produced, which carry an acetyl-lysine at a position specified by an amber stop codon in the gene of interest (Fig. 1.11b).

The material that can be obtained with the GCEC, is natively folded and quantitatively and site-specifically acetylated. Thus, the this system represents a unique tool for the study of post-translational lysine-acetylation in a site-specific manner and has been successfully scaled up to yield protein of sufficient purity and quality to perform biophysical analysis including X-ray crystallography (Lammers et al., 2010). By contrast, previous methods relied either on chemical acetylation

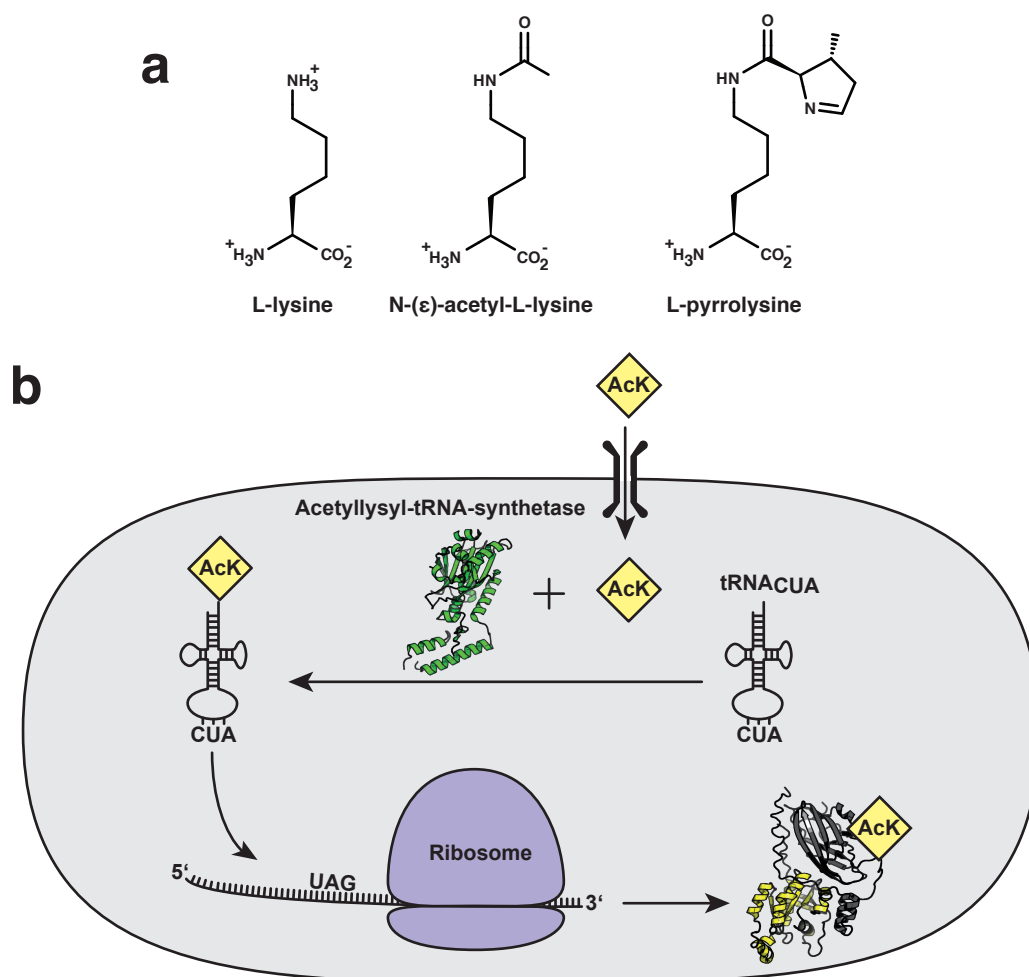


FIGURE 1.11: **The genetic code expansion concept (GCEC).** (a) Chemical structures of L-lysine, N-( $\epsilon$ )-acetyl-L-lysine and L-pyrrolysine. (b) Scheme of the genetic code expansion concept used to co-translationally incorporate N-( $\epsilon$ )-acetyl-L-lysine into recombinant proteins in *E. coli*.

using, for instance, acetic anhydride or enzymatic acetylation with purified KAT complexes. Both methods have several disadvantages, such as non-homogeneous and/or unspecific acetylation of the desired proteins. The often challenging purification of KAT complexes is an additional complicating factor. In the present work, the GCEC was of critical importance since it enabled the biophysical and biochemical study of Ran acetylation in a site-specific manner.

### 1.3 Aim of the thesis

The available proteomics data show that Ran is a target of post-translational lysine-acetylation. However, the role of Ran-acetylation was not known at the beginning of this study. Two questions were addressed in the present work:

1. What is the impact of Ran-acetylation on nuclear export and GAP-mediated GTP-hydrolysis?

The acetylation sites K37, K60, K71, K99 and K159 were the first that were discovered in human Ran (Choudhary et al., 2009). Based on the available structural data, it seemed likely that acetylation at some lysine residues could have an impact on GTP hydrolysis and export complex formation. To test this specifically, acetylated Ran and the binding partners involved in GTPase activation and export complex formation (RanGAP, RanBP1 and CRM1) were purified. The methods of choice for the subsequent experiments were, on the one hand, isothermal titration calorimetry (ITC) for the measurement of binding constants, thermodynamic parameters and stoichiometries of binding and, on the other hand, high pressure liquid chromatography (HPLC) for the determination of GDP/GTP ratios.

2. How is Ran-acetylation regulated by KATs and KDACs?

To gain insight into possible physiological role of Ran acetylation, I first sought to identify its KATs by their overexpression in cell culture and subsequent identification by immunoblotting and/or MS. With the site-specifically acetylated Ran variants at hand, it was also possible to analyze the specificity of their deacetylation. To this end, an initial *in vitro* screen was performed with purchased recombinant deacetylases. The results of this screen suggested an unexpected degree of specificity of Sirtuin deacetylases in a full-length protein context, which was then further characterized on the basis of other known Sirtuin substrates.

## 2 Material and Methods

### 2.1 Materials

#### 2.1.1 Chemicals, kits and enzymes

Unless otherwise stated, chemicals were purchased from AppliChem, Carl Roth and VWR in highest available purity. Guanine nucleotides were obtained from Analytik Jena. Suberoylanilide hydroxamic acid (SAHA) was purchased from Cayman Chemical and Sirtinol from Calbiochem/Merck. N-( $\epsilon$ )-acetyl-L-lysine was purchased from Chem-Impex International. Custom peptides were synthesized by the AG Neundorf, Institute for Biochemistry, University of Cologne. All enzymes were obtained from New England Biolabs. QIAGEN reagent kits were used for DNA isolation and purifications. Malate dehydrogenase (Ultra pure grade) was purchased from Amresco.

#### 2.1.2 Primers

Primers were purchased from Eurofins Genomics in 'Salt free' grade. Primers exceeding 35 nucleotides were ordered in 'HPSF' grade. The primers used for cloning and site-directed mutagenesis are listed in Table 2.1 and Table 2.2, respectively.

TABLE 2.1: Cloning primers

Name	Sequence (5' → 3')	Enzyme
RSFohGSTfo	ctttaataaggagatataccatgtcccctatactaggttattgg	CPEC
RSFohGSTre	gctagttattgctcagcggtcagtcacgatgcggccgctcg	CPEC
GSTohRSFfo	cgagcgccgcatcgtgactgaccgctgagcaataactagc	CPEC
GSTohRSFre	ccaataacctagtataggggacatggtatatactccttattaaag	CPEC
pGEX-MmCRM1-fo	gaaaacctttattttcagggcggaatgccagcaattatgacaatgttagc	CPEC
pGEX-MmCRM1-re	ccgggagctgcatgtgtcagaggtaatcacacatttcttctgg	CPEC
MmCRM1-pGEX-re	gctaacattgtcataattgctggcattccgccctgaaataaaggttttc	CPEC
MmCRM1-pGEX-fo	ccagaagaaatgtgtgattaacctctgacacatgcagctcccgg	CPEC
DuSirt1-225Ba-fo	gcggtaccgattaatatcctttcagaaccacc	<i>Bam</i> HI
DuSirt1-664Xho-r	ccgctcgagcggtagtcatcttcagagtctgaatatacc	<i>Xho</i> I
Sirt2-50DuBfo	gcggtaccgagcctgggcagccag	<i>Bam</i> HI
Sirt2-356DuXfo	ccgctcgagcggttacgactgggcatctatgc	<i>Xho</i> I
Sirt2-43-foB	cggtaccacttattctccagacgctcagc	<i>Bam</i> HI
Sirt2-370-revE	cggaattccgttacttgggggaagctgaagtgtctgg	<i>Eco</i> RI
Sir2Ba34fopG	cgcggtaccgagaagcagacatg	<i>Bam</i> HI
Sir2No356repG	tttcttttgcggccgctttttcttttacgactgggcatctatgc	<i>Not</i> I
Sirt3for118Bam	cgcggtaccgacaaggggaagctttccctgcag	<i>Bam</i> HI
Sirt3re399Xho	gaaactgggaagcttgatggaccagacaataaccgctcgagcgg	<i>Xho</i> I
pGEXp53-Ba-fo	cggtaccatggaggagccgagtc	<i>Bam</i> HI
pGEXp53-Eco-rev	cggaattccgtcagctgagtcaggcccttc	<i>Eco</i> RI
PEPCK1-DuBafo	cgcggtaccggaatgctcctcagctgcaaacg	<i>Bam</i> HI
PEPCK1-DuKpnre	gggtacccttacatctggttattctttgcttcaagc	<i>Kpn</i> I
RanBP11foB	cggtaccatggcgccccaaggacac	<i>Bam</i> HI
RanBP1201revE	cggaattccgttattgcttctcctcagc	<i>Eco</i> RI
RanGAPSp1foB	cgcggtaccgcatgtcgctttttc	<i>Bam</i> HI
RanGAPSp386reE	cggaattctcaaatatgagcttttg	<i>Eco</i> RI
Ranf.l.foB	cggtaccatggctgagcaggag	<i>Bam</i> HI
Ranf.l.revE	cggaattccgttacaggtcatcatcctc	<i>Eco</i> RI
RSFRanf.lfoB	cgcggtaccggaatggctgagcaggagagc	<i>Bam</i> HI
DuRanf.l.revX	ccgctcgagcggttacaggtcatcatcctc	<i>Xho</i> I
HsSpn1-foB	cggtaccatggaagagttgagtcaggcc	<i>Bam</i> HI
HsSpn1-revE	cggaattccgttaattctccatgagcagc	<i>Eco</i> RI
Tip60BamTriEXfo	cggtaccgagtgaggaggtgggggagataatcgag	<i>Bam</i> HI
Tip60XhoTriEXrev	ccgctcgagcggttaccactccccctcttctccagtc	<i>Xho</i> I
pcDNA-noKTag-fw	gtaccaggtaccagtggtgg	
pcDNA-noKTag-rev	atcgtcatcgtctacagatccc	

TABLE 2.2: Primers for site-directed mutagenesis

Name	Sequence (5' → 3')
p53-K120a	gcattctgggacagcctagtctgtgacttgacag
p53-K120a-re	cgtgcaagtcacagactaggctgtcccagaatgc
p53-K164a	gccatggccatctactagcagtcacagcacatg
p53-K164a-re	catgtgctgtgactgctagtagatggccatggc
p53-K381a	gtctacctcccgcattagaaactcatgttcaag
p53-K381a-re	cttgaacatgagtttctaatggcgggaggtagac
p53-K382a	ctacctcccgcataaaatagctcatgttcaagacag
p53-K382a-re	ctgtcttgaacatgagctatttatggcgggaggtag
p53-K381/382a	gtctacctcccgcattagtagctcatgttcaagac
p53-K381/382a-re	gtcttgaacatgagctactaatggcgggaggtagac
p53-K372a	cagccacctgaagtcttagaagggtcagcttacc
p53-K372a-re	ggtagactgaccttctaggacttcaggtggctg
p53-K373a	cacctgaagtcctaaatagggtcagcttacctcc
p53-K373a-re	ggaggtagactgacctatgttgacttcaggtg
p53-K372/373a	cagccacctgaagtccttagtaggtcagcttacc
p53-K372/373a-re	ggtagactgacctactaggacttcaggtggctg
QC-PEPCK1-K71a	catcctcaggcggctgtagaagtatgacaactgc
QC-PEPCK1-K71a-re	gcagttgtcacttctacagccgcctgaggatg
QC-PEPCK1-K71-72a	ctcaggcggctgtagtagtatgacaactgctgg
QC-PEPCK1-K71-72a-re	ccagcagttgtcactactacagccgcctgag
QC-PEPCK1-K72a	catcctcaggcggctgaagttagtatgacaactgc
QC-PEPCK1-K72a-re	gcagttgtcactacttcagccgcctgaggatg
QC-PEPCK1-K594a	ggtggaagacatcgagtagtatctggtggatcaag
QC-PEPCK1-K594a-re	cttgatccaccagatactactcgatgtctccacc
QCPEPCK1-EFE-fw	ggaagagggcacctcagtttgagtagtagtatgacaac
QCPEPCK1-EFE-rev	gttgtcactactactcaaactcgaggatgcctcttcc
QCPEPCK1-VAT-fw	cggtgtagtagtatgtagccacctggttgctctcactg
QCPEPCK1-VAT-rev	cagtgagagccaaccaggtggctacatactactacagccg
QCRan37amber	ggtgaatttgagtagaagtatgtagccaccttggg
QCRan38amberfo	ggtgaatttgagaagttagtatgtagccaccttggg
QCRanK60amber	caacagaggacctatttagttcaatgtatgggac
QCRanK71amber	cacagccggcaggagtagttcggtagtagtagag
QCRanK99amber	gagagtacttactagaatgtgcctaactgg
QCRanK159amber	gtaactacaactttgaaatagcccttctctggttgc
QCRan-K37R-K38amb-fw	ctggtgaatttgagagtagtagtagtagccac
QCRan-K37R-K38amb-fev	gtggctacatactacctctcaaattcaccag
QCRan-K37A-K38amb-fw	ctggtgaatttgaggcgtagtagtagtagccac
QCRan-K37A-K38amb-fev	gtggctacatactacgctctcaaattcaccag
QCRan-K37Q-K38amb-fw	ctggtgaatttgagcagtagtagtagtagccac
QCRan-K37Q-K38amb-fev	gtggctacatactactgctcaaattcaccag

### 2.1.3 Vectors and constructs

For the expression of Glutathione-S-transferase (GST)-tagged proteins, a modified pGEX-4T1 (GE healthcare) was used, in which a Tobacco Etch Virus (TEV)-protease cleavage site was inserted between the Thrombin cleavage site and the multiple cloning site (MCS). This vector was named pGEX-4T5. Hexahistidine

(His<sub>6</sub>)-tagged proteins were expressed from a modified pRSF-Duet-1 (Novagen) coding for a Gly2Pro substitution, which prevents  $\alpha$ -N-6-phosphogluconoylation at the N-terminus (Geoghegan et al., 1999).

To allow for the post-translational incorporation of N-( $\epsilon$ )-acetyl-L-lysine, the pRSF-Duet-1 was further modified by insertion of the synthetically evolved *M. barkeri pylS* (termed *AcKRS-3*) under control of an *glnS* promoter/terminator using an *SphI* restriction site and *pylT* under control of an *lpp* promoter/*rrnC* terminator using an *XbaI* restriction site (Neumann et al., 2008). This gave rise to pRSFDuet-1-pylT-AcKRS-3.

p53 was expressed from pRSFGST-pylT-AcKRS-3. It was generated by replacing both MCS of pRSFDuet-1-pylT-AcKRS-3 with the GST-ORF-MCS from pGEX-4T5 using circular polymerase extension cloning (CPEC) (see 2.2.4).

For expression of Ran in HEK293T (human embryonic kidney 293T) cells, a modified pcDNA3.1C vector was used. Specifically, a lysine codon in the N-terminal tag was deleted to prevent the occurrence of acetylation at this site. All lysine-acetyltransferases (HAT) were expressed from pCMV-C-Myc, except for TIP60, which was expressed from pTriEx-2.

Maps of the vectors for recombinant protein expression can be found in Appendix A.1. The constructs used in this work are listed in Table 2.3.

TABLE 2.3: Constructs for recombinant protein expression

Vector / Protein	Amino acids	Species	Accession (UniProt)
<u>pGEX-4T5:</u>			
CRM1	full-length	<i>M. musculus</i>	Q6P5F9
RanBP1	full-length	<i>M. musculus</i>	P34022
RanGAP	full-length	<i>S. pombe</i>	P41391
RanWT	full-length	<i>H. sapiens</i>	P62826
SIRT2	34-356	<i>H. sapiens</i>	Q8IXJ6
SIRT2	43-370	<i>H. sapiens</i>	Q8IXJ6
SIRT2	50-356	<i>H. sapiens</i>	Q8IXJ6
SIRT3	118-399	<i>H. sapiens</i>	Q9NTG7
Spn1	full-length	<i>H. sapiens</i>	O95149
<u>pRSFDuet-1:</u>			
His <sub>6</sub> -RanWT	full-length	<i>H. sapiens</i>	P62826
His <sub>6</sub> -SIRT2	50-356	<i>H. sapiens</i>	Q8IXJ6
SIRT1	225-664	<i>H. sapiens</i>	Q96EB6
<u>pRSFGST-pylT-AcKRS-3:</u>			
p53	full-length	<i>H. sapiens</i>	P04637
<u>pRSFDuet-1-pylT-AcKRS-3:</u>			
His <sub>6</sub> -Ran-AcK	full-length	<i>H. sapiens</i>	P62826
PEPCK1	full-length	<i>H. sapiens</i>	P35558

## 2.1.4 Crystallization screens

Table 2.4 lists the crystallization screens used in this work. Screens were aliquoted (50 µl) into 96-well sitting drop iQ plates (TPPlabtech), sealed with HDclear tape (Duck, Henkel) and stored at 4°C until use.

TABLE 2.4: Crystallization screens

Name	Manufacturer
JCSG	Molecular Dimensions
PACT premier	Molecular Dimensions
MORPHEUS	Molecular Dimensions
Clear Strategy Screen I HT-96	Molecular Dimensions
Clear Strategy Screen II HT-96	Molecular Dimensions
PGA-LM HT-96 Crystallization Screen	Molecular Dimensions
Index Screen	Hampton Research
PEG/Ion Screen	Hampton Research
PEG/Ion 2 Screen	Hampton Research
PEG/Ion 2 Screen	Hampton Research
Structure Screen 1	Hampton Research
Structure Screen 2	Hampton Research

### 2.1.5 Buffers

PBS(T):	140 mM 2.7 mM 10.1 mM 1.8 mM pH (0.1% (v/v))	NaCl KCl Na <sub>2</sub> HPO <sub>4</sub> KH <sub>2</sub> PO <sub>4</sub> 7.4-7.6 Tween-20
Standard buffer:	50 mM 100 mM 5 mM 2 mM	Tris/HCl, pH 7.4 NaCl MgCl <sub>2</sub> $\beta$ -ME
GST-Wash buffer:	50 mM 500 mM 5 mM 2 mM	Tris/HCl, pH 7.4 NaCl MgCl <sub>2</sub> $\beta$ -ME
Ni-Wash buffer:	50 mM 1 M 5 mM 10 mM 2 mM	Tris/HCl, pH 7.4 NaCl MgCl <sub>2</sub> Imidazole $\beta$ -ME
Ni-Elution-I buffer:	50 mM 100 M 5 mM 10 mM 2 mM	Tris/HCl, pH 7.4 NaCl MgCl <sub>2</sub> Imidazole $\beta$ -ME
Ni-Elution-II buffer:	50 mM 100 M 5 mM 500 mM 2 mM	Tris/HCl, pH 7.4 NaCl MgCl <sub>2</sub> Imidazole $\beta$ -ME
Laemmli buffer:	50 mM 50% (v/v) 500 mM 10% /w/v 0.5% (w/v)	Tris/HCl, pH 6.8 Glycerol DTE SDS Bromphenol blue
SDS-PAGE Running buffer:	25 mM 192 mM 2% (w/v)	Tris/HCl, pH 8.3 Glycine SDS
Transfer buffer:	25 mM 150 mM 10% (v/v)	Tris, base Glycine Methanol
Staining solution:	40% (v/v) 10% (v/v) 0.4% (w/v) 0.4% (w/v)	Methanol Acetic acid Coomassie brilliant blue R-250 Coomassie brilliant blue G-250

Destaining solution:	10% (v/v)	Ethanol
	10% (v/v)	Acetic acid
HPLC buffer:	100 mM	KP <sub>i</sub> , pH 6.4
	10 mM	Tetra- <i>n</i> -butylammonium bromide (TBAB)
	2% (v/v)	Acetonitrile
KDAC-assay buffer:	25 mM	Tris/HCl, pH 8.0
	137 mM	NaCl
	2.7 mM	KCl
	1 mM	MgCl <sub>2</sub>
	0.1 mg/ml	BSA
	0.5 mM	NAD <sup>+</sup>
PEPCK1-assay buffer:	50 mM	Tris/HCl, pH 7.4
	20 mM	NaHCO <sub>3</sub>
	0.5 mM	Phosphoenolpyruvate
	1 mM	MnCl <sub>2</sub>
	0.2 mM	GDP
	0.1 mM	NADH
	2 U/ml	Malate Dehydrogenase (Amresco, Ultra Pure)
Developer solution:	5 µg/ml	Trypsin (diss. in 10 mM acetic acid)
	100 mM	Nicotinamide
2×BBS:	50 mM	(N,N-bis(Hydroxyethyl)- 2-Aminoethansulfonat, pH 6.96
	1.5 mM	Na <sub>2</sub> HPO <sub>4</sub>
	270 mM	NaCl
Pull-down lysis buffer:	10 mM	Tris/HCl, pH 8.0
	100 mM	NaH <sub>2</sub> PO <sub>4</sub>
	100 mM	NaCl
	2 mM	β-Mercaptoethanol
	8 M	Urea
	10 mM	Imidazole
	0.05% (v/v)	Tween 20
Pull-down wash buffer:	10 mM	Tris/HCl, pH 8.0
	100 mM	NaH <sub>2</sub> PO <sub>4</sub>
	300 mM	NaCl
	2 mM	β-Mercaptoethanol
	8 M	Urea
	20 mM	Imidazole
	0.05% (v/v)	Tween 20
Pull-down elution buffer:	10 mM	Tris/HCl, pH 8.0
	100 mM	NaH <sub>2</sub> PO <sub>4</sub>
	300 mM	NaCl
	2 mM	β-Mercaptoethanol
	8 M	Urea
	250 mM	Imidazole
	0.05% (v/v)	Tween 20

## 2.1.6 Media, Antibiotics and inhibitors

Lysogeny broth (LB)-medium (11):	10 g	NaCl
	10 g	Tryptone
	5 g	Yeast extract

	<b>Stock</b>	<b>Working concentration</b>
Ampicillin	100 mg/ml	0.1 mg/ml
Kanamycin	25 mg/ml	0.025 mg/ml
Trichostatin A (TSA)	5 mM	1 $\mu$ M
SAHA	10 mM	2 $\mu$ M
Sirtinol	10 mM	10 $\mu$ M
Na-Butyrate	1 M	1 mM
Nicotinamide	2 M	10 mM

## 2.2 Molecular biology techniques

### 2.2.1 Purification of DNA

Isolation of plasmid DNA from *E. coli* was performed with the QIAprep Spin Miniprep Kit or QIAprep Spin Midiprep Kit. Digested plasmid DNA or PCR products were purified using the QIAquick PCR Purification Kit or, alternatively, the QIAquick Gel Extraction Kit if fragments were isolated after agarose gel electrophoresis.

### 2.2.2 Polymerase chain reaction (PCR)

The Phusion polymerase kit (NEB) was used for preparative PCR reactions according to the manufacturers protocol. PCR reactions were performed in a VWR Collection Thermal Cycler DOPPIO. Primer melting temperatures ( $T_m$ ) were calculated with the NEB  $T_m$  Calculator ([tmcalculator.neb.com](http://tmcalculator.neb.com)). The desired restriction enzyme sites were included at the 5'-termini of the primers with 5-10 additional bases for optimal digestion efficiency. Reactions were typically carried out in a 50  $\mu$ l volume according to the following pipetting scheme and PCR program:

10 $\mu$ l	5x HF Buffer			
1.5 $\mu$ l	DMSO	98°C	2 min	
1 $\mu$ l	dNTPs (10 mM each)	98°C	10 s	25-35 cycles
1 $\mu$ l	Forward primer (10 $\mu$ M)	55-72°C	10 s	
1 $\mu$ l	Reverse primer (10 $\mu$ M)	72°C	15 s/kb	
1 $\mu$ l	Template DNA (2-10 ng/ $\mu$ l)	72°C	2 min	
0.5 $\mu$ l	Phusion polymerase (2 units/ $\mu$ l)			
35 $\mu$ l	ddH <sub>2</sub> O			

For colony-PCR, the MasterMix (5 PRIME) was used according to the manufacturers instructions. Since this kit includes the *Taq*-polymerase, the extension time was adjusted to 1 min/kb.

### 2.2.3 Restriction enzyme-based cloning

All restriction enzymes were used according to the manufacturers instructions. For the insertion of DNA fragments into the desired vector, purified PCR products and vector DNA (3  $\mu$ g) were digested with 20 units (U) of each respective restriction enzyme for 2 h at 37°C and subsequently purified by PCR purification or agarose gel extraction (see 2.2.1). The DNA concentration of each fragment was then determined on a BioPhotometer Plus (Eppendorf) at 260 nm ( $A_{260}$ ). For ligation, 50 ng of digested vector DNA was mixed with the insert DNA at a 1:3 to 1:5 molar ratio and 1 U T4 DNA Ligase in the manufacturers reaction buffer in a final volume of 20  $\mu$ l. The ligation mixture was incubated at 23°C for 20 min and subsequently used for transformation of *E. coli* DH5  $\alpha$  (see 2.2.6).

### 2.2.4 Circular polymerase extension cloning (CPEC)

CPEC is a polymerase based cloning method, allowing for seamless assembly of multiple DNA fragments (Quan and Tian, 2009). Primers were designed with  $\sim$ 25 nt complementarity to the fragment to be amplified and a  $\sim$ 25 nt 5'-overhang matching the sequence of the adjacent fragment. Tms were adjusted to not differ more than  $\pm$ 3°C between all overhangs. After a PCR for each fragment, the resulting amplicons were purified by agarose gel extraction. 100 ng of amplified vector DNA and an equimolar amount of insert fragments were used in a 25  $\mu$ l reaction (as described in 2.2.2). The reaction was run with the respective annealing

temperature, elongation time and for 5-10 cycles. The whole reaction was used for transformation of *E. coli* DH5 $\alpha$  (see 2.2.6).

### 2.2.5 Site-directed mutagenesis

For the directed introduction of point mutations into DNA sequences, the Quik-change<sup>TM</sup> method (Stratagene, La Jolla, USA) was used. Forward and reverse primers were designed to contain the desired mutation flanked by 15 bp complementary sequences. The reaction was carried out as detailed in 2.2.2 but with 100 ng template and subsequently digested with *DpnI* for 2 h at 37°C. The entire reaction was used for transformation of *E. coli* DH5 $\alpha$  (see 2.2.6).

### 2.2.6 Transformation of *E. coli*

Chemically competent *E. coli* DH5 $\alpha$  and BL21(DE3) were generated by the CaCl<sub>2</sub>-method (Mandel and Higa, 1970). In brief, 400 ml LB medium were inoculated with a fresh 5 ml pre-culture and grown until an OD<sub>600</sub> of 0.3. The culture was then centrifuged at 500  $\times$  *g* for 10 min in eight pre-chilled 50 ml centrifuge tubes. Each pellet was resuspended in 25 ml sterile ice-cold 0.1 M CaCl<sub>2</sub>, incubated on ice for 20 min and again centrifuged as before. Each pellet was then resuspended in 2 ml ice-cold 0.1 M CaCl<sub>2</sub>/15% glycerol and incubated on ice for 1-4 hours. 200  $\mu$ l aliquots were snap-frozen in liquid N<sub>2</sub> and stored at -80°C. For transformation, cells were thawed on ice, incubated with plasmid DNA for 30 min, heat-shocked at 42°C for 1 min, chilled on ice for 2 min and subsequently recovered with 1 ml of LB for 1 h at 37°C. The cells were pelleted for 1 min at 8.000  $\times$  *g* and plated on LB agar containing the appropriate antibiotic.

## 2.3 Biochemical methods

### 2.3.1 Expression of recombinant proteins

For expression of recombinant proteins, 200 ml LB-medium with the appropriate antibiotic were inoculated with several colonies from a plate of *E. coli* BL1(DE3) transformed with the desired construct. The culture was grown at 37°C for 3-4 h

or over night and then used for inoculation of 10l of LB-medium at a ratio of 1:50. This culture was grown at 160 rpm and 37°C until an OD<sub>600</sub> of 0.8 and then induced with 250 µM Isopropyl-β-D-thiogalactopyranosid (IPTG). Expression of SIRT2 was induced at a higher OD<sub>600</sub> of 1.5. For the expression of acetylated proteins, the culture was supplemented with 10 mM of N-(ε)-acetyl-L-lysine and 20 mM nicotinamide at an OD<sub>600</sub> of 0.5.

After induction, the temperature was lowered to 18°C and the culture was grown for another 16-18 h. The culture was subsequently centrifuged at 4000 × *g* and 4°C for 10 min. The supernatant was discarded and the bacterial pellets were resuspended in 100 ml Standard buffer supplemented with 100 µM phenylmethanesulfonylfluoride (PMSF). The resuspended cells were either stored at −80°C or directly subjected to lysis.

### 2.3.2 Lysis of cells

Lysis of cells was performed by sonication with a Branson Sonifier 250 for 3 min at 60% duty cycle and micro-tip limit 8. The lysate was cleared by centrifugation at 4°C and 48,254 × *g* for 45 min.

### 2.3.3 Purification of GST-tagged proteins

Proteins tagged with GST from *Schistosoma japonicum* were purified by affinity-chromatography using PureCube Glutathione Agarose (Cube Biotech). The cleared lysate was applied to a GST-Wash-buffer equilibrated column packed with 40-60 ml affinity resin at a flow-rate of 1-1.5 ml/ml using an ÄKTApurifier (GE healthcare) or a peristaltic pump (Carl Roth). The unbound proteins were washed off with 5-10 column volumes (CV) GST-Wash buffer followed by a 2 CV wash with Standard buffer to reduce the NaCl-concentration. To cleave the GST-fusion protein, 0.5-1 mg TEV-protease was applied to the column and circulated overnight at a flow-rate of 1 ml/min. The protein was eluted with 50 ml Standard buffer and concentrated to 1-2 ml for a final size exclusion chromatography (SEC) using a centricon with an appropriate molecular weight cut-off (AmiconUltra, Millipore). Depending on the molecular weight and multimerization tendency, a HiLoad Superdex 75 pg or S200 pg column was used (GE healthcare). After SEC with Standard buffer, the fractions containing the desired protein were again concentrated

to 5-20 mg/ml, aliquoted and snap-frozen in liquid N<sub>2</sub>. Proteins were then stored at -80°C until use.

The column-bound GST-p53 fusion protein was inefficiently cleaved by TEV-protease and was thus eluted with 50 ml GSH-Elution buffer. TEV-cleavage was performed in solution overnight with slow agitation. The solution containing GST, p53 and uncleaved GST-p53 was concentrated and subjected to SEC with a S200 column. p53 eluted shortly after the size exclusion peak.

### 2.3.4 Purification of His<sub>6</sub>-tagged proteins

Proteins tagged with His<sub>6</sub> were purified by affinity-chromatography using Ni-Sepharose 6 Fast Flow resin (GE healthcare). The binding and washing steps were carried out as described for GST-tagged proteins (2.3.3) but with Ni-Wash buffer. The His<sub>6</sub>-tagged protein was eluted by a 300 ml imidazole-gradient using Ni-Elution-I and Ni-Elution-II buffers. 5 ml fractions were collected. The fractions containing the desired protein were pooled and further processed as described above (2.3.3).

### 2.3.5 Determination of protein concentration

Protein concentrations were determined by measuring absorbance at 280 nm ( $A_{280}$ ) using UV Cuvettes micro (Brand) in BioPhotometer Plus (Eppendorf). The instrument was blanked with the respective buffer before measurement. The concentration can be determined based on the Lambert-Beer law according to the following formula:

$$A_x = \epsilon_x \cdot c \cdot l \quad (2.1)$$

- $A_x$ : Absorbance at wavelength  $\lambda = x$  nm
- $\epsilon_x$ : Molar extinction coefficient ( $M^{-1}cm^{-1}$ ) at wavelength  $\lambda = x$  nm
- $c$ : Protein concentration (M)
- $l$ : Path length (cm)

ExpASy ProtParam (Gasteiger et al., 2005) was used to obtain extinction coefficients and molecular weights of proteins. For the extinction coefficient of Ran, the absorbance of guanine nucleotides at 280 nm ( $7765 \text{ cm}^{-1} \text{ M}^{-1}$ ) was taken into account (Smith and Rittinger, 2002). Alternatively, the concentration of Ran was determined with BradfordUltra (Expedeon) according to the manufacturers protocol but with a 5 min room temperature incubation step before readout at 595 nm (Bradford, 1976). A standard curve was generated using a dilution series of bovine serum albumin (BSA).

### 2.3.6 SDS-polyacrylamide gel electrophoresis (SDS-PAGE)

Protein samples were separated by denaturing, discontinuous SDS-polyacrylamide gel electrophoresis (Laemmli, 1970). To this end, samples were supplemented with 5x Laemmli buffer and denatured at  $95^{\circ}\text{C}$  for 5 min. Gels were prepared as follows:

	Seperation gel (5%)	Stacking gel (12%)
2 M Tris-Cl, pH 8.8 (ml)	7.4	-
1 M Tris-Cl, pH 6.8 (ml)	-	2.4
30% Acrylamide (ml)	16	3.3
10% SDS ( $\mu\text{l}$ )	400	200
TEMED ( $\mu\text{l}$ )	24	16
ddH <sub>2</sub> O(ml)	16	13.9
10% APS ( $\mu\text{l}$ )	240	160

Gels were run at 200 V for 45 - 60 min with SDS-PAGE Running buffer. Gels were either stained with Staining solution or used for Western blotting. Destaining of gels was carried out with Destaining solution.

### 2.3.7 Western blotting and immunodetection

Proteins separated by SDS-PAGE were blotted on PVDF membrane (GE health-care) by semi-dry transfer in Transfer buffer at 150 mA for 45 min. Prior to blotting, PVDF membranes were activated in methanol for 1 min. Successful protein transfer was monitored by Ponceau S staining (Sigma) for 1 min and a brief subsequent wash with ddH<sub>2</sub>O. Membranes were blocked in 5% (w/v) skim milk

powder/PBST for 1 h at room temperature and subsequently incubated with primary antibody (AB) overnight at 4°C. After three 10 min washes with PBST, the membranes were incubated with HRP-coupled secondary AB for 1 h at room temperature. After another three washes for 10 min with PBST, the membranes were ready for detection using Roti-Lumin (Carl Roth) as HRP-substrate. Depending on signal strength, detection was carried out either with SuperRX Fujifilms (Fuji) or with a CCD camera-based Vilber Fusion Express detection system. For long-term storage, membranes were stripped with 0.2 M NaOH for 20 min, rinsed with ddH<sub>2</sub>O and then dried. For re-activation, membranes were incubated in methanol and again blocked as described. Table 2.7 details the ABs and working dilutions used in this work. The Gel Analyzer tool of the ImageJ software was used for quantitative densitometric analysis of gel band intensities.

TABLE 2.7: Antibodies

Antigen	Catalog #	Species	Dilution
Ran	ab4781	rabbit	1:2500
acetyl-lysine	ab21623	rabbit	1:1500
RanAcK37	-	rabbit	1:75
His <sub>6</sub> -tag	ab18184	mouse	1:2000
Sirt2	ab75436	rabbit	1:500
Sirt3	sc-49744 (Santa Cruz)	1:500	
GST	71097 (Novagen)	mouse	1:1000
Myc	ab24740	rabbit	1:1000
rabbit-IgG (HRP)	ab6721	goat	1:10000
mouse-IgG (HRP)	ab6728	rabbit	1:10000

### 2.3.8 Generation of the RanAcK37-specific antibody

The RanAcK37-specific AB was generated by Thermo Fisher custom antibody services. Two rabbits were immunized with an acetyl-TGEFE(AcK)KYVAT-[C]-peptide and the immune response was monitored at 0, 28, 56 and 72 days. To this end, crude sera were used at a dilution of 1:1000 for immunodetection of whole cell lysate, RanWT and RanAcK37. The 72-day-bleed was chosen for further purification by negative adsorption with the non-acetylated peptide. The flow-through was further purified by positive adsorption using the acetylated peptide. The resulting RanAcK37 AB had a concentration of 0.11 mg/ml and was used at a dilution of 1:75.

### 2.3.9 Exchange of Ran-bound nucleotides

Ran purified from *E. coli* is predominantly GDP-bound. To exchange GDP against GTP, 5-10 mg of Ran were incubated in Standard buffer with 10 mM EDTA (pH 8.4) and a 100-fold molar excess of GTP for 1 h at room temperature in a total volume of 500  $\mu$ l. Afterwards, 15 mM MgCl<sub>2</sub> were added to the exchange reaction.

For the exchange against the non-hydrolyzable GTP-analog Guanosine-5'-[( $\beta,\gamma$ )-imido]triphosphate (GppNHp), 5-10 mg of Ran were incubated in Standard buffer with a five-fold molar excess of GppNHp, 10 U of calf intestinal phosphatase (CIP) and 0.3  $\mu$ M of GST-RCC1 for 2 h at room temperature in a total volume of 500  $\mu$ l. GST-RCC1 was removed by adding 20  $\mu$ l equilibrated PureCube Glutathione Agarose and incubation for 15 min at 4°C. The solution was then separated from the beads by it through a micro-spin filter (CIRO).

In both cases, the reactions were centrifuged at 17,000  $\times g$  for 5 min and subjected to analytical SEC using a S75 Superdex 75 10/300 GL column (GE healthcare) with Standard buffer as mobile phase to remove excess nucleotides. The fractions containing Ran were subsequently pooled and concentrated with a 10 kDa cut-off centricon (AmiconUltra, Millipore), snap-frozen in liquid N<sub>2</sub> and stored at -80°C until use.

### 2.3.10 High pressure liquid chromatography (HPLC)

To determine the ratios of Ran-bound nucleotides, isocratic reversed-phase high pressure liquid chromatography (RP-HPLC) was used with a Chromolith Performance RP-18 endcapped (100-4.6 mm) column (Merck) as the stationary phase and HPLC buffer at 2 ml/min as the mobile phase. A Merck-Hitachi L-4000 UV detector and a L-6000-A pump were used. The ion-pairing reagent TBAB contained in the HPLC buffer binds to negatively charged phosphate groups of nucleotides. The more phosphate groups are present, the more TBAB molecules bind. The binding of TBAB increases the hydrophobicity and thus the retention time and allows for the separation of different nucleotides based on charge. For the measurement, 30  $\mu$ l of a 150  $\mu$ M protein solution was heated to 95°C for 5 min and subsequently centrifuged at 17,000  $\times g$  for 5 min. 25  $\mu$ l of the supernatant were injected and the UV absorbance at 254 nm was recorded over 10 min. The peaks

were assigned based on retention times obtained from standard solutions containing 150  $\mu\text{M}$  of the respective nucleotide. To calculate the ratios of nucleotides, the area of each nucleotide was divided by the sum of the areas of the assigned peaks. Peak analysis was carried out using Clarity Lite software (DataApex).

### 2.3.11 Activity assay for deacetylases

Activity assays for purified deacetylases were performed in KDAC-assay buffer using fluorogenic substrates (as specified in Table 2.8) at 5  $\mu\text{M}$ . Reactions were set up in triplicates in black 96-well plates with a reaction volume of 50  $\mu\text{l}$  (1000 pmol/reaction). The enzyme concentration was adjusted to theoretically allow for a complete deacetylation of substrate within 1 h at 37°C based on the activities stated by the manufacturer. After incubation at 37°C for 30 min, 5  $\mu\text{l}$  Developer solution were added to the reaction, which was subsequently incubated for another 30 min at room temperature. Fluorescence readout was carried out on a Beckman Paradigm (Wavelength: excitation 350 nm, emission 450 nm).

### 2.3.12 KDAC-screen

The activities of the purchased classical KDACs and Sirtuins that were determined experimentally differed substantially from the manufacturers specifications. Thus, a correction factor was calculated for each enzyme by choosing a 40-fold increase of signal intensity over background in the activity assay as the reference point. Given that 100 pmol of recombinant Ran were to be used per reaction in the screen, instead of 1000 pmol of substrate as in the activity assay, the enzyme amount was calculated as follows: correction factor  $\times$  (enzyme amount in activity assay/10). The KDAC-screen was carried out in KDAC-assay buffer as triplicate reactions with 20  $\mu\text{l}$  volume in a 96-well PCR plate. Ran incubated without enzyme served as a negative control. After incubation for 2 h at 30°C, the 2  $\mu\text{l}$  of each reaction were spotted on a nitrocellulose membrane, which was then subjected to co-immunodetection with ABs against acetyl-lysine (AcK) and His<sub>6</sub> (2.3.7). Fluorescent anti-rabbit-Alexa Fluor 680- and anti-mouse-Alexa Fluor 778-coupled secondary ABs (1:40,000) were used for the simultaneous detection of anti-AcK- and anti-His<sub>6</sub>-immunoreactivity, respectively. Acquisition was carried out on a Odyssey CLx scanner (LI-COR). The spot intensities were quantified using the

ImageJ Gel Analyzer tool. The signal intensities obtained from detection with the anti-AcK AB were corrected based on the anti-His<sub>6</sub> loading control.

TABLE 2.8: Recombinant KDACs used for the screen

Supplier/ Enzyme	Construct	Catalog #	Fluorogenic KDAC substrate	Amount in screen (ng/per reaction)
<u>Biomol:</u>				
KDAC1	full-length	50051	HDAC Substrate 3 <sup>1</sup>	4.28
KDAC2	full-length	50002	HDAC Substrate 3	0.69
KDAC3	full-length	50003	HDAC Substrate 3	0.74
KDAC4	627-1084	50004	HDAC Substrate Class2a <sup>2</sup>	5.24
KDAC5	657-1123	50005	HDAC Substrate Class2a	1.13
KDAC6	full-length	50006	HDAC Substrate 3	6.61
KDAC7	518-end	50007	HDAC Substrate Class2a	0.32
KDAC8	full-length	50008	HDAC Substrate Class2a	2.02
KDAC9	604-1066	50009	HDAC Substrate Class2a	2.35
KDAC10	1-481	50010	HDAC Substrate 3	0.44
KDAC11	full-length	50011	HDAC Substrate Class2a	1226
Sirt3	102-399	50014	SIRT Substrate 1 <sup>3</sup>	3100
<u>Sigma:</u>				
Sirt1	full-length	S8446	SIRT Substrate 1	3100
Sirt6	full-length	SRP5273	SIRT Substrate 1	4000
Sirt7	full-length	SRP5274	SIRT Substrate 1	4000
<u>Self-made:</u>				
His <sub>6</sub> -Sirt2	50-356	-	SIRT Substrate 1	1000

<sup>1</sup> Fluorogenic HDAC Substrate 3, Biomol, Catalog # 50037

<sup>2</sup> Fluorogenic HDAC Class2a, Biomol, Catalog # 50040

<sup>3</sup> SIRT Substrate 1, fluorogenic, Sigma, Catalog # SRP0308

### 2.3.13 Deacetylase assays

Deacetylase assays were carried out Standard buffer supplemented with 1 mM NAD<sup>+</sup> at 23°C unless stated otherwise. Acetylated proteins were incubated with deacetylase at concentrations as stated in the figure legends. 20 µl samples were taken at indicated time points and then heated for 5 min at 95°C to stop the reaction. The first time point (t=0) did not contain enzyme.

### 2.3.14 PEPCK1 activity assay

To measure the activity of PEPCK1, a coupled enzyme assay as outlined in Fig. 2.1 was used. The assay was carried with a LS55 Fluorescence spectrometer (Perkin

Elmer) and Quartz SUPRASIL cuvettes (10 mm light path, Hellma Analytics). The four cuvettes were first calibrated with 150  $\mu$ l of PEPCK1-assay buffer (excitation wavelength of 345 nm and a readout wavelength of 470 nm). Then, PEPCK1 was added at a final concentration of 0.2  $\mu$ M and the fluorescence drop was followed over 60 min.

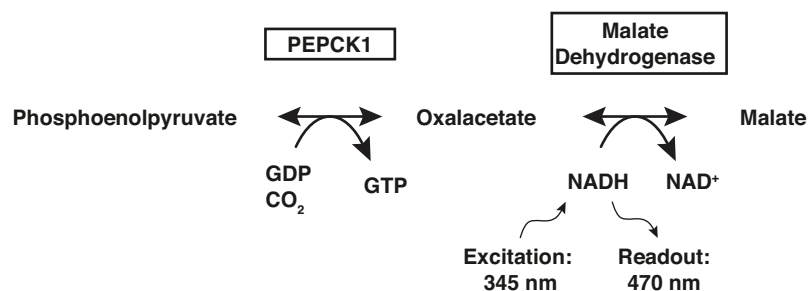


FIGURE 2.1: Scheme of PEPCK1 activity assay.

## 2.4 Cell culture

### 2.4.1 Cultivation of cell lines

HEK293T cells were cultured in Dulbeccos modified Eagles medium (DMEM) supplemented with 1% (v/v) non-essential amino acids, 1% (v/v) Penicillin/Streptomycin (Gibco) and 5% heat-inactivated fetal calf serum (PAN-Biotech). For passaging, cells were washed with PBS (PAN-Biotech) and then incubated with 0.25% trypsin-EDTA-solution (Sigma) for 5 min at 37°C. The cells were diluted with fresh pre-warmed growth medium and distributed to new culture plates (TC Dish 100 or 150 Standard, Sarstedt) to yield the desired cell density. Stocks of cells were prepared by resuspending trypsinized cells in ice-cold DMEM/10% (v/v) DMSO and slow cooling to  $-80^{\circ}\text{C}$  in a Mr. Frosty Freezing Container (Thermo). For long-term storage, stocks were then kept at  $-150^{\circ}\text{C}$ .

### 2.4.2 Transfection

HEK293T cells were transfected by calcium phosphate precipitation (Graham and van der Eb, 1973). In brief, cells were seeded 24 h before transfection to yield

approximately 50% confluency by the next day and fresh medium was given 1-4 h before transfection. For a 150 mm dish, the transfection solution was prepared as follows:

20 $\mu$ g	DNA
<i>ad</i> 900 $\mu$ l	ddH <sub>2</sub> O
100 $\mu$ l	CaCl <sub>2</sub> (2.5 M)
After mixing:	
1000 $\mu$ l	2 $\times$ BBS

The mixture was vortexed for 15 s, incubated for 15 min at room temperature and then carefully applied to the cells.

### 2.4.3 Ni<sup>2+</sup>-NTA pull-down

For pull-down of His<sub>6</sub>-tagged proteins, HEK293T cells in 15 cm dishes were transfected as described in 2.4.2. Cells were washed with 10 ml ice-cold PBS 16 h after transfection and harvested with a cell-scraper in 5 ml ice-cold PBS. Cells were then centrifuged for 3 min at 500  $\times g$  and 4°C. The cell pellet was resuspended in 1.8 ml Pull-down lysis buffer and sonicated twice for 30 sec with a Branson Sonifier 250 using a microtip (25% duty cycle and micro-tip limit 2). The lysates were subsequently transferred into 2 ml tubes and cleared by centrifugation for 10 min at 17,500  $\times g$ . The supernatant was then transferred to fresh 2 ml tubes and a 50  $\mu$ l input sample was taken. The lysates were incubated with 50  $\mu$ l Ni<sup>2+</sup>-NTA magnetic beads (5 Prime) for 2 h or over night at 4°C with agitation. After washing thrice with 1 ml Pull-down wash buffer, His<sub>6</sub>-tagged proteins were eluted by the addition of 50  $\mu$ l Pull-down elution buffer. For western blotting, the samples were not heated to 95°C since heating in Urea led to strong unspecific signals when detection was performed with the anti-AcK AB.

## 2.5 Biophysical methods

### 2.5.1 Isothermal titration calorimetry (ITC)

Isothermal titration calorimetry (ITC) was carried out on a MicroCal ITC200 or an Auto-ITC200 instrument (GE healthcare) (Wiseman et al., 1989). Unless stated otherwise, measurements were performed in Standard buffer at 20°C, a stirring speed of 1000 rpm, 2 µl injections (0.5 µl/sec), an injection-spacing of 120 s and a target differential power (DP) value of 6 µcal/sec. Protein concentrations are indicated in the figure or table legends.

ITC allows for the thermodynamic characterization of interactions between molecules. Depending on the binding mechanism heat is either released (negative  $\Delta H$ , exothermic) or absorbed (positive  $\Delta H$ , endothermic) when interaction between molecules takes place. If used in the so-called power compensation mode, one binding partner at a high concentration is titrated in a step-wise manner into a solution containing the other lower concentrated binding partner. The instrument tries to keep the temperature in the measurement cell constant and records the heating power over time that is required to do so with respect to a reference cell. For each injection, a peak can be observed in the isotherm until saturation of the lower concentrated binding partner in the cell is reached. The area of each peak is then plotted and fitted to a one-site-binding model, which allows for the direct determination of the reaction enthalpy  $\Delta H$ , the equilibrium association constant  $K_A$  and the stoichiometry. The reaction entropy  $\Delta S$  and the Gibbs energy  $\Delta G$  can be calculated using the following formula:

$$\Delta G = \Delta H - T\Delta S = -RT\ln K_a \quad (2.2)$$

### 2.5.2 Mass spectrometry (MS)

For generation of tryptic or Glu-C peptides, filter-aided sample preparation (FASP) was used as described (Wisniewski et al., 2009). Separation of peptides was performed by ultra-HPLC with a binary buffer system A (0.1% (v/v) formic acid in H<sub>2</sub>O) and B (0.1% (v/v) formic acid in acetonitrile) and an Easy nano-flow LC 1000 system (Thermo Fisher Scientific). The linear gradient was set up as follows:

4 to 30% B in 40 min, 95% B for 10 min, and followed by re-equilibration to 5% B in 5 min. The gradient was run on a 50 cm column (75  $\mu\text{m}$  internal diameter) packed with C18 (resin diameter 1.8  $\mu\text{m}$ ) at a flow rate of 250 nL/min. The column temperature was kept constant at 45°C over the course of the separation. Ultra-HPLC-separated was coupled to a quadrupole based QExactive Plus mass spectrometer via a nano-electrospray ionization source (both Thermo Fisher Scientific). For acquisition of MS spectra, the automatic gain control target was set to  $3 \cdot 10^6$  at a resolution of 70,000 (200 m/z) in a mass range of 350-1650 m/z. For ion accumulation, the maximum injection time was set to 60 ms. MS/MS spectra were generated according to the Top10 method in the high mass accuracy Orbitrap after HCD (Higher energy C-Trap Dissociation) fragmentation at 25 eV collision energy in a 100-1650 m/z mass range. The settings were as follows: a resolution 35,000 at 200 m/z, an injection time of 120 ms and an AGC target of  $5 \cdot 10^5$ .

Raw files were analyzed with MaxQuant (version 1.5.2.) with the embedded Andromeda search engine (Cox and Mann, 2008; Cox et al., 2011). Uniprot proteome databases for *H. sapiens* were used for the assignment of electron spray ionization-(ESI)-MS/MS fragmentation spectra. The database was complemented with the expected amino acid sequence of the according Ran construct (*i.e.* from pRSFDuet-1-pyIT-AcKRS-3 or pcDNA3.1C). Search parameters were set to default except that the trypsin cleavage was allowed anywhere and the minimum score for modified peptides was set to zero. For *in vivo* His<sub>6</sub>-Ran pulldown, the total intensities of unmodified Ran peptides after label-free quantification were used for normalization (to an arbitrary value of  $1 \cdot 10^{11}$ ) of the intensities of the modified peptides in each condition. For experiments with recombinant acetylated Ran, the raw intensities of unmodified Ran peptides were used for normalization. Hendrik Nolte created the heat map and performed the hierarchical clustering using the R heatmap.2 function. It represents the average intensity values of two independent experiments. The Euclidian method was used to calculate distances. Complete mode was used for the calculation of linkage.

## 2.6 Crystallographic methods

### 2.6.1 Crystallization

Three different SIRT2 constructs expressed from pGEX-4T5 were tested for their propensity to crystallize with the Ran-derived 13-mer peptides (see 2.3). Sufficiently high purity and amounts were obtained with the described purification protocol (2.3.3). For the initial screen, each construct was adjusted to a concentration of 10 mg/ml in Standard Buffer and supplemented with a 1.2-fold molar excess of the respective peptide. To remove aggregated protein, the mixture was centrifuged for 10 min at  $17,000 \times g$  and  $4^\circ\text{C}$  and the supernatant was transferred to a fresh tube. 150 nl drops of protein solution were pipetted into the three wells of 96-well sitting drop plates, in which screening conditions had been aliquoted (see 2.1.4). Then 150 nl of the reservoir solution was then pipetted onto the protein drop. Both steps were carried out with a mosquito Crystal pipetting robot (TTPlabtech) under humidified atmosphere. The plates were immediately sealed with HDclear tape (Duck, Henkel) and kept at  $20^\circ\text{C}$ . This so-called Sparse-Matrix Sampling screening method allows for the evaluation of a range of different buffers, pH, additives and precipitants for their effect on crystal formation. The different conditions have been empirically derived from known crystallization conditions of various proteins (Cudney et al., 1994; Jancarik and Kim, 1991).

### 2.6.2 Preparation of crystals for data collection

Crystals were shock-frozen in liquid  $\text{N}_2$  to protect them from disintegration and radiation damage during data collection. To this end, crystals were captured under a stereo microscope with an appropriately sized nylon cryoloop attached to a mounting pin with a magnetic base (CrystalCap HT, Hampton Research). The crystals were washed twice in mother liquor, which was supplemented with 15% and 30% D-glucose/10% glycerol as cryoprotectant, respectively. The crystals were then stored in liquid  $\text{N}_2$  until data collection.

### 2.6.3 Data collection and processing

Crystal diffraction data were collected at the Swiss Light Source (SLS) of the Paul Scherrer Institute (PSI) in Villigen, Switzerland using the X06DA/PX3 beamline. The dataset was recorded at a wavelength of 1.0 Å and 100 K using a Dectris PILATUS 2M detector in a distance of 165 mm. The oscillation range was 0.1 and 1200 frames were recorded. Indexing and integration was performed with MOSFLM (Leslie and Powell, 2007). The program AIMLESS was used for scaling (Evans and Murshudov, 2013). The data was assessed for redundancy, completeness of reflexes, signal to noise ratio of  $I/\sigma I$  and resolution. An additional measure of data quality were  $R_{sym}$  and  $R_{meas}$ , which are calculated as follows:

$$R_{sym} = \frac{\sum_{hkl} \sum_{i=1}^N |I_{i,hkl} - \langle I_{hkl} \rangle|}{\sum_{hkl} \sum_{i=1}^N I_{hkl}} \quad (2.3)$$

and

$$R_{meas} = \frac{\sum_{hkl} \sqrt{\frac{N_{hkl}}{N_{hkl}-1}} \sum_{i=1}^N |I_{i,hkl} - \langle I_{hkl} \rangle|}{\sum_{hkl} \sum_{i=1}^N \langle I_{hkl} \rangle} \quad (2.4)$$

with miller indices  $hkl$  and reflex intensities  $I$  (Diederichs and Karplus, 1997).

The collected data contains information about the electron density in the unit cell but this is limited to the Intensity  $I$  and does not include phase information  $\alpha_{hkl}$ . However, the phase information is required to determine the electron density as a function of position  $x, y, z$  via Fourier transformation (referred to as the phase information):

$$\rho(x, y, z) = \frac{1}{V} \sum_{hkl} |F_{hkl}| e^{-2\pi i(hx+ky+lz)+i\alpha_{hkl}} \quad (2.5)$$

$\rho(xyz)$ : Electron density at coordinates  $x, y, z$

$|F_{hkl}|$ : Amplitude of the reflex structure factor ( $h, k, l$ )

$\alpha_{hkl}$  Phase angle of the reflex ( $h, k, l$ )

One way of deriving the phase information is so-called molecular replacement, which can be used if structures of homologous proteins are already available. For the structure of SIRT2(50-356)·RanTFAcK37-13-mer-peptide, the initial phases were determined with the program Phaser (as part of the suite Phenix-dec-1893; Adams et al., 2010) and by using the SIRT2(43-370)·S2iL5 structure as search model (PDB: 4L3O; Yamagata et al., 2014). With the program Coot 0.7.1, the model was build into the  $2F_o - F_c$  (countered at  $1.0 \sigma$ ) and  $F_o - F_c$  (countered at  $3.0 \sigma$ ) electron density maps in iterative rounds of refinement, which were carried out with Phenix.refine (Afonine et al., 2012; Emsley et al., 2010). The quality of the structure model was assessed with Molprobity (Davis et al., 2007). The quality factor  $R_{work}$  is calculated according to the following formula:

$$R_{work} = \frac{\sum ||F_{obs}| - |F_{calc}||}{|\sum F_{obs}|} \quad (2.6)$$

with  $F_o$  and  $F_c$  as the observed and calculated structure factor amplitudes, respectively.

To account for possible overfitting, typically 5–10% of the reflection data is excluded from each refinement, which is referred to as the ‘test set’ (as opposed the other 90–95% of the data termed the ‘work set’). The test set is used to determine the free R factor  $R_{free}$  with the above formula. In the final model, the difference of  $R_{free}$  to  $R_{work}$  should not exceed 5% (Bruenger, 1992). Structure figures were prepared with MacPyMOL (Schrödinger).

## 3 Results

### 3.1 Ran acetylation: Effects and regulation

The use of the GCEC allows for the in-depth analysis of the impact of lysine-acetylation on protein function. The high-throughput mass spectrometry data obtained by Choudary et al. (2009) was the motivation to investigate the effects and the regulation of Ran acetylation. In the PhD thesis of S. de Boor (2015) a number of important results are shown regarding the influence of Ran acetylation on RCC1-mediated nucleotide exchange, nuclear import of Ran by NTF2 and the binding to importin- $\beta$ . The present work aims to complete this emerging picture by the analysis of further interaction partners mainly involved in the control of nuclear export as well as intrinsic and RanGAP-stimulated nucleotide hydrolysis. Furthermore, results are presented that give insights into the regulation of Ran acetylation and deacetylation.

#### 3.1.1 Purification of acetylated Ran

Acetylated Ran was expressed in *E. coli* by using the described GCEC and purified with a two-step protocol involving a Ni-NTA affinity chromatography and a subsequent size-exclusion chromatography (SEC). As an example, purification of RanAcK71 is shown in Fig. 3.1. Depending on the position of the modified lysine residue in Ran, the purification yields varied between approximately 1.5 and 6.0 mg/l of culture volume. Ran wildtype (RanWT) was expressed as a GST-fusion protein and purified by GSH-affinity chromatography. The yields of RanWT purifications were usually 3-4 mg/l of culture volume. After removal of the GST-tag by on-column TEV-protease cleavage, the RanWT protein was subjected to SEC. Both wild type and acetylated variants of recombinant Ran eluted as a single

peak suggesting that the purified proteins were properly folded and that acetylation does not result in multimerization or aggregation of Ran. Recombinant Ran could be concentrated to more than 20 mg/ml and was stable for several hours at room temperature.

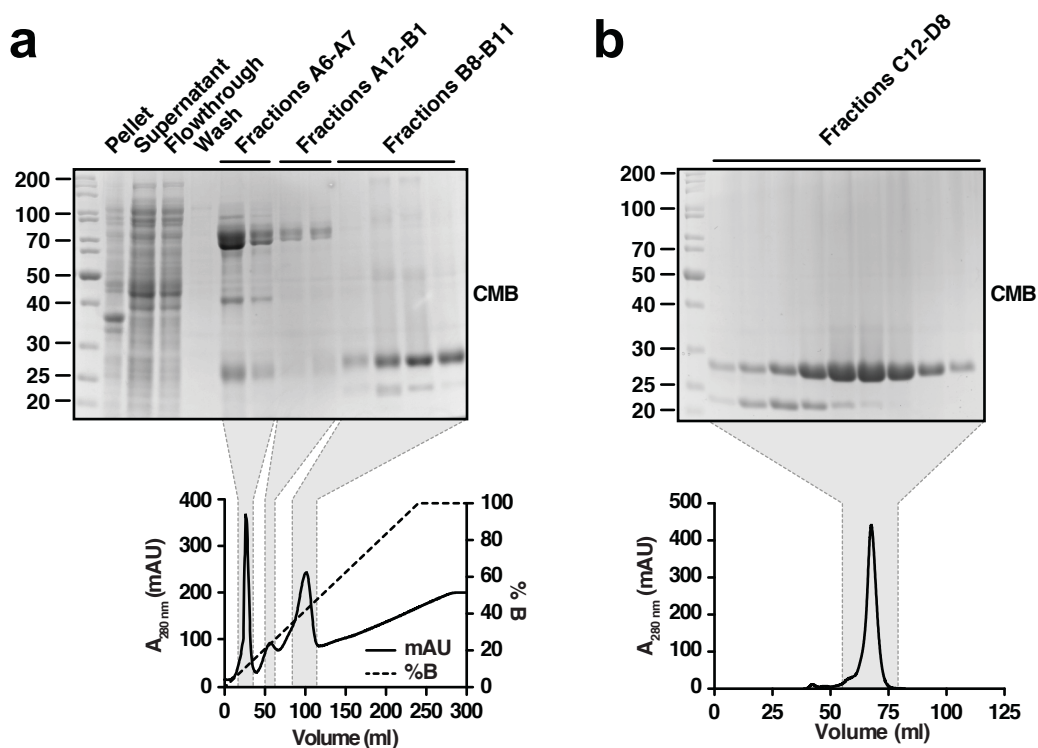
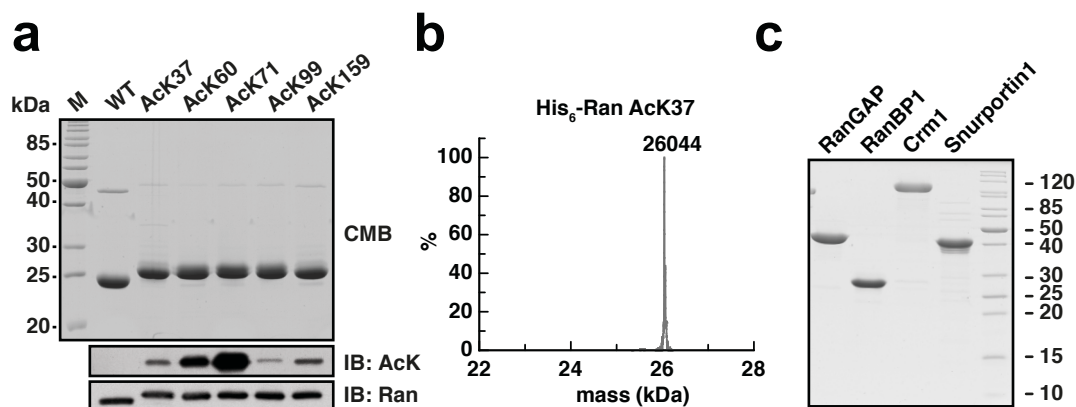


FIGURE 3.1: **Exemplary purification of acetylated Ran (RanAcK71).** (a) SDS-PAGE of samples of the cell lysis as well as the imidazol-gradient. The chromatogram of the imidazol-gradient shows the absorbance at 280 nm and the concentration of the elution buffer (% B). (b) SDS-PAGE of samples of the S75 (16/60) size exclusion chromatography with the according chromatogram. The gels were stained with Coomassie brilliant blue (CMB).

To judge the purity of the resulting protein, 5  $\mu$ g were analysed by SDS-PAGE. In addition, 250 ng of protein were subjected to Western blotting and detected with an anti-Ran and a pan-anti-acetyl-lysine (AcK) antibody (AB). As depicted in Fig. 3.2a, all Ran variants were obtained with more than 90% purity, each one showing a single major band corresponding to the molecular weight (MW) of RanWT or His<sub>6</sub>-tagged acetylated Ran (24.6 kDa and 26.1 kDa, respectively). Ran tends to show a second higher MW band, which most likely corresponds to a dimer, as described for other proteins subjected to SDS-PAGE at high concentrations (Egerman et al., 2015). As opposed to detection with the anti-Ran-AB, which results in similar signals for all Ran variants, only the supposedly acetylated Ran variants are immunoreactive to the pan-anti-AcK-AB indicating the

incorporation of AcK. Interestingly, the signals obtained vary depending on which site is acetylated, which likely reflects a preference of the anti-AcK-AB for certain sequence contexts surrounding each site (and possibly also for structural elements to some extent).



**FIGURE 3.2: Purification of acetylated Ran and Ran interaction partners.** (a) SDS-PAGE of 5  $\mu$ g of indicated Ran variants stained with Coomassie brilliant blue (CMB) and Western blot of 250 ng of Ran variants detected with indicated antibodies. (b) Representative ESI-MS spectrum of RanAcK37 with the measured molecular weight as indicated. Theoretical mass: 26043.6 Da. (c) CMB stained gel after SDS-PAGE of 5  $\mu$ g of indicated Ran interaction partners. (Parts of this figure are published in the PhD thesis of S. de Boor, 2015. The remaining ESI-MS spectra can be found in the appendix thereof.)

The RanAcKs were subjected to electrospray-ionization mass spectrometry (ESI-MS), which allows for the determination of their MWs and thus to infer if an acetyl-moiety is present. Moreover, based on SDS-PAGE alone it could not be ruled out that the proteins obtained were not a mixture of acetylated and non-acetylated species, which however is detectable by ESI-MS as additional peak(s) in the obtained spectra. Each RanAcK gave rise to a single peak corresponding to a MW of  $\sim$ 26044 Da, consistent with the quantitative incorporation of an acetyl-moiety at an N-( $\epsilon$ )-amino group of a lysine residue and distinct from the MW of non-acetylated protein (expected MW for His<sub>6</sub>-RanWT and His<sub>6</sub>-RanAcK lacking the first methionine residue: 26001.6 Da and 26043.6 Da, respectively) (see Fig. 3.2b and the appendix of the PhD thesis of S. de Boor, 2015).

Given their high purity and stability, the purified Ran constructs appeared suitable for biochemical and biophysical assays to analyze the effects of acetylation on Ran function. To this end, interaction partners were also purified by GSH-affinity

chromatography followed and subsequent SEC, similar to the purification process shown for RanWT in Fig. 3.1b. As shown in Fig. 3.2c, RanGAP (*S. pombe*), RanBP1 (*H. sapiens*), CRM1 (*M. musculus*) and Spn1 (*H. sapiens*) were obtained in estimated purities of 85-95%. The quantities varied depending on the protein but were in each case in the range of 1-5 mg/l of culture volume and thus sufficient for the purpose of this study. Given the successful purification of both, non-acetylated/acetylated Ran and these interaction partners, it was feasible to study the molecular effects of Ran acetylation on protein export and GTP-hydrolysis.

### 3.1.2 Effect of Ran acetylation on intrinsic GTP hydrolysis

The intrinsic GTP hydrolysis is very slow with reported rates of  $5.4 \times 10^{-5} \text{ s}^{-1}$  at 37°C (Klebe et al., 1995) and thus of limited physiological relevance. Given the positioning of lysines in the switch regions, it was possible that acetylation at these sites might interfere with the intrinsic GTP hydrolysis rate of Ran. In particular, K71 is in close proximity to the catalytic Q69 known to be important for GTP hydrolysis and could thus potentially influence its orientation upon acetylation (Fig. 3.3a).

For the determination of GTP hydrolysis rates, Ran was loaded with GTP given that is predominantly GDP-bound after purification from *E. coli* (as a result of its intrinsic ability to hydrolyze GTP). In brief, the nucleotide exchange is achieved by incubation with EDTA to chelate  $\text{Mg}^{2+}$  (crucial for nucleotide binding) and the addition of a 100-fold molar excess of GTP. After this incubation step,  $\text{MgCl}_2$  is added to allow for the binding of nucleotide and the protein is separated from excess nucleotide and salts by SEC. This procedure reliably resulted in Ran that was at least 75% GTP-loaded (hereafter referred to as RanGTP).

The intrinsic hydrolysis rates were determined by incubation of RanGTP (150  $\mu\text{M}$ ) at 30°C in Standard buffer. As mentioned above, the intrinsic hydrolysis rate of Ran has previously been determined at 37°C. However, RanAcK159 was slightly unstable at these elevated temperatures, so that measurements were instead carried out at 30°C. Samples were taken at indicated time points and subjected to RP-HPLC to separate the different nucleotide species (see 2.3.10). As shown in the exemplary RP-HPLC trace in Fig. 3.3b, GDP has a shorter retention time than GTP due to its lower charge (resulting in fewer TBAB molecules bound). The area

of each peak was determined and the peak area ratio of GTP was calculated. Importantly, this ratio is largely unaffected by the total amount of nucleotide loaded onto the column allowing for relatively accurate determination of hydrolysis rates. In fact, for RanWT a rate of  $5.88 \times 10^{-5} \text{ s}^{-1}$  was obtained at  $37^\circ\text{C}$ , which is consistent with the reported value mentioned above (not shown). As expected, at  $30^\circ\text{C}$  this rate was slightly decreased ( $2.61 \times 10^{-5} \text{ s}^{-1}$ ). Measurement of the acetylated Ran variants revealed that Ran acetylation at K71 has the strongest effect on the intrinsic GTP hydrolysis rate, leading to an increase by approximately 1.5-fold (Fig. 3.3c).

### 3.1.3 GAP-catalyzed nucleotide hydrolysis and binding to RanGAP is not affected by Ran acetylation

The slow intrinsic GTP hydrolysis of Ran is greatly accelerated by binding of RanGAP. Analysis of the crystal structure of Ran in complex with RanBP1 and RanGAP suggested that acetylation at K71<sup>Ran</sup> might also affect RanGAP-mediated activation of GTP hydrolysis, given the presence of a salt bridge to D103<sup>RanGAP</sup> (Fig. 3.4a). Since RanGAP shifts the catalytic Q69<sup>Ran</sup> closer to the catalytic center, interruption of the saltbridge between K71<sup>Ran</sup> and D103<sup>RanGAP</sup> could influence the extent of GTPase activation. Moreover, K99<sup>Ran</sup> faces an acidic patch in RanGAP (E336-E345<sup>RanGAP</sup>). It was thus possible that acetylation of K99<sup>Ran</sup> would electrostatically and sterically interfere with this interaction.

The RanGAP-mediated GTP hydrolysis was determined using the same method as described for measurement of the intrinsic hydrolysis rates. In this case however, the temperature was decreased to  $25^\circ\text{C}$  and catalytic amounts (5 nM) of the purified RanGAP were added to the reaction. This drastically accelerated the hydrolysis rate as expected, showing that RanGAP was active. Surprisingly, RanGAP-stimulated GTP hydrolysis appears to be largely unaffected by Ran acetylation (Fig. 3.4b).

Next, it was tested whether Ran acetylation would have an influence on the binding affinity to RanGAP. RanGAP binds to Ran with a much higher affinity if Ran is GTP-bound compared to its GDP-bound form (Seewald et al., 2003). Since GTP would be rapidly hydrolyzed as a consequence of this interaction, making the determination of the binding affinity impossible, it was necessary to instead

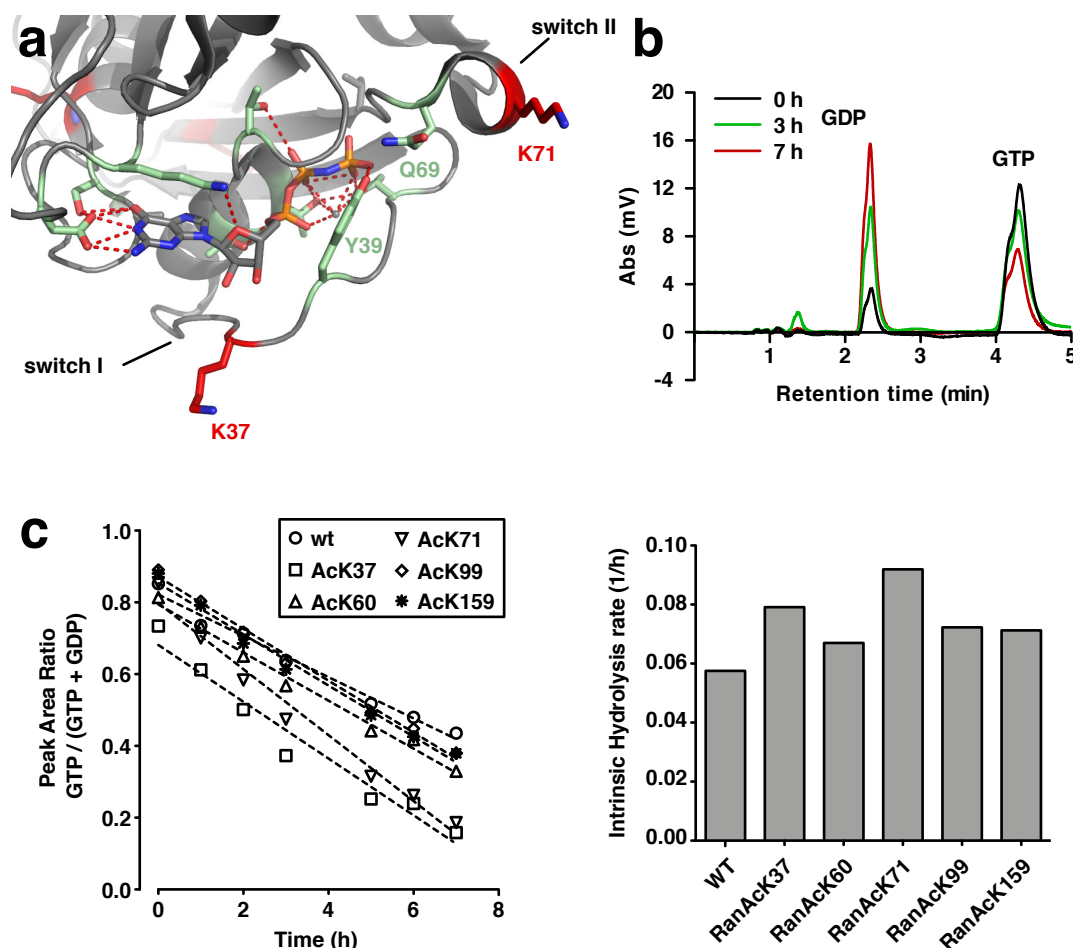


**FIGURE 3.3: Effect of Ran acetylation on intrinsic GTP hydrolysis.** (a) Ribbon-presentation of RanGppNHp (grey) with important residues for nucleotide binding and hydrolysis (green) and potentially acetylated lysines shown as sticks (red) (from the Ran-importin- $\beta$  structure, PDB: 1IBR). The polar interactions towards the GDP molecule are also shown in red. (b) Representative RP-HPLC traces of RanWT intrinsic GTP hydrolysis. Traces of three time points are shown (0 h, 3 h, 7 h). 25  $\mu$ l of 150  $\mu$ M RanGTP were loaded. The peaks are assigned based retention times of pure nucleotide standards. (c) Intrinsic hydrolysis at 30°C with RanWT and acetylated variants. Samples were taken at indicated time points and the data were fitted using a linear regression model in Graphpad/Prism.

load Ran with the non-hydrolyzable analog GppNHp. This was achieved by a different method than described for GTP-loading. In this case only a 5-fold excess of nucleotide (GppNHp) was used and catalytic amounts of the GST-tagged RCC1 were added to accelerate nucleotide exchange. The addition of calf intestinal phosphatase leads to the dephosphorylation of GDP to GMP, which is thus withdrawn from the reaction equilibrium. GST-RCC1 was then removed from the reaction

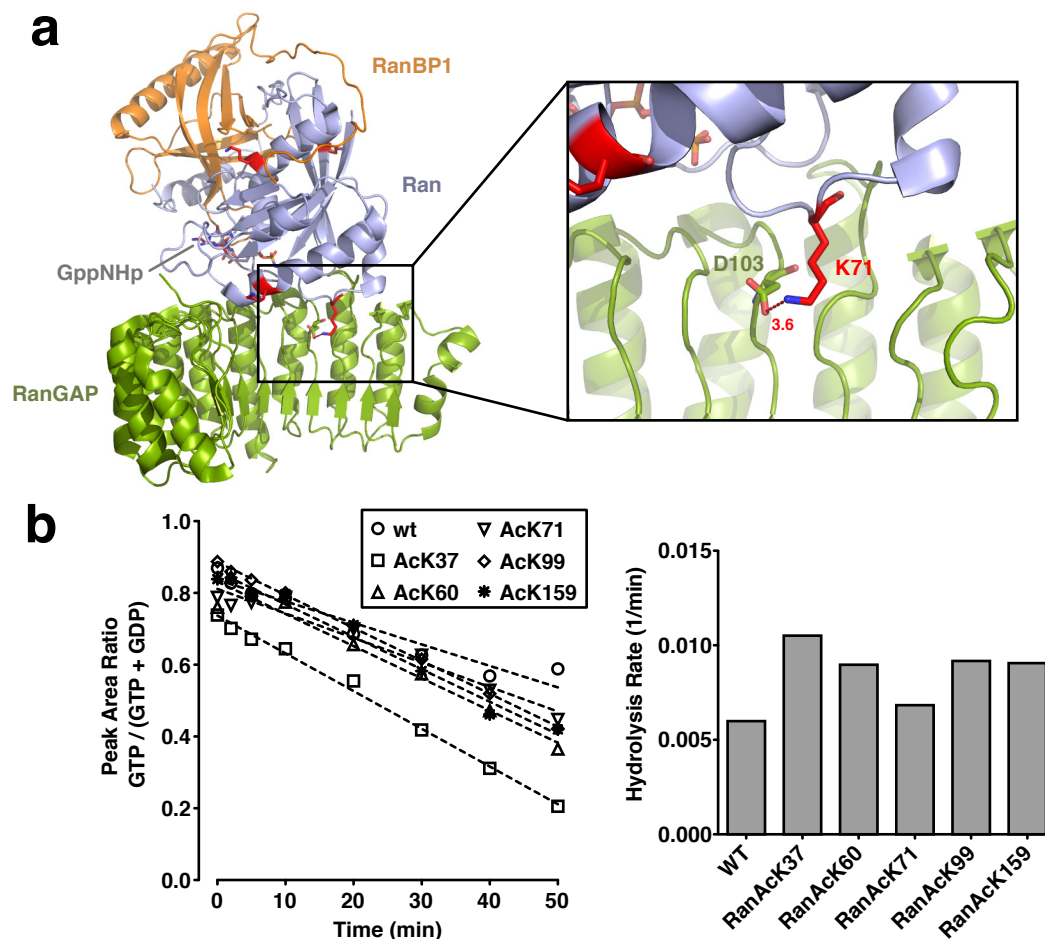


FIGURE 3.4: **Effect of Ran acetylation on RanGAP-stimulated hydrolysis.** (a) Ribbon plot of the ternary RanGAP·RanGppNHp·RanBP1 complex with potentially acetylated lysines shown as red sticks. The inset shows details of the salt-bridge involving K71<sup>Ran</sup> in Ran-RanGAP interface. (b) RanGAP-mediated hydrolysis of RanWT and acetylated variants at 25°C measured by RP-HPLC. Samples were taken at indicated time points and the data were fitted using a linear regression model in Graphpad/Prism.

by incubation with GSH-sepharose beads and Ran was subsequently purified by analytical SEC. With this protocol GppNHp loading of at least 75% were achieved.

ITC was used to determine the binding affinity of Ran to RanGAP. To this end, 20  $\mu$ M of RanGAP was titrated with 200  $\mu$ M RanGppNHp. However, no heat signals were detected, even when different NaCl concentrations (0 mM, 100 mM) and temperatures were used (10, 20, 30°C) (not shown). Possibly, higher protein concentrations would be required to allow for this interaction to be measured by ITC. As an alternative, it was tested whether interaction with RanGAP could be measured if it is titrated with a preformed complex of RanGppNHp and

RanBP1. In fact, this situation reflects more accurately the sequence of binding events occurring during nuclear export since the interaction between RanBP1 and RanGTP is very tight and thus the RanGTP·RanBP1 complex most likely represents the physiological RanGAP substrate. As shown in Fig. 3.5a, the binding reaction of RanGAP and RanGppNHp·RanBP1 (at 200 and 40/40  $\mu\text{M}$ , respectively) is endothermic and solely entropically driven. Surprisingly, the observed stoichiometry of the reaction was 0.5 if RanGAP was the titrant and 1.5 or higher if the RanGppNHp·RanBP1 complex was titrated against RanGAP (Fig. 3.5a). This suggests that, at the concentrations used, either one binding site of the RanGppNHp·RanBP1 complex is inaccessible for RanGAP or that RanGAP can bind two complexes. The affinity of the interaction measured by ITC was 540 nM, which is comparable to the reported affinity of 2  $\mu\text{M}$  determined by *stopped-flow* (Seewald et al., 2003). Moreover, none of the buffer controls showed a signal comparable to measurement of the complex with RanGAP. It was thus assumed that the observed isotherms represent the specific interaction of RanGAP with the RanGppNHp·RanBP1 complex.

For all RanAcKs binding to RanGAP was observed with a similar entropically driven mechanism (Fig. 3.5c). However, differences in  $\Delta\text{H}$  and  $\Delta\text{S}$  were observed. In particular, RanAcK71 shows a less positive  $\Delta\text{H}$  but is also less entropically favored. Overall this leads to only a small change in  $\Delta\text{G}$  and affinity (800 nM) but points towards a slight change in binding mechanism. The disruption of the salt-bridge between K71<sup>Ran</sup> and D103<sup>RanGAP</sup> thus has only a small effect on the Ran-RanGAP interaction. By contrast, RanAcK99 shows both a less favorable  $\Delta\text{H}$  and  $\Delta\text{S}$  and the affinity is lowered to 17  $\mu\text{M}$ . This suggests that indeed acetylation at K99<sup>Ran</sup> disturbs the interaction of Ran with the aforementioned acidic patch of RanGAP.

Since RanAcK99 showed no effect on RanGAP-mediated GTP hydrolysis (Fig. 3.5c), it was possible that the observed decrease in affinity of Ran for RanGAP upon acetylation at K99<sup>Ran</sup> was RanBP1-dependent. The RanGAP-stimulated GTP hydrolysis was thus tested in presence of RanBP1 for RanWT and RanAcK99. However, no difference was observed for RanAcK99 in the presence of RanBP1 (Fig. 3.5d), suggesting that the decreased binding affinity does not adversely affect the RanGAP-mediated hydrolysis. However, it should be noted that the measurements of RanGAP-stimulated GTP hydrolysis were performed under multiple

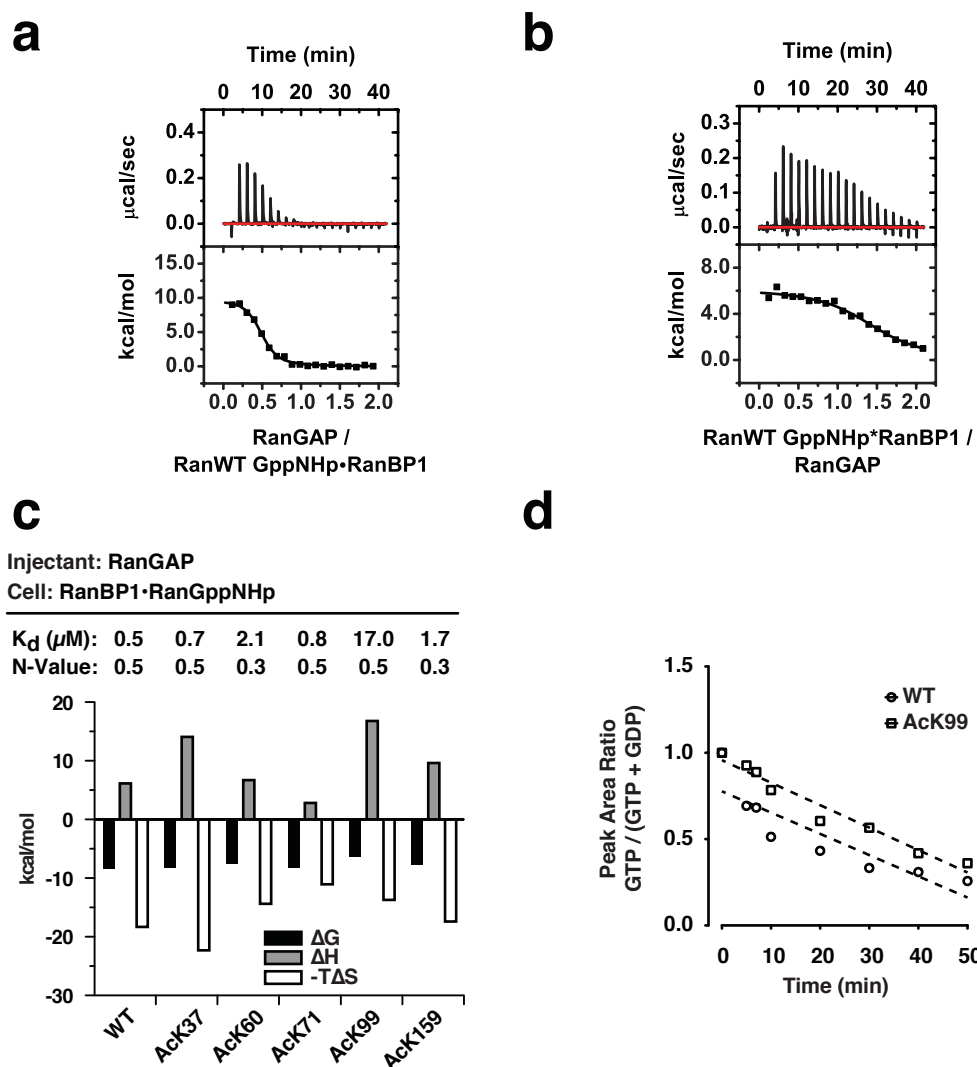


FIGURE 3.5: Interaction of RanGAP with RanGppNHp·RanBP1. (a) ITC trace of RanGppNHp·RanBP1 (40/40  $\mu\text{M}$ ) titrated with RanGAP (200  $\mu\text{M}$ ) at 20°C. (b) Same as in (a) but with tritrant and analyte exchanged. (c) Signature plots, N-values and affinities observed for binding of RanGAP to RanBP1 in complex with acetylated Ran variants under the conditions used in (a). The ITC traces can be found in the Appendix A.2. (d) RanGAP-stimulated GTP hydrolysis of Ran in the presence of RanBP1 for RanWT and RanAcK99 as indicated.

turnover conditions. Thus, an effect of K99<sup>Ran</sup> acetylation on RanGAP-stimulated GTP hydrolysis might in fact be observed under single turnover conditions.

### 3.1.4 Impact of Ran acetylation on the interaction with RanBP1

Next, it was tested whether Ran acetylation would interfere with binding to RanBP1, as an important regulator of export complex disassembly. RanBP1 binds to both RanGDP and RanGTP but with markedly different affinities, which is due to a much higher dissociation rate between RanGDP and RanBP1. This is important for the release of Ran from RanBP1 after RanGAP-mediated hydrolysis (Kuhlmann et al., 1997). The C-terminal tail of Ran containing the DEDDDL motif forms electrostatic interactions with a basic patch on RanBP1 and with K37<sup>Ran</sup> and K152<sup>Ran</sup>. The interactions of Ran with its own C-terminus are not resolved in the structure of RanGAP·RanGppNHp·RanBP1 (PDB: 1K5D) but are present in both the structure of the CRM1·RanBP1·RanGTP complex (PDB: 3M1I) and the RanBD1·RanGppNHp complex (PDB: 1RRP). It has been proposed that RanBP1 sequesters the C-terminal tail of Ran to mediate its dissociation from nuclear transport receptors (Koyama and Matsuura, 2010; Vetter et al., 1999).

Given this the involvement of K37<sup>Ran</sup> in the interaction of Ran and RanBP1, it was interesting to test if it was affected by acetylation of Ran. First, the binding of RanBP1 towards RanGDP was characterized using ITC. To this end, 20  $\mu\text{M}$  RanBP1 was titrated with 200  $\mu\text{M}$  RanGDP, which resulted in an affinity of 7.1  $\mu\text{M}$  in an exothermic reaction (Fig. 3.6a). This value correlates well with the reported affinity for this interaction of about 10  $\mu\text{M}$  (Kuhlmann et al., 1997). Since affinity of RanBP1 for RanGTP was reported to be in the low nanomolar range, the protein concentrations were lowered to 5  $\mu\text{M}$  RanGppNHp and 50  $\mu\text{M}$  RanBP1 in order to increase the sensitivity of the measurements (exchange of titrant and analyte was chosen for better quality). Under these conditions, an affinity of 3 nM was observed.

Most RanAcKs showed binding to RanBP1 in both the GDP- and the GppNHp-loaded form with affinities similar to RanWT (Fig. 3.6c and d). Unexpectedly, the most pronounced effect was observed for RanAcK159, which showed a different thermodynamic profile but unaltered affinity in the GDP-bound form and an approximately 10-fold decrease in affinity in the GppNHp-bound form (33  $\mu\text{M}$ ). However, binding to RanBP1 was not affected by acetylation of K37<sup>Ran</sup>.

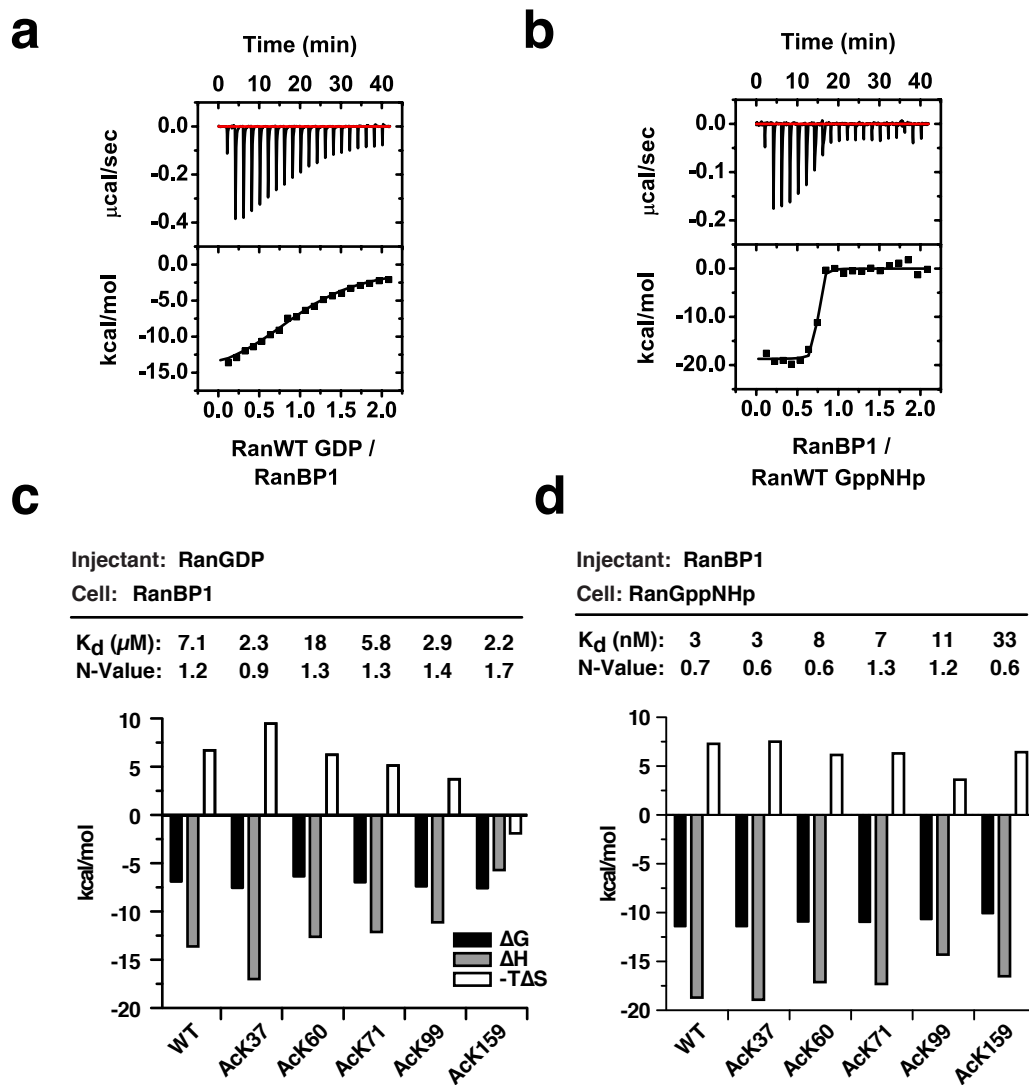


FIGURE 3.6: **Interaction of RanBP1 with acetylated Ran.** (a) ITC trace of RanBP1 (20  $\mu\text{M}$ ) titrated with RanGDP (200  $\mu\text{M}$ ) at 20°C. (b) RanGppNHp (5  $\mu\text{M}$ ) titrated with RanGppNHp (50  $\mu\text{M}$ ) at 20°C. (c and d) Signature plots, N-values and affinities observed for binding of RanBP1 to acetylated RanGDP or RanGppNHp variants, respectively. Conditions were as in (a) and (b), respectively. The ITC traces can be found in the Appendix A.3 and A.4.

### 3.1.5 Ran acetylation interferes with export complex formation

According to the current model, RanGTP and cargo cooperatively bind to export receptors to mediate the cargo export (Monecke et al., 2013). CRM1 is a major export receptor for many different cargo proteins, which bind to CRM1 via an NES. To model export complex formation *in vitro*, Spn1 was used as a cargo protein, which itself is an import adapter for spliceosomal snRNPs and thus has to

be recycled into the cytoplasm by nuclear export (Huber et al., 1998). The reason for this choice was that it has been studied extensively for its binding mechanism to CRM1, including the solution of the crystal structure of Spn1 in complex with CRM1 and RanGTP (Monecke et al., 2009).

To establish an ITC-based export complex formation assay, the different combinations of interaction partners were first tested for binding. The measurements had to be carried out at 10°C and a lower stirring speed (700 rpm) since CRM1 showed a tendency to precipitate at higher temperatures and at the usual stirring speed of 1000 rpm. First, binding of Spn1 to CRM1 was measured at 200  $\mu\text{M}$  and 20  $\mu\text{M}$ , respectively. The resulting binding isotherm is similar to those of previously reported ITC experiments and yields a comparable affinity of 1.2  $\mu\text{M}$  (Fig. 3.7 top left; reported affinity: 1.4  $\mu\text{M}$ ). Also in accordance with published data, the titration of CRM1 with RanGppNHp did not produce an isotherm that would indicate a binding event (Dong et al., 2009) (Fig. 3.7 bottom left). Other groups have reported that RanGTP binds to CRM1 with a  $K_D$  in the micromolar range, which is lowered to a low nanomolar value in the presence of Spn1 (Paraskeva et al., 1999; Petosa et al., 2004). When determined by ITC, an improvement in binding was indeed observed in presence of Spn1, yielding a  $K_D$  of 2  $\mu\text{M}$  for the interaction of RanGppNHp with CRM1 (Fig. 3.7 top right). This affinity is however about three orders of magnitude lower than previously described. A possible explanation for this discrepancy might be that binding constants have previously been determined with an indirect GAP-protection assay, in which the RanGAP-stimulated GTP hydrolysis is used as a readout for the amount of CRM1-bound RanGTP (a state in which GTP hydrolysis cannot occur). As suggested by the cooperative model of export complex formation, the interaction of Spn1 and CRM1 was also improved in presence RanGppNHp, resulting in a  $K_D$  of 280 nM instead of 1.2  $\mu\text{M}$  (Fig. 3.7 bottom right). Albeit the difference regarding the binding affinity of Ran to the CRM1·Spn1-complex, the ITC-based *in vitro* assay thus overall reflected the proposed mechanism of export complex formation (Fig. 3.7 center) (Monecke et al., 2013).

In the crystal structure of the CRM1·Spn1·RanGTP CRM1 complex, Ran is embedded in the center of the ring-shaped CRM1. Spn1, in turn, is bound to outer surface of of this ring, not directly contacting Ran. However, given the cooperativity in binding to CRM1, there is a clear indirect influence of Ran on the CRM1·Spn1 interaction and *vice versa*. CRM1 and Ran have a large binding interface

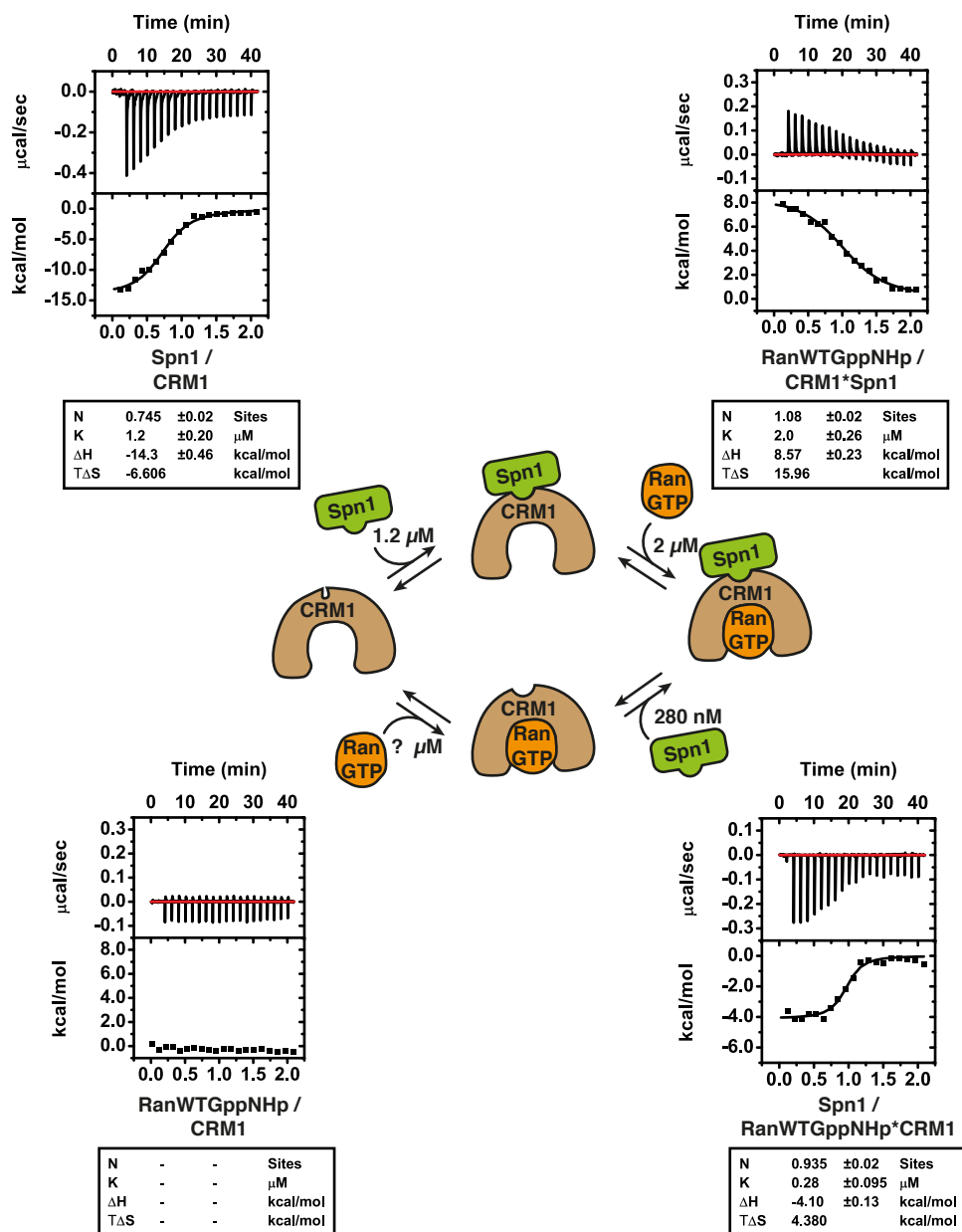


FIGURE 3.7: ITC-based *in vitro* export complex formation assay. Isotherms of ITCs with indicated proteins or protein complexes. All measurements were carried out at 10°C. In each case, for the titrant, a concentration of 200 µM was used and 20 µM for the analyte. Complexes were preformed with a two-fold molar excess of Ran or Spn1 as indicated. The model in the center illustrates the different binding combinations with affinities measured by ITC in this study.

involving two electrostatic interactions between K37<sup>Ran</sup> and D931/T932<sup>CRM1</sup>, and between K71<sup>Ran</sup> and D436/E843<sup>CRM1</sup> (Fig. 3.8a, PDB: 3GJX).

Ran acetylation could either directly influence the Ran-CRM1 interaction or could indirectly alter the ability of RanGTP to promote binding of Spn1 to CRM1. The first scenario was tested by titration of the preformed Spn1·CRM1 complex with GppNHp-loaded acetylated Ran variants using the same conditions as described above for RanWT. The binding of RanGppNHp to Spn1·CRM1 was largely unaffected by acetylation. Only RanAcK71 showed a decreased  $\Delta H$  and an about 5-fold decrease in affinity (Fig. 3.8b).

The second scenario was tested by performing the RanGppNHp·CRM1 complex and subsequent titration with Spn1, also as described above for RanWT. Again all acetylated Ran variants were able to bind and, in case of RanAcK37, 99 and 159, the affinity was increased about 4 to 7-fold (Fig. 3.8c). For RanAcK37 and 159, this is due to a more favorable entropic contribution while for RanAcK99 both the enthalpy and entropy contribute to the higher affinity. Given these increased affinities, it is possible that acetylation of K37, 99 and 159 would promote export complex formation.

### 3.1.6 *in vivo* acetylation of Ran by KAT overexpression

Acetylated Ran was so far only found by high-throughput MS, for which enrichment of acetylated peptides with an anti-AcK antibody-resin is a crucial step. Thus, it was interesting to test under which conditions Ran acetylation would be upregulated. However, detection of acetylation turned out to be challenging. In initial attempts, anti-AcK agarose beads from ImmuneChem were used to immunoprecipitate Ran from whole cell lysates of HeLa and HEK293T cells and the eluate was subsequently probed with an anti-Ran-AB. Although these beads have been used for AcK-peptide enrichment in high-throughput MS screen, this approach was unsuitable mainly for two reasons: First, the immunoprecipitation (IP) is ideally carried out under native conditions to ensure the integrity of the antibody, which however also allows for co-immunoprecipitation of Ran by an acetylated binding partner. Second, Ran bound non-specifically to the agarose beads, making the specific detection of acetylated Ran impossible with this method.

As an alternative, Ran was overexpressed by transfection as a His<sub>6</sub>-tagged construct in HEK293T cells. This approach has the major advantage that Ran can be isolated by Ni-NTA pulldown under denaturing conditions in buffer containing

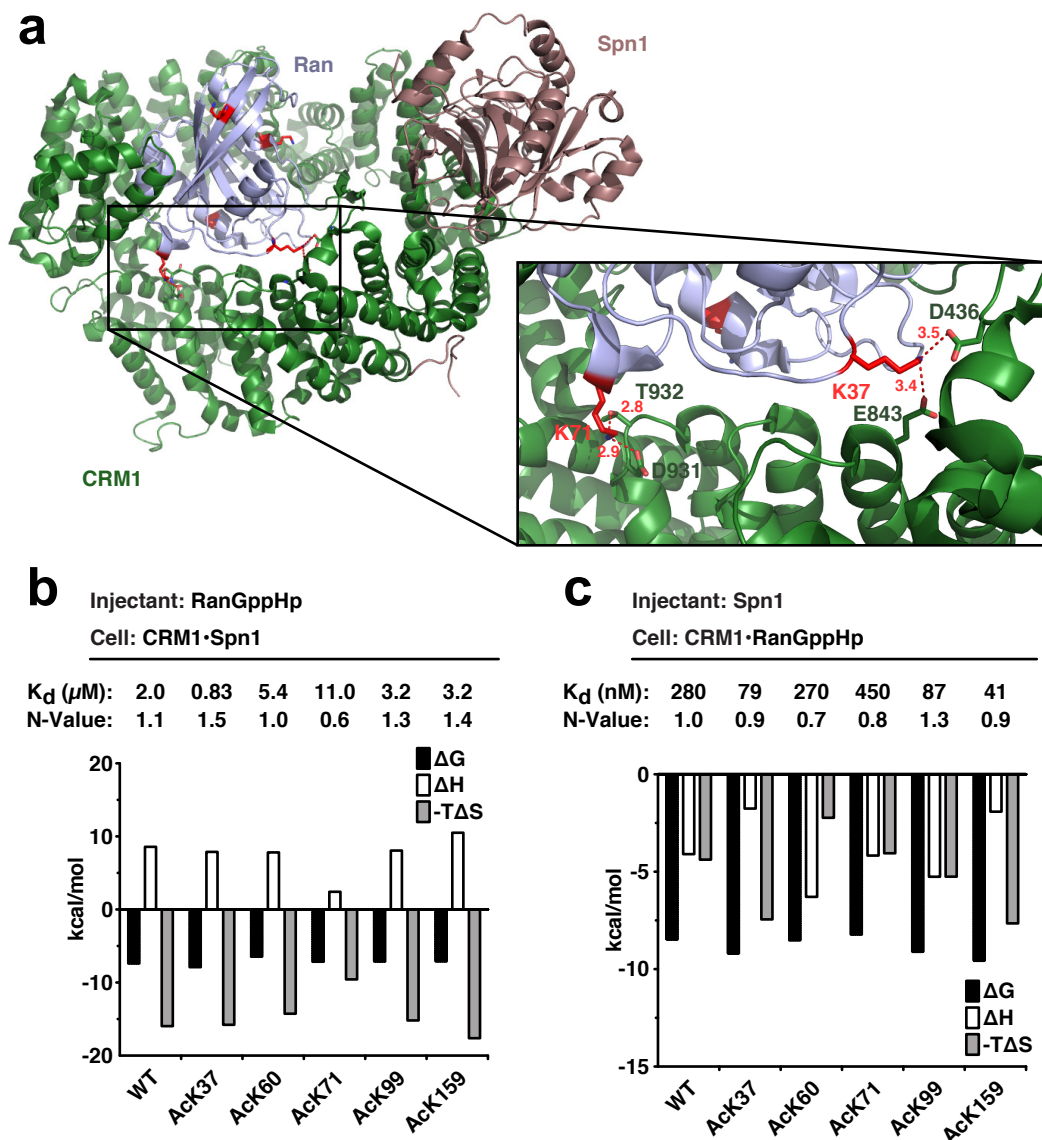


FIGURE 3.8: **Impact of Ran acetylation on *in vitro* export complex formation.** (a) Ribbon plot of the ternary Spn1·RanGppNHp·CRM1 complex with potentially acetylated lysines shown as red sticks. The inset shows details of the salt-bridges involving K37<sup>Ran</sup> and K71<sup>Ran</sup> in the Ran-CRM1 interface (PDB: 3GJX). (b and c) Signature plots, N-values and affinities observed for binding of (b) RanGppNHp (200  $\mu\text{M}$ ) to the Spn1·CRM1 complex (40/20  $\mu\text{M}$ ) or (c) of Spn1 (200  $\mu\text{M}$ ) to the RanGppNHp·CRM1 complex (40  $\mu\text{M}$ /20  $\mu\text{M}$ ). All measurements were carried out at 10°C. The ITC traces can be found in the Appendix A.5 and A.6.

8 M Urea. Under these conditions proteolysis and loss of post-translational modifications is minimized due to the rapid denaturation and hence inactivation of most enzymes in the lysate. After pulldown of His<sub>6</sub>-Ran the eluate was probed with the pan-AcK AB. This method however does not involve enrichment for acetylated

proteins as with the anti-AcK agarose and is thus not suitable for the detection of low-stoichiometry acetylation. Due to the overexpression, it is also not suitable for the analysis of potentially acetylated proteins that are normally present at low levels since the respective KATs may not be sufficiently active for their quantitative modification. An additional complicating factor in the analysis is the fact that detection sensitivity with the anti-AcK-AB varies from site to site. In case of recombinant Ran, the sites AcK37, 99 and 159 showed particularly weak signals even when 250 ng of purified acetylated protein were used for immunoblotting.

As shown in Fig. 3.9a by detection with the anti-Ran-AB, the expression and isolation of His<sub>6</sub>-Ran from the cell lysate worked efficiently. However, no AcK-signal was detected when His<sub>6</sub>-Ran from HEK293T (not shown). Within the limitations of this assay, it can thus be assumed that the stoichiometry of Ran acetylation is low under the cellular condition tested. Also, coexpression of His<sub>6</sub>-Ran with selected KATs (one for each KAT family) did not result in an acetylation signal for Ran, although all KATs were overexpressed as intended (Fig. 3.9a).

To further investigate the acetylation state of Ran, the samples (isolated His<sub>6</sub>-Ran with or without KAT coexpression) were subjected to tryptic digest and subsequently analyzed by tandem MS. Label-free quantification with the MaxQuant software was used to account for differences in protein amounts between samples. The intensities of the acetylated peptides were then normalized by the collected intensities of unmodified Ran peptides in each sample. To increase the statistical robustness of the analysis, the experiment was performed twice. With this method, surprisingly, none of the lysines were found acetylated that have previously described for human samples. Instead, acetylation at K134, K142 and K152 was detected, with AcK152 being only present upon  $\alpha$ -Tubulin overexpression while both AcK134 and AcK152 were found in all but the  $\alpha$ -Tubulin- and Gcn5-samples. Peptide intensities of these latter sites were approximately 2-fold increased upon coexpression with TIP60, CBP and p300 suggesting that these KATs directly or indirectly affect Ran acetylation (Fig. 3.9b).

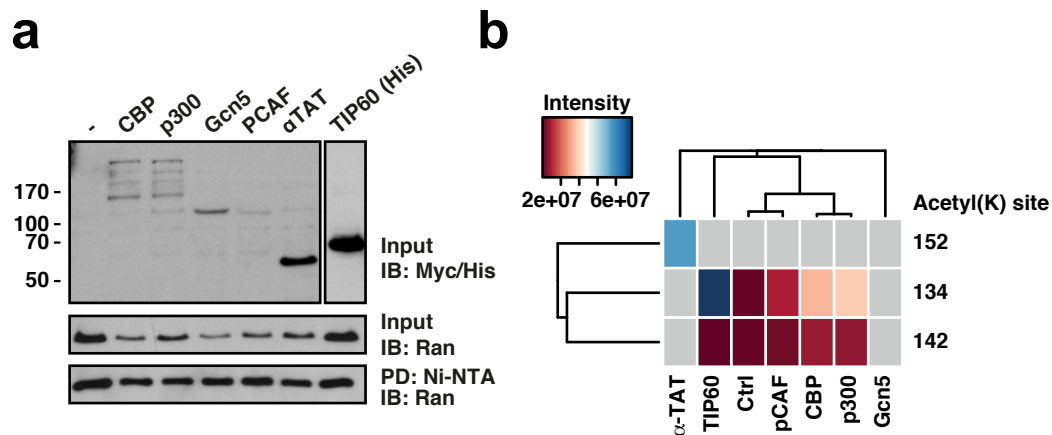


FIGURE 3.9: MS based detection of acetylated Ran in HEK293T cells. (a) Representative immunoblot of input and eluate samples of a Ni-NTA pull-down of His<sub>6</sub>-Ran. The eluate samples containing His<sub>6</sub>-Ran were used for tandem MS-analysis. (b) Intensity plot and hierarchical clustering of acetylated peptides detected by tandem MS. Results from two independent experiments were combined. Grey fields are shown if the corresponding sample was not found in the respective sample.

### 3.1.7 An *in vitro* KDAC screen identifies SIRT1-3 as Ran deacetylases

Next, the regulation of Ran by deacetylases was investigated. Given that, over the course of this work, acetylated Ran was purified in a homogeneous and site-specific manner, opened the possibility to individually test each site for deacetylation by human KDACs. To this end, all eleven ‘classical’ KDACs (Class I, II and IV) and the Sirtuins 1, 3, 6 and 7 (Class III) were obtained from commercial sources as recombinant proteins. The enzymes had been expressed in *E. coli* or in cell lines (insect or mammalian) and tested for activity with fluorogenic acetylated substrate peptides (Fluor-de-Lys assay). At this point, the only KDAC that was not purchased was SIRT2, which was instead purified from *E. coli* in the laboratory. It turned out that the activities of the purchased enzymes differed substantially from the manufacturers specifications. As evident from the data of our own Fluor-de-Lys assay, the signals vary drastically between KDACs although in each case the amount of enzyme was calibrated to theoretically yield the same fold increase over background (Fig. 3.10a and b).

Based on the newly obtained activities, a screen was performed to identify deacetylases of the five investigated acetylation sites of Ran. For this screen, 100 pmol

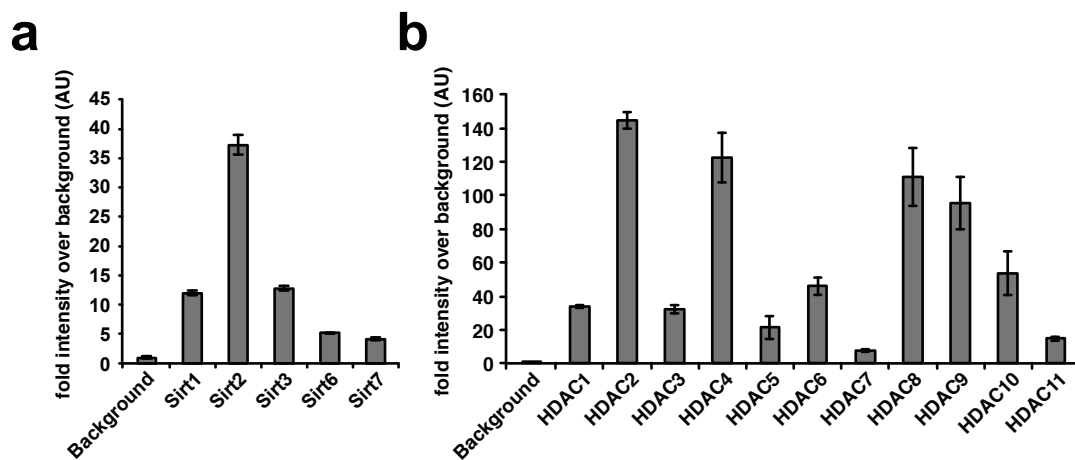


FIGURE 3.10: **Activities of recombinant KDACs used for *in vitro* deacetylase screen.** (a) Fluor-de-Lys assay of recombinant Sirtuins (Class III s). The intensities obtained by fluorescence readout (Ex: 350 nm/ Emission: 450 nm) were normalized to the background signal and are shown as fold increase. Error bars indicate the variation among technical triplicate measurements. (b) The same as in (a) is shown for the classical KDACs (Class I, II and IV).

of recombinant acetylated Ran were mixed with enzyme and incubated at 30°C for 2h (sufficiently long to allow for complete deacetylation if deacetylation of the respective site was as efficient as deacetylation of the fluorogenic peptide substrate). The reactions were run in triplicates and then spotted onto nitrocellulose membranes, which were then subjected to co-immunodetection with antibodies against AcK and His<sub>6</sub>. To allow for densitometric quantification and simultaneous detection of both the AcK and His<sub>6</sub> signals, fluorescent secondary antibodies in different colors were used and fluorescent readout was carried out on a digital scanner. As shown in Fig. 3.11a, none of the Ran acetylation sites were deacetylated by classical KDACs by more than 40%. This is in contrast to the Sirtuin deacetylases (Class III). Here, incubation with SIRT2 led to an almost complete loss of AcK immunoreactivity for RanAcK71. Also, the signal of RanAcK37 was substantially decreased when incubated with SIRT1, -2 and -3 (Fig. 3.11b).

To confirm that SIRT1-3 can deacetylate Ran *in vitro*, the experiment was repeated in a similar fashion but this time analyzed by Western blotting. Again, Ran was robustly deacetylated at K37 by SIRT1-3 and at K71 by SIRT2 after two hours. Deacetylation only occurred in presence of the obligatory co-factor NAD<sup>+</sup> and was inhibited by the pan-Sirtuin inhibitor Nicotinamide (NAM; Fig. 3.12a). Following the reaction over 90 minutes furthermore revealed that deacetylation of

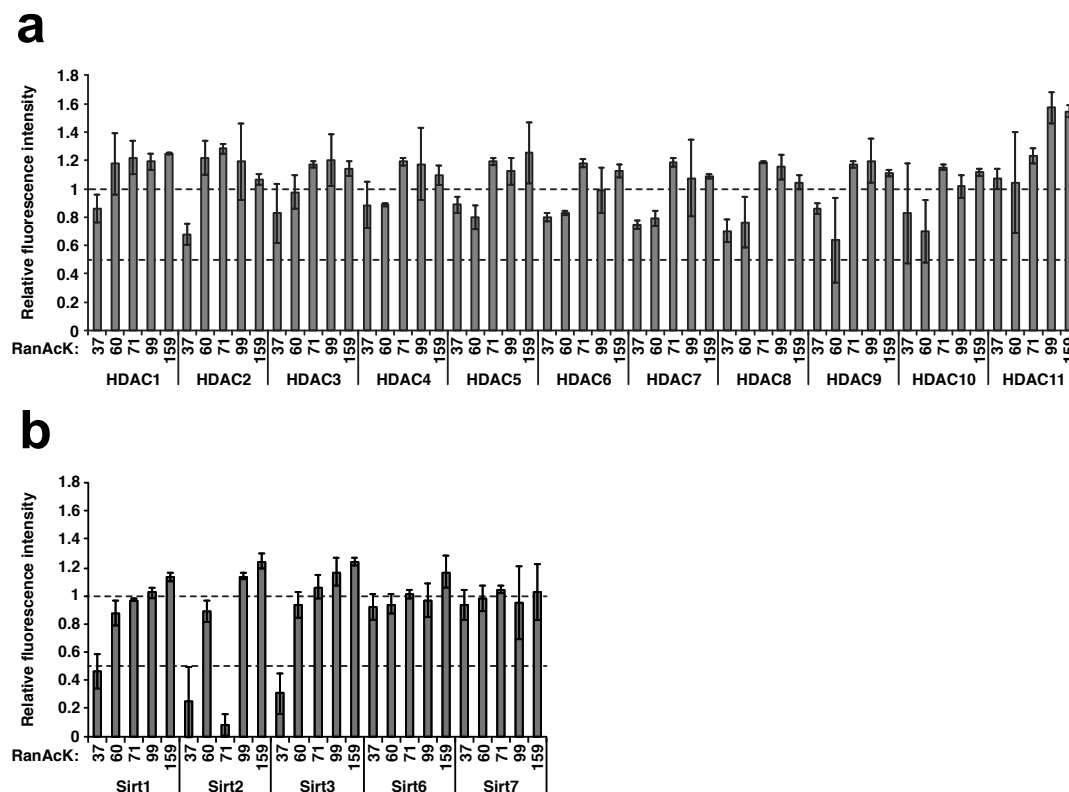


FIGURE 3.11: *In vitro* deacetylase screen for recombinant Ran. (a) Classical KDACs (Class I, II and IV) were tested for deacetylation of Ran acetylated at the indicated sites (incubation for 2 h at 30°C). Detection was performed with an anti-AcK-AB and signals were adjusted based on the anti-His<sub>6</sub> loading control. Signals were normalized to a control reaction without enzyme. Error bars indicate the variation among technical triplicate measurements. (b) As in (a) but for Sirtuin deacetylases (Class III).

RanAcK37 occurred fastest with SIRT2 and again showed the specific deacetylation of RanAcK71 by SIRT2, which however was slower than deacetylation at K37 (Fig. 3.12b). Interestingly, in a microarray-based peptide screen for deacetylation by Sirtuins, neither the RanAcK37 nor -AcK71 peptide was deacetylated, suggesting that immobilization of the peptides prevented deacetylation or that secondary structure elements are required for substrate recognition by these Sirtuins (Rauh et al., 2013).

Since small GNBPs such as Ran change their conformation depending on the bound nucleotide, it was possible to test the influence of structural changes on the deacetylation. Both K37 and K71 are located in the switch regions of Ran (switch I and II, respectively), which change their conformation most dramatically. When GDP- and GppNHp-loaded forms of Ran were compared regarding their deacetylation by SIRT2, RanAcK37 was not differentially deacetylated whereas an increased rate

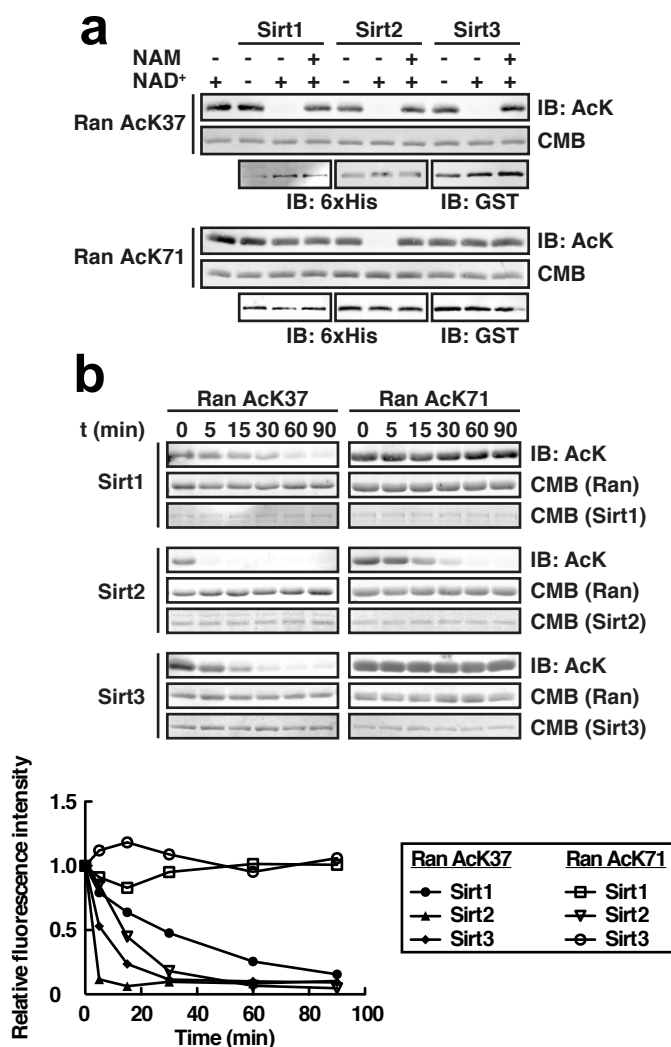


FIGURE 3.12: **Deacetylation of RanAcK37 and -AcK71 by SIRT1-3.** (a) Western blot of deacetylation experiment. Ran was incubated with Sirtuins for 2 h. SIRT1 and -2 are detected with an anti-His<sub>6</sub>-AB. SIRT3 is detected with an anti-GST-AB. Concentration of Ran was 12  $\mu$ M, the concentrations of Sirtuins were chosen according to the activities determined in this study (SIRT1: 0.7  $\mu$ M, SIRT2: 0.5  $\mu$ M, SIRT3: 0.9  $\mu$ M). NAM: Nicotinamide (10 mM). (b) Time course experiment under the same conditions as in (a). Samples were taken at indicated time points. The graph shows the densitometric quantification of the anti-AcK-AB detection.

of deacetylation was observed for GppNHP-loaded RanAcK71 (Fig. 3.13a and b). This is surprising given that the switch II adapts are more rigid confirmation when Ran is GTP-bound and may thus indicate that SIRT2, in addition to a certain sequence context, requires structural elements for substrate recognition, which are not present in the more flexible switch II loop of RanGDP.

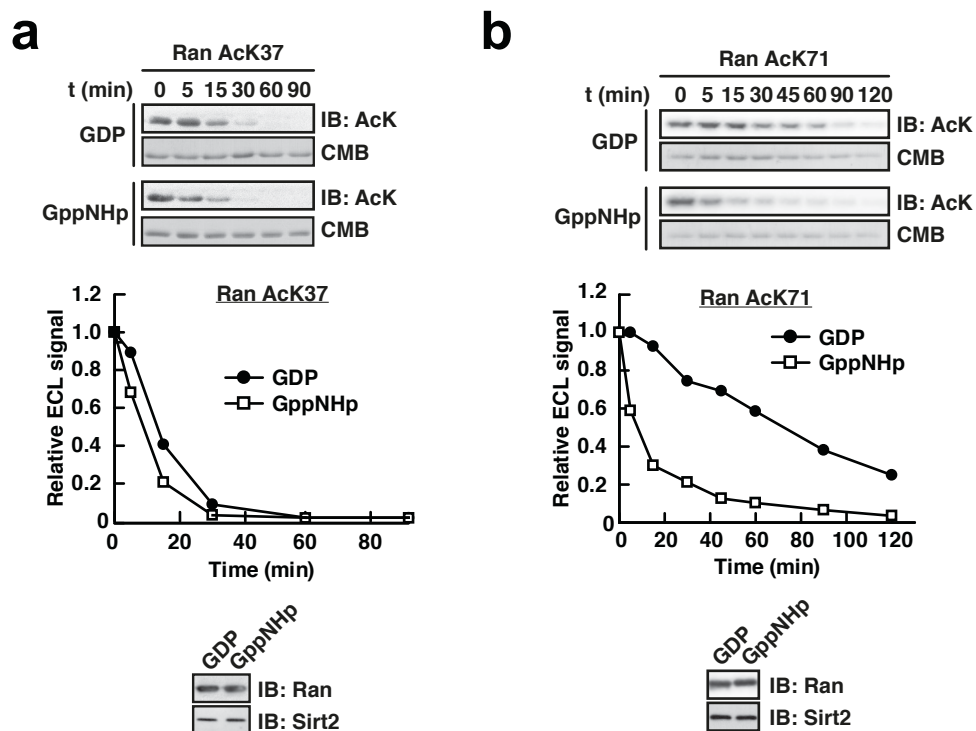


FIGURE 3.13: **Deacetylation of RanGDP and -GppNHp by SIRT2.** (a and b) Time-resolved deacetylation of Ran loaded with GDP or GppNHp as indicated. Concentration of Ran was  $12\ \mu\text{M}$ . The concentration of SIRT2 was  $0.14\ \mu\text{M}$  for RanAcK37 (molar ratio 1:86) (a) and  $0.53\ \mu\text{M}$  for RanAcK71 (molar ratio: 1:23) (b). Samples were taken at indicated time points. The graph shows the densitometric quantification of the anti-AcK-AB detection. This experiment was conducted by and is also shown in the PhD Thesis of S. de Boer (2015).

## 3.2 Analysis of di-deacetylation by Sirtuins

The above results regarding the deacetylation of Ran were the starting point for a series of experiments, which aimed at the elucidation of Sirtuin substrate recognition. The specificity of Sirtuins is highly debated and any further insight in its underlying mechanisms should promote the understanding of Sirtuin biology. With the GCEC at hand, deacetylation could be studied on natively folded proteins rather than short peptides, making the results shown in the following second part of this work particularly valuable for the lysine-acetylation research community.

### 3.2.1 SIRT2 deacetylates Ran at two adjacent lysines

The observation that RanAcK37 is deacetylated by SIRT1-3 and the fact that Ran also contains a lysine at position 38 offered the opportunity to test the sequence specificity of deacetylation. Some studies provide evidence that SIRT1-3 predominantly act on unstructured regions and have little sequence specificity (Blander et al., 2005; Khan and Lewis, 2005) while others implicate that substrate recognition is dependent on the amino acid sequence surrounding the AcK but in a context-dependent fashion (Garske and Denu, 2006; Smith et al., 2011). If indeed SIRT1-3 deacetylate lysines in unstructured regions irrespective of the surrounding sequence, RanAcK38 should be an equally good substrate.

To put the different models of Sirtuin substrate recognition to the test, RanAcK38 and moreover the di-acetylated variant RanAcK37/38 were purified as described above for the other acetylation sites. Both purifications were successful and AcK immunoreactivity indicated the incorporation of AcK as desired. However, the di-acetylated RanAcK37/38 was less pure and lower yields were obtained suggesting that incorporation of AcK is translationally less efficient than that of natural amino acids under the conditions used. A RanAcK37 specific antibody that was initially raised against the peptide TGEFE(AcK)KYVAT to detect acetylation at this site in cell lysates was useful to discriminate between different acetylation states of Ran. It shows high reactivity against RanAcK37, none against RanAcK38 and very weak reactivity against RanAcK37/38 (Fig. 3.14a).

When the three different acetylated Ran variants AcK37, AcK38 and AcK37/38 were tested with SIRT2 in a time course experiment, deacetylation of AcK37 was

substantially faster than that of AcK38 indicating that the amino acid sequence plays a role in substrate recognition. Surprisingly, deacetylation of AcK37/38 was faster than that of the mono-acetylated RanAcK38, showing a rate similar to RanAcK37 (Fig. 3.14b). Measurement of the affinities towards SIRT2 via ITC supports this observation in that both RanAcK37 and -AcK37/38 show an isotherm consistent with an exothermic binding reaction and an affinity of 24 and 9.7  $\mu\text{M}$ , respectively. This in contrast to RanAcK38, which shows no such thermodynamic profile and thus probably binds SIRT2 with much weaker affinity (for the ITCs, SIRT2 without an His<sub>6</sub>-tag was used; concentrations: 45  $\mu\text{M}$  Ran and 450  $\mu\text{M}$  SIRT2; Fig. 3.14c).

### 3.2.2 Mass spectrometric analysis of Ran di-deacetylation

Given the slow rate of AcK38-deacetylation, it seemed likely that deacetylation of RanAcK37/38 occurs sequentially with AcK38 being deacetylated first. To test this hypothesis, RanAcK37, -AcK38 and AcK37/38 were incubated with a two-fold molar excess of SIRT2 and increasing NAD<sup>+</sup> concentrations up to a molar NAD<sup>+</sup>:Ran ratio of 1:1. Due to the excess of SIRT2, deacetylation was expected to occur as a single turnover reaction and to be limited by the availability of the co-factor NAD<sup>+</sup>. As a result, only partial deacetylation of Ran was expected with submolar NAD<sup>+</sup> ratios. The reactions were blotted and either detected with the anti-AcK-AB or the aforementioned specific antibody against RanAcK37 (anti-RanAcK37-AB) using ECL and a CCD-camera system. As anticipated, the acetylation signals of RanAcK37 and -AcK38 decrease with increasing NAD<sup>+</sup>-concentrations when detection was performed with the anti-AcK-AB while the signal of RanAcK37/38 drops only to an intermediate level, indicative of an incomplete di-deacetylation due to the NAD<sup>+</sup>-limitation (two molecules of NAD<sup>+</sup> are needed per di-acetylated substrate).

When detected with the specific anti-RanAcK37-AB, the signal of RanAcK37 drops with increasing NAD<sup>+</sup> amounts (as observed before with the anti-AcK-AB) while, as expected, RanAcK38 shows no signal. Strikingly, the signals of the RanAcK37/38 samples increase toward a NAD<sup>+</sup>:Ran ratio of 1.0, indicating the formation of RanAcK37 during the deacetylation of RanAcK37/38 (Fig. 3.15a and b). However, a substantial difference is observed between the maximum signals of RanAcK37/38 and RanAcK37 when detected with the anti-RanAcK37-AB. This

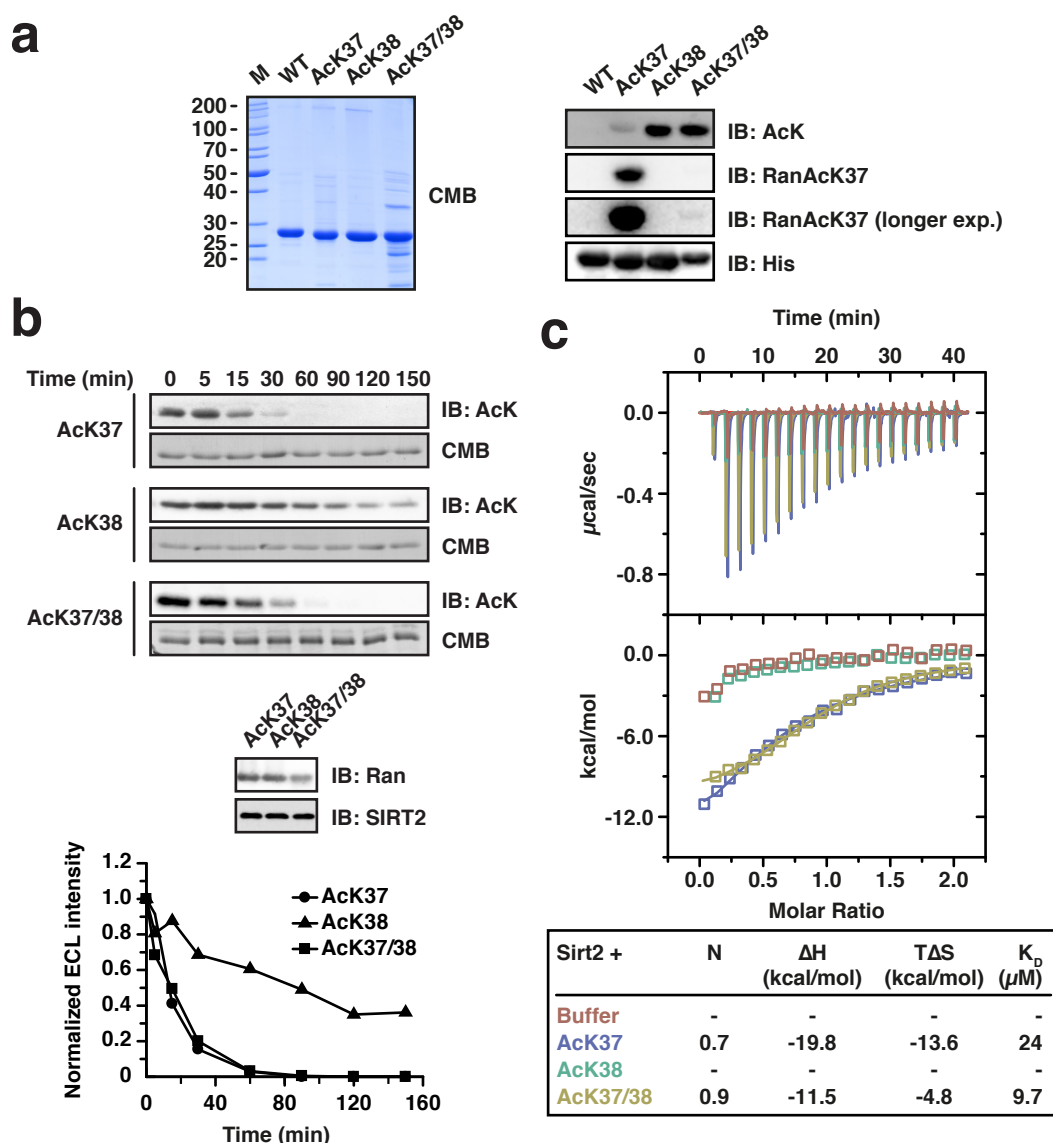


FIGURE 3.14: **SIRT2 can deacetylate Ran at two neighboring lysines.** (a) SDS-PAGE of 5  $\mu g$  of indicated Ran variants stained with Coomassie brilliant blue (CMB) and Western-blot of 250 ng of Ran variants detected with indicated antibodies. (b) Time course of Ran deacetylation by SIRT2. Concentration of Ran was 12  $\mu M$ . The concentration of SIRT2 was 0.14  $\mu M$  (molar ratio 1:86). This experiment was conducted by and is also shown in the PhD Thesis of S. de Boer (2015). (c) Isotherms of ITCs with 45  $\mu M$  Ran and 450  $\mu M$  SIRT2. Measurements were carried out at 20°C in Standard buffer supplemented 10 mM Nicotinamide.

could be due to two different reasons: Deacetylation of RanAcK37/38 might have occurred at both sites with similar preference resulting in one Ran fraction acetyl-modified at K37 (which is detected) and another fraction acetyl-modified at K38

(which is not detected). Alternatively, the reaction product may comprise a mixture of RanAcK37/38, RanAcK37 and fully deacetylated Ran. The latter scenario would be consistent with the fast deacetylation rate observed for RanAcK37/38 since no RanAcK38 would form during the reaction.

To understand in more detail the deacetylation reactions in this experiment, the samples of RanAcK37/38 were subjected to tandem MS. Given the inability of trypsin to cut C-terminally of acetylated lysines, which would result in an undesirably long peptide for the di-acetylated form, GluC was chosen for digestion instead. The data was scanned for peptides containing K37/38, including those that were acetyl-modified. Of these unmodified and acetylated peptides, only a minor fraction was identified by MS/MS as opposed to a larger fraction that was found by matching. While this is not a problem for the di-acetylated peptide since it stands out through its higher mass, identification by matching does not allow the distinction between the AcK37 and the AcK38 peptide due to their same theoretical mass. Moreover, even mono-acetylated peptides that were fragmented could not always be assigned to one particular site, which is an inherent problem of fragment ionization of di-lysine containing peptides. However, all MS/MS spectra that allowed assignment of the acetyl-moiety were consistent with its localization at K37. It thus appears likely that AcK38 peptides were not present in the samples and that mono-acetylated peptides identified by matching or with ambiguous MS/MS spectra correspond to the AcK37 state. This assumption is further corroborated by the fact that also in tryptic digests AcK38 was not found or only at background levels. Consistent with the Western blot data (RanAcK37/38 detected with anti-RanAcK37-AB), the average intensity of the mono-acetylated RanAcK37 peptide increased with increasing  $\text{NAD}^+$  concentrations. This is in contrast to the di-acetylated RanAcK37/38 peptide, the average intensity of which decreases with increasing amounts of  $\text{NAD}^+$  (Fig. 3.15c). Interestingly, also the average intensity of the unmodified is increasing towards higher  $\text{NAD}^+$  ratios, suggesting complete deacetylation of a fraction of initially di-acetylated Ran. This finding is consistent with the Western-blot data where RanAcK37/38, at an  $\text{NAD}^+:\text{Ran}$  ratio of 1.0, did not reach the same level of intensity as RanAcK37 at an  $\text{NAD}^+:\text{Ran}$  ratio of 0.0. Taken together, the above data support the model that SIRT2 first deacetylates RanAcK37/38 at K38 and subsequently at K37.

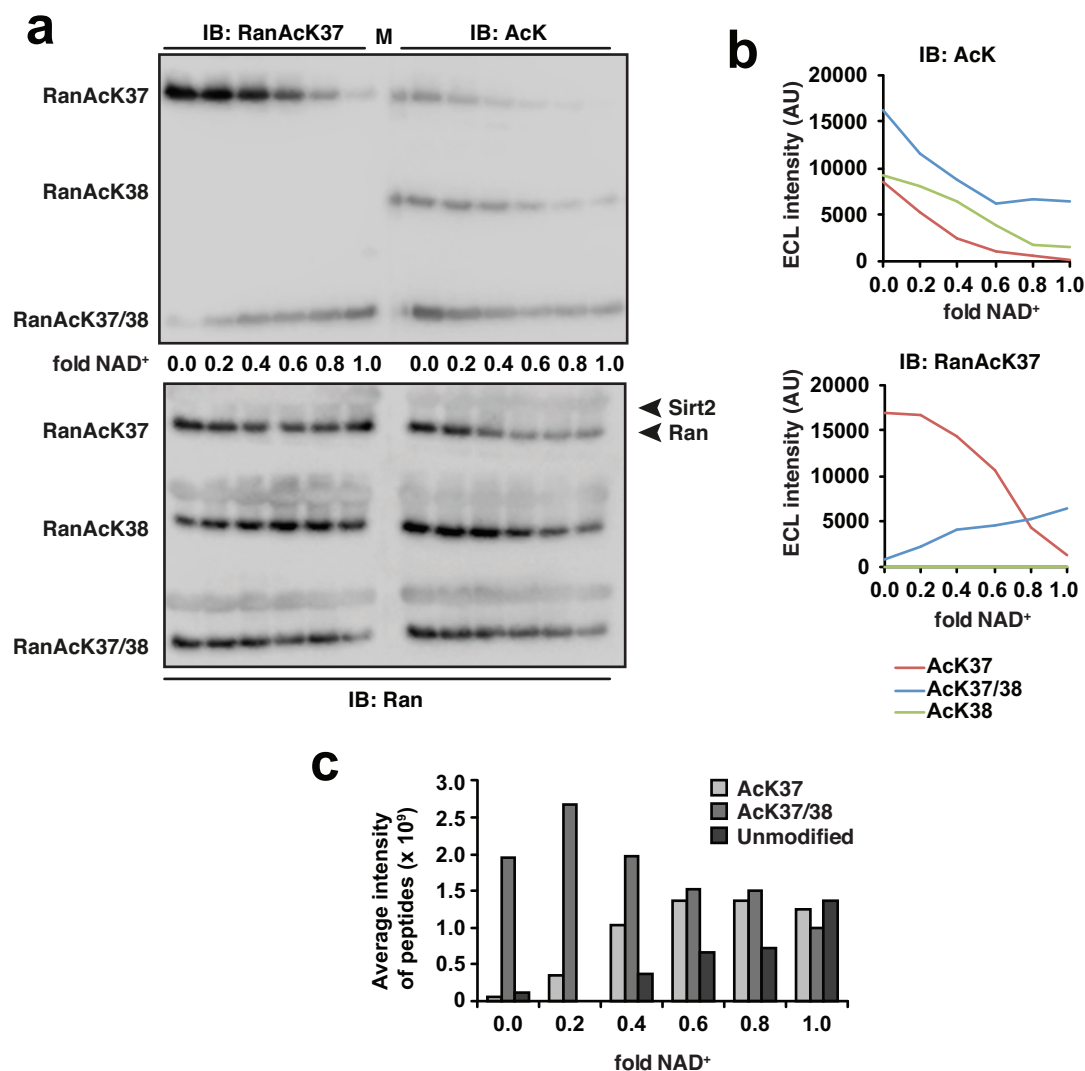


FIGURE 3.15: **Sequential deacetylation of RanAcK37/38.** (a) Ran (12  $\mu$ M) was incubated with SIRT2 (24  $\mu$ M) in presence of the indicated fold-amount of NAD<sup>+</sup>. The reaction was incubated for 10 min followed by Western blotting and detection with antibodies against AcK, RanAcK37 or Ran. (b) The graphs show the raw ECL signal intensity as measured with ImageJ for the indicated antibody detections. (c) Average peptide intensities from MS/MS data of RanAcK37/38 at different NAD<sup>+</sup> amounts. Samples are from the same experiment as in (a) and (b).

### 3.2.3 Mutational analysis of the Ran di-deacetylation site

Since acetylation of K37<sup>Ran</sup> stimulates SIRT2-mediated deacetylation of AcK38<sup>Ran</sup>, it was next investigated whether this effect could be mimicked by the introduction of different amino acids at position 37. Three mutated variants of RanAcK38 were purified, carrying an alanine, glutamine or arginine at position 37 (Fig. 3.16a). Glutamine is often used to mimic an acetylated lysine given its similar charge

characteristics. However, due to the shorter chain length, it cannot account for the sterical effects that might result from acetylation of lysine. The charge conserving mutation to arginine is often used to generate a lysine-mimetic residue that cannot be acetylated. It can however result in steric hindrance and thus effectively mimic the effect of lysine-acetylation in this regard. The mutation to alanine (as the amino acid with the smallest side chain) eliminates any special chemical features at that position.

To test which chemical property of AcK at position 37 prevails in the acceleration of AcK38-deacetylation, the three mutated variants were tested in a time course experiment with SIRT2. As shown in Fig. 3.16b, all three mutations lead to a faster deacetylation of RanAcK38. This suggests that, among those tested, a lysine at position 37 is the least favored residue for deacetylation of the neighboring AcK38. Given the accelerated deacetylation of AcK38 by both the K37Q and the K37R mutation furthermore indicates that steric and charge properties of the acetyl-moiety are important for the faster deacetylation of AcK38 observed upon acetylation of K37.

### 3.2.4 Structural insights into di-deacetylation

To gain structural insights into the recognition of the two neighboring AcK residues, it was attempted to crystallize RanAcK37 or RanAcK37/38 in complex with SIRT2. However, despite significant efforts no crystals were obtained. It should be noted that to date only structures of Sirtuins in complex with substrate peptides have been solved but none with a protein substrate. Instead of co-crystallizing SIRT2 with Ran protein, it was thus tried to use Ran-derived 13-mer peptides. Several analogs of acetyl-lysine have been described, some of which bind substantially stronger to Sirtuins than natural acetyl-lysine and can effectively not be deacetylated (Smith and Denu, 2007). Based on these data, Ran-peptides containing N-( $\epsilon$ )-trifluoroacetyl-L-lysine (TFAcK, peptide sequence: LTGEFEKKY-VATL) were synthesized with the modified residue at the position(s) corresponding to Ran K37, K38 or K37/38.

To confirm that these peptides show binding behavior similar to the full-length Ran protein, their interaction with SIRT2 was tested by ITC. As shown in Fig. 3.17a, the peptides TFAcK37 and TFAcK37/38 bind to SIRT2 with similar affinities of

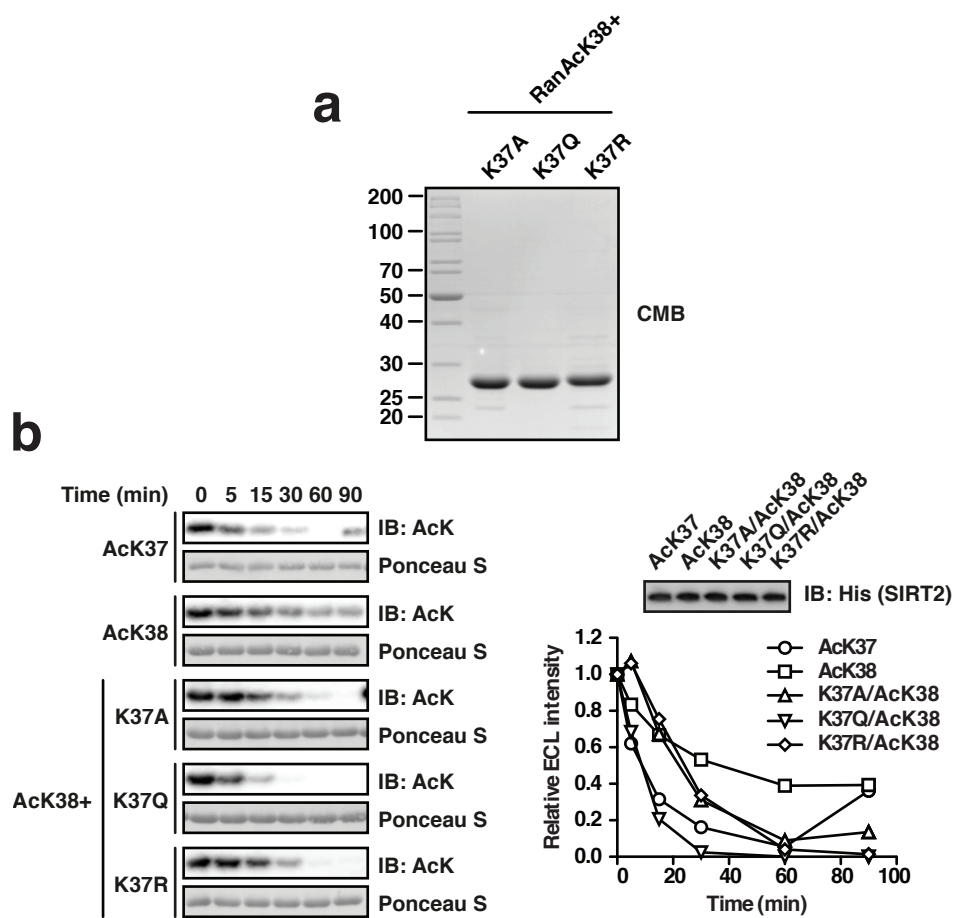


FIGURE 3.16: **Mutational analysis of RanAcK38 deacetylation.** (a) SDS-PAGE of 5  $\mu\text{g}$  of indicated Ran variants stained with Coomassie brilliant blue (CMB). (b) Time course of Ran deacetylation by SIRT2. Concentration of Ran was 12  $\mu\text{M}$ . The concentration of SIRT2 was 0.06  $\mu\text{M}$  (molar ratio 1:200). The graph shows the densitometric quantification.

1.3 and 1.0  $\mu\text{M}$ , respectively while the affinity of TFAcK38 is approximately five-fold lower. Moreover, the binding enthalpy of TFAcK37 and TFAcK37/38 is more favorable than that of TFAcK38 (-11.7 and -11.9 vs. -5.7 kcal/mol). Thus, the peptides reflect the deacetylation behavior of the acetylated Ran protein, which in turn suggests that the amino acid sequence surrounding residues K37 and K38 dictates the order of deacetylation. This conclusion is corroborated by the fact that a peptide with the same sequence containing a 'natural' acetyl-lysine at position K37 was also deacetylated as determined by a dot blot assay and detection with the anti-AcK37-AB (Fig. 3.17b). Attempts to show the same for an AcK37/38 peptide failed due to the low signal intensity upon detection with the anti-AcK-AB (peptides spotted on nitrocellulose were apparently not properly immobilized). However, based on the above data, it appeared reasonable to use these peptides

for co-crystallization with SIRT2 in order to gain insight into the mechanism of the di-deacetylation.

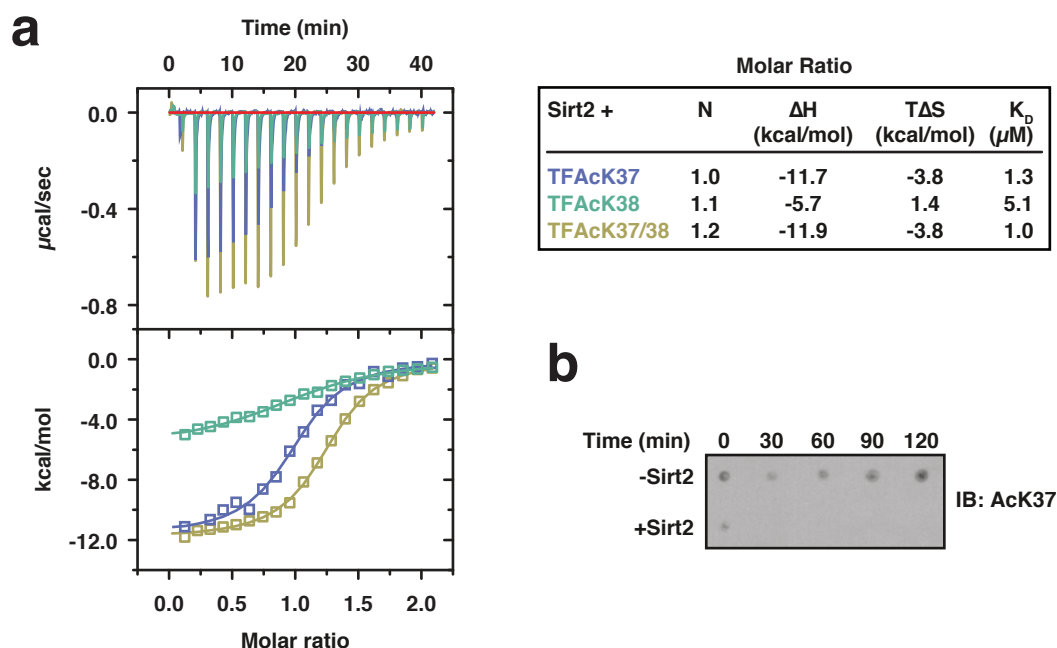


FIGURE 3.17: **Interaction of Ran-derived N-( $\epsilon$ )-trifluoroacetyl-L-lysine peptides with SIRT2.** (a) ITC data of 30  $\mu M$  SIRT2 titrated with 300  $\mu M$  of the indicated peptide. Measurements were carried out at 20°C. (b) Dot-blot showing the deacetylation of a peptide with the same sequence but containing a natural acetyl-lysine at the K37-position. Concentrations were 133  $\mu M$  for the peptide and 0.5  $\mu M$  for SIRT2.

Three SIRT2 constructs with different lengths were purified for the co-crystallization screens, two of which were previously successfully crystallized (Finnin et al., 2001; Yamagata et al., 2014). The resulting proteins were highly pure and thus suitable for crystallization (Fig. 3.18a). To set up the initial crystallization screens, each of the three SIRT2 constructs (at 10 mg/ml) was mixed with a 1.2-fold molar excess of RanTFAcK37 or RanTFAcK37/38 13-mer peptide. Sitting-drop plates were used with three wells to allow for simultaneous screen of all three constructs.

For the RanTFAcK37-13-mer peptide together with SIRT2<sub>50-356</sub>, three crystallization conditions were found (0.1 M HEPES pH 7.5/2.0 M NH<sub>4</sub>SO<sub>4</sub>, 0.2 M K-Na-tratrate pH 5.6/0.1 M Na<sub>3</sub>-citrate/2.0 M NH<sub>4</sub>SO<sub>4</sub>, 2.4 M Na<sub>2</sub>-malonate pH 7.0), all giving rise to growth of hexagonal-bipyramid crystals (Fig. 3.18b). Apart from the crystals, precipitate was present, indicating that crystallization conditions could be further optimized. However, the crystals did not reappear when optimization

screens were performed. Thus, despite their small size ( $\sim 50 \mu\text{m} \times 20 \mu\text{m} \times 50 \mu\text{m}$ ), the initially obtained crystals were used for data collection (crystals from the 0.1 M HEPES pH 7.5/2.0M  $\text{NH}_4\text{SO}_4$  condition).

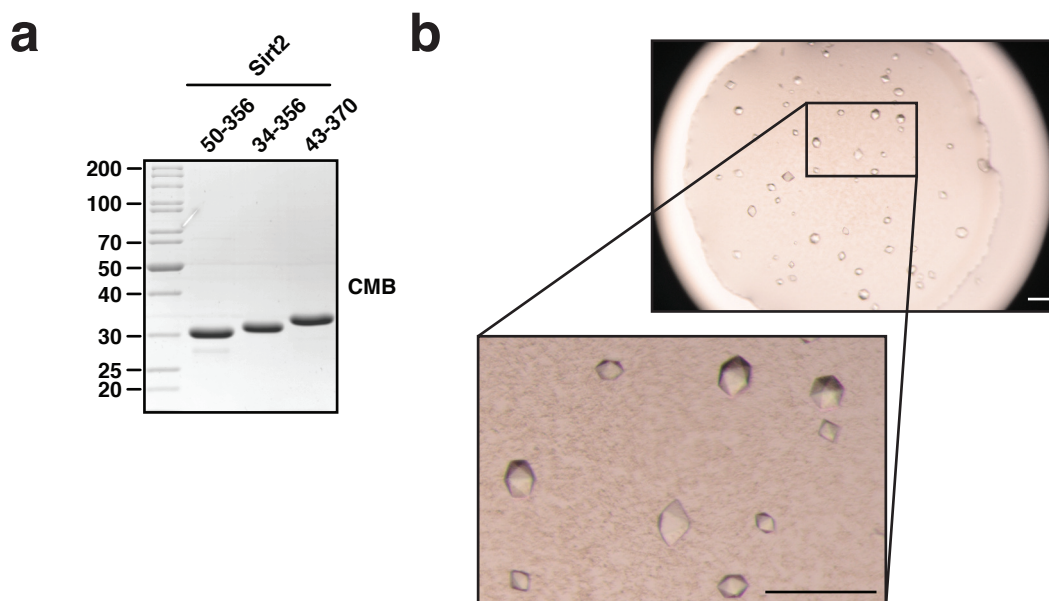


FIGURE 3.18: **Crystallisation of SIRT2 with a RanTFAcK37 13-mer.** (a) SDS-PAGE of 5  $\mu\text{g}$  of indicated SIRT2 constructs stained with Coomassie brilliant blue (CMB). (b) Micrographs of protein co-crystals of SIRT2 and the TFAcK37 13-mer grown in 2.4 M Na-malonate pH 7.0. Scale bar: 100  $\mu\text{m}$ .

The atomic structure of the complex was solved by molecular replacement and refined up to a final resolution of 3.0  $\text{\AA}$ . For molecular replacement, the previously solved structure of SIRT2 with a TFAcK-containing cyclic peptide was used as a search model (PDB: 4L3O; Yamagata et al., 2014). The crystals contained two SIRT2(50-356) $\cdot$ RanTFAcK37-13-mer complexes per asymmetric unit and belonged to the spacegroup  $P6_122$ . Data collection refinement statistics as well as the validation of the structure are shown in Table 3.2.4 and in Appendix A.7.

The solved structure of SIRT2(50-356) $\cdot$ RanTFAcK37-13-mer is shown in Fig. 3.19a. As expected, the TFAcK residue is deeply buried in the active site of SIRT2 while the N- and C-terminal residues are located along the central binding groove formed between the  $\text{Zn}^{2+}$ -binding domain and the Rossmann-fold domain. Sufficient electron density of the peptide was only observed for the residues E34–V40. Thus, the N-terminal residues L30, T31 and L32 as well as the C-terminal residues A41 and T42 are not included in the structure. This may be a result of their flexibility

TABLE 3.1: Data collection, refinement and structure validation of the SIRT2(50-356)·RanTFAcK37-13-mer-peptide structure (molecular replacement).

SIRT2(50-356)·RanTFAcK37-13-mer	
<b>Data collection</b>	
Space group	P6 <sub>1</sub> 22
Cell dimensions	
<i>a</i> , <i>b</i> , <i>c</i> (Å)	114.95, 114.95, 206.48
$\alpha$ , $\beta$ , $\gamma$ (°)	90.0 90.0 120.0
Resolution (Å) <sup>a</sup>	56.61 – 3.00 (3.18 – 3.00)
Observed reflections	187174 (31766)
Unique reflections	16888 (2655)
$R_{sym}$ or $R_{merge}$ <sup>b</sup> (%)	18.0 (72.1)
$R_{meas}$ <sup>b</sup> (%)	19.7 (78.6)
$I/\sigma I$	13.7 (3.9)
CC <sub>1/2</sub> <sup>c</sup>	0.994 (0.840)
Completeness (%)	100.0 (100.0)
Redundancy	11.1 (12.0)
<b>Refinement</b>	
Resolution (Å)	56.61 (3.0)
No. of used reflections	15978
$R_{work}/R_{free}$ <sup>b</sup>	23.16/27.11
Number of non-hydrogen atoms	
Total	4606
Protein	4417
SO <sub>4</sub> <sup>2-</sup> /Zn <sup>2+</sup>	10/2
Water	177
B-factors (Å <sup>2</sup> )	
Protein	49.05
SO <sub>4</sub> <sup>2-</sup>	72.23
Zn <sup>2+</sup>	93.43
Water	51.94
Average B-factors (Å <sup>2</sup> )	
main chain	48.75
side chain	49.35
all atoms	49.23
R.m.s. deviations	
Bond lengths (Å)	0.010
Bond angles (°)	1.537
Ramachandran plot <sup>d</sup> (%)	
Favored	95.4
Allowed	4.4
Outliers	0.2

<sup>a</sup> Values for the highest-resolution shell in parentheses.

<sup>b</sup> see Material and Methods 2.6.3.

<sup>c</sup> CC<sub>1/2</sub>: correlation coefficient from Diederichs and Karplus (2013).

<sup>d</sup> MolProbity (Chen et al., 2010).

in the SIRT2-bound state of the peptide and may furthermore indicate that these residues have a low contribution to SIRT2-binding.

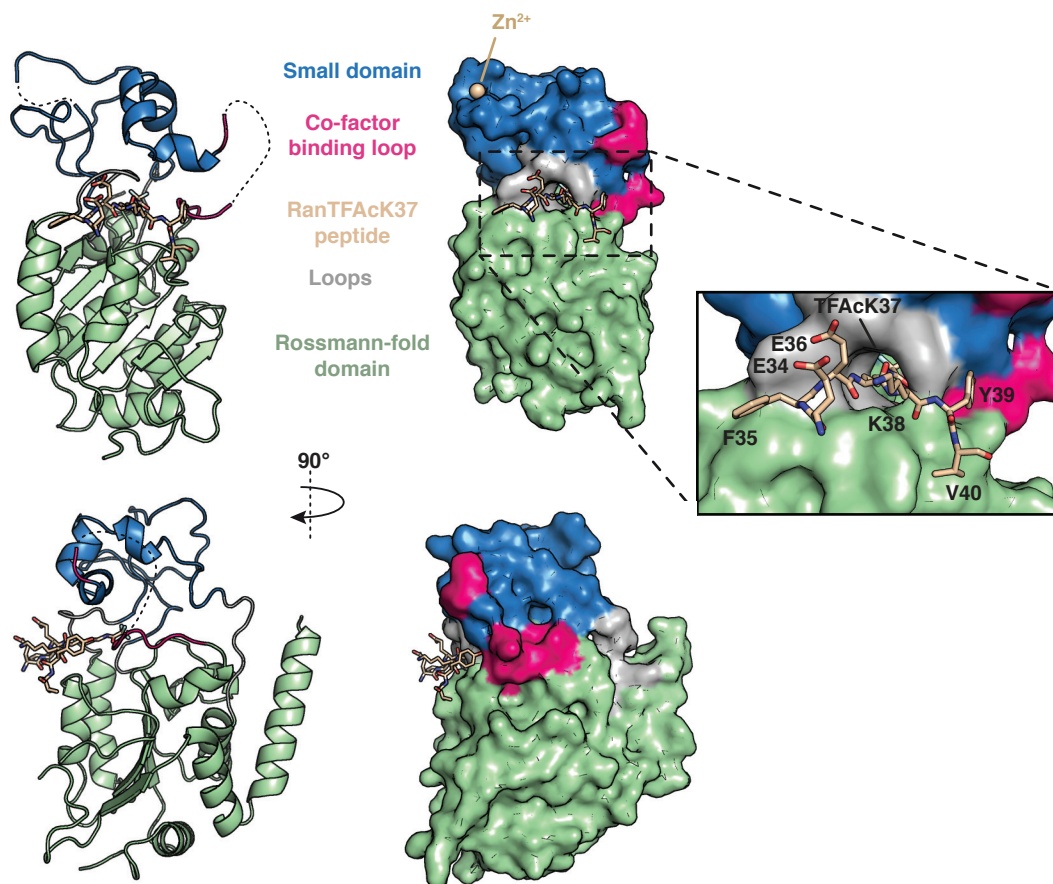


FIGURE 3.19: **Structure of SIRT2 with RanTFAcK37 13-mer peptide.** Overview of the SIRT2(50-356)·RanTFAcK37-13-mer-peptide structure is shown in ribbon and surface representation with the domains indicated in different colors (compare with Fig. 1.8). The peptide is shown as stick model. The close up shows the peptide with residue numbering according to the Ran protein sequence.

Interestingly and consistent with previous substrate-Sirtuin structures (Avalos et al., 2002; Zhao et al., 2003), the RanTFAcK37-13-mer is bound to the substrate binding groove of SIRT2 mainly via hydrogen bonds between main chain atoms of SIRT2 and the peptide (Fig. 3.20). In addition, the aromatic side chains of F35 and Y39 are possibly involved in stacking interactions with the residues F244 and F235 of SIRT2, respectively, suggesting that they have a role in the specific recognition of the peptide (and most likely also RanAcK37). In case of RanAcK38, these additional side chain interactions may not be possible due to the positional shift by one residue, which could lead to the slower deacetylation of this site by SIRT2. To clarify how SIRT2 specifically deacetylates Ran first at K38 in the di-acetylated AcK37/38 background, attempts were made to also

crystallize SIRT2 in complex with the TFAcK37/38-peptide, which however were not successful. It is thus not possible to draw conclusions about the binding of SIRT2 to this peptide.

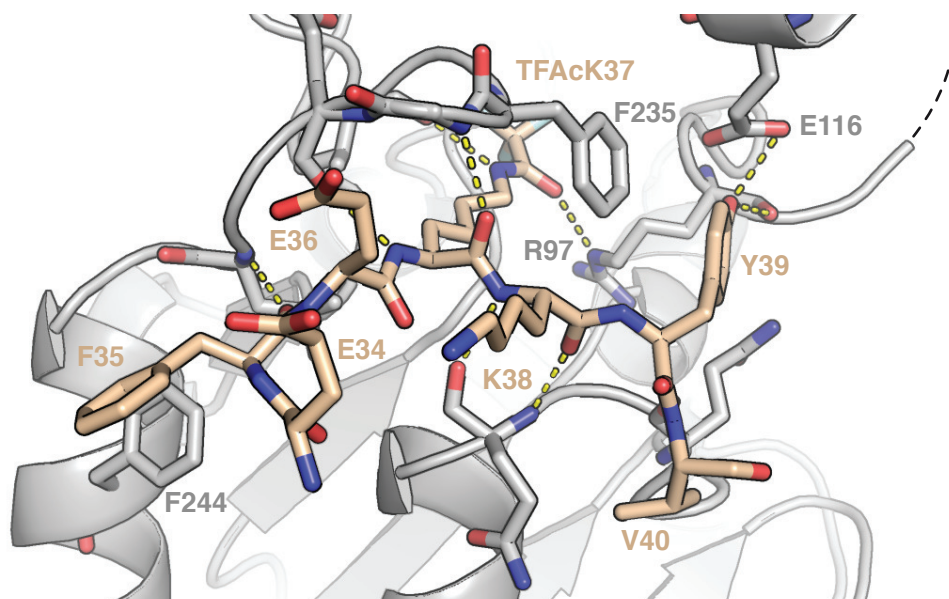


FIGURE 3.20: **Molecular interactions between SIRT2 and the Ran-TFAcK37 13-mer peptide.** Polar interactions between the peptide and SIRT2 are depicted. The peptide (brown) is shown as stick model and SIRT2 (grey) as ribbon model except for the residues participating in polar interactions.

### 3.2.5 SIRT1 and SIRT3 are able to di-deacetylate Ran

To check if the ability to deacetylate two neighboring AcKs is universal to Class I Sirtuins, SIRT1 and SIRT3 were also tested with RanAcK37/38 as a substrate. As shown above in Fig. 3.12, RanAcK37 is not only deacetylated by SIRT2 but also SIRT1 and SIRT3 and it thus appeared reasonable that the di-acetylated variant would likewise be deacetylated by these closely related enzymes. SIRT1 and SIRT3 were purified using a two-step purification strategy, involving affinity chromatography followed by SEC (Fig. 3.21a). Again, the activity of Sirtuins 1-3 was determined by a Fluor-de-Lys assay but this time at multiple concentrations and thus greater accuracy. It turned out that all three Sirtuins had similar activities so that the same molar concentrations could be used for deacetylation assays (Fig. 3.21b). When RanAcK37/38 and RanAcK38 were tested with SIRT1 and SIRT3, a robust deacetylation was observed for both, although slower than

for RanAcK37. Furthermore, similar to the behavior of SIRT2, deacetylation of RanAcK38 was slower than RanAcK37 suggesting that Sirtuins 1-3 share molecular features of substrate recognition and the ability to di-deacetylate substrate proteins.

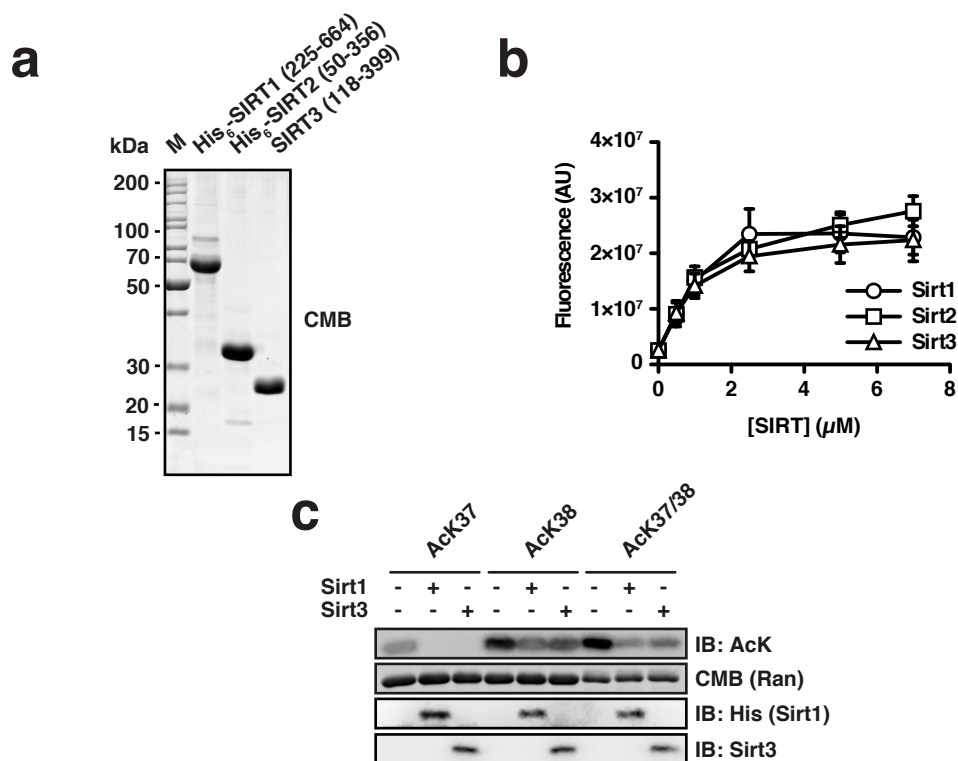


FIGURE 3.21: **Di-deacetylation by SIRT1 and SIRT3.** (a) SDS-PAGE of 5 µg of indicated Sirtuin constructs stained with Coomassie brilliant blue (CMB). (b) Fluor-de-Lys activity assay of Sirtuins. Error bars represent three independent measurements. (c) Western-blot of deacetylation experiment. The reaction was performed for 30 min. 12 µM of Ran was incubated with 0.8 µM of the indicated Sirtuin.

### 3.2.6 PEPCK1 is not deacetylated by SIRT2 *in vitro*

In a physiological context, the acetylation of a lysine residue with an unfavorable sequence context for deacetylation (such as K38 of Ran) would be relatively stable, which could result in a lasting effect on protein function and/or intracellular signaling processes. The acetylation of a neighboring lysine could then lead to a release from this situation by stimulating the deacetylation of both residues by Sirtuins 1-3.

Along these lines, the literature was screened for proteins, which have been shown to be acetylated at two neighboring lysine residues and deacetylated by SIRT1, -2 or -3. One such case is phosphoenolpyruvate carboxykinase 1 (PEPCK1), which plays a major role in gluconeogenesis and for which acetylation of residues K70, K71 and K594 has been reported. Acetylation of PEPCK1 promotes its degradation and is negatively regulated by SIRT2 (Jiang et al., 2011). Not only is PEPCK1 acetylated at two neighboring lysine residues but these two lysines are followed by a tyrosine (KKY) as is also case for RanAcK37. It appeared possible that this sequence represents a short motif for di-deacetylation. Interestingly, in an *in vitro* selection screen for cyclic peptidic inhibitors of SIRT2, 10 out of 15 isolated high affinity clones were found to contain the sequence R(I/V)(TFAcK)RY. The IC<sub>50</sub>'s of these cyclic peptides was in the low nanomolar range but also a shorter linear peptide with the sequence RI(TFAcK)RY showed an IC<sub>50</sub> of 31 nM (Morimoto et al., 2012). Given that arginine is physicochemically similar to lysine, these results seemed to support the assumption that KKY is a target motif of SIRT2.

Full-length PEPCK1-WT, -AcK70, -AcK71, -AcK70/71 and, for comparison, also -AcK594 were purified with the GCEC. The resulting protein was approximately 80% pure and, when probed with the anti-AcK-AB, the acetylated variants showed a signal while PEPCK1-WT did not (Fig. 3.22a). As an additional measure of protein quality, the enzymatic activity of the recombinant PEPCK1 was confirmed. In this activity assay, the PEPCK1-catalyzed reaction of phosphoenolpyruvate to oxalacetate is coupled with the quantitative reduction of oxalacetate to malate by malate dehydrogenase. In the latter reaction step, NADH is oxidized to NAD<sup>+</sup>, which can be traced by a drop in emission at 470 nm when excited at 350 nm (see Material and Methods 2.3.14). The specificity of the assay was tested by sequential addition of reaction components. A significant drop in fluorescence was only observed when PEPCK1 was added and the reaction was drastically accelerated upon addition of Mn<sup>2+</sup> (MnCl<sub>2</sub>), which is a PEPCK1 co-factor. The slow reaction rate observed without Mn<sup>2+</sup> suggests that only a fraction of PEPCK1 protein purified from *E. coli* is Mn<sup>2+</sup>-bound. All PEPCK1 variants displayed robust activity in this assay showing that the PEPCK1 was purified from *E. coli* in an active form. Moreover, PEPCK1-AcK71 showed an increased catalytic rate and reached a higher final fluorescence level. However, this observation has to be taken with caution since the purity between the different PEPCK1 varies and thus the true amount of enzyme in the assay cannot be accurately determined (Fig. 3.22b).

Surprisingly, none of the acetylated PEPCK1-variants were deacetylated by SIRT2 *in vitro* when tested with low amounts of enzyme in preliminary experiments (not shown). To rule out that deacetylation just occurs at a much slower rate (compared for instance to RanAcK37), PEPCK1 was incubated for 2 h at 23°C with increasing amounts of SIRT2 up to an equimolar ratio. Again, under the experimental conditions used, no deacetylation was observed (Fig. 3.22c). Since only a fraction of the purified PEPCK1 was active due to the lack of the co-factor  $Mn^{2+}$ , the experiment was repeated in  $MnCl_2$ -containing buffer. Moreover, the concentration of PEPCK1 was lowered to avoid possible multimerization or aggregation of PEPCK1, which could limit access of SIRT2 to the PEPCK1 acetylation sites. However, no deacetylation was observed at a 1:1 enzyme:substrate-ratio over the course of 2 h (Fig. 3.22d).

It was thus tested if mutation of the amino acid residues surrounding the di-acetylated site K70/71 would facilitate deacetylation by SIRT2. Two mutant variants of PEPCK1 were cloned, each coding for three amino acid substitutions N- or C-terminally of the assumed binding motif KKY by the according Ran sequence (natural PEPCK1 sequence: RRLKKYDNC, natural Ran sequence: EFEKKYVAT, 'EFE'-mutant: EFEKKYDNC, 'VAT'-mutant: RRLKKYVAT). However, in contrast to the EFE-mutant, the VAT-mutant could not be purified from *E. coli* despite significant efforts. The EFE-mutant was tested for deacetylation by SIRT2 in the di-acetylated PEPCK1-AcK70/71-background. Strikingly, as the time course experiment in Fig. 3.22e demonstrates, the PEPCK1-EFE mutant was deacetylated efficiently with a similar rate compared to RanAcK37. Since the deacetylation signal completely disappears over the course of the experiment, it is likely that both acetyl-moieties of PEPCK-70/71-EFE are removed by SIRT2. Taken together, these results suggest that, at least *in vitro*, PEPCK1 is not a substrate of SIRT2. However, mutation of three amino acids N-terminal to the assumed SIRT2 binding motif KKY is sufficient to convert PEPCK1 into a SIRT2-substrate, facilitating deacetylation of both AcK70 and AcK71. Thus, these residues (and possibly also the residues VAT, which are found C-terminally of the KKY motif in Ran) appear to dictate the substrate binding of SIRT2.

### 3.2.7 Deacetylation of p53-AcK381/382

Next, the question whether di-deacetylation is a general mechanism was further investigated with the tumor suppressor p53. The acetylation of p53 is required for its stabilization and transactivation, which in turn leads to apoptosis and/or cell-cycle-arrest. Acetylation of p53 has been described for 13 different lysines, among them also two lysine pairs (K372/373 and K381/382) in the C-terminal regulatory domain (Brooks and Gu, 2011; Reed and Quelle, 2014). To date, p53 has been described to be deacetylated by KDAC1 and SIRT1, although some evidence also points towards deacetylation by SIRT2 (Hoffmann et al., 2014; Peck et al., 2010). While KDAC1 deacetylates p53 at K320, K373 and K382 (Ito et al., 2002), SIRT1 is largely active on K382 (Vaziri et al., 2001) and potentially also K120 and K164 (Zhang et al., 2014b). Importantly, the KATs CBP and p300, *inter alia*, acetylate p53 at both lysine pairs, K372/373 and K381/382 (Gu and Roeder, 1997). Whether the di-acetylation at K381/382 can also be removed by SIRT1 has however not been tested. In a physiological context, the order and magnitude of deacetylation by SIRT1 could have direct consequences on the activation levels of p53. For instance, a preferential deacetylation of AcK382 in presence of an acetylated K381 would effectively lead to a faster inactivation of p53. On the other hand, it is also possible that acetylation of both K381 and K382 decreases the rate of deacetylation by SIRT1 and would thus promote p53 activity.

To investigate these different possible scenarios, acetylated and wild type p53 was purified using the GCEC. However, in this case the expression of His<sub>6</sub>-tagged protein and purification by Ni-NTA chromatography was not successful. Hence, p53 was cloned into a vector allowing for the expression of GST-tagged acetylated protein. With this strategy GST-p53 could be expressed but the treatment with TEV-protease to remove the GST-tag was very inefficient when performed on the column. This was possibly due the tendency of GST to dimerize plus the known tetramerization of p53, which may lead to an occluded TEV-cleavage site. Thus, GST-p53 was instead eluted first from the column and then treated with TEV-protease in solution. p53 was then separated from GST and uncleaved GST-p53 by SEC. The acetylated p53 variants AcK381, AcK382 and AcK381/382 as well as AcK120 and AcK164 were purified, the latter two sites because they have also been reported to be deacetylated by SIRT1. The result of this purification method is shown in Fig. 3.23a. As opposed to p53WT, all acetylated p53 variants showed a signal when detected with the anti-AcK-AB. Significant differences in the signal

are however observed between C-terminally acetylated p53 and p53AcK120 and -AcK164. As described above, this phenomenon was also observed with acetylated Ran and can likely be attributed to the specificity of the anti-AcK-AB.

In an initial experiment, all p53 variants were tested for deacetylation by SIRT1 at a molar ratio of 1:20. Interestingly, except for AcK164, all sites were deacetylated after two hours of incubation, overall confirming previous reports regarding the activity of SIRT1 towards p53 but for the first time showing directly that AcK381, AcK382 and the di-acetylated p53AcK381/382 are SIRT1 substrates (Fig. 3.23b). Moreover, this result speaks against previous observations that SIRT1 deacetylates p53 at K164, although it cannot be ruled out that *in vivo* additional factors mediate deacetylation of this site by SIRT1.

Next, the dynamics of deacetylation at K120, K381 and K382 were further analyzed in a time-course experiment with a p53:SIRT1-ratio of 1:20. For comparison, RanK37AcK was also included. Under the conditions used, all p53 sites were completely deacetylated after 5 to 15 min and thus slightly faster than RanAcK37 (Fig. 3.23c). Given the fast deacetylation, it was difficult to judge, which site of the lysine pair K381/382 is the preferential target of SIRT1. In another time course experiment the SIRT1 concentration was thus reduced to a ratio of 1:200. Interestingly, it turned out that both the two individual sites AcK381 and AcK382 and the di-acetylated AcK381/382 are deacetylated at almost identical rates (Fig. 3.24a).

This raised the question whether the accelerated deacetylation of RanAcK38 upon acetylation of the neighboring K37 is the result of a unique substrate recognition of SIRT2 or merely dependent on the amino acid sequence context. To test these two possibilities, the time-course experiment was repeated but in this case with SIRT2 (SIRT2:p53 ratio 1:200). As shown in Fig. 3.24b, SIRT2 is able to efficiently deacetylate p53-AcK381, -AcK382 and -AcK381/382. Although SIRT2 has previously been described as p53 deacetylase, this experiment demonstrates this activity for the first time in a direct manner (Ding et al., 2013; Hoffmann et al., 2014; Jin et al., 2008; Peck et al., 2010). Strikingly, no strong differences between the three p53 variants were observed regarding the SIRT2-catalyzed deacetylation rates. This result suggests that the sequence context of the di-acetylation site determines if its di-deacetylation is favored over the mono-deacetylation of one of the individual sites. Furthermore, this appears to be true for both SIRT1 and SIRT2.

### 3.2.8 Deacetylation of p53-AcK372/373

In order to further corroborate the assumption that the different deacetylation rates of neighboring AcK residues are due to the sequence context, the other di-acetylation site of p53 (K372/372) was also tested for deacetylation with SIRT1 and SIRT2. The result of the purifications of p53-AcK372, -AcK373 and -AcK372/-373 is shown in Fig. 3.25a. Interestingly, these acetylated variants all show a double band when CMB-stained after SDS-PAGE. Likewise, two bands are visible when the proteins are detected with the anti-p53-AB. In contrast, detection with the anti-AcK-AB results in two band only for the supposedly di-acetylated p53-AcK372/373. These findings are consistent with the lower band being a translational termination fragment, which is the result of unsuccessful incorporation of AcK at the desired positions. Since this fragment is of similar size as the full-length protein product and most likely able to tetramerize, it cannot easily be removed during the purification. In case of p53-AcK372/373, the premature translational termination can occur twice and thus result either in a shortened non-acetylated or a shortened acetylated variant (containing the AcK372 residue). The latter fragment was detected with the anti-AcK-AB, visible as a double band in Fig. 3.25a (panel IB: AcK). Interestingly, freshly prepared dilutions of the anti-AcK-AB detected the termination fragment only weakly compared to the full-length p53-AcK372/373 protein (Fig. 3.25c and d).

The fact that a significant amount of p53 protein synthesized with the GCEC is not full-length product also has implications for the results shown above regarding the other p53 di-acetylation site K381/382. It is likely that in this case a fraction of the protein is not acetylated or, in case of p53-AcK381/382 purifications, only carries one C-terminal AcK-residue. The molecular weight between the termination fragment and full-length protein is however too small to be visualized via standard SDS-PAGE. This would also explain why in deacetylation assays p53-AcK381/382 showed residual background AcK-immunoreactivity (see Fig. 3.23c and 3.24a,b).

The acetylation site K372/373 has so far not directly been shown to be deacetylated by SIRT1. However, interactions between p53-AcK373 and SIRT1 have been described as well as a decrease in p53 acetylation at K373 upon SIRT1 inhibition (Frazzi et al., 2013; Knights et al., 2006). In fact, p53-AcK372, -AcK373 and -AcK372/373 were efficiently deacetylated by SIRT1 *in vitro* (Fig. 3.25b). Next

the kinetics of reaction were again further characterized by a time course experiment with SIRT1 at a substrate:enzyme ratio of 1:200. As shown in Fig. 3.25c, SIRT1 discriminates between the three different variants. At this enzyme concentration, deacetylation of p53-AcK372 and p53-AcK372/373 is not detectable or relatively slow, respectively, while p53-AcK373 is completely deacetylated after 90 min. When the deacetylation was tested with SIRT2, no such discrimination between the two mono- or the di-acetylated variant was observed (Fig. 3.25d). Taken together, these results show that, in contrast to the di-acetylation of p53 at K381/382, di-acetylation at K372/373 has an inhibitory influence on the deacetylation of the AcK373 site. However, this seems to apply only to SIRT1 and not to SIRT2 for this set of sites.

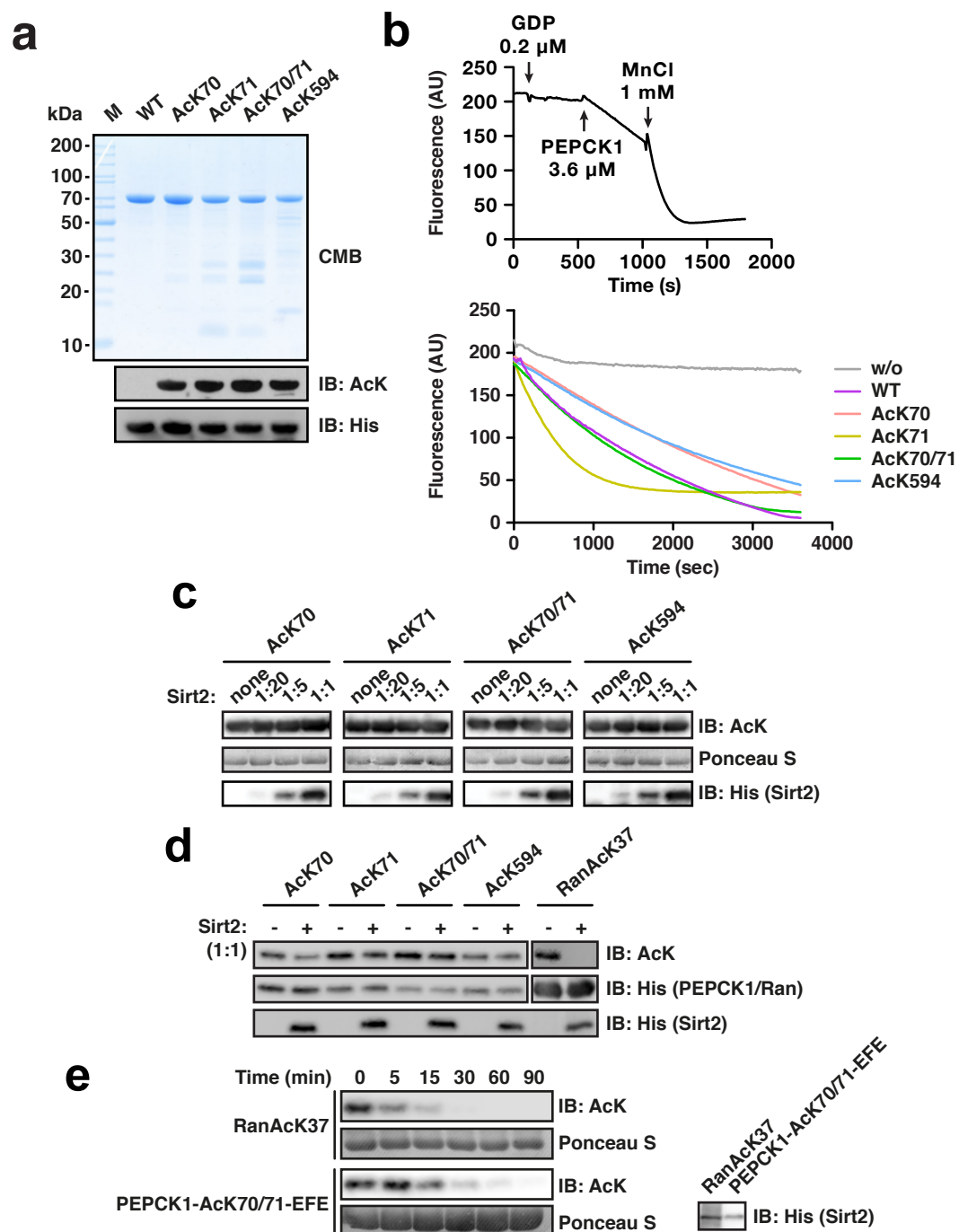


**FIGURE 3.22: Analysis of PEPCK1 deacetylation.** (a) SDS-PAGE of 5  $\mu\text{g}$  of indicated PEPCK1 constructs stained with Coomassie brilliant blue (CMB). (b) Coupled enzymatic activity assay for PEPCK1. (c) Deacetylation assay with increasing concentrations of SIRT2. Molar ratios of SIRT2:PEPCK1 are indicated. The reaction was performed for 2 h at 23°C. The concentration of PEPCK1 was 12  $\mu\text{M}$ . (d) Experiment as in (c) but with addition of 1 mM  $\text{MnCl}_2$  and lower concentration of PEPCK1 (0.6  $\mu\text{M}$ ). (e) Time course of deacetylation with PEPCK1 EFE-mutant and Ran. 20  $\mu\text{M}$  substrate protein was incubated for the indicated time with 0.1  $\mu\text{M}$  SIRT2.

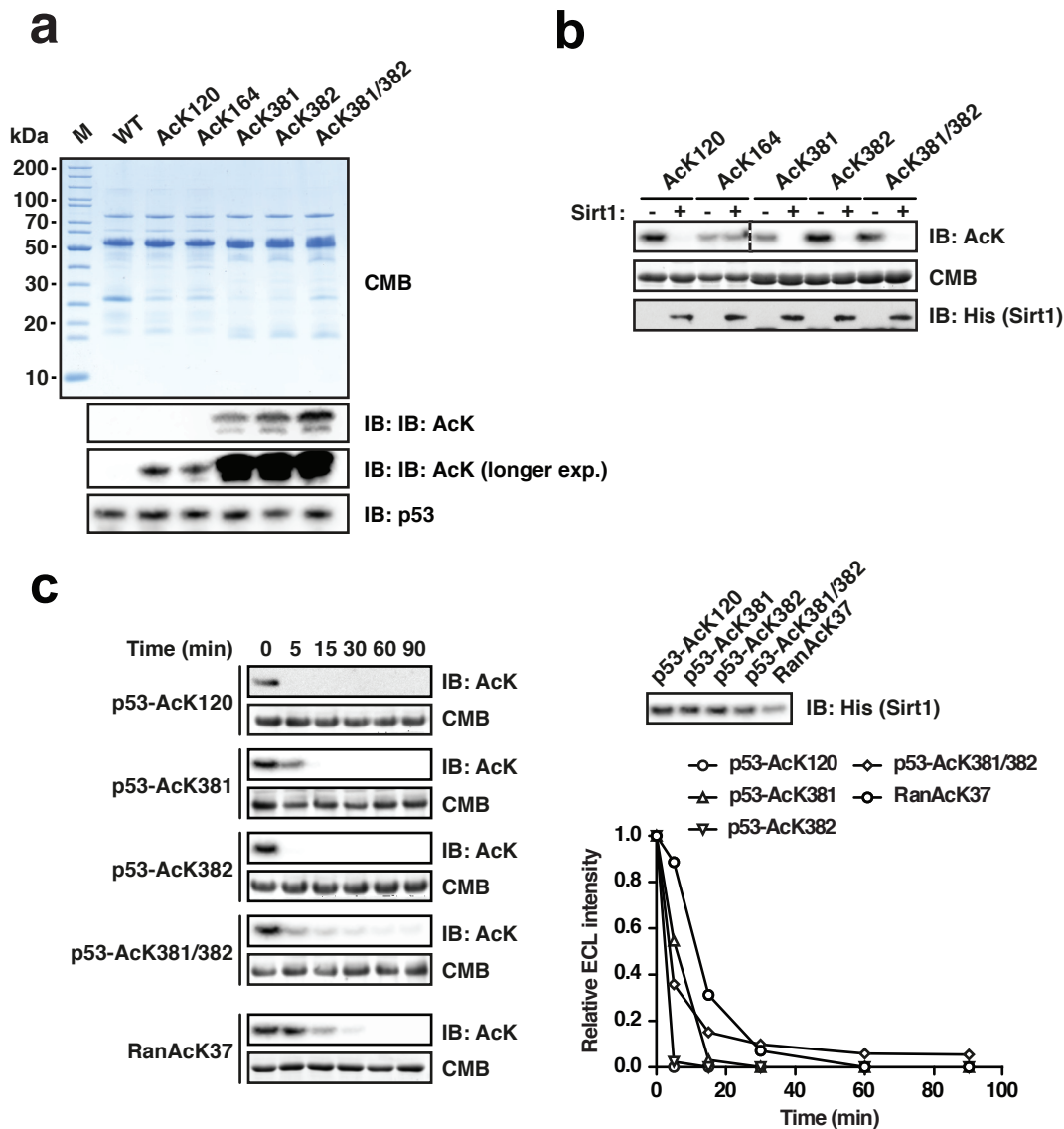


FIGURE 3.23: **Deacetylation of p53 by SIRT1.** (a) SDS-PAGE of 5  $\mu$ g of indicated p53 constructs stained with Coomassie brilliant blue (CMB). (b) Deacetylation assay with SIRT1 at molar SIRT1:p53 ratio of 1:20 (p53: 12  $\mu$ M; SIRT1: 0.6  $\mu$ M). The reaction was performed for 2 h at 23°C. (c) Time course of deacetylation experiment with same concentrations as in (b). Samples were taken at indicated time points. The graph shows the densitometric quantification.

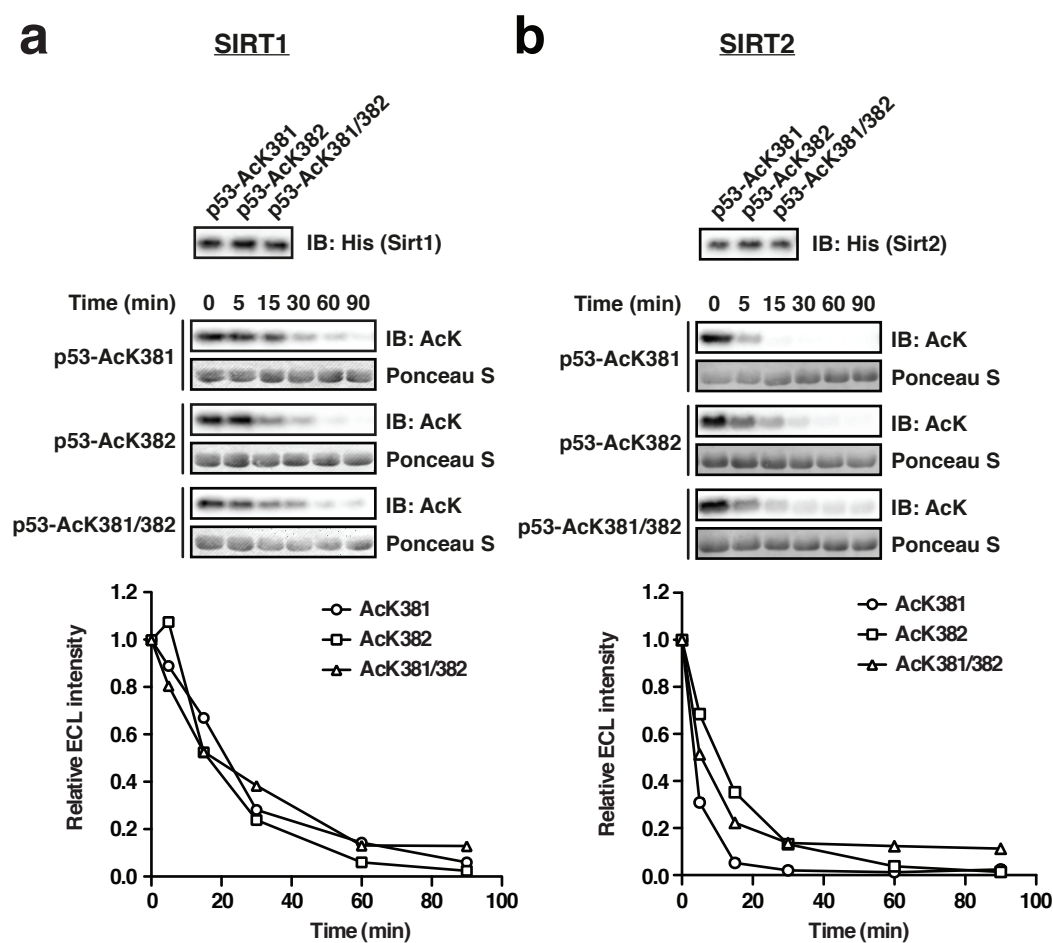


FIGURE 3.24: Dynamics of p53 deacetylation at the di-acetylation site K381/382. (a) Time course of deacetylation experiment with a molar SIRT1:p53 ratio of 1:200 (p53: 12  $\mu$ M; SIRT1: 0.06  $\mu$ M). (b) Same as in (a) but with SIRT2. Samples were taken at indicated time points. The graphs show the densitometric quantification.

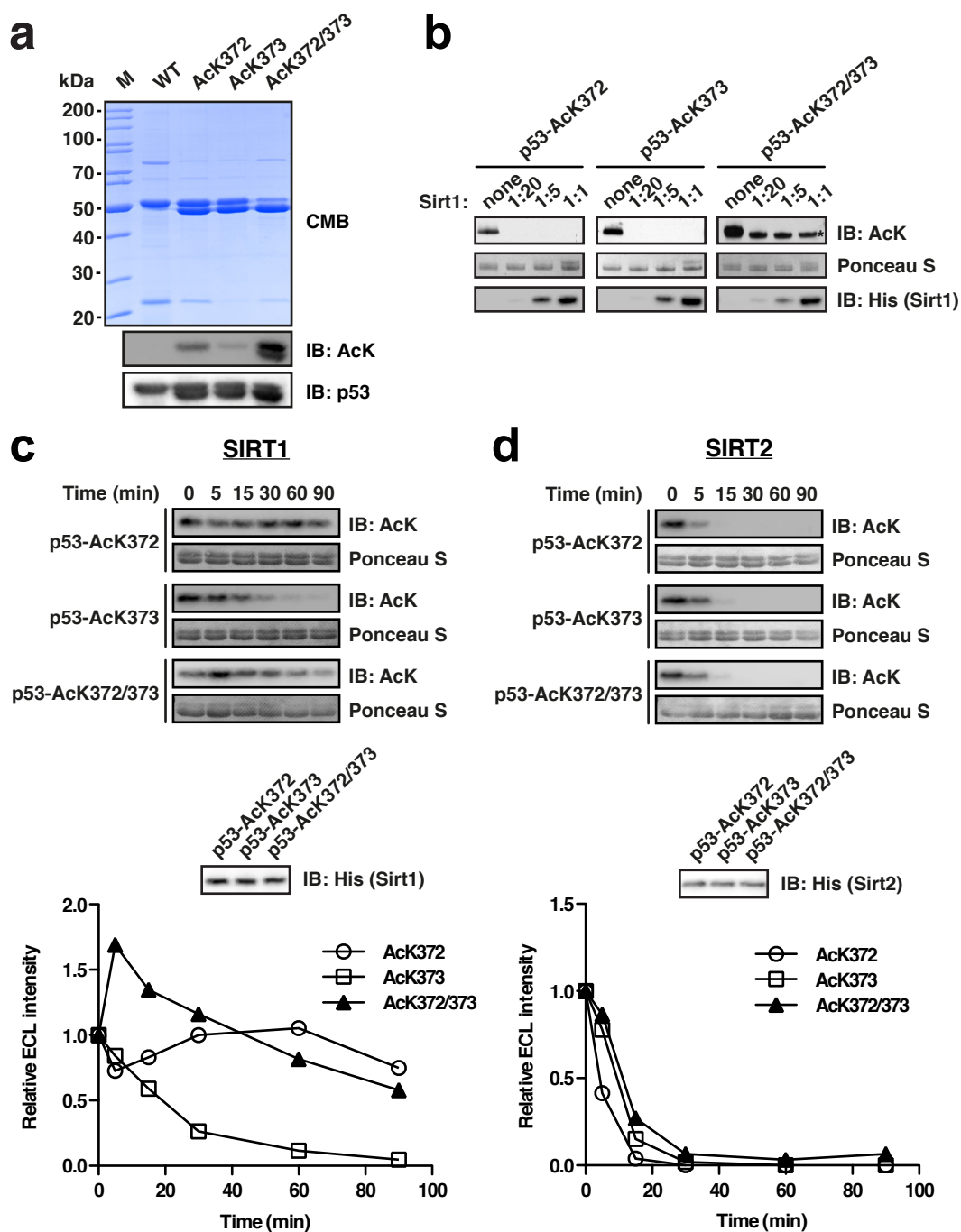


FIGURE 3.25: Deacetylation of p53 at the di-acetylation site K372/K373. (a) SDS-PAGE of 5  $\mu$ g of indicated p53 constructs stained with Coomassie brilliant blue (CMB). (b) Deacetylation assay with indicated molar SIRT1:p53 ratios (p53: 12  $\mu$ M). The reaction was performed for 2 h at 23°C. The asterisk indicates the acetylated translational termination fragment. (c) Time course of deacetylation experiment with 12  $\mu$ M p53 and 0.06  $\mu$ M SIRT1. Samples were taken at indicated time points. The graph shows the densitometric quantification. (d) Same as in (c) but with SIRT2.

## 4 Discussion

In the present work, the impact of lysine-acetylation on protein function of the small GGBP Ran has been studied. The focus lay on intrinsic and RanGAP-mediated nucleotide exchange as well as export complex formation between Ran, CRM1 and Spn1. In a separate study conducted by S. de Boor (PhD Thesis, 2015), the other major molecular functions of Ran, that is intrinsic and RCC1-mediated nucleotide exchange as well as interaction with importin-beta and NTF2, were studied with regard to their sensitivity to Ran acetylation. Based on the proteome-wide acetylation screen by Choudary et al. (2009), five acetylation sites of Ran (K37, K60, K71, K99, and K159) were chosen for investigation, for many of which it appeared likely that they would alter the above functions of Ran. The extensive biophysical characterization performed in both studies was based on the possibility to produce site-specifically lysine-acetylated Ran protein with the GCEC. Moreover, the GCEC allowed for the identification of enzymes possibly involved in the regulation of Ran acetylation.

### 4.1 Incorporation of acetyl-lysine with the GCEC

The purification of acetylated Ran with the GCEC was successful for all five sites as demonstrated by specific immunoreactivity of these variants against a pan-anti-AcK-AB and by the expected mass-shift in ESI-MS spectra consistent with an added acetyl-moiety (Fig. 3.2b). Ran was also purified with two co-translationally incorporated AcK residues (AcK37 and AcK38). Although sufficient material was obtained for the purpose of this study, the yield and purity was substantially lower for di-acetylated than for mono-acetylated Ran (Fig. 3.14a). Similarly, the purification of acetylated PEPCK1 and p53 was more challenging than of the corresponding wildtype protein and, moreover, this effect was even more pronounced

for the di-acetylated variants. In fact, differences in yield were also observed between purifications of different mono-acetylated Ran variants despite their similar stability in subsequent biochemical/-physical assays. These observations lead to the conclusion that, with the *E. coli* strain and growth conditions used in this study, the co-translational incorporation of acetyl-lysine in response to an amber-stop-codon is less efficient than that of natural amino acids. However, the extent to which the protein yields are reduced seems to be influenced by the position and the amino acid context of the desired acetyl-lysine residue within the polypeptide chain. While generally lower yields with the GCEC can be intuitively understood in light of possibly suboptimal expression levels of *PylRS/pylT* and the competition with the endogenous release factor 2 (RF2), the reason for the positional effects observed for AcK incorporation is less clear. It is known that the speed of translation is influenced by the codon composition of the corresponding mRNA stretch. In particular, sequences that contain many codons whose tRNAs are underrepresented or poly-proline coding sequences are translated substantially slower than average (Pavlov et al., 2009; Zhang et al., 2009). The positioning of codons for low abundance tRNAs often demarcates domain boundaries and thus assists in individual domain folding by slowing down translation. Moreover, non-highly expressed genes are enriched for such low-frequency codons (Thanaraj and Argos, 1996) while faster translated sequences often code for specific protein secondary structures such as  $\alpha$ -helices (Makhoul and Trifonov, 2002). Of course, such regulatory mechanisms do not apply to heterologous gene expression. However, the efficiency of AcK-incorporation at a certain position may well be affected by the usage-frequency of surrounding codons and, *vice versa*, translational pausing due to the incorporation of AcK may be particularly detrimental to the folding of certain structural elements in a recombinantly produced protein.

## 4.2 Ran acetylation in regulation of export complex formation and release

The biophysical experiments performed in this study were focused on the role of Ran acetylation in nuclear export complex formation and GTP-hydrolysis. One aspect in which Ran is influenced by acetylation is its intrinsic GTP-hydrolysis rate, which was increased  $\sim 1.5$ -fold for RanAcK71 (Fig. 3.3c). The RanGAP-stimulated GTP-hydrolysis was however largely unaffected by acetylation at each

of the sites tested (Fig. 3.4b). Although a 34-fold decrease in binding affinity of RanGAP towards RanAcK99·RanBP1 was observed (0.5  $\mu$ M for WT vs. 17  $\mu$ M for AcK99; see Fig. 3.5c), this was not reflected in a slower RanGAP-stimulated GTP-hydrolysis of Ran in complex with RanBP1 (Fig. 3.5d). These results suggest that the RanGAP-mediated inactivation of Ran in the cytoplasm is most likely not affected by Ran acetylation.

The intrinsic GTP-hydrolysis rate of Ran is very low if compared for instance to Ras (Klebe et al., 1995). While for Ras a relatively fast GAP-independent inactivation might be important to avoid sustained ‘on’-signaling, it would merely lead to a dissipation of the RanGTP gradient and therefore interfere with nuclear transport (Brucker et al., 2010). However, it remains an open question how significant a  $\sim$ 1.5-fold increase in intrinsic GTP-hydrolysis upon K71-acetylation would be in a physiological context. The work of S. de Boer (PhD Thesis, 2015) has shown that RanAcK71 is not able to bind to NTF2, the nuclear import carrier for RanGDP, due to the disruption of an essential salt bridge. Thus, acetylation at this site could adversely affect the Ran gradient in two respects: Less Ran would be transported into the nucleus and the RanGTP:RanGDP ratio would be shifted towards RanGDP. As a consequence, these two effects combined might lead to an impaired nucleocytoplasmic transport in the cell.

Another aspect of Ran function that is affected by acetylation is the assembly and, possibly, disassembly of nuclear export complexes. The assembly of nuclear export complexes requires the cooperative binding of RanGTP and the respective substrate to an export receptor (Monecke et al., 2009, 2013; Petosa et al., 2004). In the present study, this cooperative binding was modeled *in vitro* with purified components, one being the export receptor CRM1 and the other being one of its substrates, Spn1. As expected, Spn1 showed a higher affinity towards CRM1·RanGppNHp than to CRM1 alone. *Vice versa*, the binding of RanGppNHp to CRM1 could only be detected in ITC when CRM1 was bound Spn1 (Fig. 3.7). While acetylation of Ran did not directly affect its binding to CRM1, it did promote binding of Spn1 to CRM1·RanGppNHp in case of K37-, K99- and K159-acetylation (Fig. 3.8b and c). Interestingly, acetylation of these sites also increased the affinity of RanGppNHp for importin- $\beta$  (PhD thesis S. de Boer, 2015). These two effects taken together support a model in which Ran acetylation, on the one hand, enhances import substrate release in the nucleus and, on the other hand, promotes the assembly of nuclear export complexes. Moreover, the disassembly of

nuclear export complexes might be affected by Ran acetylation given the reduced affinity of RanAcK159 for RanBP1 ( $\sim 10$ -fold reduction in affinity in the GppNHp-bound form of Ran; see Fig. 3.6b). Specifically, as a result of acetylation at this site, RanBP1 might less efficiently bind to RanGTP complexed with CRM1 and, thus, export complexes would be more stable in the cytoplasm (Lounsbury and Macara, 1997; Maurer et al., 2001; Yaseen and Blobel, 1999). However, this effect depends on whether the lower affinity of RanAcK159 for RanBP1 is a result of an altered on- or the off-rate.

Additional effects of Ran acetylation were shown in the PhD thesis of S. de Boor (2015). RCC1-mediated nucleotide exchange is dramatically altered upon acetylation of Ran at K71 and K99. Interestingly, while both K71- and K99-acetylation of Ran impair RCC1-mediated nucleotide exchange, different molecular mechanisms are involved: GDP-bound RanAcK99 exhibits a decreased affinity for RCC1 and a drastically reduced RCC1-induced nucleotide dissociation rate, which essentially represents a loss-of-function phenotype. By contrast, Ran acetylation at K71 leads to a drastically increased affinity for RCC1 and, as for acetylation at K99, a slower RCC1-induced nucleotide release. With these properties, RanAcK71 resembles the dominant negative Ran mutant T24N (Dasso et al., 1994).

The above results demonstrate the broad regulatory spectrum of lysine-acetylation (for an overview of the most pronounced effects of Ran acetylation see the model in Fig. 4.1). Especially for proteins with many different interactions partners such as Ran and other members of the Ras superfamily, the consequences of lysine-acetylation for protein function are complex and difficult to predict. An interesting aspect in this regard is the fact that the alterations in protein-protein interactions or catalytic activity observed in case of Ran acetylation could not always be attributed to an obvious structural cause. This suggests that acetylation can lead to global structural rearrangements in a protein (or at least in Ran) beyond the small-scale changes in the immediate surrounding of the AcK residue (compare Fig. 1.7).

### 4.3 Regulation of Ran acetylation

An important question is under which conditions Ran becomes acetylated to such a significant level that it has a major impact on cellular function and at which sites

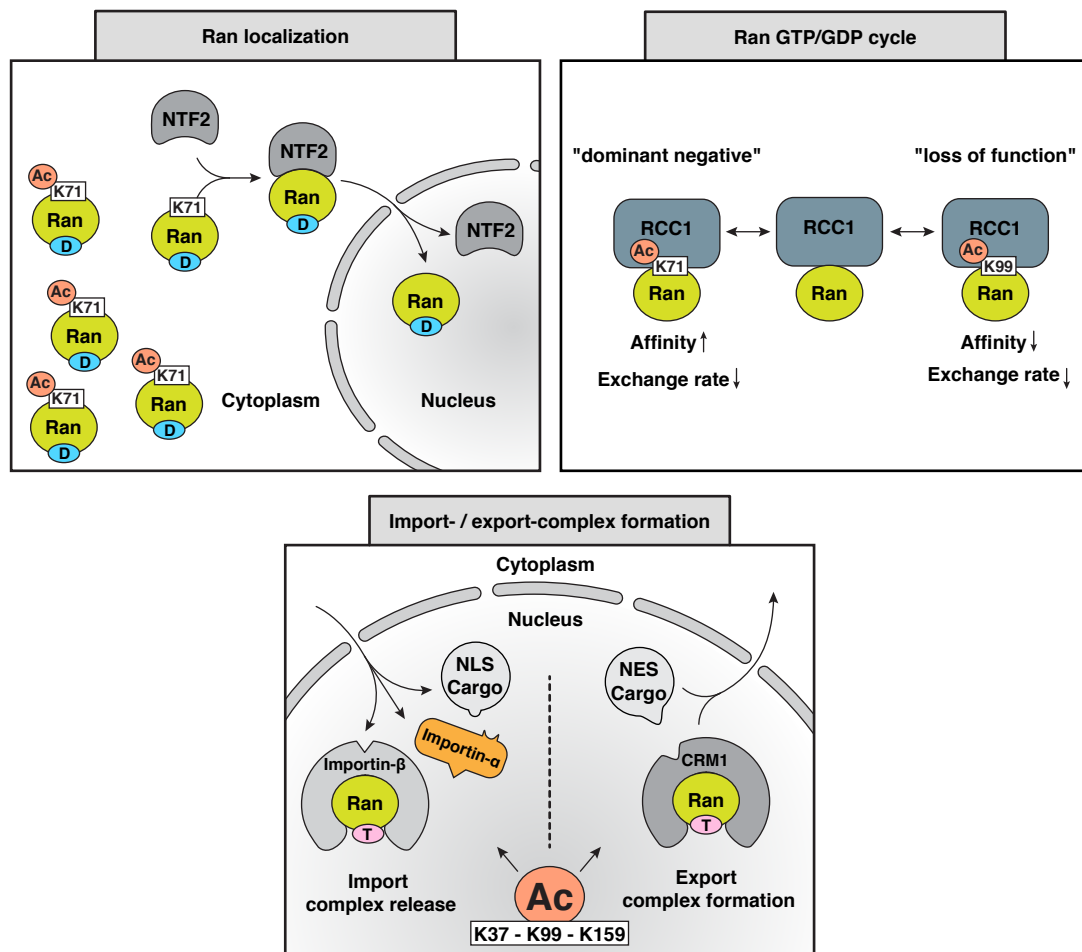


FIGURE 4.1: **Regulation of Ran functions by lysine-acetylation.** Overview of the most pronounced effects of Ran acetylation found in this study and the PhD thesis of S. de Boor (2015) (D: GDP, T: GTP).

Ran acetylation occurs most frequently. Ran is one of the most abundant proteins in the cell (Bischoff and Ponstingl, 1991b), which, on one the hand, highlights its essential cellular role and, on the other hand, suggests that substantial KAT activity towards Ran would be required to perturb or regulate its function. However, this assumption does not necessarily hold true in all situations, for example, if acetylation leads to a dominant-negative effect. As mentioned above, the acetylation of Ran at K71 represents such a case with regard to the interaction with RCC1. The significance of this finding is underscored by the fact that RCC1 is about 25 times less abundant than Ran (Bischoff and Ponstingl, 1991a), meaning that even relatively low amounts of RanAcK71 could have a strong influence on cell physiology.

Over the course of the present study, the above question was addressed by several means. Since initial attempts to isolate endogenous acetylated Ran from cultured human cells that were treated with KDAC inhibitors failed, His<sub>6</sub>-tagged Ran was co-expressed with selected KATs in HEK293T cells and subsequently isolated under denaturing conditions. Immunodetection of these samples with an anti-AcK-AB did not result in a signal, suggesting that Ran only a minor fraction was acetylated or, alternatively, that Ran was acetylated predominantly at sites that were not or only weakly detected by the anti-AcK-AB. In fact, upon MS/MS analysis three acetylation sites were detected in Ran (K134, K142 and K152), the intensities of the corresponding peptides were in some cases increased in a KAT-dependent manner (Fig. 3.9b).

To date, twelve acetylation sites have been identified in Ran. The acetylation sites studied here (K37, K60, K71, K99 and K159) were identified in several human cell lines of different origin: MV-4-11 (myeloid leukemia cells), Jurkat (lymphoid origin), A549 (epithelial origin), U20S (osteosarcoma cells) and HeLa S3 (cervical cancer cells) (Beli et al., 2012; Choudhary et al., 2009; Mertins et al., 2013). However, the three sites found in this study were so far only detected in rat and/or mouse tissue samples. It should be noted that tissue-specific global acetylation patterns have been found in rat tissues (Zhao et al., 2010) and that lysine-acetylation sites are often evolutionary conserved (Wang et al., 2010; Weinert et al., 2011). The only human tissue samples that have been analyzed for lysine-acetylation in a proteome-wide manner are skeletal muscle biopsies where no acetylated Ran was detected (Lundby et al., 2012; Zhao et al., 2010). Collectively, these findings point toward a tissue-specific occurrence of acetylated Ran, with different patterns of acetylation sites being present in each tissue. Regarding this notion, it has also to be taken into account that proteomic analyses are potentially biased towards certain acetylation sites as a result of antibody-based AcK-specific enrichment of peptides/proteins. As shown in this study and by others, even polyclonal anti-AcK-ABs detect sites with different sensitivity depending on the sequence context (Fig. 3.2a, Shaw et al., 2011), a fact that may significantly skew acetylome data towards certain acetylation sites.

Ran is the Ras superfamily member for which the most acetylation sites have been found, with Cdc42 being ranked second with seven known acetylation sites (see Table 4.1). For Ras, only one acetylation site is known, which has a negative effect on nucleotide exchange catalyzed by its GEF SOS (Son of Sevenless, Yang et al.,

2012). It is tempting to speculate that the high number of acetylation sites in Ran is due to its predominantly nuclear localization, which may result in an increased probability to encounter one of the many nuclear KATs. In the present study, the Ran acetylation sites K134 and K142 were detected in 6 out of 8 samples and K134-acetylation was upregulated upon coexpression of TIP60, CBP and p300 although it is not clear whether this is due to a direct or an indirect effect. When recombinant Ran was incubated with KATs *in vitro*, additional acetylation sites were identified (K23, K28, K37, K60, K99 and K123), three of which are among those discovered by others in human cells (PhD Thesis S. de Boor, 2015). This underscores the propensity of Ran to serve as a substrate for KATs even though the exact conditions that lead to Ran acetylation at particular sites *in vivo* have yet to be found out. Several factors might promote KAT activity towards Ran *in vivo*, such as an increase in acetyl-CoA levels (Donohoe et al., 2012; Wellen et al., 2009), alterations in the localization of KATs (Keck and Pemberton, 2011) or the presence of stimulatory cofactors (Li et al., 2003b). It will be interesting to see if, under these different conditions, the acetylation of Ran fulfills specific regulatory functions or if it rather reflects a disease state of the respective cell or tissue.

TABLE 4.1: Lysine-acetylation sites of Ras superfamily members.

GNBP	Lysine-acetylation sites found by MS <sup>a</sup>		
	Human	Mouse	Rat
Ran	K37,60,71,99,152,159	K60,71,159	K23,28,37,60,99,134,152,159
K-Ras	K104	-	-
N-Ras	-	-	-
H-Ras	-	-	-
Rap1A	-	-	K151
Rap1B	-	-	K151
RhoA	-	-	K133,135
RhoB	-	-	-
RhoC	-	-	-
Cdc42	K135,144,153	-	K128,133,135,144,150,153,166
Rac1	-	K132, K133	K147,153
Rab1A	K61	-	K61,132,140
Rab1B	K58	-	-
Rab7A	-	-	K32
Rab7B	-	-	-
Rab7L	-	-	-
Arl1	-	-	K152
Arf1	K36,142	K142	K36,142

<sup>a</sup> Acetylation sites from Phosphosite Plus are shown (Hornbeck et al., 2015).

To understand the role of acetylation for the function of a protein, it is equally important to know how this modification is reversed by KDACs. The site-specifically acetylated protein that can be produced with the GCEC allows for the identification of KDAC activity towards any given acetylation site (provided the protein can be recombinantly produced). Different experimental approaches can be envisioned to this end. For instance, acetylated recombinant protein may be incubated with whole cell lysates to globally test for the presence of KDAC activity and then (if applicable) further narrowed down to a particular enzyme by systematic knockdown/-out of KDAC genes. In the present study, KDACs of Ran were identified by an *in vitro* screen with all 18 human KDACs (Fig. 3.11), the activity of which was verified beforehand in a fluorimetric deacetylation assay (Fig. 3.10). The screen led to the identification of SIRT2 as a specific KDAC for RanAcK71 and of SIRT1-3 as KDACs for RanAcK37. The fact that SIRT3 is predominantly found in mitochondria makes it an unlikely candidate for *in vivo* Ran deacetylation while the localization of SIRT1 and SIRT2 would allow these enzymes to deacetylate Ran in the nucleus and the cytoplasm (Jin et al., 2007; Michishita et al., 2005; North and Verdin, 2007).

Like many other small GNBPs such as Ras, Cdc42 and Rac, Ran is only slowly turned over with a protein half-life of 2.6-3 days in mouse liver tissues and HeLa cells and ~9.2 days in mouse brain tissue (Cambridge et al., 2011; Price et al., 2010; Sandoval et al., 2013; Shukla et al., 2014). Thus, acetylated Ran may accumulate significantly depending on the rate at which its acetylation is happening. This may apply in particular to post-mitotic cells (such as neurons) and to tissues with high Ran expression, including some cancer types, in which Ran expression has been found to be upregulated (Azuma et al., 2004; Vanegas et al., 2003). In light of these considerations, it seems surprising that KDACs of Ran were only found for two sites (K37 and K71) in the KDAC screen performed here. However, as for the identification of KATs by means of *in vitro* experiments or KAT-overexpression, it cannot be ruled out that other KDACs are involved in Ran deacetylation *in vivo*. This is particularly the case for classical KDACs given their extensive regulation by small molecules and interactions with other proteins (see below, Guenther et al., 2000; Laherty et al., 1997; Watson et al., 2012).

In a broader sense, it is an interesting question whether a majority of the many acetylation sites found in proteomic screens is targeted by the relatively few

KDACs or if particularly the ones with a low stoichiometry are removed concurrently with protein turnover. In this regard, it seems reasonable to hypothesize that an ongoing co-evolution exists between KATs, KDACs and acetyl-acceptor sites, at least for proteins in the cytosol and the nucleus. The outcome of this co-evolution might be a large number of low-stoichiometry acetylation sites, many with tolerable effects for cell physiology and some which have to be tightly controlled due to otherwise detrimental consequences. Finally, there are the often high-stoichiometry acetylation events that are part of signaling cascades and other dynamically regulated processes. An important step towards an understanding of the acetylome is the recent development of MS tools for the absolute quantification of acetylation sites (Baeza et al., 2014; Weinert et al., 2014). Nevertheless, to discriminate between the above possibilities for so many identified acetylation sites remains a formidable challenge for the scientific community and does not only apply to acetylation but also to other post-translational modifications.

#### 4.4 Implications for the substrate specificity of classical KDACs

In the *in vitro* KDAC screen, none of the classical KDACs showed substantial activity towards Ran, albeit the reportedly low sequence specificity of many of these enzymes (Riester et al., 2007). However, it should be noted that their specificity was tested only on short peptidic substrates, which were varied in the positions  $-2/-1$ ,  $-1/+1$  or  $+1/+2$  with respect to the AcK moiety (Gurard-Levin et al., 2010, 2009; Riester et al., 2007). In addition, these substrates were either labeled with fluorophores, which alter the substrate recognition (Gurard-Levin et al., 2009; Wolfson et al., 2014), or immobilized, which required for instance a cysteine residue in a fixed position (Gurard-Levin et al., 2010, 2009). In other studies, attempts were made to identify substrates of classical KDACs by using proteomic approaches in combination with specific inhibitors. The resulting number of substrates was however relatively small and validation was again performed with peptide substrates (Olson et al., 2014). Thus, relatively little is known about how classical KDACs bind to full-length protein substrates. Nevertheless, some conclusions may be drawn from comparison of the sequence context of the Ran acetylation sites with the specificity profiles observed for the peptidic substrates.

As shown in Table 4.2, except for RanAcK71 all sites are in principle suitable substrates for classical KDACs if judged based on the positions  $-2/-1$  relative to the acetyl-moiety. Similarly, the sequence context in positions  $+1/+2$  matches the observed substrate preferences of KDAC3 in case of RanAcK37 and KDAC8 in case of RanAcK60 and -AcK71. However, yet another study, in which the positions  $-1/+1$  were analyzed, suggests that none of the five Ran acetylation sites studied here is a likely substrate for the classical KDACs tested therein (KDAC2, KDAC3 and KDAC3 in complex with SMRT). On the one hand, this might explain their lack of activity towards Ran in the present study. On the other hand, this finding is surprising given that RanAcK37 and RanAcK60 fulfilled the respective substrate criteria for the same KDAC (*i.e.* KDAC3 and KDAC8, respectively) upon independent analysis of ‘upstream’ and ‘downstream’ residues. This discrepancy may reflect the limitations of peptide-based deacetylation assays and strengthens the case for using full-length proteins instead.

TABLE 4.2: Comparison of Ran acetylation sites with preferred substrate sequences of classical KDACs.

Site	Sequence	Secondary structure	Match with enzyme preference		
			$-2$ and $-1^a$	$-1$ and $+1^b$	$+1$ and $+2^c$
K37	FE-AcK-KY	Loop	KDAC3, -6	none	KDAC3
K60	PI-AcK-FN	$\beta$ -strand	KDAC8	none	KDAC8
K71	QE-AcK-FG	Loop	none	none	KDAC8
K99	TY-AcK-NV	$\alpha$ -helix	KDAC6	none	none
K159	FE-AcK-PF	$\alpha$ -helix	KDAC6	none	none

<sup>a</sup> Riester et al. (2007)

<sup>b</sup> Gurard-Levin et al. (2009)

<sup>c</sup> Gurard-Levin et al. (2010)

Given the highly divergent functions of the different submembers of classical KDACs, which have, *inter alia*, been observed in knockout studies (reviewed in Haberland et al., 2009b), it is thought that their substrate specificity is dictated by interaction with several co-factors (reviewed in Kelly and Cowley, 2013). In fact, alterations in substrate recognition and activity of KDAC3 have been observed *in vitro* when it was bound to its co-factors NCoR2 or SRMT (Guenther et al., 2001; Gurard-Levin et al., 2009; Riester et al., 2007). Since in the screen performed here, it was not low specificity that was observed but rather unexpectedly low overall activity towards Ran (despite the apparent activity towards the fluorogenic

standard peptides), it may be concluded that many co-factors of KDACs are in fact required to enable them to bind protein substrates in the first place.

## 4.5 Implications for the substrate specificity of Sirtuins

As for the classical KDACs, the substrate specificity of Sirtuins is a matter of debate. Early studies on SIRT1 and yeast Hst2 suggest that Sirtuins have little sequence preference but require the AcK moiety to be located in unstructured regions. These conclusions were in part drawn based on structural data, which show that side chains of amino acids flanking the AcK do not substantially contribute to the binding of peptide substrates to Sirtuins (Avalos et al., 2002; Zhao et al., 2003). The requirement for unstructured conformations has been shown by comparing the Hst2-mediated deacetylation of chemically acetylated Cytochrome *c* and RNase A, either in native native form or after heat-denaturation. In both cases, the heat-denatured protein turned out to be a much better substrate than its natively folded counterpart. In the same study, several peptides were shown to be deacetylated by Hst2, mostly regardless of their sequence (Khan and Lewis, 2005). Blander et al. (2005) used a degenerate library of acetyl-peptides and determined the relative abundance of each amino acid in the positions surrounding the central AcK for those peptides that were deacetylated by SIRT1. Again, it seemed that Sirtuins have no preferred target sequence. By contrast, when Garske and Denu (2006) probed SIRT1 specificity with a combinatorial library and individually identified deacetylated peptides, significant enrichment of certain sequences was found. This discrepancy is most likely due to the different methods used in these two studies, the former only yielding an average of all preferred sequences so that the apparent context-dependent substrate recognition of SIRT1 was overlooked. Since then other studies have confirmed the context-dependency of SIRT1 binding and extended this finding to SIRT3 as well as other Sirtuins (Gurard-Levin et al., 2010; Rauh et al., 2013; Smith et al., 2011).

Based on the results of the present work, it appears that, at least *in vitro*, SIRT1-3 share some features of substrate recognition. A total of 15 acetylation sites

has been analyzed for deacetylation by Sirtuins and in addition three sets of diacetylation sites. In Fig. 4.2, the sequence context of these sites shown in comparison with the specificity profile of SIRT3 obtained by Smith et al. (2011). Note that the differently sized letters do not represent relative residue frequencies for each position (as in classical consensus sequence representations) but rather reflect the discriminative weight of residues at specific positions in the prediction of SIRT3 substrate specificity. From this comparison, it is difficult to identify clear sequence-based differences that would explain the efficient deacetylation of some sites and the non-suitability of others. This applies to both the comparison among the sequences as well as the comparison to the specificity profile of SIRT3. For instance, RanAcK159 is surrounded by favorable residues at the most critical positions, namely a Tyr at  $-4$ , a Phe at  $-2$ , a Phe at  $+2$  and a Leu at  $+3$  and yet turned out to be no substrate for SIRT3. The  $-1$  Glu and  $+1$  Pro may be responsible for the lack of SIRT3 activity towards this site. However RanAcK37, -AcK38 and AcK37/38, which are SIRT3 substrates, also have disfavored residues at specificity determining positions.

Thus, a different way to understand the deacetylation of specific sites by Sirtuins might be to compare the sites' structural environments (see Fig. 4.3). Although the known protein structures of sites tested here do not offer insights into their actual positioning upon acetylation, some conclusions may nevertheless be drawn from their visual inspection in the non-acetylated state. Of the sites that were no substrates, RanK99 and PEPCK1-K594 are part of  $\alpha$ -helices and RanK60 is centrally positioned in a  $\beta$ -strand. In these cases, the N- and C-terminal amino acid residues of the AcK residue and the AcK residue itself might be less accessible for Sirtuin binding. Similarly, p53-K164 and RanK159 reside at the end of a  $\beta$ -sheet or an  $\alpha$ -helix, respectively, and thus the potentially recognizable residues are at least partially engaged in a rigid structure. Moreover, the accessibility of p53-K164 might be lowered also due to the closely spaced tetramerization domain of p53 (not shown in Fig. 4.3). PEPCK1-K71 and K72 are found in a loop and at least three residues N- and C-terminally also appear relatively accessible. Thus, it is perhaps surprising that these sites of PEPCK1 turned out to be no substrate for SIRT2. However, the fact that it was deacetylated upon mutation of three N-terminal residues suggests that either the structure of the loop was previously not sufficiently accessible (but was with the mutations) or, alternatively, that the natural N-terminal amino acid sequence was not suitable for SIRT2 binding.

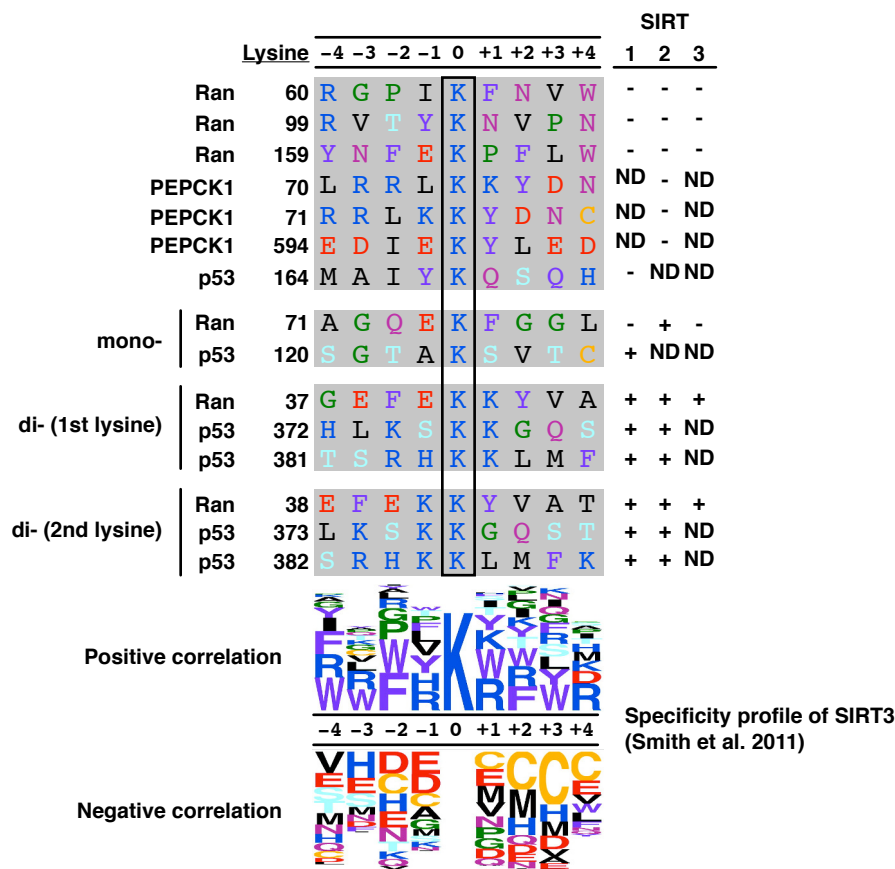


FIGURE 4.2: **Sequence context of acetylation sites tested for deacetylation.** All sites tested for deacetylation in this work are listed with their sequence context from position -4 until +4 and colored according to their sidechain characteristics. The discriminative profile of SIRT3 represents the relative contribution of residues/positions to SIRT3 specificity as differently sized letters. The total column height reflects how important the respective position is for specificity (ND: not determined; Smith et al., 2011).

The C-terminus of p53 with the acetylation sites K372/373 and K381/382 is highly disordered and thus likely behaves similar to peptides regarding the binding to the active site of Sirtuins. For each of the mono- and the di-acetylated p53 variants, deacetylation was observed, which suggests limited sequence specificity of SIRT1 and SIRT2 on disordered polypeptide stretches. The other sites that were deacetylated efficiently by Sirtuins, namely p53-K120, RanK37/38 and RanK71, all reside in loop regions and appear to be highly accessible. An interesting observation in this regard is the fact that SIRT2 deacetylated RanAcK71 faster in its GppNHp-bound than in its GDP-bound form. This is surprising given that the switch-II loop is more flexible in the GDP-bound form of Ran. However, K71<sup>Ran</sup> in RanGDP

is pointing inwards away from the solvent, which is not the case in RanGppNHp and hence perhaps allows more efficient binding by SIRT2 (Fig. 4.3).

From the structural analysis of the different acetylation sites tested here, it may be concluded that one important element of substrate recognition by Sirtuins is the accessibility and perhaps flexibility of both the AcK residue and its N- and C-terminally adjacent amino acids. In addition, there is certainly a sequence component to Sirtuin-substrate interaction. This was demonstrated with the deacetylation of RanAcK38, the rate of which is substantially lower than for the adjacent RanAcK37, and by the fact that mutation of PEPCK1 in three positions N-terminally of the two AcK residues allowed its deacetylation by SIRT2. Moreover, at least with SIRT1, the deacetylation of p53-AcK373 was somewhat preferred over that of p53-AcK372 and -AcK372/373. Taken together, a combination of structural and sequence requirements have to be fulfilled to allow for deacetylation by the Sirtuins tested here. Whether other factors play a role in substrate recognition *in vivo* and whether these findings can be generalized to the other Sirtuins is however still an open question.

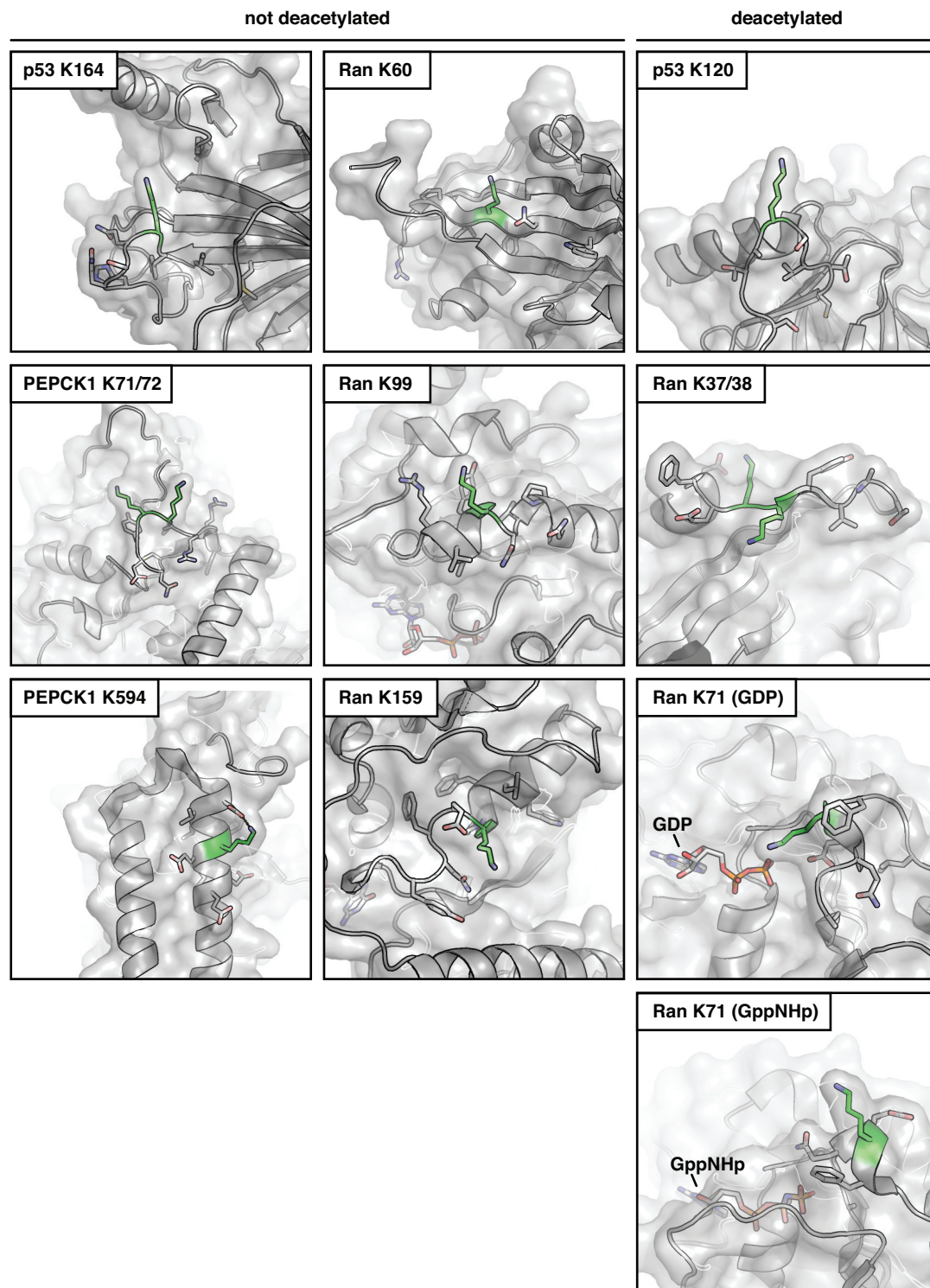


FIGURE 4.3: **Structural context of sites tested for deacetylation.** Ribbon and surface plots of structures with acetylation sites highlighted in green. The sidechains of position -4 until +4 are shown as sticks. The C-terminal sites of p53 are not shown since they are intrinsically disordered. PDB IDs – p53: 2OCJ, PEPCK1: 1KHF, RanGDP: 1BYU, RanGppNHp: 1IBR.

## 4.6 On the role of di-acetylation

In this work, the deacetylation of two adjacent lysines by Sirtuins was studied only for three proteins (Ran, PEPCK1 and p53). It should be noted however that to date the acetylation of two neighboring lysines has been found for 978 sites and 771 proteins in human (according to current entries on Phosphosite.org, Hornbeck et al., 2015), although it is difficult to assess how many of these potential di-acetylation sites have actually been identified as simultaneous modifications. Nevertheless, this large number suggests an important role for di-deacetylation *in vivo*. The acetylation of p53 has been shown to be of major importance for the regulation of its anti-tumorigenic effects and it is only poorly understood how the many different sites are regulated by a multitude of KATs and KDACs (reviewed in Reed and Quelle, 2014). It is thus an important finding that deacetylation of p53 by SIRT1 and SIRT2 occurs even upon acetylation of two adjacent lysines. In addition, a number of di-acetylation sites are also found in histones. With regard to the ‘histone code’, which has been proposed to explain the interplay of different histone modifications (Strahl and Allis, 2000), di-acetylation and/or its removal might be an important mechanism for the regulation of gene expression. The fact that histones possess many lysine residues in their N-terminal tails may also lead to off-target acetylation events catalyzed by KATs, which could be counteracted by Sirtuins even if two adjacent lysines are affected.

## 4.7 Conclusions and Outlook

In this and the accompanying work by S. de Boor (PhD Thesis, 2015), five Ran acetylation sites were studied regarding their effects on Ran protein function. Ran acetylation was found to influence the interaction of Ran with RCC1, NTF2, RanBP1 and the nuclear transport receptors CRM1 and importin- $\beta$ . These results not only demonstrate the broad regulatory spectrum of lysine-acetylation for Ran function but more generally implicate that the molecular effects of lysine-acetylation are diverse and often not easy to predict. Since the GCEC enables the site-specific incorporation of acetyl-lysine into recombinant protein and hence the study of individual acetyl-modifications, it is a valuable tool for the understanding of these molecular effects.

Another central aspect regarding the impact of lysine-acetylation on protein function is its stoichiometry. The results shown in the present and the accompanying study suggest a low stoichiometry of Ran acetylation, at least under the conditions and the cell lines tested. Nevertheless, Ran acetylation sites were identified in HEK293T cells and these were upregulated in response to coexpression with KATs. In addition, *in vitro* KAT assays showed that Ran is a potential substrate of KATs. Interestingly, the acetylation sites identified in Ran isolated from HEK293T cells were different from those previously found in human. Based on high-throughput MS data of mouse and rat tissue samples, the patterns of Ran acetylation sites appear to be highly tissue-specific, which may be a result of different metabolic states and/or differential expression of KATs. The above findings together with the strong and, in some cases, dominant-negative consequences of Ran acetylation on its function suggest that it has a significant impact on cell physiology. To establish the conditions under which Ran becomes acetylated to what level and at which sites is an important but challenging future task, which will likely require further high-throughput MS data and further advances in MS-based quantification techniques.

The *in vitro* KDAC screen, which was performed to gain insights into the negative regulation of Ran acetylation, revealed several, in part unexpected, aspects of KDAC biology. Despite their reportedly low specificity for peptidic substrates, none of the classical KDACs was found to deacetylate Ran. Whether this was due to the absence of additional co-factors or does in fact reflect a high specificity towards full-length protein substrates remains to be resolved. As opposed to the classical KDACs, Sirtuins did show activity towards Ran, at least for two sites. The further results regarding the deacetylation of these two sites as well as sites in p53 and PEPCK1 support the conclusion that, in a full-length protein context, Sirtuins preferentially deacetylate AcK residues that are located in loop structures with high accessibility. Nevertheless, the analysis of four di-acetylation sites shows an additional sequence dependency of substrate recognition. The fact that SIRT1-3 are able to deacetylate two adjacent AcK residues underscores the context-dependent sequence requirements of Sirtuins, which has previously been observed on peptidic substrates. How exactly this is achieved is an interesting question for future studies. A major step forward, regarding both the structural and the sequence requirements, would be the solution of further structures of Sirtuins bound to their substrates, in particular to a full-length protein and to a peptide

---

of a di-deacetylation site. In light of the recent discovery of additional lysine-acyl-modifications, it will be interesting to see how Sirtuins (and KDACs in general) are influenced by the presence of such modifications in the vicinity of their target AcK sites.

# A Appendix

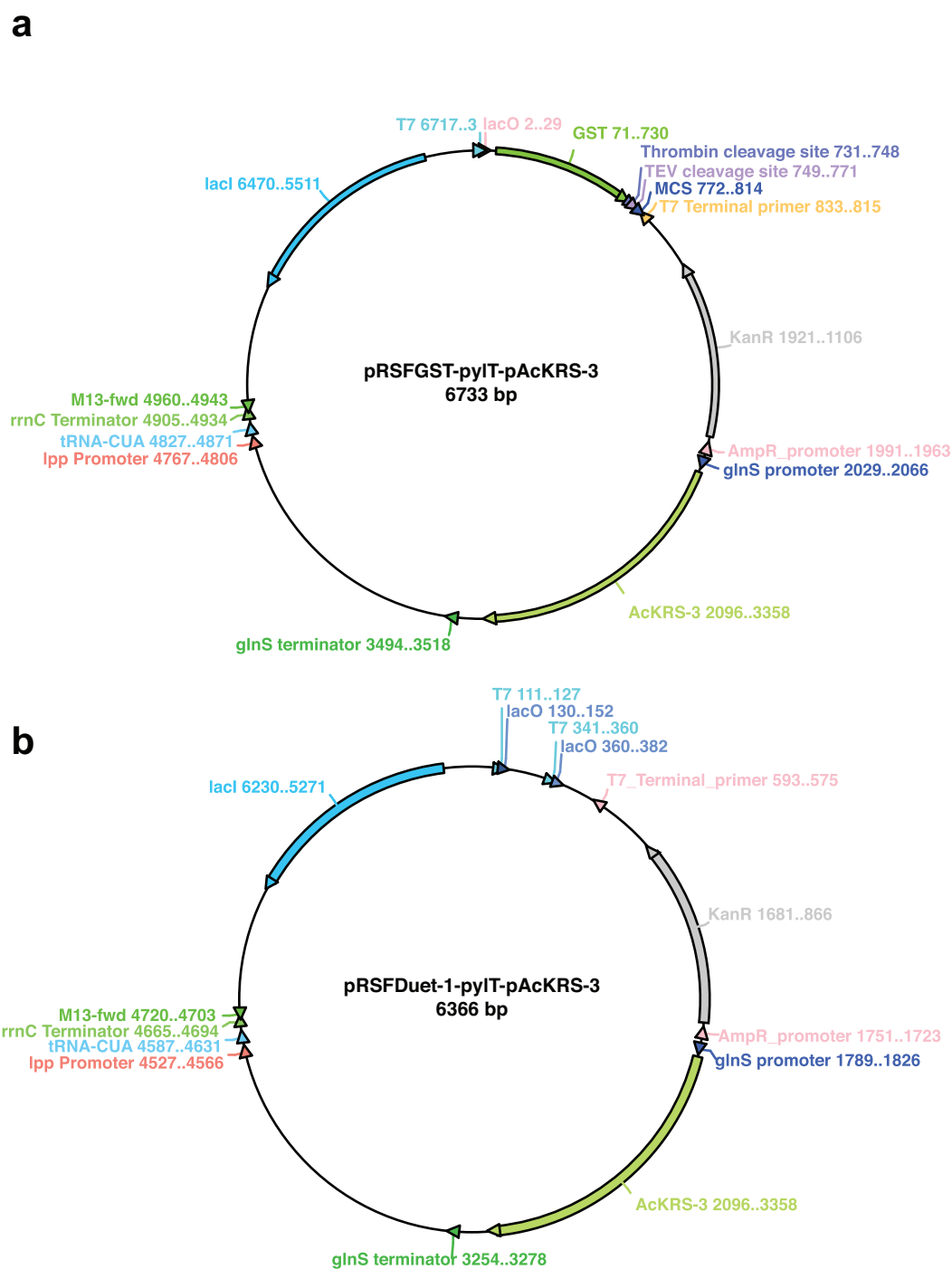


FIGURE A.1: Maps of vectors used for GCEC. (a) Vector for the purification of acetylated proteins with GST-tag. (b) Vector for the purification of acetylated proteins with His<sub>6</sub>-tag

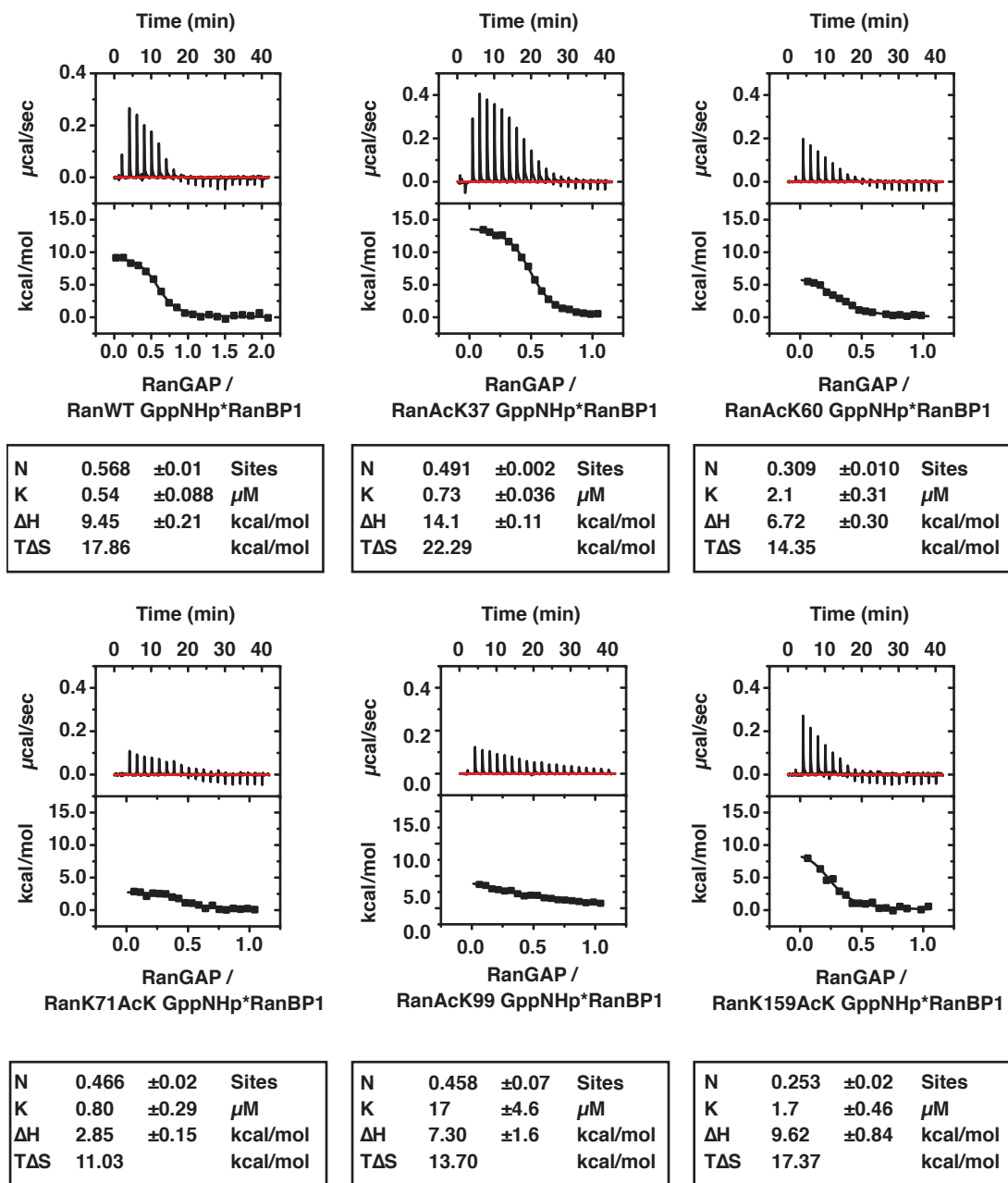


FIGURE A.2: ITC measurements of RanGppNHp-RanBP1 and RanGAP. RanGppNHp-RanBP1 (40/40 μM) was titrated with RanGAP (200 μM) at 20°C.

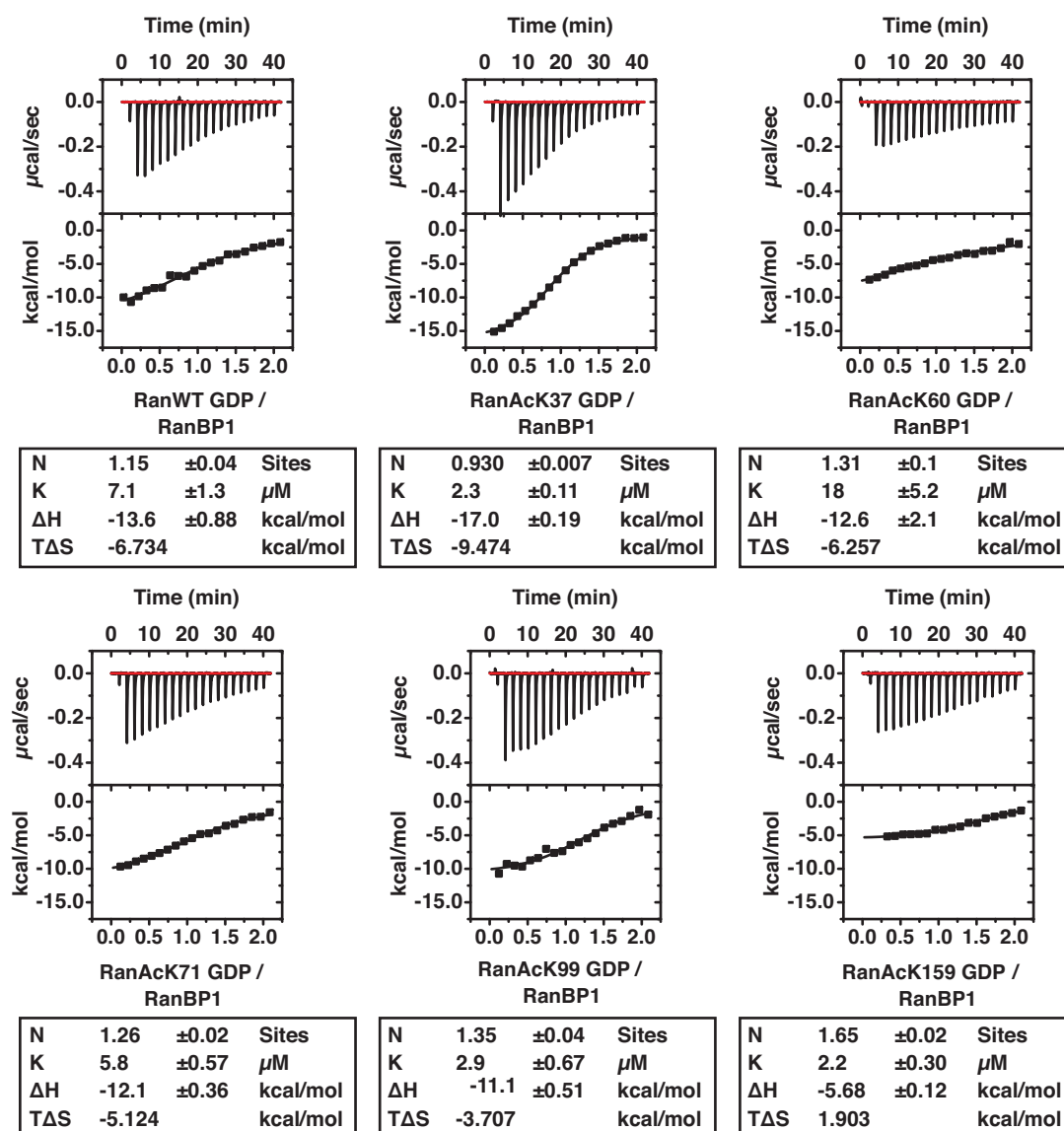


FIGURE A.3: ITC measurements of RanGDP and RanBP1. RanBP1 ( $20\ \mu\text{M}$ ) was titrated with RanGDP ( $200\ \mu\text{M}$ ) at  $20^\circ\text{C}$ .

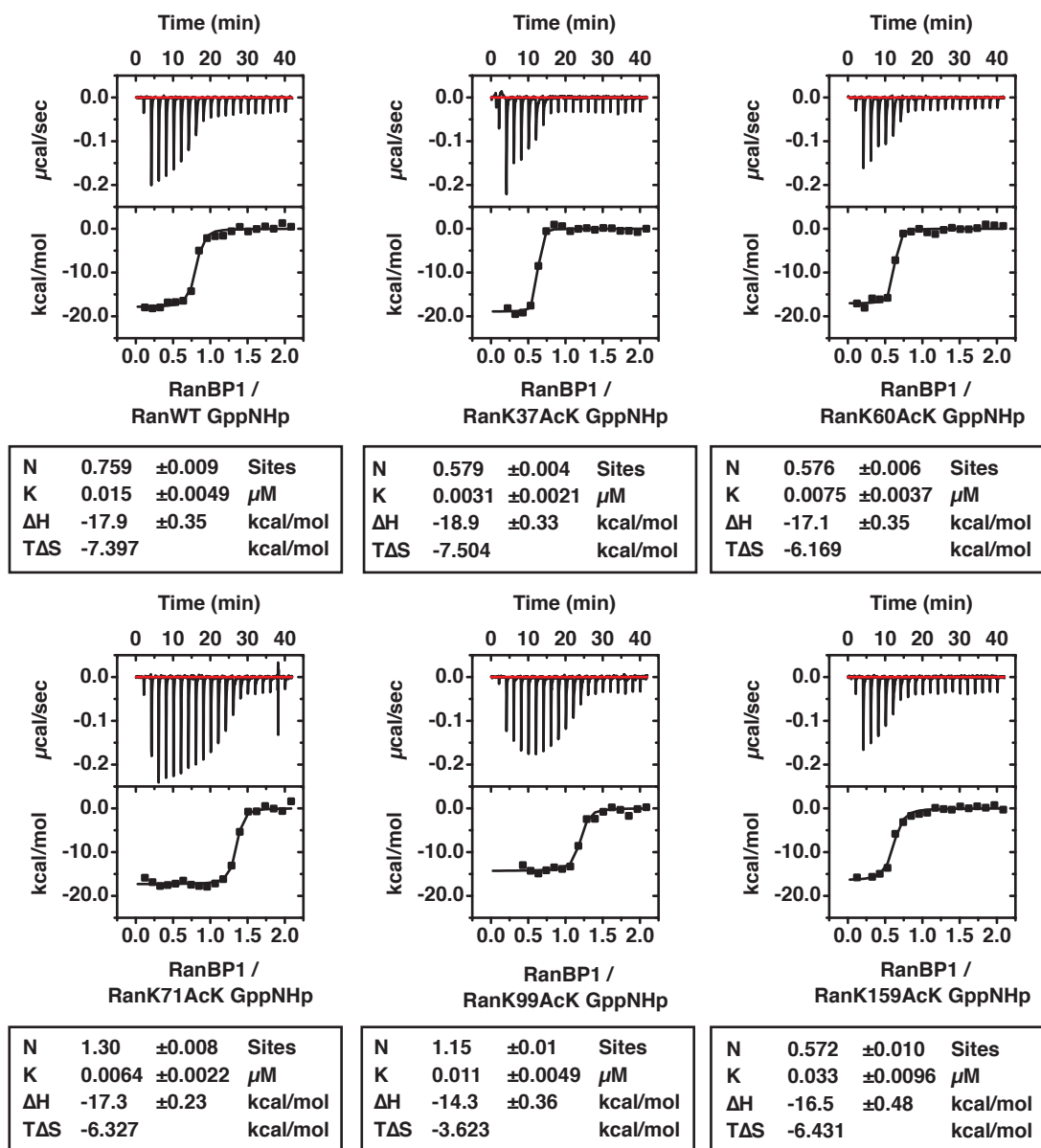


FIGURE A.4: ITC measurements of RanGppNHp and RanBP1. RanGppNHp (5  $\mu\text{M}$ ) was titrated with RanBP1 (50  $\mu\text{M}$ ) at 20°C.

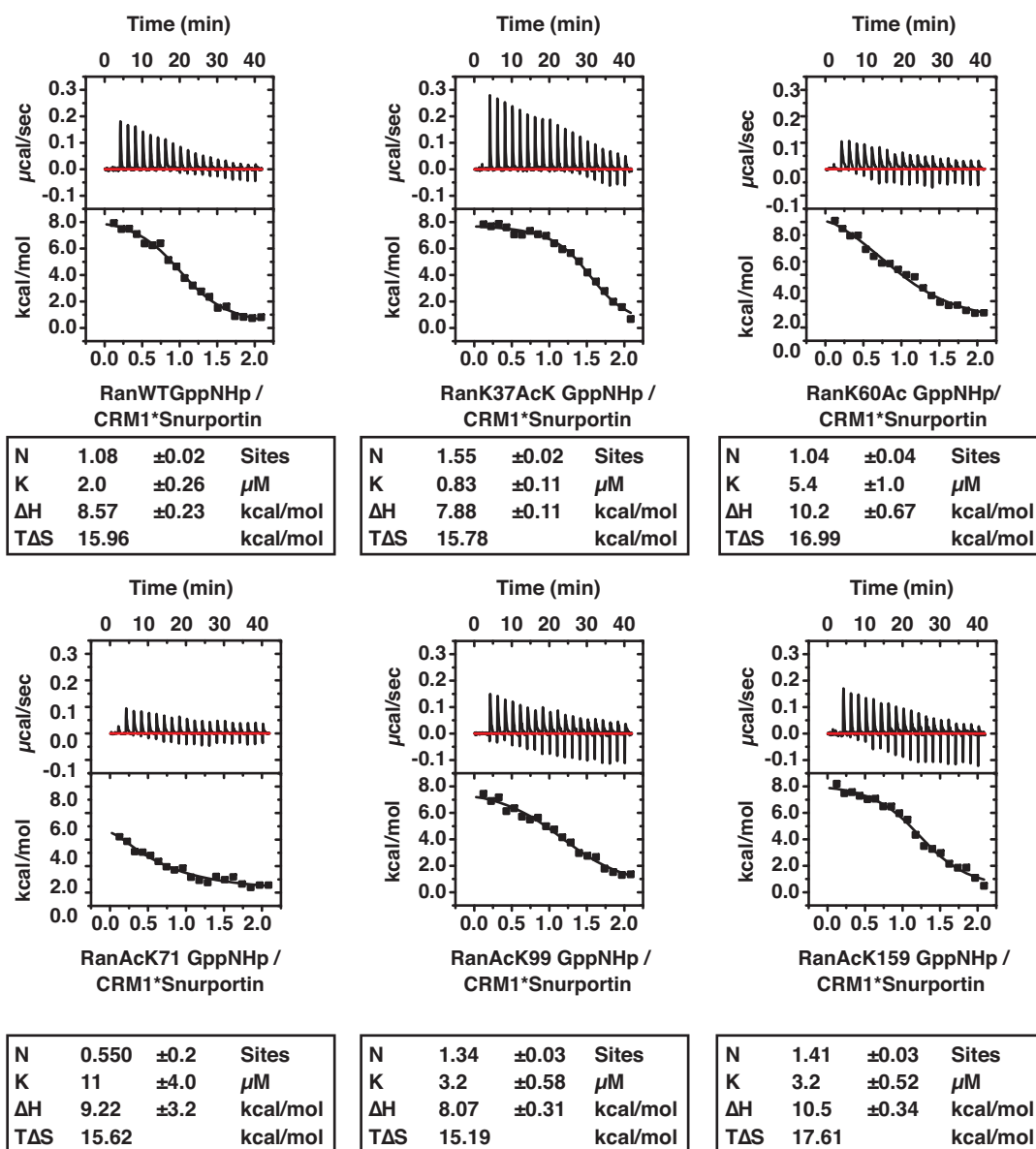


FIGURE A.5: ITC measurements of RanGppNHp and CRM1·Spn1. CRM1·Spn1 (20/40 µM) was titrated with RanGppNHp (200 µM) at 10°C.

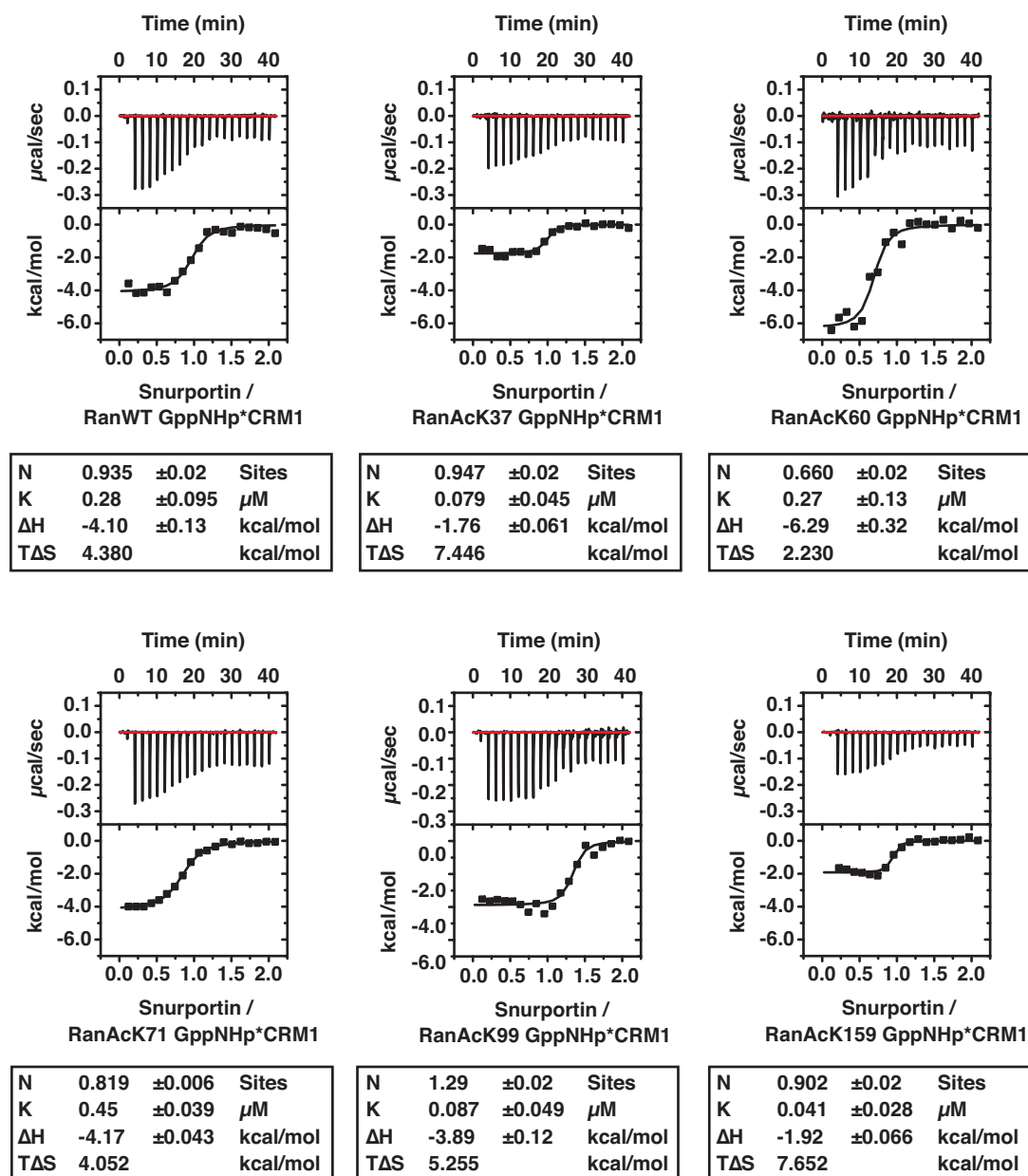


FIGURE A.6: ITC measurements of RanGppNHp·CRM1 and Spn1. RanGppNHp·CRM1 (20/40 µM) was titrated with Spn1 (200 µM) at 10°C.

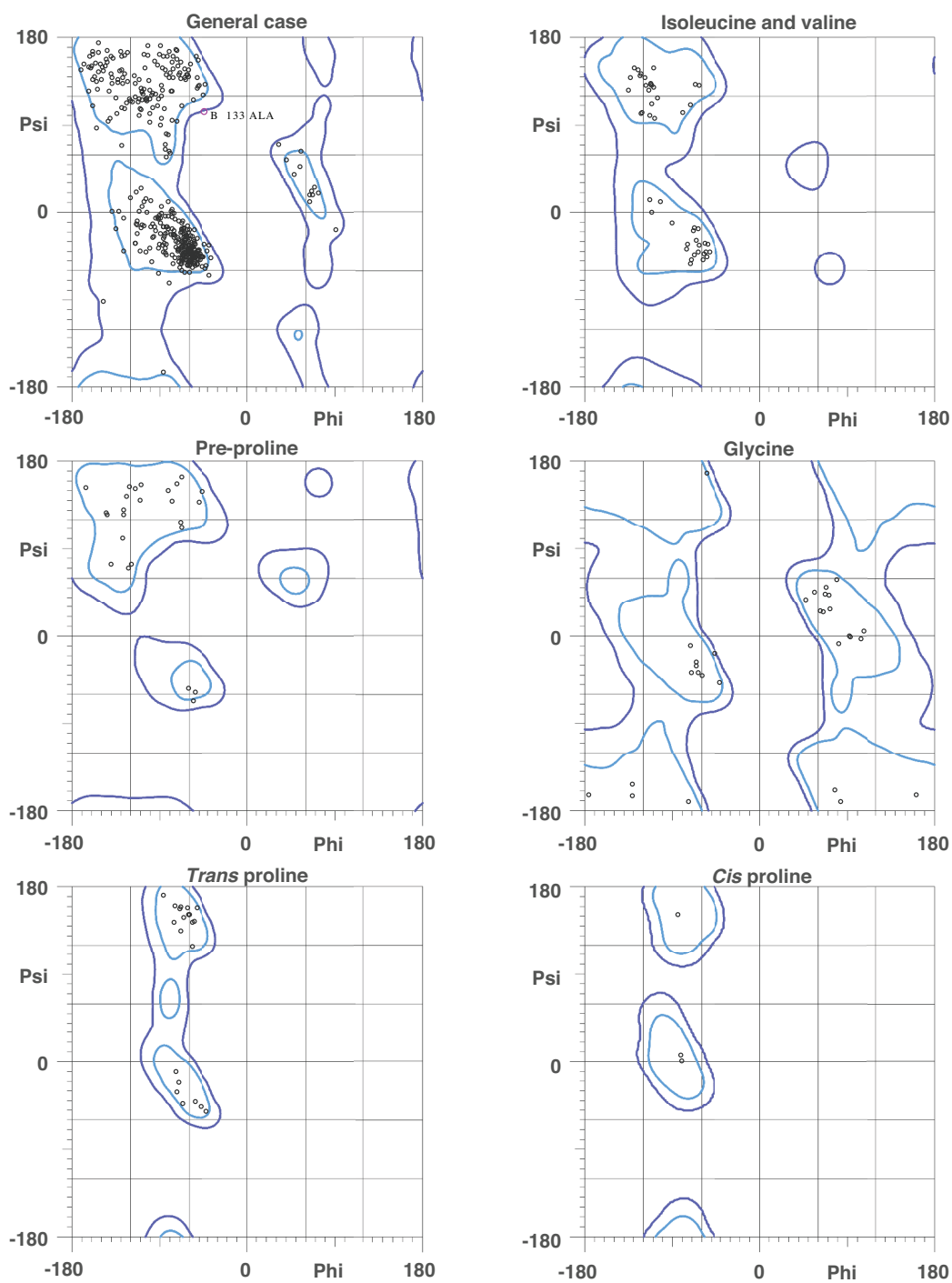


FIGURE A.7: **Ramachandran plots by residue type.** Ramachandran analysis was performed with MolProbity version 4.2 (Chen et al., 2010; Lovell et al., 2003). 95.4% (516/541) of all residues were in favored (98%) regions. 99.8% (540/541) of all residues were in allowed (>99.8%) regions. There was one outlier (phi, psi): Chain B Ala 133 (-44.7, 104.2).

# Abbreviations

<b>AB</b>	Antibody
<b>AcK</b>	Acetyl-L-lysine
<b>CMB</b>	Coomassie Brilliant Blue
<b>CRM1</b>	Chromosomal maintenance 1
<b>CV</b>	Column volume
<b>ESI</b>	Electrospray-ionization
<b>GAP</b>	GTPase activating protein
<b>GCEC</b>	Genetic code expansion concept
<b>GDP / GTP</b>	Guanosine diphosphate / triphosphate
<b>GppNHp</b>	Guanosine-5'-[( $\beta$ , $\gamma$ )-imido]triphosphate
<b>GEF</b>	Guanine nucleotide exchange factor
<b>GNBP</b>	Guanine nucleotide binding protein
<b>GST</b>	Glutathione-S-transferase
<b>HDACs</b>	Histone deacetylase
<b>(RP)-HPLC</b>	(Reversed-phase) high pressure liquid chromatography
<b>IB</b>	Immunoblot
<b>IP</b>	Immunoprecipitation
<b>IPTG</b>	Isopropyl- $\beta$ -D-thiogalactopyranosid
<b>ITC</b>	Isothermal titration calorimetry
<b>KATs</b>	Lysine-acetyl-transferase
<b>KDACs</b>	Lysine-deacetylase
<b>LB</b>	Lysogeny broth
<b>MCS</b>	Multiple cloning site
<b>MS</b>	Mass spectrometry
<b>MW</b>	Molecular weight
<b>NAD</b>	Nicotinamide adenine dinucleotide
<b>NAM</b>	Nicotinamide
<b>NE</b>	Nuclear envelope
<b>NES</b>	Nuclear export signal
<b>NLS</b>	Nuclear localization signal

---

<b>NPC</b>	Nuclear pore complex
<b>NTF2</b>	Nuclear transport receptor 2
<b>PBS</b>	Phosphate buffered saline
<b>PDB</b>	Protein database
<b>PEPCK1</b>	Phosphoenolpyruvate carboxykinase 1
<b>RanBP</b>	Ran binding protein
<b>RCC1</b>	Regulator of chromosome condensation 1
<b>rpm</b>	Rotations per minute
<b>SEC</b>	Size exclusion chromatography
<b>Spn1</b>	Snurportin 1
<b>SUMO</b>	Small ubiquitin-like modifier
<b>TBAB</b>	Tetra- <i>n</i> -butylammonium bromide
<b>TEV</b>	Tobacco etch virus
<b>TFAcK</b>	N-( $\epsilon$ )-trifluoroacetyl-L-lysine
<b>WT</b>	wildtype

# Bibliography

- Ach, R. A. and Gruissem, W. (1994). A small nuclear GTP-binding protein from tomato suppresses a *Schizosaccharomyces pombe* cell-cycle mutant. *Proceedings of the National Academy of Sciences of the United States of America*, 91(13):5863–5867.
- Adams, P. D., Afonine, P. V., Bunkczi, G., Chen, V. B., Davis, I. W., Echols, N., Headd, J. J., Hung, L.-W., Kapral, G. J., Grosse-Kunstleve, R. W., McCoy, A. J., Moriarty, N. W., Oeffner, R., Read, R. J., Richardson, D. C., Richardson, J. S., Terwilliger, T. C., and Zwart, P. H. (2010). PHENIX: a comprehensive Python-based system for macromolecular structure solution. *Acta Crystallographica. Section D, Biological Crystallography*, 66(Pt 2):213–221.
- Afonine, P. V., Grosse-Kunstleve, R. W., Echols, N., Headd, J. J., Moriarty, N. W., Mustyakimov, M., Terwilliger, T. C., Urzhumtsev, A., Zwart, P. H., and Adams, P. D. (2012). Towards automated crystallographic structure refinement with phenix.refine. *Acta Crystallographica. Section D, Biological Crystallography*, 68(Pt 4):352–367.
- Akella, J. S., Wloga, D., Kim, J., Starostina, N. G., Lyons-Abbott, S., Morrissette, N. S., Dougan, S. T., Kipreos, E. T., and Gaertig, J. (2010). MEC-17 is an  $\alpha$ -tubulin acetyltransferase. *Nature*, 467(7312):218–222.
- Aletta, J. M., Cimato, T. R., and Ettinger, M. J. (1998). Protein methylation: a signal event in post-translational modification. *Trends in Biochemical Sciences*, 23(3):89–91.
- Allen, T. D., Cronshaw, J. M., Bagley, S., Kiseleva, E., and Goldberg, M. W. (2000). The nuclear pore complex: mediator of translocation between nucleus and cytoplasm. *Journal of Cell Science*, 113 (Pt 10):1651–1659.

- Allfrey, V. G., Faulkner, R., and Mirsky, A. E. (1964). Acetylation and methylation of histones and their possible role in the regulation of RNA synthesis. *Proceedings of the National Academy of Sciences of the United States of America*, 51:786–794.
- Anderegg, R. J., Betz, R., Carr, S. A., Crabb, J. W., and Duntze, W. (1988). Structure of *Saccharomyces cerevisiae* mating hormone  $\alpha$ -factor. Identification of S-farnesyl cysteine as a structural component. *The Journal of Biological Chemistry*, 263(34):18236–18240.
- Anderson, D. J. and Hetzer, M. W. (2007). Nuclear envelope formation by chromatin-mediated reorganization of the endoplasmic reticulum. *Nature Cell Biology*, 9(10):1160–1166.
- Andres, D. A., Seabra, M. C., Brown, M. S., Armstrong, S. A., Smeland, T. E., Creemers, F. P., and Goldstein, J. L. (1993). cDNA cloning of component A of Rab geranylgeranyl transferase and demonstration of its role as a Rab escort protein. *Cell*, 73(6):1091–1099.
- Antonny, B., Beraud-Dufour, S., Chardin, P., and Chabre, M. (1997). N-terminal hydrophobic residues of the G-protein ADP-ribosylation factor-1 insert into membrane phospholipids upon GDP to GTP exchange. *Biochemistry*, 36(15):4675–4684.
- Apolloni, A., Prior, I. A., Lindsay, M., Parton, R. G., and Hancock, J. F. (2000). H-ras but not K-ras traffics to the plasma membrane through the exocytic pathway. *Molecular and Cellular Biology*, 20(7):2475–2487.
- Arnautov, A., Azuma, Y., Ribbeck, K., Joseph, J., Boyarchuk, Y., Karpova, T., McNally, J., and Dasso, M. (2005). Crm1 is a mitotic effector of Ran-GTP in somatic cells. *Nature cell biology*, 7(6):626–632.
- Arnautov, A. and Dasso, M. (2005). Ran-GTP regulates Kinetochores Attachment in Somatic Cells. *Cell Cycle*, 4(9):1161–1165.
- Arya, G. and Schlick, T. (2006). Role of histone tails in chromatin folding revealed by a mesoscopic oligonucleosome model. *Proceedings of the National Academy of Sciences of the United States of America*, 103(44):16236–16241.
- Askjaer, P., Galy, V., Hannak, E., and Mattaj, I. W. (2002). Ran GTPase cycle and importins  $\alpha$  and  $\beta$  are essential for spindle formation and nuclear envelope

- assembly in living *Caenorhabditis elegans* embryos. *Molecular Biology of the Cell*, 13(12):4355–4370.
- Avalos, J. L., Bever, K. M., and Wolberger, C. (2005). Mechanism of sirtuin inhibition by nicotinamide: altering the NAD(+) cosubstrate specificity of a Sir2 enzyme. *Molecular cell*, 17(6):855–868.
- Avalos, J. L., Celic, I., Muhammad, S., Cosgrove, M. S., Boeke, J. D., and Wolberger, C. (2002). Structure of a Sir2 enzyme bound to an acetylated p53 peptide. *Molecular Cell*, 10(3):523–535.
- Azuma, K., Sasada, T., Takedatsu, H., Shomura, H., Koga, M., Maeda, Y., Yao, A., Hirai, T., Takabayashi, A., Shichijo, S., and Itoh, K. (2004). Ran, a Small GTPase Gene, Encodes Cytotoxic T Lymphocyte (CTL) Epitopes Capable of Inducing HLA-A33restricted and Tumor-Reactive CTLs in Cancer Patients. *Clinical Cancer Research*, 10(19):6695–6702.
- Baeza, J., Dowell, J. A., Smallegan, M. J., Fan, J., Amador-Noguez, D., Khan, Z., and Denu, J. M. (2014). Stoichiometry of site-specific lysine acetylation in an entire proteome. *The Journal of Biological Chemistry*, 289(31):21326–21338.
- Baeza, J., Smallegan, M. J., and Denu, J. M. (2015). Site-specific reactivity of nonenzymatic lysine acetylation. *ACS chemical biology*, 10(1):122–128.
- Bai, P., Cant, C., Oudart, H., Brunynszki, A., Cen, Y., Thomas, C., Yamamoto, H., Huber, A., Kiss, B., Houtkooper, R. H., Schoonjans, K., Schreiber, V., Sauve, A. A., Menissier-de Murcia, J., and Auwerx, J. (2011). PARP-1 inhibition increases mitochondrial metabolism through SIRT1 activation. *Cell Metabolism*, 13(4):461–468.
- Bannister, A. J., Miska, E. A., Grlich, D., and Kouzarides, T. (2000). Acetylation of importin- $\alpha$  nuclear import factors by CBP/p300. *Current biology: CB*, 10(8):467–470.
- Bannister, A. J., Zegerman, P., Partridge, J. F., Miska, E. A., Thomas, J. O., Allshire, R. C., and Kouzarides, T. (2001). Selective recognition of methylated lysine 9 on histone H3 by the HP1 chromo domain. *Nature*, 410(6824):120–124.
- Bayliss, R., Sardon, T., Vernos, I., and Conti, E. (2003). Structural Basis of Aurora-A Activation by TPX2 at the Mitotic Spindle. *Molecular Cell*, 12(4):851–862.

- Beirowski, B., Gustin, J., Armour, S. M., Yamamoto, H., Viader, A., North, B. J., Michn, S., Baloh, R. H., Golden, J. P., Schmidt, R. E., Sinclair, D. A., Auwerx, J., and Milbrandt, J. (2011). Sir-two-homolog 2 (Sirt2) modulates peripheral myelination through polarity protein Par-3/atypical protein kinase C (aPKC) signaling. *Proceedings of the National Academy of Sciences of the United States of America*, 108(43):E952–961.
- Beli, P., Lukashchuk, N., Wagner, S. A., Weinert, B. T., Olsen, J. V., Baskcomb, L., Mann, M., Jackson, S. P., and Choudhary, C. (2012). Proteomic investigations reveal a role for RNA processing factor THRAP3 in the DNA damage response. *Molecular Cell*, 46(2):212–225.
- Beltrao, P., Albanese, V., Kenner, L. R., Swaney, D. L., Burlingame, A., Villn, J., Lim, W. A., Fraser, J. S., Frydman, J., and Krogan, N. J. (2012). Systematic Functional Prioritization of Protein Post-translational Modifications. *Cell*, 150(2):413–425.
- Bertos, N. R., Gilquin, B., Chan, G. K. T., Yen, T. J., Khochbin, S., and Yang, X.-J. (2004). Role of the tetradecapeptide repeat domain of human histone deacetylase 6 in cytoplasmic retention. *The Journal of Biological Chemistry*, 279(46):48246–48254.
- Bhaskara, S., Chyla, B. J., Amann, J. M., Knutson, S. K., Cortez, D., Sun, Z.-W., and Hiebert, S. W. (2008). Deletion of histone deacetylase 3 reveals critical roles in S phase progression and DNA damage control. *Molecular Cell*, 30(1):61–72.
- Bi, X., Corpina, R. A., and Goldberg, J. (2002). Structure of the Sec23/24-Sar1 pre-budding complex of the COPII vesicle coat. *Nature*, 419(6904):271–277.
- Bielli, A., Haney, C. J., Gabreski, G., Watkins, S. C., Bannykh, S. I., and Aridor, M. (2005). Regulation of Sar1 NH2 terminus by GTP binding and hydrolysis promotes membrane deformation to control COPII vesicle fission. *The Journal of Cell Biology*, 171(6):919–924.
- Bischoff, F. R., Krebber, H., Smirnova, E., Dong, W., and Ponstingl, H. (1995). Co-activation of RanGTPase and inhibition of GTP dissociation by Ran-GTP binding protein RanBP1. *The EMBO Journal*, 14(4):705–715.
- Bischoff, F. R., Maier, G., Tilz, G., and Ponstingl, H. (1990). A 47-kDa human nuclear protein recognized by antikinetochore autoimmune sera is homologous with the

- protein encoded by RCC1, a gene implicated in onset of chromosome condensation. *Proceedings of the National Academy of Sciences of the United States of America*, 87(21):8617–8621.
- Bischoff, F. R. and Ponstingl, H. (1991a). Catalysis of guanine nucleotide exchange on Ran by the mitotic regulator RCC1. *Nature*, 354(6348):80–82.
- Bischoff, F. R. and Ponstingl, H. (1991b). Mitotic regulator protein RCC1 is complexed with a nuclear ras-related polypeptide. *Proceedings of the National Academy of Sciences*, 88(23):10830–10834.
- Blander, G., Olejnik, J., Krzymanska-Olejnik, E., McDonagh, T., Haigis, M., Yaffe, M. B., and Guarente, L. (2005). SIRT1 shows no substrate specificity in vitro. *The Journal of Biological Chemistry*, 280(11):9780–9785.
- Boettcher, B. and Barral, Y. (2013). The cell biology of open and closed mitosis. *Nucleus*, 4(3):160–165.
- Boriack-Sjodin, P. A., Margarit, S. M., Bar-Sagi, D., and Kuriyan, J. (1998). The structural basis of the activation of Ras by Sos. *Nature*, 394(6691):337–343.
- Bos, J. L., Rehmann, H., and Wittinghofer, A. (2007). GEFs and GAPs: Critical Elements in the Control of Small G Proteins. *Cell*, 129(5):865–877.
- Bourne, H. R., Sanders, D. A., and McCormick, F. (1991). The GTPase superfamily: conserved structure and molecular mechanism. *Nature*, 349(6305):117–127.
- Boyault, C., Gilquin, B., Zhang, Y., Rybin, V., Garman, E., Meyer-Klaucke, W., Matthias, P., Mller, C. W., and Khochbin, S. (2006). HDAC6-p97/VCP controlled polyubiquitin chain turnover. *The EMBO journal*, 25(14):3357–3366.
- Bradford, M. M. (1976). A rapid and sensitive method for the quantitation of microgram quantities of protein utilizing the principle of protein-dye binding. *Analytical Biochemistry*, 72:248–254.
- Brooks, C. L. and Gu, W. (2011). The impact of acetylation and deacetylation on the p53 pathway. *Protein & cell*, 2(6):456–462.

- Brownell, J. E. and Allis, C. D. (1995). An activity gel assay detects a single, catalytically active histone acetyltransferase subunit in *Tetrahymena* macronuclei. *Proceedings of the National Academy of Sciences of the United States of America*, 92(14):6364–6368.
- Brownell, J. E., Zhou, J., Ranalli, T., Kobayashi, R., Edmondson, D. G., Roth, S. Y., and Allis, C. D. (1996). *Tetrahymena* histone acetyltransferase A: a homolog to yeast Gcn5p linking histone acetylation to gene activation. *Cell*, 84(6):843–851.
- Brucker, S., Gerwert, K., and Ktting, C. (2010). Tyr39 of ran preserves the Ran.GTP gradient by inhibiting GTP hydrolysis. *Journal of Molecular Biology*, 401(1):1–6.
- Bruenger, A. T. (1992). Free R value: a novel statistical quantity for assessing the accuracy of crystal structures. *Nature*, 355(6359):472–475.
- Bush, J. and Cardelli, J. (1993). Molecular cloning and DNA sequence of a *Dictyostelium* cDNA encoding a Ran/TC4 related GTP binding protein belonging to the ras superfamily. *Nucleic Acids Research*, 21(7):1675.
- Cambridge, S. B., Gnad, F., Nguyen, C., Bermejo, J. L., Krger, M., and Mann, M. (2011). Systems-wide proteomic analysis in mammalian cells reveals conserved, functional protein turnover. *Journal of Proteome Research*, 10(12):5275–5284.
- Capon, D. J., Seeburg, P. H., McGrath, J. P., Hayflick, J. S., Edman, U., Levinson, A. D., and Goeddel, D. V. (1983). Activation of Ki-ras2 gene in human colon and lung carcinomas by two different point mutations. *Nature*, 304(5926):507–513.
- Carazo-Salas, R. E., Guarguaglini, G., Gruss, O. J., Segref, A., Karsenti, E., and Mattaj, I. W. (1999). Generation of GTP-bound Ran by RCC1 is required for chromatin-induced mitotic spindle formation. *Nature*, 400(6740):178–181.
- Casey, P. J., Solski, P. A., Der, C. J., and Buss, J. E. (1989). p21ras is modified by a farnesyl isoprenoid. *Proceedings of the National Academy of Sciences of the United States of America*, 86(21):8323–8327.
- Cavalier-Smith, T. (1991). Intron phylogeny: a new hypothesis. *Trends in genetics: TIG*, 7(5):145–148.
- Chandra, A., Grecco, H. E., Pisupati, V., Perera, D., Cassidy, L., Skoulidis, F., Ismail, S. A., Hedberg, C., Hanzal-Bayer, M., Venkitaraman, A. R., Wittinghofer, A., and

- Bastiaens, P. I. H. (2012). The GDI-like solubilizing factor PDE sustains the spatial organization and signalling of Ras family proteins. *Nature Cell Biology*, 14(2):148–158.
- Chang, E. H., Gonda, M. A., Ellis, R. W., Scolnick, E. M., and Lowy, D. R. (1982). Human genome contains four genes homologous to transforming genes of Harvey and Kirsten murine sarcoma viruses. *Proceedings of the National Academy of Sciences of the United States of America*, 79(16):4848–4852.
- Chang, S., Young, B. D., Li, S., Qi, X., Richardson, J. A., and Olson, E. N. (2006). Histone deacetylase 7 maintains vascular integrity by repressing matrix metalloproteinase 10. *Cell*, 126(2):321–334.
- Chen, L. M., Chern, Y., Ong, S. J., and Tai, J. H. (1994). Molecular cloning and characterization of a ras-related gene of ran/tc4/spi1 subfamily in *Giardia lamblia*. *The Journal of Biological Chemistry*, 269(25):17297–17304.
- Chen, T., Muratore, T. L., Schaner-Tooley, C. E., Shabanowitz, J., Hunt, D. F., and Macara, I. G. (2007). N-terminal alpha-methylation of RCC1 is necessary for stable chromatin association and normal mitosis. *Nature Cell Biology*, 9(5):596–603.
- Chen, V. B., Arendall, W. B., Headd, J. J., Keedy, D. A., Immormino, R. M., Kapral, G. J., Murray, L. W., Richardson, J. S., and Richardson, D. C. (2010). MolProbity: all-atom structure validation for macromolecular crystallography. *Acta Crystallographica. Section D, Biological Crystallography*, 66(Pt 1):12–21.
- Chen, Y., Zhao, W., Yang, J. S., Cheng, Z., Luo, H., Lu, Z., Tan, M., Gu, W., and Zhao, Y. (2012). Quantitative acetylome analysis reveals the roles of SIRT1 in regulating diverse substrates and cellular pathways. *Molecular & cellular proteomics: MCP*, 11(10):1048–1062.
- Cheng, H.-L., Mostoslavsky, R., Saito, S., Manis, J. P., Gu, Y., Patel, P., Bronson, R., Appella, E., Alt, F. W., and Chua, K. F. (2003). Developmental defects and p53 hyperacetylation in Sir2 homolog (SIRT1)-deficient mice. *Proceedings of the National Academy of Sciences of the United States of America*, 100(19):10794–10799.
- Choudhary, C., Kumar, C., Gnad, F., Nielsen, M. L., Rehman, M., Walther, T. C., Olsen, J. V., and Mann, M. (2009). Lysine acetylation targets protein complexes and co-regulates major cellular functions. *Science (New York, N.Y.)*, 325(5942):834–840.

- Choy, E., Chiu, V. K., Silletti, J., Feoktistov, M., Morimoto, T., Michaelson, D., Ivanov, I. E., and Philips, M. R. (1999). Endomembrane trafficking of ras: the CAAX motif targets proteins to the ER and Golgi. *Cell*, 98(1):69–80.
- Clarke, S., Vogel, J. P., Deschenes, R. J., and Stock, J. (1988). Posttranslational modification of the Ha-ras oncogene protein: evidence for a third class of protein carboxyl methyltransferases. *Proceedings of the National Academy of Sciences of the United States of America*, 85(13):4643–4647.
- Cohen, H. Y., Miller, C., Bitterman, K. J., Wall, N. R., Hekking, B., Kessler, B., Howitz, K. T., Gorospe, M., de Cabo, R., and Sinclair, D. A. (2004). Calorie restriction promotes mammalian cell survival by inducing the SIRT1 deacetylase. *Science (New York, N.Y.)*, 305(5682):390–392.
- Colicelli, J. (2004). Human RAS superfamily proteins and related GTPases. *Science's STKE: signal transduction knowledge environment*, 2004(250):RE13.
- Cox, J. and Mann, M. (2008). MaxQuant enables high peptide identification rates, individualized p.p.b.-range mass accuracies and proteome-wide protein quantification. *Nature Biotechnology*, 26(12):1367–1372.
- Cox, J., Neuhauser, N., Michalski, A., Scheltema, R. A., Olsen, J. V., and Mann, M. (2011). Andromeda: a peptide search engine integrated into the MaxQuant environment. *Journal of Proteome Research*, 10(4):1794–1805.
- Creaven, M., Hans, F., Mutskov, V., Col, E., Caron, C., Dimitrov, S., and Khochbin, S. (1999). Control of the histone-acetyltransferase activity of Tip60 by the HIV-1 transactivator protein, Tat. *Biochemistry*, 38(27):8826–8830.
- Cudney, R., Patel, S., Weisgraber, K., Newhouse, Y., and McPherson, A. (1994). Screening and optimization strategies for macromolecular crystal growth. *Acta Crystallographica Section D: Biological Crystallography*, 50(4):414–423.
- Dasso, M., Seki, T., Azuma, Y., Ohba, T., and Nishimoto, T. (1994). A mutant form of the Ran/TC4 protein disrupts nuclear function in *Xenopus laevis* egg extracts by inhibiting the RCC1 protein, a regulator of chromosome condensation. *The EMBO journal*, 13(23):5732–5744.

- Davis, I. W., Leaver-Fay, A., Chen, V. B., Block, J. N., Kapral, G. J., Wang, X., Murray, L. W., Arendall, W. B., Snoeyink, J., Richardson, J. S., and Richardson, D. C. (2007). MolProbity: all-atom contacts and structure validation for proteins and nucleic acids. *Nucleic Acids Research*, 35(Web Server issue):W375–383.
- de Vos, A. M., Tong, L., Milburn, M. V., Matias, P. M., Jancarik, J., Noguchi, S., Nishimura, S., Miura, K., Ohtsuka, E., and Kim, S. H. (1988). Three-dimensional structure of an oncogene protein: catalytic domain of human c-H-ras p21. *Science (New York, N.Y.)*, 239(4842):888–893.
- Dequiedt, F., Kasler, H., Fischle, W., Kiermer, V., Weinstein, M., Herndier, B. G., and Verdin, E. (2003). HDAC7, a thymus-specific class II histone deacetylase, regulates Nur77 transcription and TCR-mediated apoptosis. *Immunity*, 18(5):687–698.
- Dever, T. E., Glynnias, M. J., and Merrick, W. C. (1987). GTP-binding domain: three consensus sequence elements with distinct spacing. *Proceedings of the National Academy of Sciences of the United States of America*, 84(7):1814–1818.
- Dhalluin, C., Carlson, J. E., Zeng, L., He, C., Aggarwal, A. K., and Zhou, M. M. (1999). Structure and ligand of a histone acetyltransferase bromodomain. *Nature*, 399(6735):491–496.
- Diederichs, K. and Karplus, P. A. (1997). Improved R-factors for diffraction data analysis in macromolecular crystallography. *Nature Structural Biology*, 4(4):269–275.
- Diederichs, K. and Karplus, P. A. (2013). Better models by discarding data? *Acta Crystallographica. Section D, Biological Crystallography*, 69(Pt 7):1215–1222.
- Ding, G., Liu, H.-D., Huang, Q., Liang, H.-X., Ding, Z.-H., Liao, Z.-J., and Huang, G. (2013). HDAC6 promotes hepatocellular carcinoma progression by inhibiting P53 transcriptional activity. *FEBS letters*, 587(7):880–886.
- Dokmanovic, M., Clarke, C., and Marks, P. A. (2007). Histone deacetylase inhibitors: overview and perspectives. *Molecular cancer research: MCR*, 5(10):981–989.
- Dompierre, J. P., Godin, J. D., Charrin, B. C., Cordelires, F. P., King, S. J., Humbert, S., and Saudou, F. (2007). Histone deacetylase 6 inhibition compensates for the transport deficit in Huntington’s disease by increasing tubulin acetylation. *The Journal of Neuroscience: The Official Journal of the Society for Neuroscience*, 27(13):3571–3583.

- Dong, X., Biswas, A., and Chook, Y. M. (2009). Structural basis for assembly and disassembly of the CRM1 nuclear export complex. *Nature Structural & Molecular Biology*, 16(5):558–560.
- Donohoe, D., Collins, L., Wali, A., Bigler, R., Sun, W., and Bultman, S. (2012). The Warburg Effect Dictates the Mechanism of Butyrate-Mediated Histone Acetylation and Cell Proliferation. *Molecular Cell*, 48(4):612–626.
- Dorigo, B., Schalch, T., Bystricky, K., and Richmond, T. J. (2003). Chromatin fiber folding: requirement for the histone H4 N-terminal tail. *Journal of Molecular Biology*, 327(1):85–96.
- Downs, J. A., Allard, S., Jobin-Robitaille, O., Javaheri, A., Auger, A., Bouchard, N., Kron, S. J., Jackson, S. P., and Ct, J. (2004). Binding of chromatin-modifying activities to phosphorylated histone H2a at DNA damage sites. *Molecular Cell*, 16(6):979–990.
- Du, J., Zhou, Y., Su, X., Yu, J. J., Khan, S., Jiang, H., Kim, J., Woo, J., Kim, J. H., Choi, B. H., He, B., Chen, W., Zhang, S., Cerione, R. A., Auwerx, J., Hao, Q., and Lin, H. (2011). Sirt5 is a NAD-dependent protein lysine demalonylase and desuccinylase. *Science (New York, N.Y.)*, 334(6057):806–809.
- Egerman, M. A., Cadena, S. M., Gilbert, J. A., Meyer, A., Nelson, H. N., Swalley, S. E., Mallozzi, C., Jacobi, C., Jennings, L. L., Clay, I., Laurent, G., Ma, S., Brachat, S., Lach-Trifilieff, E., Shavhlakadze, T., Trendelenburg, A.-U., Brack, A. S., and Glass, D. J. (2015). GDF11 Increases with Age and Inhibits Skeletal Muscle Regeneration. *Cell Metabolism*, 22(1):164–174.
- Eissenberg, J. C. (2012). Structural biology of the chromodomain: Form and function. *Gene*, 496(2):69–78.
- Ellis, R. W., Defeo, D., Shih, T. Y., Gonda, M. A., Young, H. A., Tsuchida, N., Lowy, D. R., and Scolnick, E. M. (1981). The p21 src genes of Harvey and Kirsten sarcoma viruses originate from divergent members of a family of normal vertebrate genes. *Nature*, 292(5823):506–511.

- Emsley, P., Lohkamp, B., Scott, W. G., and Cowtan, K. (2010). Features and development of Coot. *Acta Crystallographica. Section D, Biological Crystallography*, 66(Pt 4):486–501.
- Evans, P. R. and Murshudov, G. N. (2013). How good are my data and what is the resolution? *Acta Crystallographica. Section D, Biological Crystallography*, 69(Pt 7):1204–1214.
- Eyers, P. A., Erikson, E., Chen, L. G., and Maller, J. L. (2003). A Novel Mechanism for Activation of the Protein Kinase Aurora A. *Current Biology*, 13(8):691–697.
- Farria, A., Li, W., and Dent, S. Y. R. (2015). KATs in cancer: functions and therapies. *Oncogene*, 34(38):4901–4913.
- Feldman, J. L., Baeza, J., and Denu, J. M. (2013). Activation of the protein deacetylase SIRT6 by long-chain fatty acids and widespread deacylation by mammalian sirtuins. *The Journal of Biological Chemistry*, 288(43):31350–31356.
- Feldman, J. L., Dittenhafer-Reed, K. E., and Denu, J. M. (2012). Sirtuin Catalysis and Regulation. *The Journal of Biological Chemistry*, 287(51):42419–42427.
- Feuerstein, J., Goody, R. S., and Webb, M. R. (1989). The mechanism of guanosine nucleotide hydrolysis by p21 c-Ha-ras. The stereochemical course of the GTPase reaction. *The Journal of Biological Chemistry*, 264(11):6188–6190.
- Filippakopoulos, P., Picaud, S., Mangos, M., Keates, T., Lambert, J.-P., Barsyte-Lovejoy, D., Felletar, I., Volkmer, R., Mller, S., Pawson, T., Gingras, A.-C., Arrow-smith, C. H., and Knapp, S. (2012). Histone recognition and large-scale structural analysis of the human bromodomain family. *Cell*, 149(1):214–231.
- Finnin, M. S., Donigian, J. R., and Pavletich, N. P. (2001). Structure of the histone deacetylase SIRT2. *Nature structural biology*, 8(7):621–625.
- Firestein, R., Blander, G., Michan, S., Oberdoerffer, P., Ogino, S., Campbell, J., Bhimavarapu, A., Luikenhuis, S., de Cabo, R., Fuchs, C., Hahn, W. C., Guarente, L. P., and Sinclair, D. A. (2008). The SIRT1 deacetylase suppresses intestinal tumorigenesis and colon cancer growth. *PloS One*, 3(4):e2020.

- Foisner, R. and Gerace, L. (1993). Integral membrane proteins of the nuclear envelope interact with lamins and chromosomes, and binding is modulated by mitotic phosphorylation. *Cell*, 73(7):1267–1279.
- Forte, G. M. A., Pool, M. R., and Stirling, C. J. (2011). N-terminal acetylation inhibits protein targeting to the endoplasmic reticulum. *PLoS biology*, 9(5):e1001073.
- Frazzi, R., Valli, R., Tamagnini, I., Casali, B., Latruffe, N., and Merli, F. (2013). Resveratrol-mediated apoptosis of hodgkin lymphoma cells involves SIRT1 inhibition and FOXO3a hyperacetylation. *International Journal of Cancer. Journal International Du Cancer*, 132(5):1013–1021.
- Friedman, J. R., Webster, B. M., Mastronarde, D. N., Verhey, K. J., and Voeltz, G. K. (2010). ER sliding dynamics and ER-mitochondrial contacts occur on acetylated microtubules. *The Journal of Cell Biology*, 190(3):363–375.
- Friedmann, D. R. and Marmorstein, R. (2013). Structure and mechanism of non-histone protein acetyltransferase enzymes. *The FEBS journal*, 280(22):5570–5581.
- Fukuda, M., Asano, S., Nakamura, T., Adachi, M., Yoshida, M., Yanagida, M., and Nishida, E. (1997). CRM1 is responsible for intracellular transport mediated by the nuclear export signal. *Nature*, 390(6657):308–311.
- Gallo, C. M., Smith, D. L., and Smith, J. S. (2004). Nicotinamide clearance by Pnc1 directly regulates Sir2-mediated silencing and longevity. *Molecular and Cellular Biology*, 24(3):1301–1312.
- Garske, A. L. and Denu, J. M. (2006). SIRT1 top 40 hits: use of one-bead, one-compound acetyl-peptide libraries and quantum dots to probe deacetylase specificity. *Biochemistry*, 45(1):94–101.
- Gasteiger, E., Hoogland, C., Gattiker, A., Wilkins, M. R., Appel, R. D., Bairoch, A., and others (2005). *Protein identification and analysis tools on the ExpASY server*. Springer.
- Geoghegan, K. F., Dixon, H. B., Rosner, P. J., Hoth, L. R., Lanzetti, A. J., Borzilleri, K. A., Marr, E. S., Pezzullo, L. H., Martin, L. B., LeMotte, P. K., McColl, A. S., Kamath, A. V., and Stroh, J. G. (1999). Spontaneous alpha-N-6-phosphogluconoylation

- of a His tag in *Escherichia coli*: the cause of extra mass of 258 or 178 Da in fusion proteins. *Analytical Biochemistry*, 267(1):169–184.
- Giustiniani, J., Daire, V., Cantaloube, I., Durand, G., Pos, C., Perdiz, D., and Baillet, A. (2009). Tubulin acetylation favors Hsp90 recruitment to microtubules and stimulates the signaling function of the Hsp90 clients Akt/PKB and p53. *Cellular Signalling*, 21(4):529–539.
- Glozak, M. A., Sengupta, N., Zhang, X., and Seto, E. (2005). Acetylation and deacetylation of non-histone proteins. *Gene*, 363:15–23.
- Goerlich, D., Kostka, S., Kraft, R., Dingwall, C., Laskey, R. A., Hartmann, E., and Prehn, S. (1995). Two different subunits of importin cooperate to recognize nuclear localization signals and bind them to the nuclear envelope. *Current biology: CB*, 5(4):383–392.
- Goerlich, D., Prehn, S., Laskey, R. A., and Hartmann, E. (1994). Isolation of a protein that is essential for the first step of nuclear protein import. *Cell*, 79(5):767–778.
- Gosser, Y. Q., Nomanbhoy, T. K., Aghazadeh, B., Manor, D., Combs, C., Cerione, R. A., and Rosen, M. K. (1997). C-terminal binding domain of Rho GDP-dissociation inhibitor directs N-terminal inhibitory peptide to GTPases. *Nature*, 387(6635):814–819.
- Graham, F. L. and van der Eb, A. J. (1973). A new technique for the assay of infectivity of human adenovirus 5 DNA. *Virology*, 52(2):456–467.
- Gruenwald, D., Singer, R. H., and Rout, M. (2011). Nuclear export dynamics of RNA-protein complexes. *Nature*, 475(7356):333–341.
- Gruss, O. J., Carazo-Salas, R. E., Schatz, C. A., Guarguaglini, G., Kast, J., Wilm, M., Le Bot, N., Vernos, I., Karsenti, E., and Mattaj, I. W. (2001). Ran Induces Spindle Assembly by Reversing the Inhibitory Effect of Importin on TPX2 Activity. *Cell*, 104(1):83–93.
- Gu, W. and Roeder, R. G. (1997). Activation of p53 sequence-specific DNA binding by acetylation of the p53 C-terminal domain. *Cell*, 90(4):595–606.

- Guenther, M. G., Barak, O., and Lazar, M. A. (2001). The SMRT and N-CoR corepressors are activating cofactors for histone deacetylase 3. *Molecular and Cellular Biology*, 21(18):6091–6101.
- Guenther, M. G., Lane, W. S., Fischle, W., Verdin, E., Lazar, M. A., and Shiekhattar, R. (2000). A core SMRT corepressor complex containing HDAC3 and TBL1, a WD40-repeat protein linked to deafness. *Genes & Development*, 14(9):1048–1057.
- Gurard-Levin, Z. A., Kilian, K. A., Kim, J., Bhr, K., and Mrksich, M. (2010). Peptide Arrays Identify Isoform-Selective Substrates for Profiling Endogenous Lysine Deacetylase Activity. *ACS Chemical Biology*, 5(9):863–873.
- Gurard-Levin, Z. A., Kim, J., and Mrksich, M. (2009). Combining Mass Spectrometry and Peptide Arrays to Profile the Specificities of the Histone Deacetylases. *ChemBiochem : a European journal of chemical biology*, 10(13):2159–2161.
- Haberland, M., Mokalled, M. H., Montgomery, R. L., and Olson, E. N. (2009a). Epigenetic control of skull morphogenesis by histone deacetylase 8. *Genes & Development*, 23(14):1625–1630.
- Haberland, M., Montgomery, R. L., and Olson, E. N. (2009b). The many roles of histone deacetylases in development and physiology: implications for disease and therapy. *Nature Reviews. Genetics*, 10(1):32–42.
- Haigis, M. C., Mostoslavsky, R., Haigis, K. M., Fahie, K., Christodoulou, D. C., Murphy, A. J., Valenzuela, D. M., Yancopoulos, G. D., Karow, M., Blander, G., Wolberger, C., Prolla, T. A., Weindruch, R., Alt, F. W., and Guarente, L. (2006). SIRT4 inhibits glutamate dehydrogenase and opposes the effects of calorie restriction in pancreatic beta cells. *Cell*, 126(5):941–954.
- Hallows, W. C., Yu, W., Smith, B. C., Devries, M. K., Devires, M. K., Ellinger, J. J., Someya, S., Shortreed, M. R., Prolla, T., Markley, J. L., Smith, L. M., Zhao, S., Guan, K.-L., and Denu, J. M. (2011). Sirt3 promotes the urea cycle and fatty acid oxidation during dietary restriction. *Molecular Cell*, 41(2):139–149.
- Hancock, J. F., Paterson, H., and Marshall, C. J. (1990). A polybasic domain or palmitoylation is required in addition to the CAAX motif to localize p21ras to the plasma membrane. *Cell*, 63(1):133–139.

- Haney, S. A. and Broach, J. R. (1994). Cdc25p, the guanine nucleotide exchange factor for the Ras proteins of *Saccharomyces cerevisiae*, promotes exchange by stabilizing Ras in a nucleotide-free state. *The Journal of Biological Chemistry*, 269(24):16541–16548.
- Harvey, J. J. (1964). An unidentified virus which causes the rapid production of tumours in mice. *Nature*, 204:1104–1105.
- Hebert, A. S., Dittenhafer-Reed, K. E., Yu, W., Bailey, D. J., Selen, E. S., Boersma, M. D., Carson, J. J., Tonelli, M., Balloon, A. J., Higbee, A. J., Westphall, M. S., Pagliarini, D. J., Prolla, T. A., Assadi-Porter, F., Roy, S., Denu, J. M., and Coon, J. J. (2013). Calorie restriction and SIRT3 trigger global reprogramming of the mitochondrial protein acetylome. *Molecular Cell*, 49(1):186–199.
- Hershko, A., Heller, H., Eytan, E., Kaklij, G., and Rose, I. A. (1984). Role of the alpha-amino group of protein in ubiquitin-mediated protein breakdown. *Proceedings of the National Academy of Sciences of the United States of America*, 81(22):7021–7025.
- Hirschey, M. D., Shimazu, T., Huang, J.-Y., Schwer, B., and Verdin, E. (2011). SIRT3 Regulates Mitochondrial Protein Acetylation and Intermediary Metabolism. *Cold Spring Harbor Symposia on Quantitative Biology*, 76:267–277.
- Hoffmann, G., Breitenbcher, F., Schuler, M., and Ehrenhofer-Murray, A. E. (2014). A Novel Sirtuin 2 (SIRT2) Inhibitor with p53-dependent Pro-apoptotic Activity in Non-small Cell Lung Cancer. *Journal of Biological Chemistry*, 289(8):5208–5216.
- Hollebeke, J., Van Damme, P., and Gevaert, K. (2012). N-terminal acetylation and other functions of N-acetyltransferases. *Biological Chemistry*, 393(4):291–298.
- Hook, S. S., Orian, A., Cowley, S. M., and Eisenman, R. N. (2002). Histone deacetylase 6 binds polyubiquitin through its zinc finger (PAZ domain) and copurifies with deubiquitinating enzymes. *Proceedings of the National Academy of Sciences of the United States of America*, 99(21):13425–13430.
- Hopper, A. K., Traglia, H. M., and Dunst, R. W. (1990). The yeast RNA1 gene product necessary for RNA processing is located in the cytosol and apparently excluded from the nucleus. *The Journal of Cell Biology*, 111(2):309–321.

- Hornbeck, P. V., Zhang, B., Murray, B., Kornhauser, J. M., Latham, V., and Skrzypek, E. (2015). PhosphoSitePlus, 2014: mutations, PTMs and recalibrations. *Nucleic Acids Research*, 43(Database issue):D512–520.
- Hubbert, C., Guardiola, A., Shao, R., Kawaguchi, Y., Ito, A., Nixon, A., Yoshida, M., Wang, X.-F., and Yao, T.-P. (2002). HDAC6 is a microtubule-associated deacetylase. *Nature*, 417(6887):455–458.
- Huber, J., Cronshagen, U., Kadokura, M., Marshallsay, C., Wada, T., Sekine, M., and Lhrmann, R. (1998). Snurportin1, an m3g-cap-specific nuclear import receptor with a novel domain structure. *The EMBO journal*, 17(14):4114–4126.
- Hwang, C.-S., Shemorry, A., and Varshavsky, A. (2010). N-terminal acetylation of cellular proteins creates specific degradation signals. *Science (New York, N.Y.)*, 327(5968):973–977.
- Imai, S., Armstrong, C. M., Kaeberlein, M., and Guarente, L. (2000). Transcriptional silencing and longevity protein Sir2 is an NAD-dependent histone deacetylase. *Nature*, 403(6771):795–800.
- Ito, A., Kawaguchi, Y., Lai, C.-H., Kovacs, J. J., Higashimoto, Y., Appella, E., and Yao, T.-P. (2002). MDM2-HDAC1-mediated deacetylation of p53 is required for its degradation. *The EMBO journal*, 21(22):6236–6245.
- Ito, A., Lai, C. H., Zhao, X., Saito, S., Hamilton, M. H., Appella, E., and Yao, T. P. (2001). p300/CBP-mediated p53 acetylation is commonly induced by p53-activating agents and inhibited by MDM2. *The EMBO journal*, 20(6):1331–1340.
- Jancarik, J. and Kim, S.-H. (1991). Sparse matrix sampling: a screening method for crystallization of proteins. *Journal of applied crystallography*, 24(4):409–411.
- Jiang, W., Wang, S., Xiao, M., Lin, Y., Zhou, L., Lei, Q., Xiong, Y., Guan, K.-L., and Zhao, S. (2011). Acetylation regulates gluconeogenesis by promoting PEPCK1 degradation via recruiting the UBR5 ubiquitin ligase. *Molecular cell*, 43(1):33–44.
- Jiang, Y., Rossi, G., and Ferro-Novick, S. (1993). Bet2p and Mad2p are components of a prenyltransferase that adds geranylgeranyl onto Ypt1p and Sec4p. *Nature*, 366(6450):84–86.

- Jin, Q., Yan, T., Ge, X., Sun, C., Shi, X., and Zhai, Q. (2007). Cytoplasm-localized SIRT1 enhances apoptosis. *Journal of Cellular Physiology*, 213(1):88–97.
- Jin, Y., Zeng, S. X., Dai, M.-S., Yang, X.-J., and Lu, H. (2002). MDM2 inhibits PCAF (p300/CREB-binding protein-associated factor)-mediated p53 acetylation. *The Journal of Biological Chemistry*, 277(34):30838–30843.
- Jin, Y.-H., Kim, Y.-J., Kim, D.-W., Baek, K.-H., Kang, B. Y., Yeo, C.-Y., and Lee, K.-Y. (2008). Sirt2 interacts with 14-3-3 / and down-regulates the activity of p53. *Biochemical and Biophysical Research Communications*, 368(3):690–695.
- John, J., Sohmen, R., Feuerstein, J., Linke, R., Wittinghofer, A., and Goody, R. S. (1990). Kinetics of interaction of nucleotides with nucleotide-free H-ras p21. *Biochemistry*, 29(25):6058–6065.
- Jkely, G. (2003). Small GTPases and the evolution of the eukaryotic cell. *BioEssays: News and Reviews in Molecular, Cellular and Developmental Biology*, 25(11):1129–1138.
- Kalab, P., Pu, R. T., and Dasso, M. (1999). The Ran GTPase regulates mitotic spindle assembly. *Current Biology*, 9(9):481–484.
- Kalebic, N., Sorrentino, S., Perlas, E., Bolasco, G., Martinez, C., and Heppenstall, P. A. (2013). TAT1 is the major  $\alpha$ -tubulin acetyltransferase in mice. *Nature Communications*, 4:1962.
- Kamita, M., Kimura, Y., Ino, Y., Kamp, R. M., Plevoda, B., Sherman, F., and Hirano, H. (2011). N(-)-Acetylation of yeast ribosomal proteins and its effect on protein synthesis. *Journal of Proteomics*, 74(4):431–441.
- Katayama, M., Kawata, M., Yoshida, Y., Horiuchi, H., Yamamoto, T., Matsuura, Y., and Takai, Y. (1991). The posttranslationally modified C-terminal structure of bovine aortic smooth muscle rhoA p21. *The Journal of Biological Chemistry*, 266(19):12639–12645.
- Katta, S. S., Smoyer, C. J., and Jaspersen, S. L. (2014). Destination: inner nuclear membrane. *Trends in Cell Biology*, 24(4):221–229.

- Keck, K. M. and Pemberton, L. F. (2011). Interaction with the histone chaperone Vps75 promotes nuclear localization and HAT activity of Rtt109 in vivo. *Traffic (Copenhagen, Denmark)*, 12(7):826–839.
- Kelly, R. D. W. and Cowley, S. M. (2013). The physiological roles of histone deacetylase (HDAC) 1 and 2: complex co-stars with multiple leading parts. *Biochemical Society Transactions*, 41(3):741–749.
- Khan, A. N. and Lewis, P. N. (2005). Unstructured conformations are a substrate requirement for the Sir2 family of NAD-dependent protein deacetylases. *The Journal of Biological Chemistry*, 280(43):36073–36078.
- Khosravi-Far, R., Lutz, R. J., Cox, A. D., Conroy, L., Bourne, J. R., Sinensky, M., Balch, W. E., Buss, J. E., and Der, C. J. (1991). Isoprenoid modification of rab proteins terminating in CC or CXC motifs. *Proceedings of the National Academy of Sciences of the United States of America*, 88(14):6264–6268.
- Kim, G.-W., Li, L., Gorbani, M., You, L., and Yang, X.-J. (2013). Mice Lacking  $\alpha$ -Tubulin Acetyltransferase 1 Are Viable but Display  $\alpha$ -Tubulin Acetylation Deficiency and Dentate Gyrus Distortion. *The Journal of Biological Chemistry*, 288(28):20334–20350.
- Kim, J., Daniel, J., Espejo, A., Lake, A., Krishna, M., Xia, L., Zhang, Y., and Bedford, M. T. (2006a). Tudor, MBT and chromo domains gauge the degree of lysine methylation. *EMBO reports*, 7(4):397–403.
- Kim, S. C., Sprung, R., Chen, Y., Xu, Y., Ball, H., Pei, J., Cheng, T., Kho, Y., Xiao, H., Xiao, L., Grishin, N. V., White, M., Yang, X.-J., and Zhao, Y. (2006b). Substrate and functional diversity of lysine acetylation revealed by a proteomics survey. *Molecular cell*, 23(4):607–618.
- Kirsten, W. H., Schauf, V., and McCoy, J. (1970). Properties of a murine sarcoma virus. *Bibliotheca Haematologica*, (36):246–249.
- Klebe, C., Bischoff, F. R., Ponstingl, H., and Wittinghofer, A. (1995). Interaction of the nuclear GTP-binding protein Ran with its regulatory proteins RCC1 and RanGAP1. *Biochemistry*, 34(2):639–647.

- Knauer, S. K., Bier, C., Habtemichael, N., and Stauber, R. H. (2006). The SurvivinCrm1 interaction is essential for chromosomal passenger complex localization and function. *EMBO Reports*, 7(12):1259–1265.
- Knights, C. D., Catania, J., Di Giovanni, S., Muratoglu, S., Perez, R., Swartzbeck, A., Quong, A. A., Zhang, X., Beerman, T., Pestell, R. G., and Avantaggiati, M. L. (2006). Distinct p53 acetylation cassettes differentially influence gene-expression patterns and cell fate. *The Journal of Cell Biology*, 173(4):533–544.
- Koonin, E. V. (2015). Origin of eukaryotes from within archaea, archaeal eukaryome and bursts of gene gain: eukaryogenesis just made easier? *Philosophical Transactions of the Royal Society B: Biological Sciences*, 370(1678).
- Koyama, M. and Matsuura, Y. (2010). An allosteric mechanism to displace nuclear export cargo from CRM1 and RanGTP by RanBP1. *The EMBO Journal*, 29(12):2002–2013.
- Kuhlmann, J., Macara, I., and Wittinghofer, A. (1997). Dynamic and equilibrium studies on the interaction of Ran with its effector, RanBP1. *Biochemistry*, 36(40):12027–12035.
- Laemmli, U. K. (1970). Cleavage of structural proteins during the assembly of the head of bacteriophage T4. *Nature*, 227(5259):680–685.
- Lagger, G., O’Carroll, D., Rembold, M., Khier, H., Tischler, J., Weitzer, G., Schuettengruber, B., Hauser, C., Brunmeir, R., Jenuwein, T., and Seiser, C. (2002). Essential function of histone deacetylase 1 in proliferation control and CDK inhibitor repression. *The EMBO journal*, 21(11):2672–2681.
- Laherty, C. D., Yang, W. M., Sun, J. M., Davie, J. R., Seto, E., and Eisenman, R. N. (1997). Histone deacetylases associated with the mSin3 corepressor mediate mad transcriptional repression. *Cell*, 89(3):349–356.
- Lammers, M., Neumann, H., Chin, J. W., and James, L. C. (2010). Acetylation regulates cyclophilin A catalysis, immunosuppression and HIV isomerization. *Nature chemical biology*, 6(5):331–337.
- Lane, N. and Martin, W. (2010). The energetics of genome complexity. *Nature*, 467(7318):929–934.

- LeDizet, M. and Piperno, G. (1987). Identification of an acetylation site of Chlamydomonas alpha-tubulin. *Proceedings of the National Academy of Sciences of the United States of America*, 84(16):5720–5724.
- Lee, J.-S., Shukla, A., Schneider, J., Swanson, S. K., Washburn, M. P., Florens, L., Bhaumik, S. R., and Shilatifard, A. (2007). Histone crosstalk between H2b monoubiquitination and H3 methylation mediated by COMPASS. *Cell*, 131(6):1084–1096.
- Legate, K. R. and Andrews, D. W. (2003). The beta-subunit of the signal recognition particle receptor is a novel GTP-binding protein without intrinsic GTPase activity. *The Journal of Biological Chemistry*, 278(30):27712–27720.
- Lenzen, C., Cool, R. H., Prinz, H., Kuhlmann, J., and Wittinghofer, A. (1998). Kinetic analysis by fluorescence of the interaction between Ras and the catalytic domain of the guanine nucleotide exchange factor Cdc25mm. *Biochemistry*, 37(20):7420–7430.
- Leo, C. and Chen, J. D. (2000). The SRC family of nuclear receptor coactivators. *Gene*, 245(1):1–11.
- Leslie, A. G. W. and Powell, H. R. (2007). Processing diffraction data with mosflm. In Read, R. J. and Sussman, J. L., editors, *Evolving Methods for Macromolecular Crystallography*, number 245 in NATO Science Series, pages 41–51. Springer Netherlands. DOI: 10.1007/978-1-4020-6316-9\_4.
- L’Hernault, S. W. and Rosenbaum, J. L. (1983). Chlamydomonas alpha-tubulin is posttranslationally modified in the flagella during flagellar assembly. *The Journal of Cell Biology*, 97(1):258–263.
- Li, H. Y., Wirtz, D., and Zheng, Y. (2003a). A mechanism of coupling RCC1 mobility to RanGTP production on the chromatin in vivo. *The Journal of cell biology*, 160(5):635–644.
- Li, Q.-J., Yang, S.-H., Maeda, Y., Sladek, F. M., Sharrocks, A. D., and Martins-Green, M. (2003b). MAP kinase phosphorylation-dependent activation of Elk-1 leads to activation of the co-activator p300. *The EMBO journal*, 22(2):281–291.
- Li, T., Diner, B. A., Chen, J., and Cristea, I. M. (2012). Acetylation modulates cellular distribution and DNA sensing ability of interferon-inducible protein IFI16. *Proceedings*

- of the National Academy of Sciences of the United States of America*, 109(26):10558–10563.
- Lin, H., Su, X., and He, B. (2012). Protein lysine acylation and cysteine succination by intermediates of energy metabolism. *ACS chemical biology*, 7(6):947–960.
- Liou, G.-G., Tanny, J. C., Kruger, R. G., Walz, T., and Moazed, D. (2005). Assembly of the SIR complex and its regulation by O-acetyl-ADP-ribose, a product of NAD-dependent histone deacetylation. *Cell*, 121(4):515–527.
- Liu, H., Wang, J.-Y. S., Huang, Y., Li, Z., Gong, W., Lehmann, R., and Xu, R.-M. (2010). Structural basis for methylarginine-dependent recognition of Aubergine by Tudor. *Genes & Development*, 24(17):1876–1881.
- Liu, L., Scolnick, D. M., Trievel, R. C., Zhang, H. B., Marmorstein, R., Halazonetis, T. D., and Berger, S. L. (1999). p53 sites acetylated in vitro by PCAF and p300 are acetylated in vivo in response to DNA damage. *Molecular and Cellular Biology*, 19(2):1202–1209.
- Longenecker, K., Read, P., Derewenda, U., Dauter, Z., Liu, X., Garrard, S., Walker, L., Somlyo, A. V., Nakamoto, R. K., Somlyo, A. P., and Derewenda, Z. S. (1999). How RhoGDI binds Rho. *Acta Crystallographica. Section D, Biological Crystallography*, 55(Pt 9):1503–1515.
- Lounsbury, K. M. and Macara, I. G. (1997). Ran-binding protein 1 (RanBP1) forms a ternary complex with Ran and karyopherin beta and reduces Ran GTPase-activating protein (RanGAP) inhibition by karyopherin beta. *The Journal of biological chemistry*, 272(1):551–555.
- Lovell, S. C., Davis, I. W., Arendall, W. B., de Bakker, P. I. W., Word, J. M., Prisant, M. G., Richardson, J. S., and Richardson, D. C. (2003). Structure validation by Calpha geometry: phi,psi and Cbeta deviation. *Proteins*, 50(3):437–450.
- Lu, L., Ladinsky, M. S., and Kirchhausen, T. (2011). Formation of the postmitotic nuclear envelope from extended ER cisternae precedes nuclear pore assembly. *The Journal of Cell Biology*, 194(3):425–440.
- Lundby, A., Lage, K., Weinert, B. T., Bekker-Jensen, D. B., Secher, A., Skovgaard, T., Kelstrup, C. D., Dmytriyev, A., Choudhary, C., Lundby, C., and Olsen, J. V. (2012).

- Proteomic analysis of lysine acetylation sites in rat tissues reveals organ specificity and subcellular patterns. *Cell Reports*, 2(2):419–431.
- Luo, J., Nikolaev, A. Y., Imai, S., Chen, D., Su, F., Shiloh, A., Guarente, L., and Gu, W. (2001). Negative control of p53 by Sir2alpha promotes cell survival under stress. *Cell*, 107(2):137–148.
- Luo, J., Su, F., Chen, D., Shiloh, A., and Gu, W. (2000). Deacetylation of p53 modulates its effect on cell growth and apoptosis. *Nature*, 408(6810):377–381.
- Mahajan, R., Delphin, C., Guan, T., Gerace, L., and Melchior, F. (1997). A small ubiquitin-related polypeptide involved in targeting RanGAP1 to nuclear pore complex protein RanBP2. *Cell*, 88(1):97–107.
- Makhoul, C. H. and Trifonov, E. N. (2002). Distribution of rare triplets along mRNA and their relation to protein folding. *Journal of Biomolecular Structure & Dynamics*, 20(3):413–420.
- Malik, S. and Roeder, R. G. (2000). Transcriptional regulation through Mediator-like coactivators in yeast and metazoan cells. *Trends in Biochemical Sciences*, 25(6):277–283.
- Maltese, W. A., Sheridan, K. M., Repko, E. M., and Erdman, R. A. (1990). Post-translational modification of low molecular mass GTP-binding proteins by isoprenoid. *The Journal of Biological Chemistry*, 265(4):2148–2155.
- Mandel, M. and Higa, A. (1970). Calcium-dependent bacteriophage DNA infection. *Journal of Molecular Biology*, 53(1):159–162.
- Manning, E. T., Ikehara, T., Ito, T., Kadonaga, J. T., and Kraus, W. L. (2001). p300 forms a stable, template-committed complex with chromatin: role for the bromodomain. *Molecular and Cellular Biology*, 21(12):3876–3887.
- Marks, P., Rifkind, R. A., Richon, V. M., Breslow, R., Miller, T., and Kelly, W. K. (2001). Histone deacetylases and cancer: causes and therapies. *Nature Reviews. Cancer*, 1(3):194–202.
- Martin, W. and Koonin, E. V. (2006). Introns and the origin of nucleocytoplasmic compartmentalization. *Nature*, 440(7080):41–45.

- Matunis, M. J., Coutavas, E., and Blobel, G. (1996). A novel ubiquitin-like modification modulates the partitioning of the Ran-GTPase-activating protein RanGAP1 between the cytosol and the nuclear pore complex. *The Journal of cell biology*, 135(6 Pt 1):1457–1470.
- Maurer, P., Redd, M., Solsbacher, J., Bischoff, F. R., Greiner, M., Podtelejnikov, A. V., Mann, M., Stade, K., Weis, K., and Schlenstedt, G. (2001). The nuclear export receptor Xpo1p forms distinct complexes with NES transport substrates and the yeast Ran binding protein 1 (Yrb1p). *Molecular biology of the cell*, 12(3):539–549.
- Maurer-Stroh, S., Dickens, N. J., Hughes-Davies, L., Kouzarides, T., Eisenhaber, F., and Ponting, C. P. (2003). The Tudor domain 'Royal Family': Tudor, plant Agenet, Chromo, PWWP and MBT domains. *Trends in Biochemical Sciences*, 28(2):69–74.
- McKinsey, T. A., Zhang, C. L., Lu, J., and Olson, E. N. (2000). Signal-dependent nuclear export of a histone deacetylase regulates muscle differentiation. *Nature*, 408(6808):106–111.
- Mertins, P., Qiao, J. W., Patel, J., Udeshi, N. D., Clauser, K. R., Mani, D. R., Burgess, M. W., Gillette, M. A., Jaffe, J. D., and Carr, S. A. (2013). Integrated proteomic analysis of post-translational modifications by serial enrichment. *Nature Methods*, 10(7):634–637.
- Meunier, S. and Vernos, I. (2011). K-fibre minus ends are stabilized by a RanGTP-dependent mechanism essential for functional spindle assembly. *Nature Cell Biology*, 13(12):1406–1414.
- Michishita, E., Park, J. Y., Burneskis, J. M., Barrett, J. C., and Horikawa, I. (2005). Evolutionarily conserved and nonconserved cellular localizations and functions of human SIRT proteins. *Molecular Biology of the Cell*, 16(10):4623–4635.
- Milburn, M. V., Tong, L., deVos, A. M., Brnnger, A., Yamaizumi, Z., Nishimura, S., and Kim, S. H. (1990). Molecular switch for signal transduction: structural differences between active and inactive forms of protooncogenic ras proteins. *Science (New York, N. Y.)*, 247(4945):939–945.

- Mohamed, J. S., Wilson, J. C., Myers, M. J., Sisson, K. J., and Alway, S. E. (2014). Dysregulation of SIRT-1 in aging mice increases skeletal muscle fatigue by a PARP-1-dependent mechanism. *Aging*, 6(10):820–834.
- Mohr, D., Frey, S., Fischer, T., Gttler, T., and Grlich, D. (2009). Characterisation of the passive permeability barrier of nuclear pore complexes. *The EMBO journal*, 28(17):2541–2553.
- Monecke, T., Gttler, T., Neumann, P., Dickmanns, A., Grlich, D., and Ficner, R. (2009). Crystal structure of the nuclear export receptor CRM1 in complex with Snurportin1 and RanGTP. *Science (New York, N.Y.)*, 324(5930):1087–1091.
- Monecke, T., Haselbach, D., Vo, B., Russek, A., Neumann, P., Thomson, E., Hurt, E., Zachariae, U., Stark, H., Grubmiller, H., Dickmanns, A., and Ficner, R. (2013). Structural basis for cooperativity of CRM1 export complex formation. *Proceedings of the National Academy of Sciences*, 110(3):960–965.
- Montgomery, D. C., Sorum, A. W., and Meier, J. L. (2014). Chemoproteomic Profiling of Lysine Acetyltransferases Highlights an Expanded Landscape of Catalytic Acetylation. *Journal of the American Chemical Society*, 136(24):8669–8676.
- Montgomery, R. L., Davis, C. A., Potthoff, M. J., Haberland, M., Fielitz, J., Qi, X., Hill, J. A., Richardson, J. A., and Olson, E. N. (2007). Histone deacetylases 1 and 2 redundantly regulate cardiac morphogenesis, growth, and contractility. *Genes & Development*, 21(14):1790–1802.
- Morimoto, J., Hayashi, Y., and Suga, H. (2012). Discovery of macrocyclic peptides armed with a mechanism-based warhead: isoform-selective inhibition of human deacetylase SIRT2. *Angewandte Chemie (International Ed. in English)*, 51(14):3423–3427.
- Morinire, J., Rousseaux, S., Steuerwald, U., Soler-Lpez, M., Curtet, S., Vitte, A.-L., Govin, J., Gaucher, J., Sadoul, K., Hart, D. J., Krijgsveld, J., Khochbin, S., Mller, C. W., and Petosa, C. (2009). Cooperative binding of two acetylation marks on a histone tail by a single bromodomain. *Nature*, 461(7264):664–668.
- Moroianu, J., Blobel, G., and Radu, A. (1996). Nuclear protein import: Ran-GTP dissociates the karyopherin alphabeta heterodimer by displacing alpha from an overlapping

- binding site on beta. *Proceedings of the National Academy of Sciences of the United States of America*, 93(14):7059–7062.
- Morrison, A. J., Highland, J., Krogan, N. J., Arbel-Eden, A., Greenblatt, J. F., Haber, J. E., and Shen, X. (2004). INO80 and gamma-H2ax interaction links ATP-dependent chromatin remodeling to DNA damage repair. *Cell*, 119(6):767–775.
- Moser, M. A., Hagelkruys, A., and Seiser, C. (2014). Transcription and beyond: the role of mammalian class I lysine deacetylases. *Chromosoma*, 123(1-2):67–78.
- Mujtaba, S., He, Y., Zeng, L., Yan, S., Plotnikova, O., Sachchidanand, n., Sanchez, R., Zeleznik-Le, N. J., Ronai, Z., and Zhou, M.-M. (2004). Structural mechanism of the bromodomain of the coactivator CBP in p53 transcriptional activation. *Molecular Cell*, 13(2):251–263.
- Muller, S., Filippakopoulos, P., and Knapp, S. (2011). Bromodomains as therapeutic targets. *Expert Reviews in Molecular Medicine*, 13:e29.
- Nachury, M. V., Maresca, T. J., Salmon, W. C., Waterman-Storer, C. M., Heald, R., and Weis, K. (2001). Importin Is a Mitotic Target of the Small GTPase Ran in Spindle Assembly. *Cell*, 104(1):95–106.
- Nachury, M. V. and Weis, K. (1999). The direction of transport through the nuclear pore can be inverted. *Proceedings of the National Academy of Sciences of the United States of America*, 96(17):9622–9627.
- Nancy, V., Callebaut, I., El Marjou, A., and de Gunzburg, J. (2002). The delta subunit of retinal rod cGMP phosphodiesterase regulates the membrane association of Ras and Rap GTPases. *The Journal of Biological Chemistry*, 277(17):15076–15084.
- Nassar, N., Hoffman, G. R., Manor, D., Clardy, J. C., and Cerione, R. A. (1998). Structures of Cdc42 bound to the active and catalytically compromised forms of Cdc42gap. *Nature Structural Biology*, 5(12):1047–1052.
- Neumann, H., Peak-Chew, S. Y., and Chin, J. W. (2008). Genetically encoding N(epsilon)-acetyllysine in recombinant proteins. *Nature chemical biology*, 4(4):232–234.

- Neumann, H., Wang, K., Davis, L., Garcia-Alai, M., and Chin, J. W. (2010). Encoding multiple unnatural amino acids via evolution of a quadruplet-decoding ribosome. *Nature*, 464(7287):441–444.
- Nogales, E., Whittaker, M., Milligan, R. A., and Downing, K. H. (1999). High-resolution model of the microtubule. *Cell*, 96(1):79–88.
- North, B. J., Marshall, B. L., Borra, M. T., Denu, J. M., and Verdin, E. (2003). The human Sir2 ortholog, SIRT2, is an NAD<sup>+</sup>-dependent tubulin deacetylase. *Molecular cell*, 11(2):437–444.
- North, B. J. and Verdin, E. (2007). Interphase nucleo-cytoplasmic shuttling and localization of SIRT2 during mitosis. *PLoS One*, 2(8):e784.
- Ohtsubo, M., Okazaki, H., and Nishimoto, T. (1989). The RCC1 protein, a regulator for the onset of chromosome condensation locates in the nucleus and binds to DNA. *The Journal of Cell Biology*, 109(4 Pt 1):1389–1397.
- Olson, D. E., Udeshi, N. D., Wolfson, N. A., Pitcairn, C. A., Sullivan, E. D., Jaffe, J. D., Svinkina, T., Natoli, T., Lu, X., Paulk, J., McCarren, P., Wagner, F. F., Barker, D., Howe, E., Lazzaro, F., Gale, J. P., Zhang, Y.-L., Subramanian, A., Fierke, C. A., Carr, S. A., and Holson, E. B. (2014). An unbiased approach to identify endogenous substrates of "histone" deacetylase 8. *ACS chemical biology*, 9(10):2210–2216.
- Orjalo, A. V., Arnaoutov, A., Shen, Z., Boyarchuk, Y., Zeitlin, S. G., Fontoura, B., Briggs, S., Dasso, M., and Forbes, D. J. (2006). The Nup107-160 nucleoporin complex is required for correct bipolar spindle assembly. *Molecular Biology of the Cell*, 17(9):3806–3818.
- Ossareh-Nazari, B., Bachelier, F., and Dargemont, C. (1997). Evidence for a role of CRM1 in signal-mediated nuclear protein export. *Science (New York, N.Y.)*, 278(5335):141–144.
- Outeiro, T. F., Kontopoulos, E., Altmann, S. M., Kufareva, I., Strathearn, K. E., Amore, A. M., Volk, C. B., Maxwell, M. M., Rochet, J.-C., McLean, P. J., Young, A. B., Abagyan, R., Feany, M. B., Hyman, B. T., and Kazantsev, A. G. (2007). Sirtuin 2 inhibitors rescue alpha-synuclein-mediated toxicity in models of Parkinson's disease. *Science (New York, N.Y.)*, 317(5837):516–519.

- Owen, D. J., Ornaghi, P., Yang, J. C., Lowe, N., Evans, P. R., Ballario, P., Neuhaus, D., Filetici, P., and Travers, A. A. (2000). The structural basis for the recognition of acetylated histone H4 by the bromodomain of histone acetyltransferase gcn5p. *The EMBO journal*, 19(22):6141–6149.
- Pai, E. F., Kabsch, W., Krengel, U., Holmes, K. C., John, J., and Wittinghofer, A. (1989). Structure of the guanine-nucleotide-binding domain of the Ha-ras oncogene product p21 in the triphosphate conformation. *Nature*, 341(6239):209–214.
- Pan, X., Eathiraj, S., Munson, M., and Lambright, D. G. (2006). TBC-domain GAPs for Rab GTPases accelerate GTP hydrolysis by a dual-finger mechanism. *Nature*, 442(7100):303–306.
- Paraskeva, E., Izaurralde, E., Bischoff, F. R., Huber, J., Kutay, U., Hartmann, E., Lhrmann, R., and Grlich, D. (1999). CRM1-mediated recycling of snurportin 1 to the cytoplasm. *The Journal of cell biology*, 145(2):255–264.
- Patel, D., Huang, S. M., Baglia, L. A., and McCance, D. J. (1999). The E6 protein of human papillomavirus type 16 binds to and inhibits co-activation by CBP and p300. *The EMBO journal*, 18(18):5061–5072.
- Pavlov, M. Y., Watts, R. E., Tan, Z., Cornish, V. W., Ehrenberg, M., and Forster, A. C. (2009). Slow peptide bond formation by proline and other N-alkylamino acids in translation. *Proceedings of the National Academy of Sciences of the United States of America*, 106(1):50–54.
- Pearson, M., Carbone, R., Sebastiani, C., Cioce, M., Fagioli, M., Saito, S., Higashimoto, Y., Appella, E., Minucci, S., Pandolfi, P. P., and Pelicci, P. G. (2000). PML regulates p53 acetylation and premature senescence induced by oncogenic Ras. *Nature*, 406(6792):207–210.
- Peck, B., Chen, C.-Y., Ho, K.-K., Di Fruscia, P., Myatt, S. S., Coombes, R. C., Fuchter, M. J., Hsiao, C.-D., and Lam, E. W.-F. (2010). SIRT inhibitors induce cell death and p53 acetylation through targeting both SIRT1 and SIRT2. *Molecular Cancer Therapeutics*, 9(4):844–855.
- Peng, C., Lu, Z., Xie, Z., Cheng, Z., Chen, Y., Tan, M., Luo, H., Zhang, Y., He, W., Yang, K., Zwaans, B. M. M., Tishkoff, D., Ho, L., Lombard, D., He, T.-C.,

- Dai, J., Verdin, E., Ye, Y., and Zhao, Y. (2011). The first identification of lysine malonylation substrates and its regulatory enzyme. *Molecular & cellular proteomics: MCP*, 10(12):M111.012658.
- Petosa, C., Schoehn, G., Askjaer, P., Bauer, U., Moulin, M., Steuerwald, U., Soler-Lpez, M., Baudin, F., Mattaj, I. W., and Mller, C. W. (2004). Architecture of CRM1/Exportin1 suggests how cooperativity is achieved during formation of a nuclear export complex. *Molecular Cell*, 16(5):761–775.
- Petry, S., Groen, A., Ishihara, K., Mitchison, T., and Vale, R. (2013). Branching Microtubule Nucleation in *Xenopus* Egg Extracts Mediated by Augmin and TPX2. *Cell*, 152(4):768–777.
- Pfaller, R., Smythe, C., and Newport, J. W. (1991). Assembly/disassembly of the nuclear envelope membrane: cell cycle-dependent binding of nuclear membrane vesicles to chromatin in vitro. *Cell*, 65(2):209–217.
- Phillips, D. M. (1963). The presence of acetyl groups of histones. *The Biochemical Journal*, 87:258–263.
- Pichler, A., Gast, A., Seeler, J. S., Dejean, A., and Melchior, F. (2002). The nucleoporin RanBP2 has SUMO1 E3 ligase activity. *Cell*, 108(1):109–120.
- Pillai, J. B., Isbatan, A., Imai, S.-i., and Gupta, M. P. (2005). Poly(ADP-ribose) polymerase-1-dependent cardiac myocyte cell death during heart failure is mediated by NAD<sup>+</sup> depletion and reduced Sir2alpha deacetylase activity. *The Journal of Biological Chemistry*, 280(52):43121–43130.
- Polesskaya, A. and Harel-Bellan, A. (2001). Acetylation of MyoD by p300 requires more than its histone acetyltransferase domain. *The Journal of Biological Chemistry*, 276(48):44502–44503.
- Poveda, A., Pamblanco, M., Tafrov, S., Tordera, V., Sternglanz, R., and Sendra, R. (2004). Hif1 is a component of yeast histone acetyltransferase B, a complex mainly localized in the nucleus. *The Journal of Biological Chemistry*, 279(16):16033–16043.
- Price, J. C., Guan, S., Burlingame, A., Prusiner, S. B., and Ghaemmaghami, S. (2010). Analysis of proteome dynamics in the mouse brain. *Proceedings of the National Academy of Sciences of the United States of America*, 107(32):14508–14513.

- Priv, G. G., Milburn, M. V., Tong, L., de Vos, A. M., Yamaizumi, Z., Nishimura, S., and Kim, S. H. (1992). X-ray crystal structures of transforming p21 ras mutants suggest a transition-state stabilization mechanism for GTP hydrolysis. *Proceedings of the National Academy of Sciences of the United States of America*, 89(8):3649–3653.
- Pylypenko, O., Rak, A., Durek, T., Kushnir, S., Dursina, B. E., Thomae, N. H., Constantinescu, A. T., Brunsveld, L., Watzke, A., Waldmann, H., Goody, R. S., and Alexandrov, K. (2006). Structure of doubly prenylated Ypt1:GDI complex and the mechanism of GDI-mediated Rab recycling. *The EMBO Journal*, 25(1):13–23.
- Pylypenko, O., Rak, A., Reents, R., Niculae, A., Sidorovitch, V., Cioaca, M. D., Bessolitsyna, E., Thom, N. H., Waldmann, H., Schlichting, I., Goody, R. S., and Alexandrov, K. (2003). Structure of Rab escort protein-1 in complex with Rab geranylgeranyltransferase. *Molecular Cell*, 11(2):483–494.
- Quan, J. and Tian, J. (2009). Circular polymerase extension cloning of complex gene libraries and pathways. *PloS One*, 4(7):e6441.
- Randazzo, P. A. and Kahn, R. A. (1994). GTP hydrolysis by ADP-ribosylation factor is dependent on both an ADP-ribosylation factor GTPase-activating protein and acid phospholipids. *The Journal of Biological Chemistry*, 269(14):10758–10763.
- Rardin, M. J., He, W., Nishida, Y., Newman, J. C., Carrico, C., Danielson, S. R., Guo, A., Gut, P., Sahu, A. K., Li, B., Uppala, R., Fitch, M., Riiff, T., Zhu, L., Zhou, J., Mulhern, D., Stevens, R. D., Ilkayeva, O. R., Newgard, C. B., Jacobson, M. P., Hellerstein, M., Goetzman, E. S., Gibson, B. W., and Verdin, E. (2013). SIRT5 regulates the mitochondrial lysine succinylome and metabolic networks. *Cell Metabolism*, 18(6):920–933.
- Rauh, D., Fischer, F., Gertz, M., Lakshminarasimhan, M., Bergbrede, T., Aladini, F., Kambach, C., Becker, C. F. W., Zerweck, J., Schutkowski, M., and Steegborn, C. (2013). An acetylome peptide microarray reveals specificities and deacetylation substrates for all human sirtuin isoforms. *Nature communications*, 4:2327.
- Reed, N. A., Cai, D., Blasius, T. L., Jih, G. T., Meyhofer, E., Gaertig, J., and Verhey, K. J. (2006). Microtubule acetylation promotes kinesin-1 binding and transport. *Current biology: CB*, 16(21):2166–2172.

- Reed, S. M. and Quelle, D. E. (2014). p53 Acetylation: Regulation and Consequences. *Cancers*, 7(1):30–69.
- Renault, L., Kuhlmann, J., Henkel, A., and Wittinghofer, A. (2001). Structural Basis for Guanine Nucleotide Exchange on Ran by the Regulator of Chromosome Condensation (RCC1). *Cell*, 105(2):245–255.
- Ribbeck, K., Lipowsky, G., Kent, H. M., Stewart, M., and Grlich, D. (1998). NTF2 mediates nuclear import of Ran. *The EMBO Journal*, 17(22):6587–6598.
- Riester, D., Hildmann, C., Grnewald, S., Beckers, T., and Schwienhorst, A. (2007). Factors affecting the substrate specificity of histone deacetylases. *Biochemical and Biophysical Research Communications*, 357(2):439–445.
- Rittinger, K., Walker, P. A., Eccleston, J. F., Smerdon, S. J., and Gamblin, S. J. (1997). Structure at 1.65 Å of RhoA and its GTPase-activating protein in complex with a transition-state analogue. *Nature*, 389(6652):758–762.
- Rocks, O., Peyker, A., Kahms, M., Verveer, P. J., Koerner, C., Lumbierres, M., Kuhlmann, J., Waldmann, H., Wittinghofer, A., and Bastiaens, P. I. H. (2005). An acylation cycle regulates localization and activity of palmitoylated Ras isoforms. *Science (New York, N.Y.)*, 307(5716):1746–1752.
- Rojas, A. M., Fuentes, G., Rausell, A., and Valencia, A. (2012). The Ras protein superfamily: Evolutionary tree and role of conserved amino acids. *The Journal of Cell Biology*, 196(2):189–201.
- Rokudai, S., Laptenko, O., Arnal, S. M., Taya, Y., Kitabayashi, I., and Prives, C. (2013). MOZ increases p53 acetylation and premature senescence through its complex formation with PML. *Proceedings of the National Academy of Sciences of the United States of America*, 110(10):3895–3900.
- Roscioli, E., Di Francesco, L., Bolognesi, A., Giubettini, M., Orlando, S., Harel, A., Schinin, M. E., and Lavia, P. (2012). Importin- negatively regulates multiple aspects of mitosis including RANGAP1 recruitment to kinetochores. *The Journal of Cell Biology*, 196(4):435–450.

- Rotem, A., Gruber, R., Shorer, H., Shaulov, L., Klein, E., and Harel, A. (2009). Importin beta regulates the seeding of chromatin with initiation sites for nuclear pore assembly. *Molecular Biology of the Cell*, 20(18):4031–4042.
- Roy, S., Plowman, S., Rotblat, B., Prior, I. A., Muncke, C., Grainger, S., Parton, R. G., Henis, Y. I., Kloog, Y., and Hancock, J. F. (2005). Individual Palmitoyl Residues Serve Distinct Roles in H-Ras Trafficking, Microlocalization, and Signaling. *Molecular and Cellular Biology*, 25(15):6722–6733.
- Rudoni, S., Colombo, S., Coccetti, P., and Martegani, E. (2001). Role of guanine nucleotides in the regulation of the Ras/cAMP pathway in *Saccharomyces cerevisiae*. *Biochimica et Biophysica Acta (BBA) - Molecular Cell Research*, 1538(23):181–189.
- Ryu, D., Jo, Y. S., Lo Sasso, G., Stein, S., Zhang, H., Perino, A., Lee, J. U., Zeviani, M., Romand, R., Hottiger, M. O., Schoonjans, K., and Auwerx, J. (2014). A SIRT7-dependent acetylation switch of GABP1 controls mitochondrial function. *Cell Metabolism*, 20(5):856–869.
- Sagot, I., Schaeffer, J., and Daignan-Fornier, B. (2005). Guanylic nucleotide starvation affects *Saccharomyces cerevisiae* mother-daughter separation and may be a signal for entry into quiescence. *BMC cell biology*, 6(1):24.
- Sahakian, E., Powers, J. J., Chen, J., Deng, S. L., Cheng, F., Distler, A., Woods, D. M., Rock-Klotz, J., Sodre, A. L., Youn, J.-I., Woan, K. V., Villagra, A., Gabrilovich, D., Sotomayor, E. M., and Pinilla-Ibarz, J. (2015). Histone deacetylase 11: A novel epigenetic regulator of myeloid derived suppressor cell expansion and function. *Molecular Immunology*, 63(2):579–585.
- Sakin, V., Richter, S. M., Hsiao, H.-H., Urlaub, H., and Melchior, F. (2015). Sumoylation of the GTPase Ran by the RanBP2 SUMO E3 Ligase Complex. *The Journal of Biological Chemistry*, 290(39):23589–23602.
- Sampath, S. C., Ohi, R., Leismann, O., Salic, A., Pozniakovski, A., and Funabiki, H. (2004). The chromosomal passenger complex is required for chromatin-induced microtubule stabilization and spindle assembly. *Cell*, 118(2):187–202.

- Sanders, B. D., Jackson, B., and Marmorstein, R. (2010). Structural basis for sir-tuin function: what we know and what we don't. *Biochimica Et Biophysica Acta*, 1804(8):1604–1616.
- Sandoval, P. C., Slentz, D. H., Pisitkun, T., Saeed, F., Hoffert, J. D., and Knepper, M. A. (2013). Proteome-wide measurement of protein half-lives and translation rates in vasopressin-sensitive collecting duct cells. *Journal of the American Society of Nephrology: JASN*, 24(11):1793–1805.
- Santos-Rosa, H., Valls, E., Kouzarides, T., and Martinez-Balbs, M. (2003). Mechanisms of P/CAF auto-acetylation. *Nucleic Acids Research*, 31(15):4285–4292.
- Saraste, M., Sibbald, P. R., and Wittinghofer, A. (1990). The P-loop—a common motif in ATP- and GTP-binding proteins. *Trends in Biochemical Sciences*, 15(11):430–434.
- Sasaki, T., Kikuchi, A., Araki, S., Hata, Y., Isomura, M., Kuroda, S., and Takai, Y. (1990). Purification and characterization from bovine brain cytosol of a protein that inhibits the dissociation of GDP from and the subsequent binding of GTP to smg p25a, a ras p21-like GTP-binding protein. *The Journal of Biological Chemistry*, 265(4):2333–2337.
- Scheffzek, K., Ahmadian, M. R., Kabsch, W., Wiesmiller, L., Lautwein, A., Schmitz, F., and Wittinghofer, A. (1997). The Ras-RasGAP complex: structural basis for GTPase activation and its loss in oncogenic Ras mutants. *Science (New York, N.Y.)*, 277(5324):333–338.
- Schiltz, R. L., Mizzen, C. A., Vassilev, A., Cook, R. G., Allis, C. D., and Nakatani, Y. (1999). Overlapping but distinct patterns of histone acetylation by the human coactivators p300 and PCAF within nucleosomal substrates. *The Journal of Biological Chemistry*, 274(3):1189–1192.
- Schulze, E., Asai, D. J., Bulinski, J. C., and Kirschner, M. (1987). Posttranslational modification and microtubule stability. *The Journal of Cell Biology*, 105(5):2167–2177.
- Schweins, T., Geyer, M., Scheffzek, K., Warshel, A., Kalbitzer, H. R., and Wittinghofer, A. (1995). Substrate-assisted catalysis as a mechanism for GTP hydrolysis of p21ras and other GTP-binding proteins. *Nature Structural Biology*, 2(1):36–44.

- Scrofani, J., Sardon, T., Meunier, S., and Vernos, I. (2015). Microtubule Nucleation in Mitosis by a RanGTP-Dependent Protein Complex. *Current Biology*, 25(2):131–140.
- Seewald, M. J., Kraemer, A., Farkasovsky, M., Korner, C., Wittinghofer, A., and Vetter, I. R. (2003). Biochemical Characterization of the Ran-RanBP1-RanGAP System: Are RanBP Proteins and the Acidic Tail of RanGAP Required for the Ran-RanGAP GTPase Reaction? *Molecular and Cellular Biology*, 23(22):8124–8136.
- Seewald, M. J., Krner, C., Wittinghofer, A., and Vetter, I. R. (2002). RanGAP mediates GTP hydrolysis without an arginine finger. *Nature*, 415(6872):662–666.
- Shahbazian, M. D. and Grunstein, M. (2007). Functions of site-specific histone acetylation and deacetylation. *Annual Review of Biochemistry*, 76:75–100.
- Shaw, P. G., Chaerkady, R., Zhang, Z., Davidson, N. E., and Pandey, A. (2011). Monoclonal antibody cocktail as an enrichment tool for acetylome analysis. *Analytical Chemistry*, 83(10):3623–3626.
- Shema-Yaacoby, E., Nikolov, M., Haj-Yahya, M., Siman, P., Allemand, E., Yamaguchi, Y., Muchardt, C., Urlaub, H., Brik, A., Oren, M., and Fischle, W. (2013). Systematic identification of proteins binding to chromatin-embedded ubiquitylated H2b reveals recruitment of SWI/SNF to regulate transcription. *Cell Reports*, 4(3):601–608.
- Shiseki, M., Nagashima, M., Pedeux, R. M., Kitahama-Shiseki, M., Miura, K., Okamura, S., Onogi, H., Higashimoto, Y., Appella, E., Yokota, J., and Harris, C. C. (2003). p29ing4 and p28ing5 bind to p53 and p300, and enhance p53 activity. *Cancer Research*, 63(10):2373–2378.
- Shogren-Knaak, M., Ishii, H., Sun, J.-M., Pazin, M. J., Davie, J. R., and Peterson, C. L. (2006). Histone H4-K16 acetylation controls chromatin structure and protein interactions. *Science (New York, N.Y.)*, 311(5762):844–847.
- Shukla, S., SankarAllam, U., Ahsan, A., Chen, G., Krishnamurthy, P. M., Marsh, K., Rumschlag, M., Shankar, S., Whitehead, C., Schipper, M., Basrur, V., Southworth, D. R., Chinnaiyan, A. M., Rehemtulla, A., Beer, D. G., Lawrence, T. S., Nyati, M. K., and Ray, D. (2014). KRAS Protein Stability Is Regulated through SMURF2: UBC5 Complex-Mediated -TrCP1 Degradation. *Neoplasia (New York, N.Y.)*, 16(2):115–128.

- Smith, A., Brownawell, A., and Macara, I. G. (1998). Nuclear import of Ran is mediated by the transport factor NTF2. *Current biology: CB*, 8(25):1403–1406.
- Smith, B. C. and Denu, J. M. (2007). Acetyl-lysine analog peptides as mechanistic probes of protein deacetylases. *The Journal of Biological Chemistry*, 282(51):37256–37265.
- Smith, B. C., Settles, B., Hallows, W. C., Craven, M. W., and Denu, J. M. (2011). SIRT3 substrate specificity determined by peptide arrays and machine learning. *ACS chemical biology*, 6(2):146–157.
- Smith, S. J. and Rittinger, K. (2002). Preparation of GTPases for structural and biophysical analysis. In *GTPase Protocols*, pages 13–24. Springer.
- Spang, A., Saw, J. H., Jrgensen, S. L., Zaremba-Niedzwiedzka, K., Martijn, J., Lind, A. E., van Eijk, R., Schleper, C., Guy, L., and Ettema, T. J. G. (2015). Complex archaea that bridge the gap between prokaryotes and eukaryotes. *Nature*, 521(7551):173–179.
- Srinivasan, G., James, C. M., and Krzycki, J. A. (2002). Pyrrolysine encoded by UAG in Archaea: charging of a UAG-decoding specialized tRNA. *Science (New York, N.Y.)*, 296(5572):1459–1462.
- Stade, K., Ford, C. S., Guthrie, C., and Weis, K. (1997). Exportin 1 (Crmlp) is an essential nuclear export factor. *Cell*, 90(6):1041–1050.
- Strahl, B. D. and Allis, C. D. (2000). The language of covalent histone modifications. *Nature*, 403(6765):41–45.
- Strambio-De-Castillia, C., Niepel, M., and Rout, M. P. (2010). The nuclear pore complex: bridging nuclear transport and gene regulation. *Nature Reviews Molecular Cell Biology*, 11(7):490–501.
- Sykes, S. M., Mellert, H. S., Holbert, M. A., Li, K., Marmorstein, R., Lane, W. S., and McMahon, S. B. (2006). Acetylation of the p53 DNA-binding domain regulates apoptosis induction. *Molecular Cell*, 24(6):841–851.
- Tammsalu, T., Matic, I., Jaffray, E. G., Ibrahim, A. F. M., Tatham, M. H., and Hay, R. T. (2014). Proteome-wide identification of SUMO2 modification sites. *Science Signaling*, 7(323):rs2.

- Tang, Y., Luo, J., Zhang, W., and Gu, W. (2006). Tip60-dependent acetylation of p53 modulates the decision between cell-cycle arrest and apoptosis. *Molecular Cell*, 24(6):827–839.
- Tang, Y., Zhao, W., Chen, Y., Zhao, Y., and Gu, W. (2008). Acetylation Is Indispensable for p53 Activation. *Cell*, 133(4):612–626.
- Tanny, J. C. and Moazed, D. (2001). Coupling of histone deacetylation to NAD breakdown by the yeast silencing protein Sir2: Evidence for acetyl transfer from substrate to an NAD breakdown product. *Proceedings of the National Academy of Sciences of the United States of America*, 98(2):415–420.
- Thanaraj, T. A. and Argos, P. (1996). Protein secondary structural types are differentially coded on messenger RNA. *Protein Science: A Publication of the Protein Society*, 5(10):1973–1983.
- Tong, L. and Denu, J. M. (2010). Function and metabolism of sirtuin metabolite O-acetyl-ADP-ribose. *Biochimica Et Biophysica Acta*, 1804(8):1617–1625.
- Tsai, M.-Y., Wiese, C., Cao, K., Martin, O., Donovan, P., Ruderman, J., Prigent, C., and Zheng, Y. (2003). A Ran signalling pathway mediated by the mitotic kinase Aurora A in spindle assembly. *Nature Cell Biology*, 5(3):242–248.
- Tsai, Y.-C., Greco, T. M., Boonmee, A., Miteva, Y., and Cristea, I. M. (2012). Functional proteomics establishes the interaction of SIRT7 with chromatin remodeling complexes and expands its role in regulation of RNA polymerase I transcription. *Molecular & cellular proteomics: MCP*, 11(5):60–76.
- Tse, C., Sera, T., Wolffe, A. P., and Hansen, J. C. (1998). Disruption of Higher-Order Folding by Core Histone Acetylation Dramatically Enhances Transcription of Nucleosomal Arrays by RNA Polymerase III. *Molecular and Cellular Biology*, 18(8):4629–4638.
- Tseng, L.-C. and Chen, R.-H. (2011). Temporal control of nuclear envelope assembly by phosphorylation of lamin B receptor. *Molecular Biology of the Cell*, 22(18):3306–3317.
- Tsuchida, N., Ryder, T., and Ohtsubo, E. (1982). Nucleotide sequence of the oncogene encoding the p21 transforming protein of Kirsten murine sarcoma virus. *Science (New York, N.Y.)*, 217(4563):937–939.

- Van Damme, P., Hole, K., Pimenta-Marques, A., Helsens, K., Vandekerckhove, J., Martinho, R. G., Gevaert, K., and Arnesen, T. (2011). NatF contributes to an evolutionary shift in protein N-terminal acetylation and is important for normal chromosome segregation. *PLoS genetics*, 7(7):e1002169.
- VanBogelen, R. A., Hutton, M. E., and Neidhardt, F. C. (1990). Gene-protein database of *Escherichia coli* K-12: edition 3. *Electrophoresis*, 11(12):1131–1166.
- Vanegas, N., Garca-Sacristn, A., Lpez-Fernndez, L. A., Prraga, M., del Mazo, J., Hernandez, P., Schwartzman, J. B., and Krimer, D. B. (2003). Differential expression of Ran GTPase during HMBA-induced differentiation in murine erythroleukemia cells. *Leukemia Research*, 27(7):607–615.
- Vaziri, H., Dessain, S. K., Ng Eaton, E., Imai, S. I., Frye, R. A., Pandita, T. K., Guarente, L., and Weinberg, R. A. (2001). hSIR2(SIRT1) functions as an NAD-dependent p53 deacetylase. *Cell*, 107(2):149–159.
- Verdel, A., Curtet, S., Brocard, M. P., Rousseaux, S., Lemerrier, C., Yoshida, M., and Khochbin, S. (2000). Active maintenance of mHDA2/mHDAC6 histone-deacetylase in the cytoplasm. *Current biology: CB*, 10(12):747–749.
- Vetter, I. R., Nowak, C., Nishimoto, T., Kuhlmann, J., and Wittinghofer, A. (1999). Structure of a Ran-binding domain complexed with Ran bound to a GTP analogue: implications for nuclear transport. *Nature*, 398(6722):39–46.
- Vetter, I. R. and Wittinghofer, A. (2001). The guanine nucleotide-binding switch in three dimensions. *Science (New York, N.Y.)*, 294(5545):1299–1304.
- Wagner, G. R. and Hirsche, M. D. (2014). Nonenzymatic protein acylation as a carbon stress regulated by sirtuin deacylases. *Molecular Cell*, 54(1):5–16.
- Wagner, G. R. and Payne, R. M. (2013). Widespread and enzyme-independent N-acetylation and N-succinylation of proteins in the chemical conditions of the mitochondrial matrix. *The Journal of Biological Chemistry*, 288(40):29036–29045.
- Wang, Q., Zhang, Y., Yang, C., Xiong, H., Lin, Y., Yao, J., Li, H., Xie, L., Zhao, W., Yao, Y., Ning, Z.-B., Zeng, R., Xiong, Y., Guan, K.-L., Zhao, S., and Zhao, G.-P. (2010). Acetylation of metabolic enzymes coordinates carbon source utilization and metabolic flux. *Science (New York, N.Y.)*, 327(5968):1004–1007.

- Wang, R.-H., Sengupta, K., Li, C., Kim, H.-S., Cao, L., Xiao, C., Kim, S., Xu, X., Zheng, Y., Chilton, B., Jia, R., Zheng, Z.-M., Appella, E., Wang, X. W., Ried, T., and Deng, C.-X. (2008). Impaired DNA damage response, genome instability, and tumorigenesis in SIRT1 mutant mice. *Cancer Cell*, 14(4):312–323.
- Wang, W., Yang, X., Kawai, T., Lopez de Silanes, I., Mazan-Mamczarz, K., Chen, P., Chook, Y. M., Quensel, C., Khler, M., and Gorospe, M. (2004). AMP-activated protein kinase-regulated phosphorylation and acetylation of importin alpha1: involvement in the nuclear import of RNA-binding protein HuR. *The Journal of biological chemistry*, 279(46):48376–48388.
- Watson, P. J., Fairall, L., Santos, G. M., and Schwabe, J. W. R. (2012). Structure of HDAC3 bound to co-repressor and inositol tetrakisphosphate. *Nature*, 481(7381):335–340.
- Webster, D. R. and Borisy, G. G. (1989). Microtubules are acetylated in domains that turn over slowly. *Journal of Cell Science*, 92 ( Pt 1):57–65.
- Weinert, B. T., Iesmantavicius, V., Moustafa, T., Schlz, C., Wagner, S. A., Magnes, C., Zechner, R., and Choudhary, C. (2014). Acetylation dynamics and stoichiometry in *Saccharomyces cerevisiae*. *Molecular systems biology*, 10:716.
- Weinert, B. T., Iesmantavicius, V., Wagner, S. A., Schlz, C., Gummesson, B., Beli, P., Nyström, T., and Choudhary, C. (2013). Acetyl-phosphate is a critical determinant of lysine acetylation in *E. coli*. *Molecular Cell*, 51(2):265–272.
- Weinert, B. T., Moustafa, T., Iesmantavicius, V., Zechner, R., and Choudhary, C. (2015). Analysis of acetylation stoichiometry suggests that SIRT3 repairs nonenzymatic acetylation lesions. *The EMBO journal*.
- Weinert, B. T., Wagner, S. A., Horn, H., Henriksen, P., Liu, W. R., Olsen, J. V., Jensen, L. J., and Choudhary, C. (2011). Proteome-wide mapping of the *Drosophila* acetylome demonstrates a high degree of conservation of lysine acetylation. *Science signaling*, 4(183):ra48.
- Wellen, K. E., Hatzivassiliou, G., Sachdeva, U. M., Bui, T. V., Cross, J. R., and Thompson, C. B. (2009). ATP-citrate lyase links cellular metabolism to histone acetylation. *Science (New York, N.Y.)*, 324(5930):1076–1080.

- Wiseman, T., Williston, S., Brandts, J. F., and Lin, L. N. (1989). Rapid measurement of binding constants and heats of binding using a new titration calorimeter. *Analytical Biochemistry*, 179(1):131–137.
- Wisniewski, J. R., Zougman, A., Nagaraj, N., and Mann, M. (2009). Universal sample preparation method for proteome analysis. *Nature Methods*, 6(5):359–362.
- Wolfson, N. A., Pitcairn, C. A., Sullivan, E. D., Joseph, C. G., and Fierke, C. A. (2014). An enzyme-coupled assay measuring acetate production for profiling histone deacetylase specificity. *Analytical biochemistry*, 456:61–69.
- Worthylake, D. K., Rossman, K. L., and Sondek, J. (2000). Crystal structure of Rac1 in complex with the guanine nucleotide exchange region of Tiam1. *Nature*, 408(6813):682–688.
- Yamada, M., Mattaj, I. W., and Yoneda, Y. (2004). An ATP-dependent activity that releases RanGDP from NTF2. *The Journal of Biological Chemistry*, 279(35):36228–36234.
- Yamagata, K., Goto, Y., Nishimasu, H., Morimoto, J., Ishitani, R., Dohmae, N., Takeda, N., Nagai, R., Komuro, I., Suga, H., and Nureki, O. (2014). Structural Basis for Potent Inhibition of SIRT2 Deacetylase by a Macrocyclic Peptide Inducing Dynamic Structural Change. *Structure*, 22(2):345–352.
- Yamaguchi, T., Cubizolles, F., Zhang, Y., Reichert, N., Kohler, H., Seiser, C., and Matthias, P. (2010). Histone deacetylases 1 and 2 act in concert to promote the G1-to-S progression. *Genes & Development*, 24(5):455–469.
- Yang, L., Vaitheesvaran, B., Hartil, K., Robinson, A. J., Hoopmann, M. R., Eng, J. K., Kurland, I. J., and Bruce, J. E. (2011). The fasted/fed mouse metabolic acetylome: N6-acetylation differences suggest acetylation coordinates organ-specific fuel switching. *Journal of Proteome Research*, 10(9):4134–4149.
- Yang, M. H., Nickerson, S., Kim, E. T., Liot, C., Laurent, G., Spang, R., Philips, M. R., Shan, Y., Shaw, D. E., Bar-Sagi, D., Haigis, M. C., and Haigis, K. M. (2012). Regulation of RAS oncogenicity by acetylation. *Proceedings of the National Academy of Sciences of the United States of America*, 109(27):10843–10848.

- Yaseen, N. R. and Blobel, G. (1999). GTP Hydrolysis Links Initiation and Termination of Nuclear Import on the Nucleoporin Nup358. *Journal of Biological Chemistry*, 274(37):26493–26502.
- Yeung, F., Hoberg, J. E., Ramsey, C. S., Keller, M. D., Jones, D. R., Frye, R. A., and Mayo, M. W. (2004). Modulation of NF-kappaB-dependent transcription and cell survival by the SIRT1 deacetylase. *The EMBO journal*, 23(12):2369–2380.
- Yuan, H. and Marmorstein, R. (2013). Histone Acetyltransferases: Rising Ancient Counterparts to Protein Kinases. *Biopolymers*, 99(2):98–111.
- Yuan, J., Minter-Dykhouse, K., and Lou, Z. (2009). A c-Myc-SIRT1 feedback loop regulates cell growth and transformation. *The Journal of Cell Biology*, 185(2):203–211.
- Zhang, C. and Clarke, P. R. (2000). Chromatin-independent nuclear envelope assembly induced by Ran GTPase in *Xenopus* egg extracts. *Science (New York, N.Y.)*, 288(5470):1429–1432.
- Zhang, C., Hughes, M., and Clarke, P. R. (1999). Ran-GTP stabilises microtubule asters and inhibits nuclear assembly in *Xenopus* egg extracts. *Journal of Cell Science*, 112 ( Pt 14):2453–2461.
- Zhang, C., Hutchins, J. R. A., Mhlhuser, P., Kutay, U., and Clarke, P. R. (2002). Role of importin-beta in the control of nuclear envelope assembly by Ran. *Current biology: CB*, 12(6):498–502.
- Zhang, G., Hubalewska, M., and Ignatova, Z. (2009). Transient ribosomal attenuation coordinates protein synthesis and co-translational folding. *Nature Structural & Molecular Biology*, 16(3):274–280.
- Zhang, M., Arnaoutov, A., and Dasso, M. (2014a). RanBP1 Governs Spindle Assembly by Defining Mitotic Ran-GTP Production. *Developmental Cell*, 31(4):393–404.
- Zhang, Y., Li, N., Caron, C., Matthias, G., Hess, D., Khochbin, S., and Matthias, P. (2003). HDAC-6 interacts with and deacetylates tubulin and microtubules in vivo. *The EMBO journal*, 22(5):1168–1179.

- Zhang, Z.-N., Chung, S.-K., Xu, Z., and Xu, Y. (2014b). Oct4 maintains the pluripotency of human embryonic stem cells by inactivating p53 through Sirt1-mediated deacetylation. *Stem Cells (Dayton, Ohio)*, 32(1):157–165.
- Zhao, K., Chai, X., Clements, A., and Marmorstein, R. (2003). Structure and autoregulation of the yeast Hst2 homolog of Sir2. *Nature structural biology*, 10(10):864–871.
- Zhao, S., Xu, W., Jiang, W., Yu, W., Lin, Y., Zhang, T., Yao, J., Zhou, L., Zeng, Y., Li, H., Li, Y., Shi, J., An, W., Hancock, S. M., He, F., Qin, L., Chin, J., Yang, P., Chen, X., Lei, Q., Xiong, Y., and Guan, K.-L. (2010). Regulation of cellular metabolism by protein lysine acetylation. *Science (New York, N.Y.)*, 327(5968):1000–1004.
- Zhu, S., Zhang, H., and Matunis, M. J. (2006). SUMO modification through rapamycin-mediated heterodimerization reveals a dual role for Ubc9 in targeting RanGAP1 to nuclear pore complexes. *Experimental Cell Research*, 312(7):1042–1049.

# *Acknowledgements*

Die vorliegende Arbeit wurde von Januar 2013 bis November 2015 am Institut für Genetik der Universität Köln unter der Anleitung von Dr. Michael Lammers angefertigt.

Dr. Michael Lammers danke ich sehr für die Aufnahme in seine Arbeitsgruppe, für das interessante Forschungsthema, die sehr gute Betreuung und die Gewährung der großen Freiräume beim Anfertigen dieser Arbeit.

Bei Prof. Dr. Kay Hofmann bedanke ich mich ganz herzlich für die Bereitschaft das Zweitgutachten zu übernehmen.

Mein großer Dank gilt auch den Mitarbeitern der AG Krüger und der Massenspektrometrie-Facility des CECAD Instituts, insbesondere Hendrik Nolte, Astrid Wilbrand-Hennes und Rene Grandjean, für die Hilfe bei der Gewinnung und Auswertung der massenspektrometrischen Daten.

Für die Herstellung der in dieser Arbeit verwendeten Peptide danke ich Prof. Dr. Ines Neundorf und den Mitarbeitern ihrer Gruppe.

Zudem möchte ich mich herzlich bei Dr. Magdalena Schacherl, Dr. Jan Gebauer und Prof. Dr. Ulrich Baumann für die Aufnahme der kristallographischen Daten bedanken. Prof. Dr. Ulrich Baumann danke ich zudem für die Übernahme des Prüfungsvorsitzes sowie für die Möglichkeit die Geräte und Räumlichkeiten des Instituts für Biochemie nutzen zu können.

Besonders möchte ich mich noch bei Dr. Susanne de Boor bedanken, die für das gesamte Ran-Projekt hervorragende Vorarbeit geleistet hat und mir vor allem am Anfang einen reibungslosen Start ermöglicht hat. Die Zusammenarbeit und der Austausch mit ihr war für das Gelingen dieser Arbeit sehr wichtig.

Vielen Dank an die restliche AG Lammers für die Unterstützung in allen Belangen und die Schaffung einer positiven Arbeitsatmosphäre.

Ich danke meinen Eltern, die mir diese Ausbildung ermöglicht haben und mich stets unterstützt haben. Liebe Goya, vielen Dank für alles!



# *Eidesstattliche Erklärung*

Ich versichere, dass ich die von mir vorgelegte Dissertation selbständig angefertigt, die benutzten Quellen und Hilfsmittel vollständig angegeben und die Stellen der Arbeit – einschließlich Tabellen, Karten und Abbildungen –, die anderen Werken im Wortlaut oder dem Sinn nach entnommen sind, in jedem Einzelfall als Entlehnung kenntlich gemacht habe; dass diese Dissertation noch keiner anderen Fakultät oder Universität zur Prüfung vorgelegen hat; dass sie – abgesehen von unten angegebenen Teilpublikationen – noch nicht veröffentlicht worden ist sowie, dass ich eine solche Veröffentlichung vor Abschluss des Promotionsverfahrens nicht vornehmen werde. Die Bestimmungen der Promotionsordnung sind mir bekannt. Die von mir vorgelegte Dissertation ist von Dr. Michael Lammers betreut worden.

---

Carl Philipp Graf zu Innhausen und Knyphausen